Deciphering Functional Significance of Substrate-Binding Domain of Ssa1 on Heat-Shock Response and Prion Propagation

Maynooth University
National University of Ireland Maynooth

A thesis submitted to the

Maynooth University

For the degree of

DOCTOR OF PHILOSOPHY

BY

Linan Xu. M.Sc.

June 2016

Supervisor	Co-supervisor	Head of the Department
Dr. Gary Jones	**Prof. Sarah Perrett**	**Prof. Paul Moynagh**
Department of Biology	Institute of Biophysics	Department of Biology
Maynooth University	Chinese Academy of Sciences	Maynooth University
Co. Kildare, Ireland	Beijing, China	Co. Kildare, Ireland

CONTENTS

DECLARATION OF AUTHORSHIP

This thesis has not been submitted in whole or in part, to this or any other University, for any degree and is except otherwise stated the original work of the author.

Linan Xu **Date:**

ACKNOWLEDGEMENTS

As Marcel Proust's description in *À la recherche du temps perdu*, time always fly away without any nostalgia. And three-year study at Maynooth really has flowed away but left the sand of the friendship and knowledge. In the three years, I have got so many generous and selfless guidance, assistance and encouragement, which makes my life more wonderful and colourful. So I would like to say thanks to people who helped me during those three years.

First of all, I would like to thank my supervisor Dr. Gary Jones, who granted and guided this thesis to be completed. It's impossible that I can finish this kind of level research without Gary's help. Gary is not only a great supervisor in academic, but also a good mentor in life. I also would like to extend my sincere thanks to the other members Dr. David Fitzpatrick for the registration of the ICHEC account when I started in the lab. I am thankful to the other staffs that provided selfless help in the biology department. As a member of the John and Pat Hume Scholarship, I would also like to thank the grant which ensure the most basic livelihood in those three years. And thanks to Dr. Andrea Valova from the Graduate Studies Officer for processing the scholarship nicely.

Secondly, I want to thank our collaborations in the other counties. Thanks to Dr. Andrew W. Truman for the mass spectrometry. Special thanks to Professor Sarah Perrett for supporting the biochemistry assays when I stayed in the Institute of Biophysics, Chinese Academy of Sciences. I would also like to extend my sincere thanks to the other members in Sarah's group, especially Dr. Hong Zhang, Dr. Weibin Gong, Jie Yang and Huiwen Wu for providing partial methods or performing NMRs in this project. All your generous help is foundational to complete the thesis in advance.

Furthermore, I would like to bring my sincere thanks to all of my friends in this country. I have to say that I really feel so lucky to know you guys and work with you guys. Thanks to Daragh for always picking me up at airport, helping me settling down in Maynooth and correcting this thesis. Your Charismas invitation really opened my eyes to learn the real culture in Ireland. Thanks to Elizabeth for countless helps when I just started my project in the lab and when I had English problems. Thanks to Stephen, Nicola and the others in the Biotechnology lab for bringing so much fun to my life in

Ireland. Thanks to Dr. Shuo Yang and Dr. Bingwei Wang for spending festival time with me and dispersing my homesick. I cannot imagine how boring and humdrum my life would be in the past three years without you all. No words for you guys but sincere thanks only.

Finally, I would like to sincerely acknowledge the understanding, supporting, blessing and encouragement from my parents in the other side of the earth. You did not give me the rich childhood and wonderful education resources, but you did give me all the best things you had. And one day, I will let you feel proud of me, and I am on that way. I would extend my heartiest thanks to my sister who take care our parents when I am abroad. No matter where I am, I always feel blessing and refuge from you all and that is family meant to be.

By Linan Xu
At Maynooth University
28.02.2016

PUBLICATIONS

Peer reviewed paper:

1. Chong, X., Lu, X., Wang, Y., Chang, A.K., **Xu, L.**, Wang, N., Sun, Y., Jones, G.W., Song, Y., Song, Y.B. and He, J., 2015. Distinct structural changes in wild-type and amyloidogenic chicken cystatin caused by disruption of C95-C115 disulfide bond. Journal of Biomolecular Structure and Dynamics, (just-accepted), pp.1-22.
2. Wang, N., He, J., Chang, A.K., Wang, Y., **Xu, L.,** Chong, X., Lu, X., Sun, Y., Xia, X., Li, H. and Zhang, B., 2015. (−)-Epigallocatechin-3-gallate Inhibits Fibrillogenesis of Chicken Cystatin. Journal of agricultural and food chemistry, 63(5), pp.1347-1351.
3. He, J., Wang, Y., Chang, A.K., **Xu, L.,** Wang, N., Chong, X., Li, H., Zhang, B., Jones, G.W. and Song, Y., 2014. Myricetin prevents fibrillogenesis of hen egg white lysozyme. Journal of agricultural and food chemistry, 62(39), pp.9442-9449.

Published abstract:

1. Deciphering the regulation of the substrate-binding domain of Hsp70. Best poster presentation, Biology Departmental Research Day, June 2016.
2. Deciphering the Role of Hsp70 in Prion Propagation. Cell Stress Society International Congress on Stress and Health, Huangshan, China, September 2015

ABBREVIATIONS

AAA+	*A*TPases *A*ssociated with diverse cellular *A*ctivities
Aβ	Amyloid β peptide
ACD	α-crystallin domain
AD	Alzheimer's disease
ADP	Adenosine triphosphate
AFM	Atomic force microscopy
APP	Amyloid precursor protein
APS	Ammonium persulfate
ATP	Adenosine triphosphate
Bip	Binding immunoglobulin protein
BSA	Bovine serum albumin
BSE	Bovine spongiform encephalopathy
CD	Circular dichroism
CNS	Central nervous system
CR	Congo red
CTE	C-terminal extension
CWI	cell well integrity
DD	C-terminal dimerization domain
DNA	Deoxyribonucleic acid
dNTP	Deoxynucleotide triphosphate
DTT	Dithiothreitol
EDTA	Ethylenediaminetetraacetic acid
ER	Endoplasmic reticulum

Gdn-HCl	Guanidine Hydrochloride
GSP	General stress proteins
HAT	Histone Acetyl Transferase
HDAC	Histone Deacetylase
HO*	hydroxyl radical
HSE	Heat shock element
HSF	Heat shock factor
Hsp	Heat shock protein
HSR	Heat-shock response
hTERT	human telomerase reverse transcriptase
ICHEC	Ireland's High-Performance Computing Centre
kDa	Kilo Dalton
LB	Luria Broth
LiAc	Lithium acetate
MCAC	Metal chelate affinity chromatography
MD	Molecular dynamics simulation
md	middle domain
MG132	Z-L-Leu-D-Leu-L-Leu-al
mm	millimetre
MW	molecular weight
MWCO	Molecular weight cut-off
NBD	Nucleotide-binding domain
NEF	Nucleotide exchange factors
NF-kB	nuclear factor-kB

nm	nanometre
NMR	Nuclear magnetic resonance
NTD	N-terminal domain
OD	Optical density
O_2^-	superoxide radical anion
OPR	Oligopeptide repeat region
PCR	Polymerase chain reaction
PEG	Polyethylene glycol
PMSF	Phenylmethanesulfonylfluoride
PrP	Prion protein
PrD	Prion forming domain
PTM	post-translational modification
PVDF	Polyvinylidene difluoride
QNR	Glutamine Asparagine rich
RAC	Ribosome-associated complex
RF	Release factors
RMSD	Root-Mean-Square Deviation
RMSF	Root-Mean-Square Fluctuations
RNA	Ribonucleic acid
ROS	reactive oxygen species
RPD	Reduced Potassium Dependency
rpm	Revolutions per minute
RT	Room temperature
SAXS	small-angle x-ray scattering

SBD	Substrate-binding domain
SBDα	α-helix subdomain of the SBD
SBDβ	β-sheets subdomain of the SBD
SC	Synthetic complete
SDM	Site directed mutagenesis
SDS	Sodium dodecyl sulphate
SDS-PAGE	Sodium Dodecyl Sulphate-Poly acrylamide gel electrophoresis
SGD	*Saccharomyces* Genome Database
SMD	Steered molecular dynamics simulation
Ssa	Stress seventy subfamily A
Ssb	Stress seventy subfamily B
SSBP	Single-stranded binding protein
SUMO	Small ubiquitin-like modifier
TBS	Tris buffered saline
TCA	Trichloroacetic acid
TEM	Transmission electron microscopy
TEMED	Tetramethylethylenediamine
ThT	thioflavin T
TSE	Transmissible spongiform encephalopathies
UPS	Ubiquitin-proteasome system
UV	Ultraviolet
v/v	Volume per total volume
WAXS	the wide-angle x-ray scattering
WT	Wide type

w/v	Weight per total volume
w/w	Weight per total weight
YPD	Yeast Peptone Dextrose
2D	2-dimensional
3D	3-demensional
5-FOA	5-fluoro-orotic acid

LIST OF TABLES

LIST OF FIGURES

ABSTRACT

The Hsp70 (70kDa heat shock protein) is highly conserved in all species and has been implicated in a variety of important cellular functions such as heat shock response, prion propagation, protein folding and refolding, translocation across membranes and assembly of macromolecular complexes. A variety of evidence has accumulated to show that Hsp70 machinery is a key modulator of the stress response, such as heat shock and oxidant stress. Moreover, many human neurodegenerative diseases such as Alzheimer's, Parkinson's and the prion disease Creutzfeldt-Jacob Disease (CJD) are also intimately linked to Hsp70. Structurally, Hsp70 is comprised of two domains: nucleotide-binding domain (NBD) and substrate-binding domain (SBD). In this work, a well-established yeast system and a combination of computational biology, genetics, structural biology, biochemistry and molecular biology were utilized to decipher the role of the SBD of Hsp70 in regulation of heat shock response and [PSI^+] prion propagation.

It was found that mutations (F475S and L483W) located in a region termed β6-β7 dramatically decreased the stability of the SBD and the size of side chain contributes to maintain the hydrophobic core of SBD. Introduction of smaller amino acid side chains at residue 475, such as alanine and serine, resulted in temperature sensitivity and [PSI^+] impairment. When the side chain of residue 475 is larger than Cysteine, no matter if it is polar or nonpolar (tyrosine and phenylalanine), thermotolerance and [PSI^+] can be maintained. However, there is a limit to side-chain size as too large, such as tryptophan, Ssa1 will lose intrinsic function and fail to support cell viability. By contrast, residue 483 prefer to smaller size amino acid to remain the hydrophobic core of SBD. Therefore, mutations on those two residues easily disturb the integrity of SBD and thus promote the degradation of SBD *in vitro* and *in vivo*.

Inter-domain communication between the NBD and SBD is affected through disruption of the important hydrophobic core and disturbance of a critical interface between the two domains. Disruption of the SBD structure abolishes repression of ATP hydrolysis of the NBD, reduces protein refolding activity and alters interactions with co-chaperones, especially Hsp104 and Hsp26, but decreased the interactions with Sup35. Degradation of the SBD in *vivo* is dependent on the action of vacuolar carboxypeptidase (Pep4) rather than the proteasome and occurs in WT cells at high temperature. Finally,

SBD degradation is negatively regulated by the acetylation of four reversible hyperacetylated lysine residues, K86, K185, K354 and K562 of Ssa1. And, the thermotolerance regulation is independent from [PSI^{+}] prion and alteration of the genome-wide translation caused by the read-through. The reversible hyperacetylated residues did not influence the basal expression level of the Hsp70 machinery, but rapidly respond the heat-shock stress by deacetylating themselves to stabilize SBD of Hsp70.

Key Words: Hsp70, substrate-binding domain, inter-domain communication, SBD degradation, acetylation, prion, heat shock

CHAPTER ONE

INTRODUCTION

1.1 Heat shock proteins

Heat shock proteins (HSPs) are a group of proteins that are induced under stresses such as heat shock, heavy metal ions and pro-oxidants. HSPs are the most common molecular chaperones and can cope with denatured proteins which induce stresses as seen in the pioneering work of Ritossa (Ritossa 1962). The stress response based on HSPs has been reported to be the most highly conserved mechanism in all organisms from archaebacteria to animals (Lindquist & Craig 1988). Although the expression of HSPs was transiently elevated against other cellular stresses, HSPs actually have multifunctional roles under physiological conditions to maintain normal cellular functions such as cell cycle, cell proliferation, cell survival and cell death, gene expression, protein folding and signalling transduction (Rutherford & Lindquist 1998; Nollen & Morimoto 2002; Sreedhar & Csermely 2004; Ritossa 1962; Rüdiger et al. 1997).

HSPs can be assigned according to a typical molecular weight (MW) and sequence homology (Gething 1997). Briefly, there are six major families which are HSP100, HSP90, HSP70, HSP60, HSP40, and the small HSPs (Table 1.1).

Table 1.1 Heat-shock protein families

Approximate molecular weight (kDa)	Prokaryotic protein (eg.)	Eukaryotic proteins (eg.)		Function
		Yeast	Mammalian	
100	ClpA, ClpB, ClpC, ClpX, ClpY	Hsp104	Hsp100	Response to extreme temperature and disassemble aggregation
90	HtpG	Hsp82, Hsp90	Hsp90, Grp94, TRAP1	Assists protein folding, against heat stress, protein degradation
70	DnaK	Ssa1-4, Ssb1-2, Grp78	Hsp70, Hsc70	Protein folding and refolding, stress response, regulation of cell cycle, transmembrane transport of proteins
60	GroEL	Hsp60	Hsp60	Protein folding and

			(Group 1 mitochondrial chaperone)	conformation maintenance, mitochondrial protein transport and DNA metabolism.
40	DnaJ	Ydj1, Sis1	Hdj1, mDj3-11	Substrate delivery and ATPase stimulant of HSP70, related with aggregation and degradation.
10-30	GroES, GrpE	Hsp26, Hsp42	HSP10, HSP27, HSPB group	Increases thermotolerance, inhibition of apoptosis, regulation of cell development, and cell differentiation, signal transduction, Protein degradation.

Table adapted from (Schlesinger 1990; Lindquist & Craig 1988).

1.1.1 HSP100

Most eukaryotes express proteins which are more than 100 kDa to respond to extreme temperature such as Hsp104 and HSP110. HSP110 had been found in murine cells under both optimal and heat-shocked conditions (Subjeck et al. 1983). With longer heat shocks, HSP110 forms a ring-like structure surrounding the nucleolus (Welch & Suhan 2012). HSP110 is also expressed to protect ribosomes, because its deletion results in sensitivity to heat shock (Nover et al. 1986). However, HSP110 is not a member of HSP100 family, which was confused by some of research. HSP110 is actually a subfamily of HSP70 and serves as nucleotide exchange factor to load ATP onto the cytosolic HSP70s, such SSE (Stress Seventy subfamily E) (Mukai et al. 1993). HSP100 is Clp family and forms large hexameric structures with unfoldase activity in the presence of ATP (Pietrosiuk et al. 2011; Wang et al. 2010). Thus Clp proteins (in *E.coli*) and HSP104 (in *S.cerevisiae*) are classic HSP100 proteins.

HSP104 is a non-essential heat shock protein originally identified in *Saccharomyces cerevisiae* and is required for the acquisition of thermotolerance (Parsell et al. 1994). Based on sequence and functional similarities HSP104 is classified as a member of the

AAA+ (*A*TPases *A*ssociated with diverse cellular *A*ctivities) family of proteins (Sweeny & Shorter 2015). HSP104 functions as a hexameric complex (Sweeny & Shorter 2015). In conjunction with cytosolic HSP70 chaperone machinery it is responsible for the disaggregation of amorphous protein aggregates formed as a result of heat-shock or other cellular stresses (Glover et al. 1997). While HSP104 is highly conserved in fungi and bacteria, orthologues are absent from metazoa. Plants are the highest eukaryotes where an obvious HSP104 orthologue has been identified (Schirmer et al. 1994) and a clear role for this protein in heat tolerance and a variety of other cellular processes has been established (Tonsor et al. 2008; Hong & Vierling 2001; Queitsch 2000). Functional conservation of HSP104's role in thermotolerance is evident by the ability of both *Arabidopsis thaliana* and rice HSP101 proteins to complement the thermotolerance defect of a *S. cerevisiae* HSP104 deletion strain (Schirmer et al. 1994; Agarwal et al. 2003).

1.1.1.1 The structure of HSP104

There are 908 residues which form five domains in HSP104 (Desantis & Shorter 2012; Grimminger-Marquardt & Lashuel 2010). They are the N-terminal domain (NTD), two nucleotide-binding AAA+ domains (NBD1 and NBD2), a coiled-coil middle domain (md) inserted within the small domain of NBD1, and a unique C-terminal extension (Figure 1.1). The precise and completed structure of HSP104 monomer is unknown, but several structures of separated domains have been reported.

Crystal structures of the NTDs for Clp group (ClpA, ClpB, ClpC and ClpV, bacterial HSP100 proteins) have shown that the NTDs are highly conserved globular domains (Li & Sha 2003; Pietrosiuk et al. 2011; Wang et al. 2010; Xia et al. 2004). In ClpB, the NTD binds substrate and linker between NTD and NBD1, this is necessary for translocation and disaggregation of substrate (Li & Sha 2003; Zhang et al. 2012; Mizuno et al. 2012).

The NBDs of HSP104 proteins are highly conserved and consist of two subdomains, the α/β subdomain and the α-helical subdomain (Iyer et al. 2004). NBDs feature ATP binding and hydrolysis in AAA+ protein. Furthermore, NBD1 and NBD2 in HSP104 are originated from different AAA+ superfamilies but are not simple duplicates

(Erzberger & Berger 2006). NBD1 and NBD2 belong to clade 3 (members include the FtsH family, p97, NSF, and katanin) and clade 5 (members include HslU/ClpX family, RuvB, and Lon family) respectively (Erzberger & Berger 2006). All of them are able to bind and hydrolyze ATP, but with significant differences in terms of their catalytic properties (Hattendorf & Lindquist 2002). Briefly, NBD1 is low affinity, but has a high ATP turnover rate, but NBD2 is opposite (Hattendorf & Lindquist 2002). Interestingly, the basal ATPase activity of HSP104 is mainly contributed by NBD1 and communication between NBD1 and NBD2 (Hattendorf & Lindquist 2002).

There is a coiled-coil middle domain (md) inserted between NBD1 and NBD2 (Figure 1.1B). In previous reports, the md has been shown to repress the activity of the hexamer by interacting with NBD1 and NBD2 (Seyffer et al. 2012; Oguchi et al. 2012; Dulle et al. 2014). Meanwhile, md is essential for interaction between HSP104 and HSP70 (Seyffer et al. 2012). Thus, md plays a crucial role in regulating HSP104 activity. However, the mechanism of md regulation is not clear yet.

HSP104 has a CTD of 40 residues which contains 42.5% acidic amino acids and a highly conserved DDLD motif which is related with binding to HSP90 (Abbas-Terki et al. 2001). However, deficiency of the DDLD motif does not influence thermotolerance, thus the role of the motif is not clear (Abbas-Terki et al. 2001). Generally, CTD was shown to be necessary for hexamerization of HSP104 (Abbas-Terki et al. 2001).

As an AAA+ proteins HSP104 only has normal function in a ring-liked hexamer state (Sweeny & Shorter 2015). Previously research has shown that hexamers can be formed in the presence of either ADP or ATP (Schirmer et al. 2001; Schirmer et al. 1998) or without any nucleotides with low salt concentrations (Hattendorf & Lindquist 2002). ADP or ATP binding to NBD2 is crucial for hexamerization of HSP104, whereas ADP or ATP binding to NBD1 is dispensable for hexamerization (Schirmer et al. 2001; Schirmer et al. 1998).

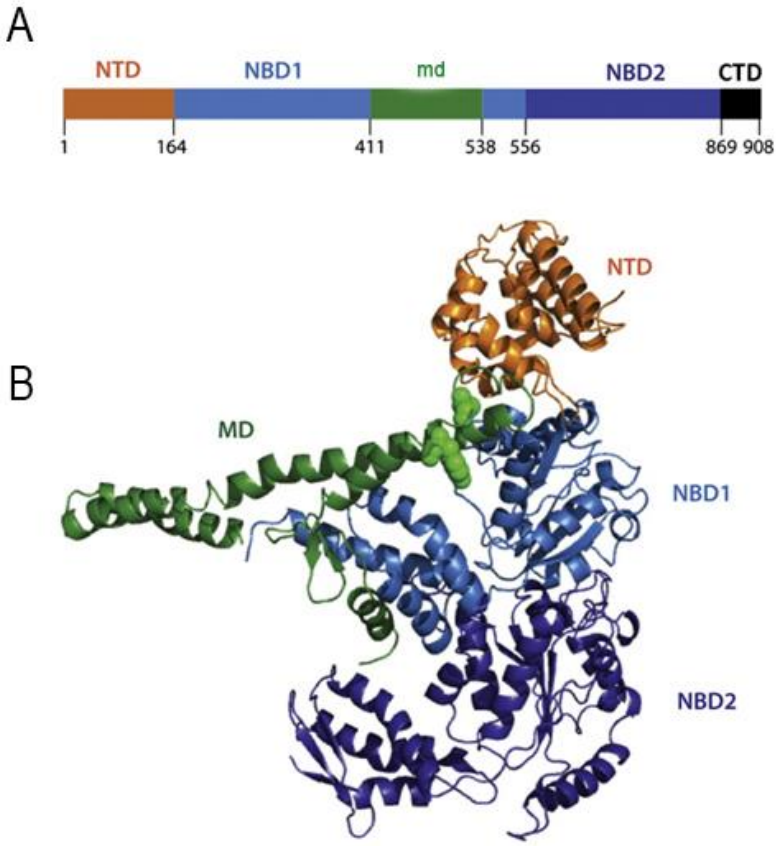

Figure 1.1. Domains organization of HSP104. (A) and predicted monomeric structure (B) Predicted structure of HSP104 based on PDB ID: 1khy and PDB ID: 1qvr. NTD shown in orange; NBD1 and NBD2 shown in light blue and dark blue respectively; md is green; and CTD shown in black. Adapted from Ref.(Sweeny & Shorter 2015).

1.1.1.2 Conformational changes of HSP104 during ATP hydrolysis

As mentioned above, ATP hydrolysis of HSP104 is a dynamic process with complicated conformational changes. The small-angle X-ray scattering (SAXS) and the wide-angle X-ray scattering (WAXS) have been used to investigate the conformational changes of several AAA+ proteins (Arias-Palomo et al. 2013; Sysoeva et al. 2013; Davies et al. 2005; Chen et al. 2010). Shorter's group reconstructed HSP104 and HSP104$^{\Delta N}$ hexamers via rudimentary domain fitting (Figure 1.2) (Sweeny et al. 2015). Moreover, large structural differences between HSP104 and HSP104$^{\Delta N}$ hexamers were displayed under different nucleotide conditions (Sweeny et al. 2015). HSP104 and HSP104$^{\Delta N}$ hexamers contract upon ATP hydrolysis and expand upon ATP binding, suggesting a pumping mechanism to drive substrate translocation (Sweeny et al. 2015). SAXS of HSP104$^{\Delta N}$ suggested that loss of the NTD results in expansion of the ends of the central

channel. It appears this is due to conformational changes of the central channel during ATP hydrolysis (Sweeny et al. 2015). Unfortunately, only a few mutations have been reported in limited nucleotide states. It is still difficult to extend and prove these finding in wild-type HSP104 directly (Sweeny & Shorter 2015).

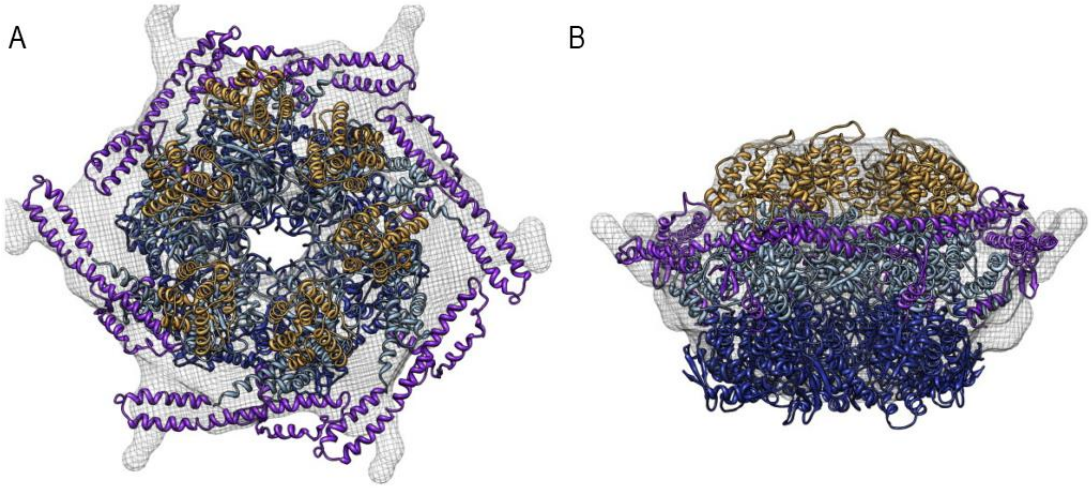

Figure 1.2. Reconstructions of the HSP104 hexamer with ATP based on SAXS. Individual HSP104 domains were homology modelled based on the ClpB crystal structure PDB ID: 1khy (NTD) and PDB ID: 1qvr (for NBD1, middle domain, and NBD2). (A) Top view. (B) Side view. NTD is shown in orange, NBD1 in light blue, middle domain in purple, and NBD2 in dark blue. Adapted from Ref. (Sweeny & Shorter 2015).

1.1.2 HSP90

HSP90 family is ATP-dependent, highly conserved and an essential molecular chaperone for eukaryotic cells (Johnson 2012). HSP90 isoforms are distributed in the cytosol and nucleus (HSP90a and HSP90b), ER (Grp94), mitochondria (TRAP1) and plastids (HSP90C) (Stankiewicz & Mayer 2012; Mayer & Le Breton 2015; Johnson 2012). Although several HSP90s are induced by heat shock or other stresses in response to signalling circuits preventing the aggregation of misfolded proteins, it cannot refold misfolded proteins like HSP60 and HSP70 (Mayer & Le Breton 2015). HSP90 is highly interactive binding receptors, transcription factors, kinases, and other unrelated proteins which are involved in signalling circuits, cell growth, cell death, proliferation and tumor progression (Echeverría et al. 2011).

1.1.2.1 Structure of HSP90

HSP90 consists of three domains, N-terminal nucleotide-binding domain (ND), a middle domain (md) and a C-terminal dimerization domain (DD) in monomeric HSP90 (Figure 1.3A). ND and md are related with ATPase activity of HSP90 and all three domains interact with different clients. The structure of ND is similar with other members of the ATPase/kinase superfamily such as DNA Gyrase B and histidine kinases; ND also binds with inhibitors such as geldanamycin and radicicol (Stebbins et al. 1997; Dutta & Inouye 2000). The md plays a central role and is highly interactive with binding parters such as HSP70 and HSF1 (Stankiewicz & Mayer 2012). DD is essential for dimerization of HSP90. The HSP90 dimer displays flexible and free conformation in Figure 1.3B. NDs appear to open or close around the DD in the apo form, ATP and ADP states. The closed NDs promote ATP hydrolysis. Furthermore, the catalytic loops of the md initiates ATP hydrolysis as well as contacting the nucleotide-binding cleft (Stankiewicz & Mayer 2012; Vaughan et al. 2009). In *E. coli*, the HtpG dimer was formed by conformational changes induced by ATP binding. ADP did not afford protection like ATP suggesting that the conformational changes of HtpG prefer ATP binding (Graf et al. 2009; Stankiewicz & Mayer 2012). Moreover, the previous report showed that charged linker (CL) between ND and md is unrelated with ATP hydrolysis but necessary for client binding (Hainzl et al. 2009). However, the detailed function of the CL is not clear yet.

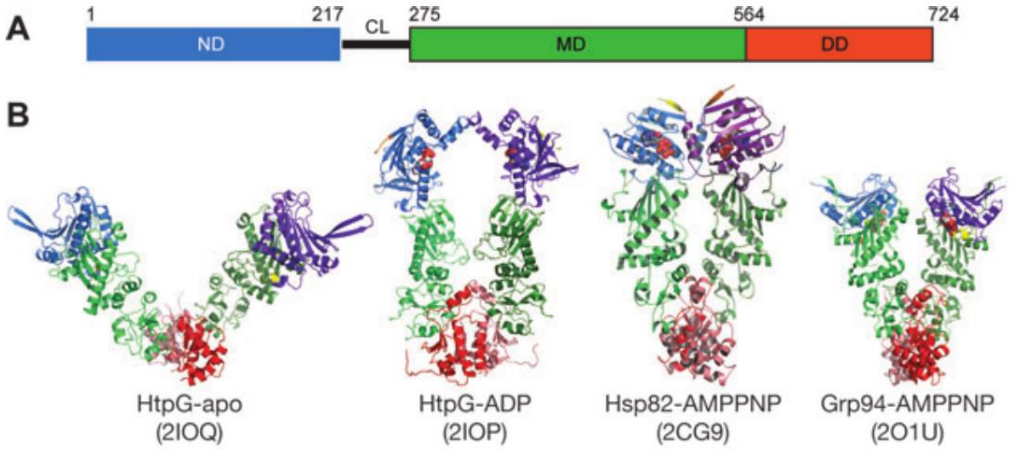

Figure 1.3. The structures of HSP90. (A) Domain organization of HSP90. (B) the dimeric structures of HSP90 at different states. ND is shown in blue. Middle domain (md) is shown in green and DD is shown in red. The changed linker (CL) is shown in black. Adapted from Ref. (Stankiewicz & Mayer 2012).

1.1.2.2 Symmetry and asymmetry of HSP90

As shown in Figure 1.3B, HSP90 dimers were symmetric in the apo form, ADP and AMPPNP bound states. However, the recently discovered structure of the mitochondrial HSP90 TRAP1 in its ATP state exhibit an asymmetric and closed dimer (Lavery et al. 2014). The structure of chain B is similar with the closed conformation of yeast HSP90, while the chain A deviates from symmetry conformation (Figure 1.4) (Mayer & Le Breton 2015). *E.coli* HSP90 also displays asymmetry using SAXS. In TRAP1 the asymmetry is related with ATP hydrolysis and dimerization (Lavery et al. 2014). Therefore, symmetry and asymmetry conformations both exist, but it is not clear whether asymmetry is a basic feature for all of the HSP90s.

Moreover, symmetry and asymmetry also happens within HSP90-chaperones complexes. In a previous report, HSP90-chaperones complexes were considered to exist symmetrically (Prodromou et al. 1999). However, many co-chaperones interact with HSP90 in a 1:2. For instance, Hop/Sti1 interacts with HSP90 in 2:2 and 1:2 stoichiometry (Ebong et al. 2011), which implied that Hop/Sti-HSP90 complex is not only symmetric but asymmetric as well. Mayer suggested that the asymmetric complexes are the foundation of an ordered succession of chaperones and a unidirectional conformational cycle of HSP90 (Mayer & Le Breton 2015). It is not clear whether the asymmetric HSP90 complexes can be extended to the whole HSP90 family with their clients.

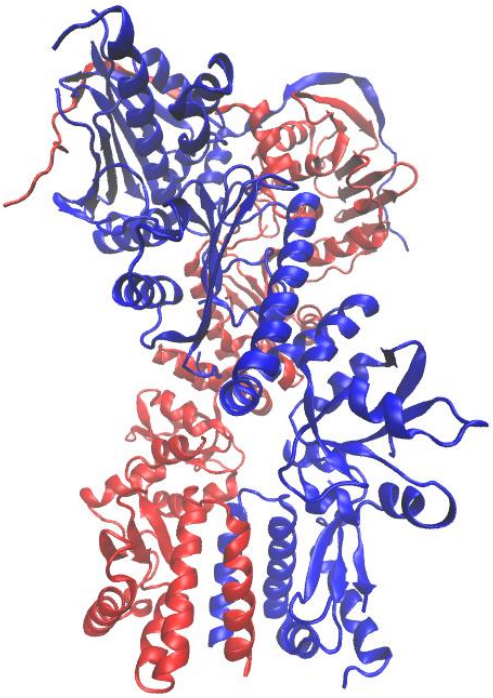

Figure 1.4. Asymmetric structure of HSP90 TRAP1. TRAP1 (PDB code: 4IPE) is in ribbon schematic representation and two chains of TRAP1 were shown in different colours (chain A is blue and chain B is red).

1.1.2.3 HSP90 and disease

HSP90 is overexpressed in cancer cells and a lot of oncogenic proteins are clients of HSP90 (Mahalingam et al. 2009). HSP90 increases cell survival by activating NF-kB (nuclear factor-kB) as a negative regulator of apoptosis (Mahalingam et al. 2009). Therefore, HSP90 has been targeted for cancer therapy. For example, it has been found that HSP90 inhibitors could enhance the efficiency of DNA-damage-inducing agents in the eradication of tumours with *p53* mutation (Whitesell et al. 1998). HSP90 inhibition also perturbs telomerase assembly and hTERT (human telomerase reverse transcriptase) enzymatic activity to reduce the proliferative capacity of tumours (Xu & Neckers 2007). Moreover, HSP90 with other heat shock proteins (eg. HSP70, HSP40 and HSP27) is also related with neurodegenerative diseases. More details about molecular chaperones and neurodegenerative diseases will be discussed in Section 1.3.4.

1.1.3 HSP70

HSP70 is a key molecular chaperone in all species and have been found in the cytoplasm, mitochondria, endoplasmic reticulum and chloroplast (Karlin & Brocchieri 1998). Three HSP70 proteins have been found in *E.coli* which are DnaK, HscA and HscC (Zhu et al. 1996). *Saccharomyces cerevisiae* has 14 HSP70 with 9 located in the cytosol, 2 of them are present in the ER (Kar2 and Lhs1) and 3 are in the mitochondrion (Ssc1, Ecm10 and Ssq1) (Kominek et al, 2013). In human cells 13 HSP70 homologue have been found, with the exception of Bip (binding immunoglobulin protein) and mtHSP70 the others are all present in the cytosol or nucleus (Boswell-Casteel et al. 2014).

Cytosolic HSP70 can be categorized into two groups. One is heat shock cognate (Hsc) 70, which is expressed constitutively and involved in most cellular activities such as translocation and protein folding. The other group is inducible HSP70 which charges for biotic or abiotic stress responses by refolding denatured proteins (Kominek et al, 2013). There are four subfamilies of cytosolic HSP70 in *Saccharomyces cerevisiae* which then contain the Ssa, Ssb, Sse, and Ssz subfamilies. The Ssa subfamily has four members Ssa1-4 and play crucial roles in protein folding, translocation and refolding denatured protein so that at least one of them is necessary for viability (Werner-Washburne et al. 1987; Albanèse et al. 2006). Ssb members Ssb1-2 appear to influence membrane proteins response to salt (Peisker et al. 2010). Sse1 and Sse2 proteins are ATPase components of the HSP90 chaperone complex which play a role in prion propagation and unfolded protein. Ssz1 can form a heterodimeric ribosome-associated complex with HSP40 Zuotin to stimulate the ATPase activity of Ssb (Fiaux et al. 2010). ER HSP70, Bips is involved in the ER pathway to respond to ER stress resulting in an accumulation of unfolded or misfolded proteins (Kleizen & Braakman 2004). Mitochondrial HSP70 Ssc1 is part of the Translocase of the Inner Mitochondrial membrane (TIM23 complex) which is involved in protein translocation (Neupert & Herrmann 2007).

1.1.3.1 Evolution of HSP70

Figure 1.5 shows the identification of several ancient and advanced groups of HSP70s. Notably, there are four distinct groups, cytoplasmic, ER, mitochondrial and plastid, for eukaryotic HSP70s based on there localization of proteins in *vivo*. Cytoplasmic and ER HSP70s of Eukaryotes share approximately 50% identity with those of prokaryotes and organelles of prokaryotic origin. Members in the same subfamily are more similar to each other, especially cytoplasmic subfamilies such as Ssa subfamily (Ssa1-4). Otherwise, even if some of the residues had been changed, many of them are still conservative in nature. Phylogenetic analysis of the C-terminal domain suggests that Ssb1 results from a gene duplication event prior to that which gave rise to the HSP70s of the ER (Boorstein et al. 1994).

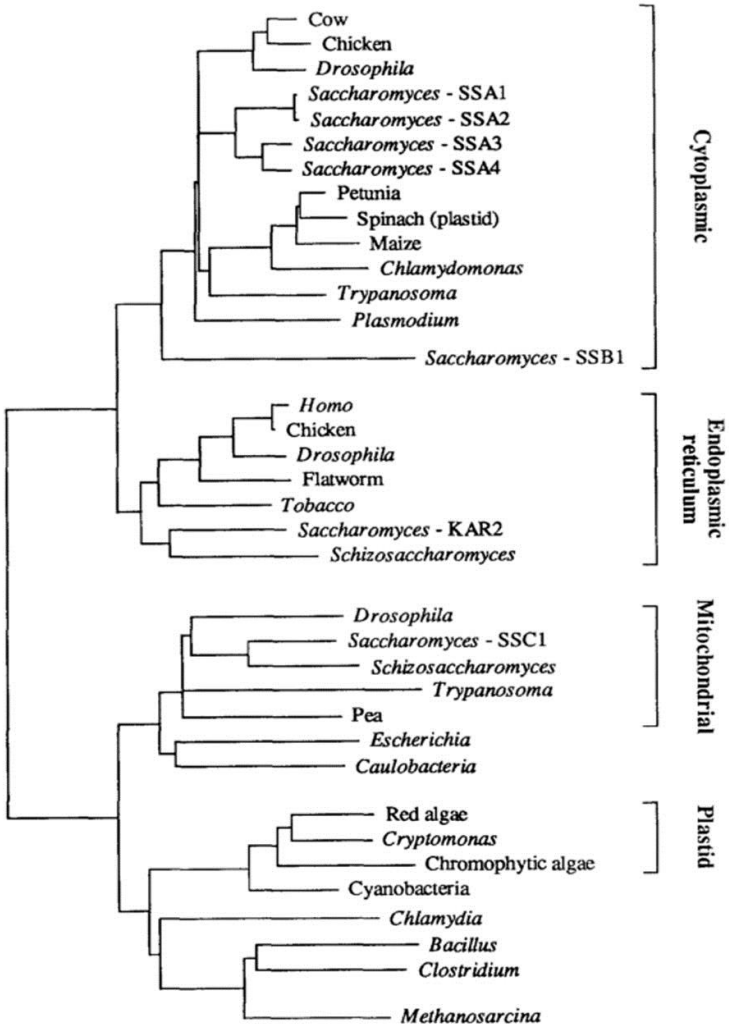

Figure 1.5. Phylogenetic tree of HSP70 based on 25 different species. Adapted from Ref. (Boorstein et al. 1994).

The 11 yeast HSP70 fall into 4 groups based on the phylogenetic tree in Figure 1.6. The Ssa subfamily shares identity from 84% to 99%. The other two cytoplasmic Ssb subfamily members are 99% identical. Ssc subfamily members (Ssc1, Ssq1 and ECM10) are highly conserved mitochondrial HSP70. The other two Kar2 and Lhs1 are ER HSP70 among them, Kar2 is close to the cytoplasmic HSP70 from an evolutionary perspective. Lhs1 is the most distantly related to other yeast HSP70s. Obviously, cytoplasmic HSP70s (Ssa and Ssb subfamilies) are the most conserved compared to ER and mitochondrial subfamilies. One of the reasons for this is that multiple members are related with diverse functions, require higher protein levels, or respond to stresses rapidly in the cytoplasm (Boorstein et al. 1994).

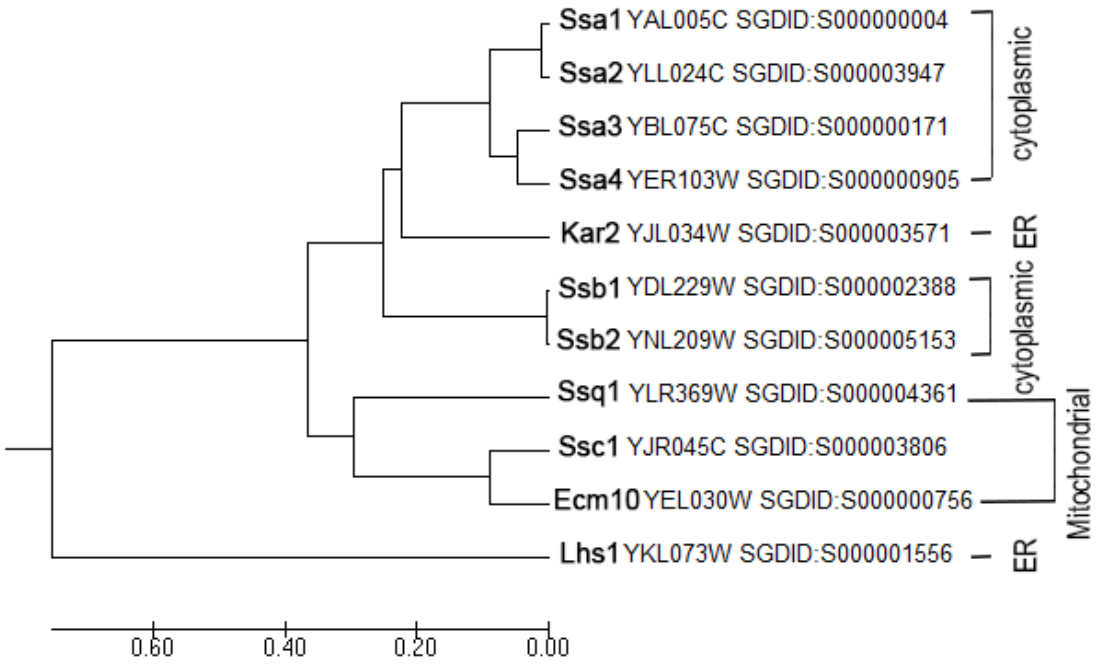

Figure 1.6. Phylogenetic tree of the HSP70 in yeast. The evolutionary history was computed using the UPGMA statistical method using the MEGA7 programme (Kumar et al. 2016). The optimal tree with the sum of branch length = 2.87833404 is shown. The evolutionary distances were computed using the Poisson correction method and are in the units of the number of amino acid substitutions per site. The analysis involved 11 HSP70 members. All positions contain gaps and missing data were eliminated. There were a total of 581 positions in the final dataset.

1.1.3.2 The structure of HSP70

The structure of HSP70s is highly conserved in all species. Briefly, HSP70 is comprised of two domains: N-terminal 45 kDa nucleotide binding domain (NBD), which is enriched in α-helix and confers ATP hydrolysis (Figure 1.7 A,B and C); C-terminal 25 kDa substrate-binding domain (SBD) (Figure 1.7 A,B and D), which consists of a β-sheet rich substrate-binding domain (SBDβ) with peptide-binding sites, a α-helical lid region (SBDα) over the substrate-binding cavity and a disordered tail of around 30 residues containing an highly conserved EEVD motif which docks with chaperones such as Hop, Sti1 and Chip (Figure 1.7 A, B and D) (Morshauser et al. 1985; Zhu et al. 1996; Mayer & Kityk 2015). The NBD has a similar structure with actin and sugar kinases and can be divided into lobe Ⅰ and lobe Ⅱ. Each lobe can be divided into two subdomains further (ⅠA, ⅠB, ⅡA, ⅡB, Figure 1.7C) (Flaherty et al. 1990). ATP hydrolysis happens in the deep site of the cleft formed by these four subdomains (Figure 1.7 C) (Flaherty et al. 1990). SBDβ is composed of eight β-sheets like sandwiches with two layers containing a substrate-binding cleft (Figure 1.7 D) (Zhu et al. 1996). Hydrophobic peptides dock into the cleft and directly interact with L12 and L34 (Figure 1.7D) (Zhu et al. 1996). SBDα consisting of five α-helixes regulates the substrate binding by a closed or opened conformation (Figure 1.7D) (Zahn et al. 2013).

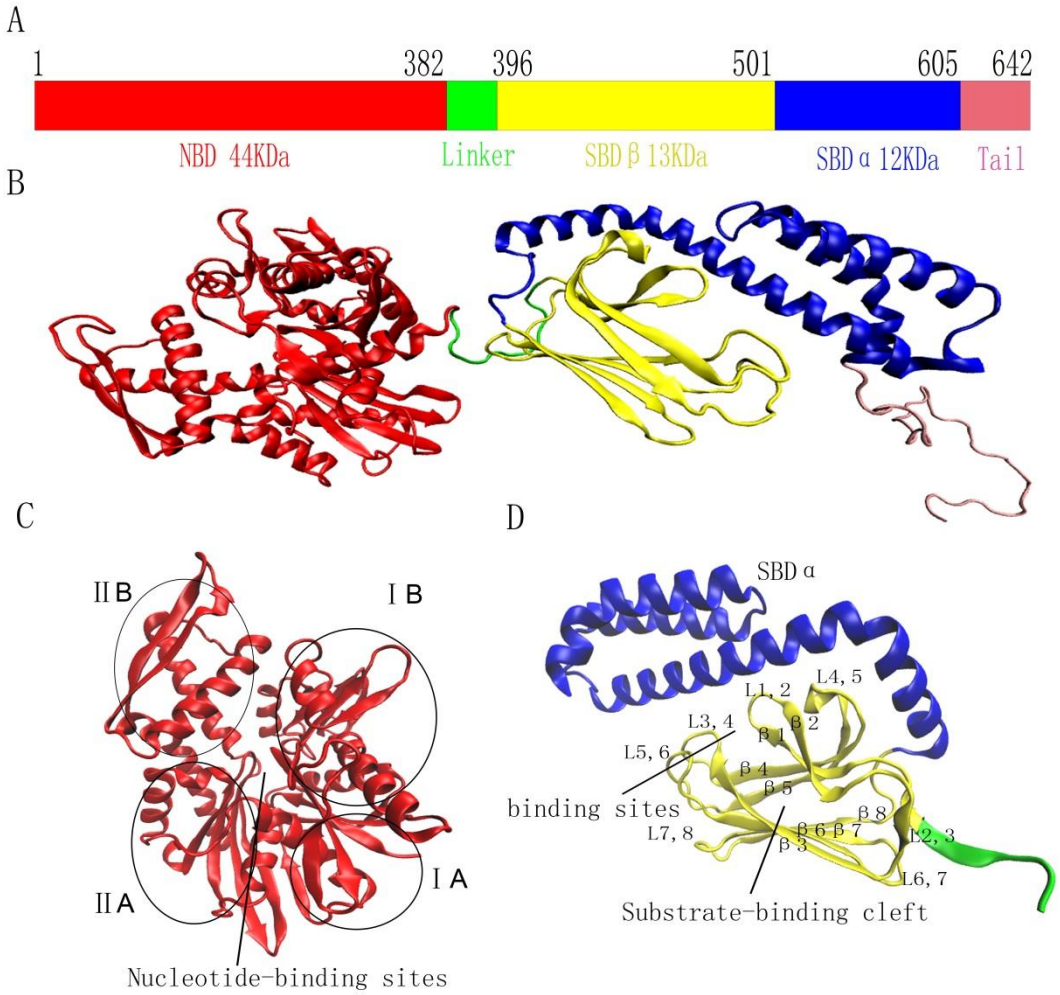

Figure 1.7. The structures of HSP70. (A) Domain organization of HSP70. NBD is shown in red. Linker is shown in green. SBDα and SBDβ are shown in yellow and blue respectively. Disordered tail is shown in pink. (B) The structure of HSP70 at ADP state. Full-length Ssa1 model was constructed by Modeller 9v8 (Fiser & Šali 2003) based on DnaK (PDB code: 2KHO) (Bertelsen et al. 2009). (C) The structure of the DnaK NBD at ATP state (PDB code: 4B9Q) (Kityk et al. 2012). (D) The structure of DnaK SBD at peptide-binding state (PDB code: 4EZW (Zahn et al. 2013).

1.1.3.3 Allostery of HSP70

There is a bidirectional allosteric intramolecular regulation between NBD and SBD (Figure 1.8). Briefly, ATP binding and hydrolysis of the NBD regulates the substrate capture of the SBD. Substrate binding of the SBD then increases ATP hydrolysis (Mayer & Kityk 2015). Compared with the DnaK-ADP state the DnaK-ATP state is more compact. In the ATP state, the lid detaches from the substrate-binding pocket

completely and docks onto one side of the NBD; the linker is then buried into the cleft of the NBD to steer the SBD docking onto another side of the NBD (Kityk et al. 2012; Bertelsen et al. 2009). Several residues which are part of the NBD and SBD interface have been reported such as Arg151, Arg167, Asp326, Asp393, Lys414, Asp481 (residue numbers in DnaK) (Kityk et al. 2012; Kityk et al. 2015). Therefore, the stability of the interface plays a critical role in allosteric regulation and intramolecular communication in HSP70. In particular, Asp481 and Lys414 which connect the NBD subdomain IA and IIA respectively as a clamp to fix the NBD and SBD interaction in the ATP state strongly decrease intrinsic ATPase activity without stimulation from substrate and HSP40 (Kityk et al. 2015).

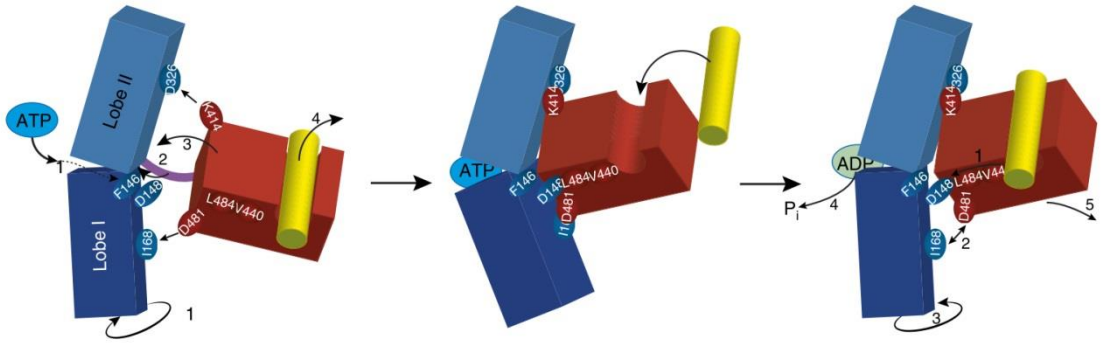

Figure 1.8. Model of allosteric regulation of HSP70. Adapted from Ref. (Kityk et al. 2015). After ATP binding, lobe I of the NBD is rotated (1). The linker then buries into the cleft of the NBD (2); this corrects the positions of Ile16 and Asp326 to face and interacts with the SBD (3). The interactions between NBD and SBD through Asp481 and Lys414 result in the open conformation of SBD which allows the substrate to bind. The incoming substrate pushes through the lever (Vala440, Leu484), triggers NBD conformational changes by Asp148 (2), and releases the SBD from the NBD (5) allowing lobe I back rotation (3) and ATP hydrolysis (4) with concomitant trapping of the substrate.

1.1.3.4 Post-translational modifications of HSP70

Protein post-translational modifications (PTM) are widely used to mediate cellular processes and stress responses. For years, proteome mapping of PTMs has provided dramatic information for analysing the functional relevance, deviation and developing a disease pathogenesis strategy. For example, yeast Rsp5 (Nedd4 homolog in mammalian cell) targets cytosolic misfolded proteins and increases ubiquitination levels upon heat shock (Fang et al. 2014). Hul5 is another ubiquitin ligase which ubiquitylates cytosolic

proteins under heat shock, but Rsp5 and Hul5 target heat-induced substrates independently (Fang et al. 2014). Acetylation of proteins is important in the regulation of chromatin organization, mitochondrial metabolism, protein synthesis and the other cellular processes (Henriksen et al. 2012). Sumoylation regulates many proteins which are included in cancer, Huntington's, Alzheimer's and Parkinson's diseases (Sarge & Park-Sarge 2009). As a highly complex HSP70, Ssa1 has been reported with multiple PTM sites (Table 1.2).

In a previous phosphoproteome of the yeast *Saccharomyces cerevisiae* report, serine phosphorylation was found to be most common (around 83%); threonine phosphorylation accounted for the rest. The phosphorylation of HSP70 promotes dimerization of itself (Morgner et al. 2015). Table 1.2 shows the multiple phosphoprotein sites of Ssa1. Among them, highly conserved T36 phosphorylation in Ssa1 creates displacement of Ydj1, allowing binding between Ssa1 and the G1 cyclin Cln3 thus promoting its degradation (Truman et al. 2012).

Lysine acetylation is a reversible PTM and widely used to regulate a series of cellular processes *in vivo*. Lysine acetylation on its ε-amino group is catalysed by HATs (also known as KATs, Histone Acetyl Transferase) and can be reversed by HDACs (Histone Deacetylase) (Yang & Seto 2007). Lysine acetylation is an evolutionary conserved PTM from bacteria to mammalian cells, suggesting that its regulatory roles may be conserved during evolution (Yang & Seto 2007). Recently research has shown that multiple acetylation sites of HSP70 contributes to dimer stability of HSP70 (Morgner et al. 2015). However, it is not clear which kinds of cellular functions are affected by acetylation of HSP70.

Table 1.2. Post-translational modifications of Ssa1

Site	Modification	Reference
T35	phosphorylation	(Albuquerque et al. 2008)
T36	phosphorylation	(Albuquerque et al. 2008)
T43	phosphorylation	(Albuquerque et al. 2008)

K54	ubiquitination	(Swaney et al. 2013)
K54	acetylation	(Henriksen et al. 2012)
K54	succinylation	(Weinert et al. 2013)
S62	phosphorylation	(Albuquerque et al. 2008)
S62	phosphorylation	(Swaney et al. 2013)
K69	acetylation	(Henriksen et al. 2012)
K69	succinylation	(Weinert et al. 2013)
K86	acetylation	(Henriksen et al. 2012)
K86	succinylation	(Weinert et al. 2013)
K98	ubiquitination	(Swaney et al. 2013)
K110	ubiquitination	(Swaney et al. 2013)
K126	ubiquitination	(Swaney et al. 2013)
S131	phosphorylation	(Albuquerque et al. 2008)
S131	phosphorylation	(Swaney et al. 2013)
K136	ubiquitination	(Swaney et al. 2013)
S151	phosphorylation	(Albuquerque et al. 2008)
S151	phosphorylation	(Swaney et al. 2013)
T156	phosphorylation	(Swaney et al. 2013)
K157	ubiquitination	(Swaney et al. 2013)
T219	phosphorylation	(Swaney et al. 2013)
T223	phosphorylation	(Swaney et al. 2013)
K243	ubiquitination	(Swaney et al. 2013)
K316	ubiquitination	(Swaney et al. 2013)
K354	ubiquitination	(Swaney et al. 2013)

T378	phosphorylation	(Albuquerque et al. 2008)
S415	phosphorylation	(Swaney et al. 2013)
K420	ubiquitination	(Swaney et al. 2013)
K448	ubiquitination	(Swaney et al. 2013)
K455	ubiquitination	(Swaney et al. 2013)
S459	phosphorylation	(Albuquerque et al. 2008)
S486	phosphorylation	(Albuquerque et al. 2008)
T492	phosphorylation	(Albuquerque et al. 2008)
S495	phosphorylation	(Albuquerque et al. 2008)
K497	ubiquitination	(Swaney et al. 2013)
K504	ubiquitination	(Swaney et al. 2013)
K509	ubiquitination	(Swaney et al. 2013)
K521	ubiquitination	(Swaney et al. 2013)
K521	ubiquitination	(Kolawa et al. 2013)
K521	ubiquitination	(Peng et al. 2003)
K523	ubiquitination	(Kolawa et al. 2013)
S535	phosphorylation	(Swaney et al. 2013)
K536	ubiquitination	(Swaney et al. 2013)
K536	ubiquitination	(Peng et al. 2003)
S541	phosphorylation	(Albuquerque et al. 2008)
S545	phosphorylation	(Albuquerque et al. 2008)
S551	phosphorylation	(Albuquerque et al. 2008)
K556	ubiquitination	(Swaney et al. 2013)
K556	acetylation	(Henriksen et al. 2012)

K556	ubiquitination	(Fang et al. 2014)
K556	succinylation	(Weinert et al. 2013)
K562	acetylation	(Henriksen et al. 2012)
K562	succinylation	(Weinert et al. 2013)
S603	phosphorylation	(Albuquerque et al. 2008)

Table adapted from SGD: http://www.yeastgenome.org/locus/S000000004/protein

1.1.3.5 The versatility of HSP70

HSP70 is probably the most versatile of all of the chaperones involved in the protein folding network (Mayer & Kityk 2015). There are four possible reasons for this. First of all, HSP70 has a lot of homologues in cells. Although they have complementary or variant functions *in vivo*, they are involved in much more cellular processes. Secondly, HSP70 has the degenerate recognition motif, which consists of a core of five hydrophobic amino acids flanked by positively charged residues which are favourable for binding (Mayer & Kityk 2015). Thirdly, HSP70 interacts with wide chaperones forming a complex network (Figure 1.9), especially with HSP40. There are 22 HSP40s in *S. cerevisiae* and even more (47) in human cells (Kampinga & Craig 2010; Mayer & Kityk 2015). Finally, the complete allosteric regulation of HSP70 is the most important reason for its versatility (Mayer & Kityk 2015).

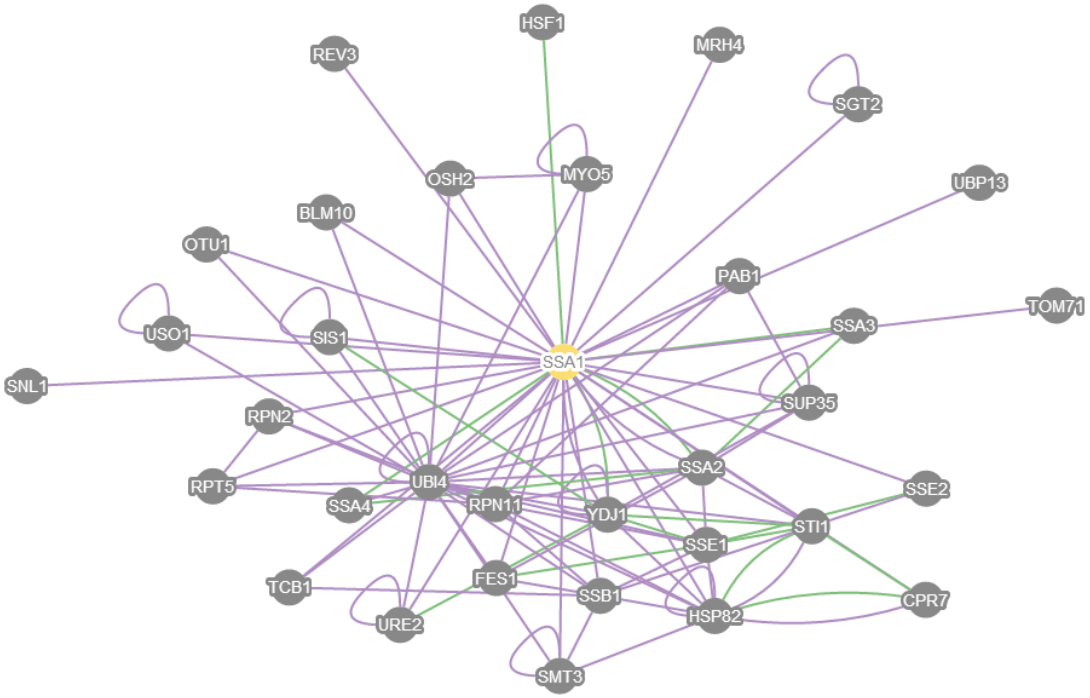

Figure1.9. Interactome of Ssa1. Ssa1 presents in yellow and binding partners are in gray. Physical interaction network was presented in purple; and genetic interactions are presented in green. Adapted from SGD: http://www.yeastgenome.org/locus/S000000004/interaction.

1.1.3.6 HSP70 as an environmental monitor

Beside versatile cellular functions, HSP70 is expressed/induced under environmental stress like pro-oxidants or heavy metal ions (Schröder et al. 2000; Barnes et al. 2002), therefore HSP70 is used widely in environmental toxicology as a biomarker in pollution research. For instance, in green algae and with earthworms, HSP70 had been utilized as a very sensitive biomarker to detect different pollutants (Bierkens et al. 1998; Nadeau et al. 2001). Juvenile rainbow trout exposed to water with heavy metal showed a significant increase in HSP70 levels in their gills (Williams et al. 1996). Researchers have also employed recombinant DNA technology to fuse HSP70 and reporter genes like lacZ or fluorescent protein. For instance, Guven's group constructed the HSP70-lacZ fusion gene in *Caenorhabditis elegans* to study soil ecotoxicology (Guven et al. 1995; Guven et al. 1994). Halloran cloned the green fluorescent protein gene under the promoter of inducible HSP70 in zebrafish (Halloran et al. 2000). Blechinger used the same zebrafish model to the calculate toxicity of cadmium (Blechinger et al. 2002).

1.1.4 HSP40

HSP40, the so called J protein are members of a family containing a J domain. HSP40 plays crucial roles in protein translation, folding, refolding, translocation and degradation progresses (Qiu et al. 2006). ATP hydrolysis of HSP70 is regulated by HSP40. Briefly, HSP40 brings substrates to the SBD of HSP70 and interacts with the NBD of HSP70 to stimulate ATP hydrolysis (Kampinga & Craig 2010). Previous reports have demonstrated that the HSP40 family is related with numerous human diseases, such as Huntington's disease and cancer (Huang et al. 2014; Borrell-Pagès et al. 2006). Ydj1 has been reported to efficiently cure [*URE3*] prion in yeast (Pettett & Jones. 2008). A study on lung cancer had shown that HSP40 was overexpressed in cancerous lung tissues and it can be used in tumor diagnosis (Oka et al. 2001).

1.1.4.1 Structure and classification of the HSP40

Almost all of the HSP40 members contain the J domain which is consisted of helixes and a loop region containing a highly conserved HPD motif (Histidine, Proline and Aspartic acid sequence) (Figure 1.10) (Qian et al. 1996). With exception of the J domain, HSP40 contains another two regions, a Gly/Phe-rich region and a cysteine repeat region (Figure 1.11). Therefore, the HSP40 family can be categorized into three subfamilies (Ⅰ, Ⅱ and Ⅲ, Figure 1.11) based on these regions (Cheetham & Caplan 1998). Type Ⅰ HSP40 contains all of the J domain, Gly/Phe-rich region and the cysteine repeats region, such as DnaJ in *E.coli*. Type Ⅱ lacks the cysteine repeats region but has the rest, such as Sis1 in yeast. Type Ⅲ is J domain only, such as DjlA. More details of the subfamily member for each type have been shown in Table 1.3. Beside those three conserved regions, some HSP40 members contain additional conserved regions at the C-terminal (Figure 1.11 black). Although it is not very clear what are the functions of these C-terminal regions, some researchers have found that they are essential for dimerization and for further chaperone activity (Shi et al. 2005).

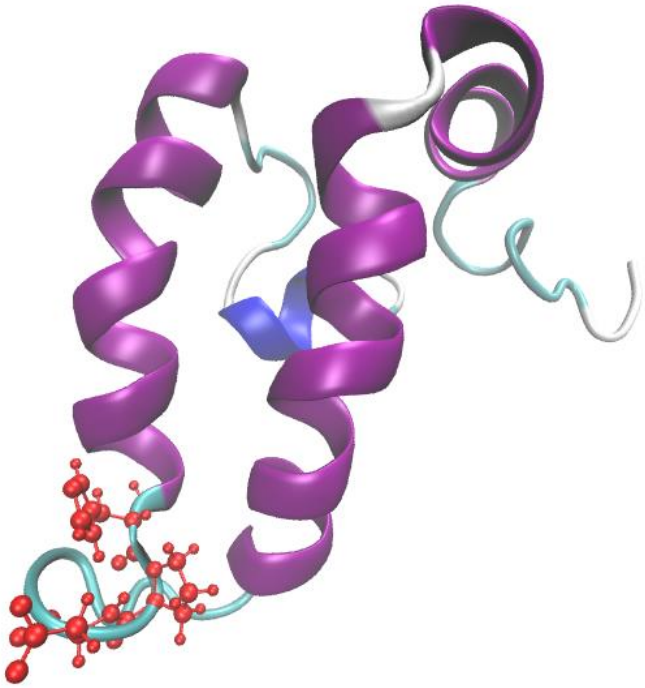

Figure 1.10. The structure of the human HSP40 HDJ-1. PDB code: 1HDJ (Qian et al. 1996). Helixes (purple), turns (silver) and main loop (cyan) are illustrated. The HPD motif is shown in red.

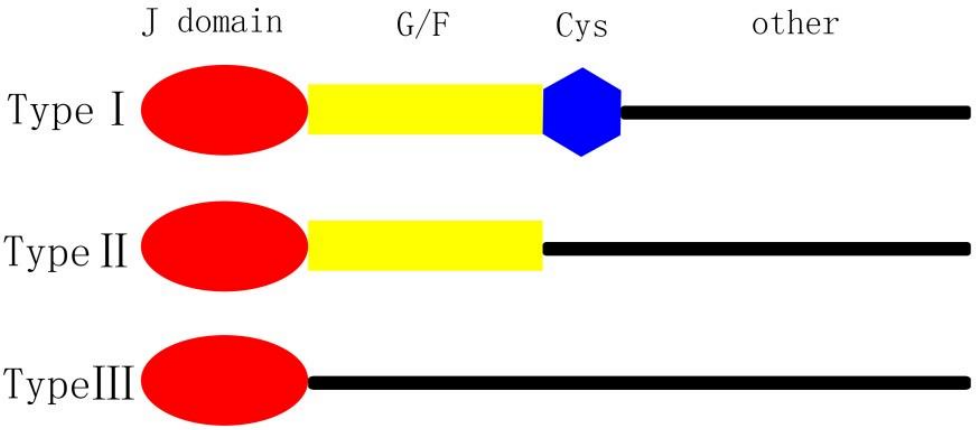

Figure 1.11. Classification of HSP40 family. HSP40 family can be categorized into three subfamilies (Ⅰ, Ⅱ and Ⅲ) based on the J domain (red), Gly/Phe-rich region (yellow) and the cysteine repeats region (blue) (Cheetham & Caplan 1998). The other regions are shown in black.

Table 1.3. HSP40 family members by type.

	Type Ⅰ	Type Ⅱ	Type Ⅲ
Eubacteria	DnaJ	Cbpa, NolC	DjiA
Archaea	DnaJ	-	-
Virus	-	-	T antigen
Yeast	Ydj1, Mdj1, Scj1, Xdj1	Sis1, Zuo1, Caj1, Hlj1, Djp1, Jjj3	Sec63, Jem1, Jjj1, Jjj2, Erj5
Plant	Anj1, Atj1	D3	-
Animals	Hdj2, Tid56	Hsj1a/b, Hdj1	p58IPK, Mtj1, auxilin, csp, MIDA1

Adapted from Ref. (Cheetham & Caplan 1998).

1.1.4.2 The distribution of cellular HSP40

HSP40 is spread across various subcellular locations and has been found in the cytosol, nucleus, endosomes, mitochondria, ER and ribosomes (Qiu et al. 2006). In multicellular organisms, it can be expressed either in all tissues or in a specific one. For instance, Hsj1 is preferentially expressed in brain tissue (Cheetham et al. 1992), but rat rDJL can be found in the liver and testis (Yang et al. 2005). The distribution of yeast HSP40s has been shown in Table 1.4 (Qiu et al. 2006). The wide distribution of cellular HSP40 is related to its versatility and even the versatility of its chaperone HSP70.

Table 1.4. Distribution of yeast HSP40s

	Nucleus	Cytoplasm	Mitochondria	ER	Ribosome
Type Ⅰ	-	Ydj1	Mdj1, Xdj1	Scj1	-
Type Ⅱ	Sis1, Caj1, Jjj3	Sis1, Djp1, Jjj3	-	Hlj1	Zou1
Type Ⅲ	Jjj1, Jjj2	Jjj2	Sec63	Sec63, Jem1, Erj5	-

1.1.4.3 Interaction between HSP40 and HSP70

Normally HSP70 has a very low ATP hydrolysis rate; however it can be stimulated by HSP40. Previous reports have shown that HSP40 actually binds with NBD and SBD both of the HSP70 (Freeman et al. 1995; Landry 2003). It has been well established that the HPD motif contributes to interactions between Ydj1 and the NBD of HSP70 (Tsai & Douglas 1996). There is no HSP40/HSP70 crystal complex directly; however a potential interaction model may become apparent with the increased understanding of the structures of HSP40 and HSP70. Figure 1.12 showed one of the models from Gruschus' group (Gruschus et al. 2004). Briefly, His874 of the HPD motif forms transient hydrogen bonds with Ala148, Try149 and Asn174 of the Hsc70 NBD, while there is a salt bridge between Asp876 of the HPD motif and Arg171 of the NBD. Furthermore, Asp876 is close to Arg155, which may form a transient salt bridge on specific occasions. Arg155 and Arg171 are both highly conserved in the HSP70 family (Gruschus et al. 2004). Considering the variety of the HSP40 and HSP70, it is not clear whether all of them have similar contacts from different species and homologs.

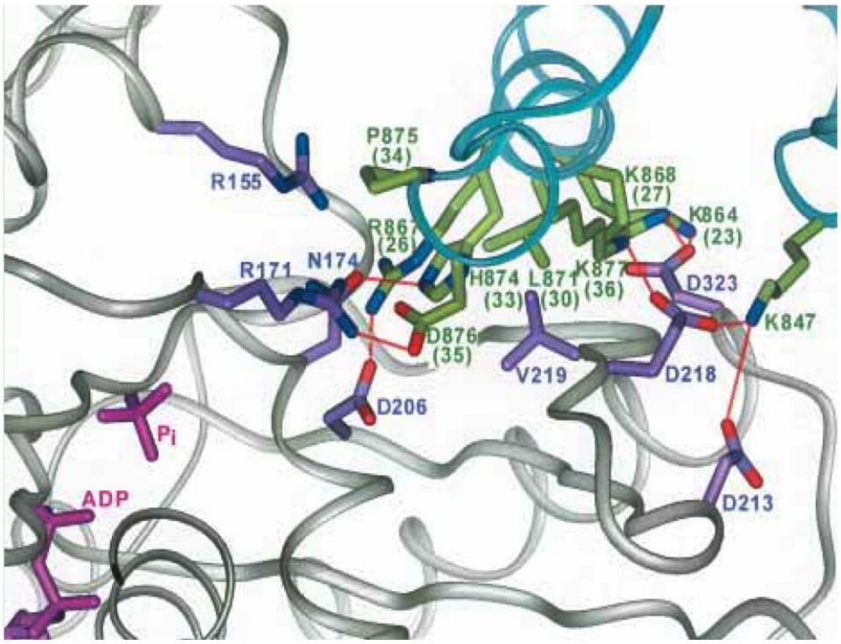

Figure 1.12. Potential interaction model for NBD/J domain complex. The auxilin J domain and NBD of the HSP70 are shown in cyan and grey respectively. The contacted residues are green for J domain and purple for NBD. Hydrogen bonds are shown as red lines. Adapted from Ref. (Gruschus et al. 2004).

1.1.4.4 Cellular functions of HSP40

HSP40 is the most important co-chaperone of HSP70. HSP40 has been reportedly involved in many cellular processes. (1) Protein folding, refolding and assembly. For example, DnaJ regulates the ATP hydrolysis of Bip to mediate protein folding and oligomerization in the ER (Hendershot et al. 1996). Scj1 helps Kar2 to fold and assemble proteins in the ER lumen (Schlenstedt et al. 1995); (2) Stress responses and translational regulation. The J-domain protein DnaJC3 in mammalian cells plays an important role in a negative feedback loop to inhibit eIF-2α signalling and to decrease the unfolded-protein response in the ER (Van Huizen et al. 2003); (3) Protein translation. Zuo1 together with Ssz1 and Ssb1/2 can regulate protein translation by forming the ribosome-associated complex (Huang et al. 2005; Gautschi et al. 2001); (4) Protein degradation, many HSP40s have been shown to be involved in proteasomal degradation, such as Hsj1 and Ydj1 (Chapple et al. 2004; Lee et al. 1996).

1.1.5 Small HSP

sHSP are highly conserved heat shock proteins with 12-43 kDa molecular weight in all species. In mammalian cells, there are ten sHSP named from HSPB1 to HSPB10 (Kappé et al. 2003). They are categorized into two types as shown in Table 1.4. The most common is type Ⅰ sHSP which are inducible and important to maintaining cell survival under stress. Type Ⅱ sHSP are normally more important in development, differentiation and specific tissue such as germ tissue (Table 1.5) (Bakthisaran et al. 2015). They are widely involved in stress responses, protein folding/refolding, degradation, cell cycle, cell death, differentiation, signal transduction, cytoskeletal-integrity maintaining and development (Ito et al. 2001; Bai et al. 2004; Haslbeck et al. 2005; Chowdary et al. 2004; Bakthisaran et al. 2015).

Table 1.5. Distribution of human sHSP

Name	WM (kDa)	PI	Distribution	Inducible	Type
HSPB1 (HSP27)	22.8	6.4	Ubiquitous, high levels in heart, striated and smooth muscles	+	Ⅰ
HSPB2 (MKBP)	20.2	4.8	Heart, skeletal and smooth muscle	-	Ⅱ
HSPB3	17.0	5.9	Heart, brain, skeletal and smooth muscle	-	Ⅱ
HSPB4 (αA-crystallin)	19.9	6.2	Abundant in eye lens. skeletal muscle, liver, spleen, adipose tissue	-	Ⅱ
HSPB5 (αB-crystallin)	20.2	7.4	Ubiquitous, abundant in eye lens. High levels in heart and muscle	+	Ⅰ
HSPB6 (HSP20)	16.8	6.4	Ubiquitous, abundant in muscle	-	Ⅰ
HSPB7 (cardiovascular HSP)	18.6	6.5	Heart and skeletal muscle. Adipose tissue (low level	-	Ⅱ
HSPB8 (HSP22)	21.6	4.7	Ubiquitous	+	Ⅰ
HSPB9	17.5	9.0	Testis	-	Ⅱ
HSPB10	28.3	8.4	Testis	-	Ⅱ

Table adapted from Ref. (Bakthisaran et al. 2015).

1.1.5.1 Structure of the sHSP

sHSP have a highly conserved α-crystallin domain (ACD) flanked by an N-terminal domain (NTD) and C-terminal extension (CTE) (Figure 1.13C). Although several ACDs have crystal structures, the structures of full-length sHSP have not been determined. Figure 1.13A shows the dimeric structure of HSPB5 ACD which has an anti-parallel and β-rich structure. With the development of EM, SAXS and NMR, several oligomeric models of HSPB5 (Figure 1.13B) and a pseudoatomic model of a 24-

mer HSPB5 assembly (Figure 1.13C) has been reported. This structural information may provide new understanding of interaction sites with the other proteins.

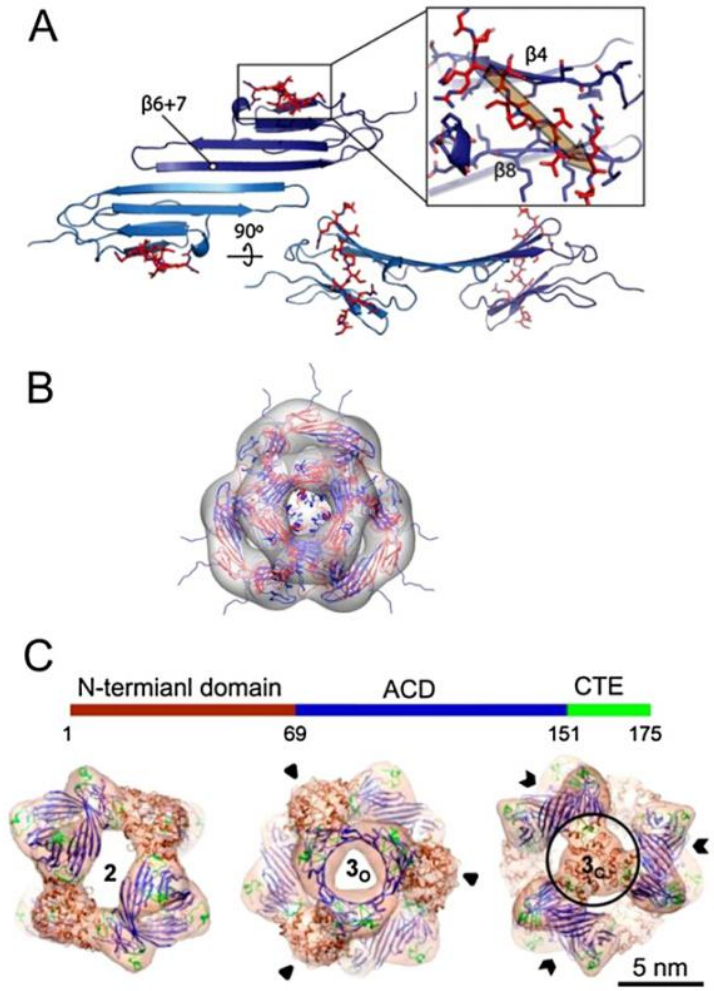

Figure 1.13. Structure of the sHSP. (A) Crystal structure of ACD dimer of HSPB5 (Hochberg et al. 2014). (B) Oligomeric (24-mer) model of HSPB5 (Jehle et al. 2011). (C) Pseudoatomic model of a 24-meri HSPB5 assembly (Braun et al. 2011). Adapted from Ref. (Bakthisaran et al. 2015).

1.1.5.2 sHSP and neurodegenerative disease

Neurodegenerative diseases such as Parkinson's and Alzheimer's disease are caused by amyloid fibres, a form of protein aggregate. sHSP have been reported to interact with unfolded or misfolded proteins and to prevent their aggregation (Wilhelmus et al. 2006; Ecroyd & Carver 2009; Duennwald et al. 2012). Human HSP27 (HSPB1) and the rat HSP25 have been reported to impair the Aβ1-42 amyloidogenesis *in vitro* (Kudva et al.

1997). Moreover, α-Crystallin inhibited the nucleation process by interacting with amyloidogenic precursors of apolipoprotein C-II (Hatters et al. 2001). In yeast, sHSP (HSP26 and HSP42) impair [*PSI*$^{+}$] prion propagation by inhibiting self-templating and preventing conformational rearrangements of molten oligomers respectively (Duennwald et al. 2012). Therefore sHSP could be used as the therapeutic targets for design of neurodegenerative drugs.

1.1.5.3 sHSP in protein degradation

There is a lot of evidence showing that sHSP are involved in the ubiquitin-proteasome degradation pathway (Bakthisaran et al. 2015). For examples, αB-crystallin plays a crucial role in cyclin D1 degradation (Lin et al. 2006). Promoting ubiquitin-dependent proteolysis of cyclin D1, this may be a way to suppress tumours since cyclin D1 is normally overexpressed in cancer cells (Barbash & Diehl 2008). Furthermore, HSP27 promotes the sumoylation which plays an important role in protein degradation in the nucleus and cytoplasm (Ahner et al. 2012). Overexpression of HSP27 promoted protein degradation through the proteasome pathway and accelerated degradation of the phosphorylated IkBα by the proteasome (Parcellier et al. 2003). HSP22 has been co-localized with the proteasome and its overexpression stimulates proteasome activity even more (Hedhli et al. 2008). All of these demonstrate that sHSP could mediate degradation of partially unfolded/misfolded, denatured and abnormal proteins.

1.2 Stress response

Cells are challenged by acute and chronic stresses like heat shock, oxidant stress, variations in pH and salt concentrations as well as other toxic chemicals (De Angelis & Gobbetti 2004). In stressed environments, proteins can undergo aggregation, unfolding or misfolding. Therefore, cells have to develop specific networks to detect, monitor and respond to those stresses from specific environments (Sreedhar et al. 2010; Merchant et al. 1998). For instance, previous researchers showed that the outer membrane protein (OMP) can sense these stress signals in *E.coli* which result in the activation and expression of stress genes (Hayden & Ades 2008). In this section, the main stresses and response mechanisms will be discussed.

1.2.1 Heat shock stress

Global warming has been high on the agenda as a global concern since it influences all organisms on the earth. The definition of heat shock is elevated temperature beyond a threshold level for physiological temperature and results in irreversible damage to an organisms growth (Wahid et al. 2007). From a cell molecular biology perspective, heat shock results in protein denaturation, as well as damage to membranes and nucleic acids (Teixeira et al. 1997). Under heat shock membrane integrity is disturbed by increasing the fluidity of membranes thus affecting the normal functions of proteins and can even lead to cell death (scchoffl 1999, wahid 2007, Kamada et al., 1995). Moreover, intracellular pH is decreased causing the distribution of the transmembrane protons by elevated temperature (Weitzel, Pilatus, & Rensing, 1987).

1.2.1.1 Heat-shock response

The heat-shock response (HSR) is a way to maintain proteostasis and protect cells from perturbation of denatured proteins (Vabulas et al. 2010). Pioneering work showed that heat shock not only causes upregulation of HSPs, but also increases the ubiquitylation of proteins that go through the proteasome degradation pathway in eukaryotic cells (Parag et al. 1987; Carlson et al. 1987). Proper function of the HSR is relevant to many human diseases such as cancer and neurodegenerative diseases (Morimoto 2008; Dai et al. 2007).

Yeast Rsp5 (Nedd4 homolog in mammalian cell) targets cytosolic misfolded proteins and increase ubiquitylation levels upon heat shock (Fang et al. 2014). Hul5 is another ubiquitin ligase which ubiquitylates cytosolic proteins under heat shock, but Rsp5 and Hul5 target heat-induced substrates independently (Fang et al. 2014). Ydj1 mediates the ubiquitylation of Rsp5 substrates and deletion of *YDJ1* impairs ubiquitylation and degradation upon heat shock (Fang et al. 2014). The Sis1, homolog of Ydj1, can cooperate with the HSP70 and Ubr1 E3 ligase to degrade misfolded cytosolic proteins (Summers et al. 2013).

1.2.1.2 Heat-shock Factor in HSR

HSF1 (heat-shock factor 1) can regulate the heat shock response in mammalian cells (Wu 1995). A model of how HSP works was proposed by Sorger and showed in Figure

1.14 (Sorger 1991). Briefly, HSF1 is low activity in the cytoplasm and nucleus under unstressed conditions. Normally HSF1 stays as a monomer by interaction with HSP90, HSP70, HSP40 and other negative regulators. Under heat shock the amount of denatured protein was elevated which bound with HSP and other chaperones this sets HSF1 free (Morimoto 1998; Shi et al. 1998; Zou et al. 1998). As a result, HSF1 accumulates and forms a DNA-binding trimer in the nucleus. Active HSF1 trimers bind with the heat shock elements (HSEs, 5'-nAGAAnnTTCTn-3') and the stress responsive elements (STREs) to activate the transcription of chaperone genes (Petesch & Lis, 2012; Wang et al., 2013; Marchler, Schüller, Adam, & Ruis, 1993; Sorger & Pelham, 1988). In *E.coli* GroEL and DnaK are significantly elevated from 37℃ to 43℃ (Gunasekera et al. 2008).

HSP/c70 has been detected in a small fraction of inactive HSF1 complex (Nunes & Calderwood 1995; Baler et al. 1996; Rabindran et al. 1994). HSF1 associated with HSP/c70 cannot be trimerized (Zou et al. 1998). However, recent reports have shown that HSP70 operated within the HSP90 chaperone system is capable of regulating a wide range of cellular clients, but HSP70 alone is not sufficient to suppress HSF1 in mammalian cells (Taipale et al. 2010). In Drosophila, human and *S.pombe* cells, HSF only bind to HSE after heat shock, but in *S.cerevisiae* binding happens both before and after heat shock (Sorger 1991). Furthermore, HSFs are highly phosphorylated after heat shock which promotes transcriptional activity (Figure 1.14).

Not only can cytoplasmic chaperones such as HSP110, HSP90, HSP70, HSP40 and small HSP be induced under heat shock but also mitochondrial chaperones such as HSP10 and HSP60 (Tan et al. 2015). Tan *et al.* found that heat shock induced the expression of SSBP1 (single-stranded binding protein 1) which is involved in mitochondrial DNA replication. SSBP1 can interact with HSF1 directly and the complex supported cell survival and other mitochondrial function under heat shock conditions (Tan et al. 2015). SSBP1 promotes the mRNA levels of HSP70 under heat shock by interaction with HSF1 directly (Tan et al. 2015). To some extent, HSF1-SSBP1 complex protects cells from heat shock and other proteotoxic stresses.

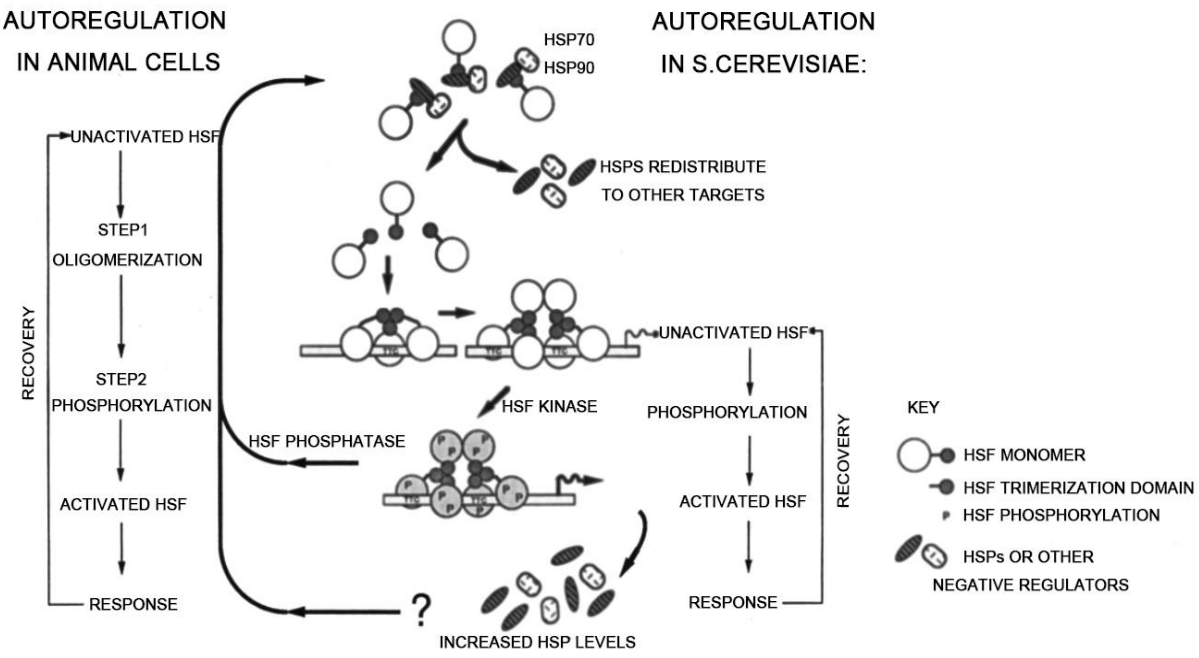

Figure 1.14. A heat-shock response model basing HSF. Adopted from Ref. (Sorger 1991).

1.2.1.3 Other pathways to respond heat shock

The PKC1-regulated MAPK pathway is another way to induce thermotolerance. The PKC1 is encoded as a homolog of α, β and γ isoforms of mammalian PKC in yeast and is proposed to activate a MAPK pathway. Damage to this pathway weakens cell wall construction resulting in a deficiency when cells grow at elevated temperatures. However, a previous report has shown that the PKC1-regulated pathway is independent from heat shock elements (Kamada et al. 1995).

Cell lysis contributes to cell survival under heat stress as well. Reports have shown that some ATP-driven proteolysis (Clp/HSP100 protease) plays an important role in the removal of non-functional damaged proteins (Porankiewlcz et al. 1999; Gottesman 1996; Alexopoulos et al. 2013). Noor suggested that cell lysis might be a mechanism to support the survival of the *E.coli* population through heat stress as a nutritional supplement (Noor 2015).

1.2.2 Oxidative stress

The definition of oxidative stress is that the production of reactive oxygen species (ROS) induce adverse effects upon cell fitness (De Angelis & Gobbetti 2004). There are three common reactive oxygen intermediates: the superoxide radical anion (O_2^-), hydrogen peroxide (H_2O_2) and hydroxyl radicals (HO*). O_2^- and H_2O_2 may contribute to the formation of the highly reactive oxidant HO* via the Fenton and Haber-Weiss reactions (Mccormick et al. 1998).

HSF1 and Ssa1 have been reported to respond to oxidative stress (Wang et al. 2012). Briefly, residues Cys15, Cys264 and Cys303 (especially Cys303) of Ssa1 located within the NBD were oxidized by H_2O_2, cadmium sulfate, diamide or N-ethyl maleimide (NEM) suggesting that Ssa1 is one of the responsers to oxidative stress (Wang et al. 2012). And then HSF1 can be activated by oxidised Ssa1 in yeast to promote Hsps expression (Wang et al. 2012). It highlights that HSP70 is a sensor for the regulation of oxidative stress.

1.2.3 Osmotic stress

The definition of osmotic stress is a sudden increase or decrease in the osmolality of the environment resulting in the movement of water from inside the cell to the outside or from outside to inside the cell, which causes changes in cell turgor pressure, cell shape and volume (De Angelis & Gobbetti 2004). Hyperosmotic stress (18% NaCl 2h) dramatically decreases the survival of *Lb. acidophilus* (Kim et al. 2001). To prevent osmotic stress and keep turgor pressure, *Lactobacilli* accumulates specific solutes which can be released rapidly to maintain turgor pressure during hyperosmotic stress. For example, *Lb. plantarum* releases glycine betaine, proline and some glutamate to remain osmotically balanced (Glaasker et al. 1996).

Cell wall integrity (CWI) plays a crucial role in maintaining cell turgor pressure and osmotic stress. Broadly, any environmental conditions that induce CWI change may cause osmotic stress in cells and not only in a hyperosmotic solution. Thus, all other stresses, such as pH changes, oxidative stress, and heat shock, have the possibility of causing extra osmotic stress. For example, high temperature weakens the CWI and osmotic stabilisers such as 1M sorbitol rescue the damage to some extent (Davenport et

al. 1995; Levin & Bartlett-Heubusch 1992). Since molecular chaperone functions are related with CWI, the mutations that destabilize the CWI at elevated temperatures are usually found in genes involved in cell wall maintenance (Paravicini et al. 1992). Thus the abnormal function of molecular chaperones is another cause of osmotic stress.

1.2.4 Other stresses

With exception to the stresses mentioned above, there are several other stresses, such as cold stress, acid stress and starvation. The definition of cold stress is the opposite to heat shock stress. After exposing cells abruptly to low temperatures, several disturbances impair the cell such as reduction of membrane fluidity, structural changes of the DNA supercoil, inhibition of DNA replication, transcription and protein synthesis (De Angelis & Gobbetti 2004). Acid stress occurs often in industry fermentation. Lactic acid is involved in balancing the cytoplasmic pH *in vivo* (Piard & Desmazeaud 1991; Kasjet 1987). The proton-translocation ATPase is possibly the most crucial regulator for bacteria (Bender & Marquis 1987). Starvation is another stress occurring in industry fermentations. When nutrition is exhausted cell growth is limited and starvation stress occurs by the accumulation of metabolic products. Carbohydrate starvation leads to cell energy depletion; phosphate starvation which damages the cells energy supply as well as DNA/ RNA synthesis. Nitrogen starvation mainly imitates protein synthesis (De Angelis & Gobbetti 2004). General stress proteins (GSP) of *E. coli* and *B. subtilis* are induced under various conditions especially under glucose starvation. The alternative sigma factor, σ^B, controls the expression of the majority of GSP. The activation of this regulation is induced by different pathways which depend on the stress condition (Antelmann et al. 1997).

1.3 Protein misfolding and related diseases

Protein misfolding means that the structure of protein differs from its native state so that it cannot maintain native functions. Misfolded protein aggregates protein oligomers easily, these protein aggregates with ordered cross-β structures called amyloid fibrils. This term was first described by Rudolph Virchow in 1854. Virchow found microscopic images of iodine stained cerebral corpora amylacea were abnormal and similar to an earlier description of other tissues such as lardaceous liver and waxy liver in 1639 (Sipe

& Cohen 2000). However, at that time Virchow considered these iodine stained substances were cellulose and it is not clear what differences there are between plant starch and animal cellulose. Friedreich and Kekule demonstrated that the amyloid fibrils were actually proteins based on their high nitrogen percentage which brought the new knowledge about amyloid fibrils to the world (Sipe & Cohen 2000).

Initially, people considered amyloid fibrils to be structurally amorphous. The Cohen group demonstrated that amyloid fibrils have different origins, however amyloid fibrils in humans and animals displayed a similar structure- containing bundles of rigid and straight fibrils (Figure 1.15) (Cohen et al. 1982; Sipe & Cohen 2000). After that, fibrils were isolated from tissues by sucrose gradient centrifugation and the structure of isolated fibrils from tissues was seen to be similar with ones observed in tissues (Figure 1.16A) (Sipe & Cohen 2000). And negative staining identified the diameter of the isolated amyloid fibrils to be 75-100 Å (Figure 1.16B) (Sipe & Cohen 2000).

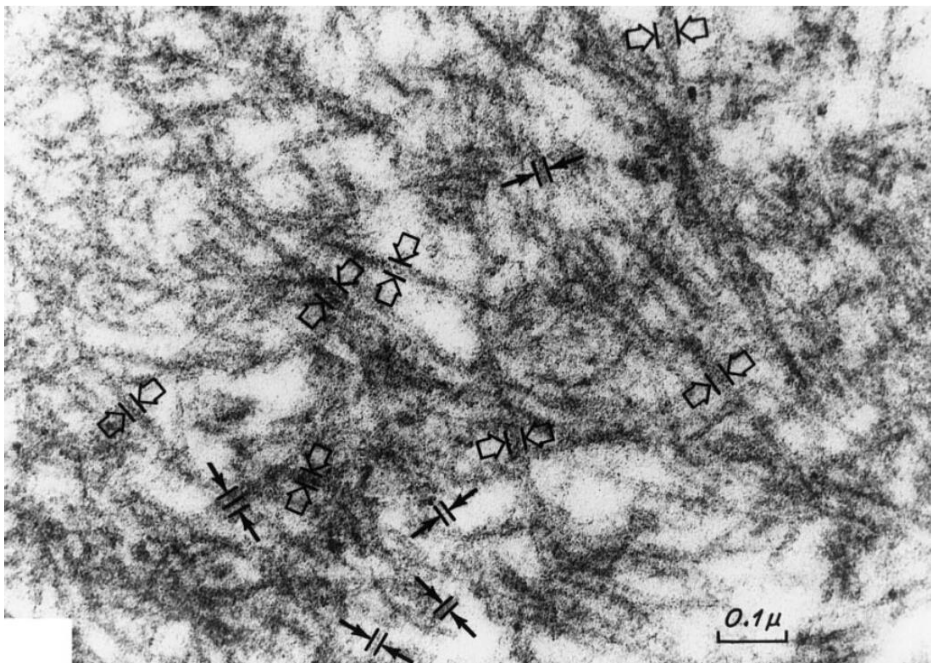

Figure 1.15. An electron micrograph of amyloid fibrils of the human amyloidootic spleen. Adapted from Ref. (Sipe & Cohen 2000) and original figure from The Journal of Cell Biology, 1967, Vol. 33, pp. 679-708.

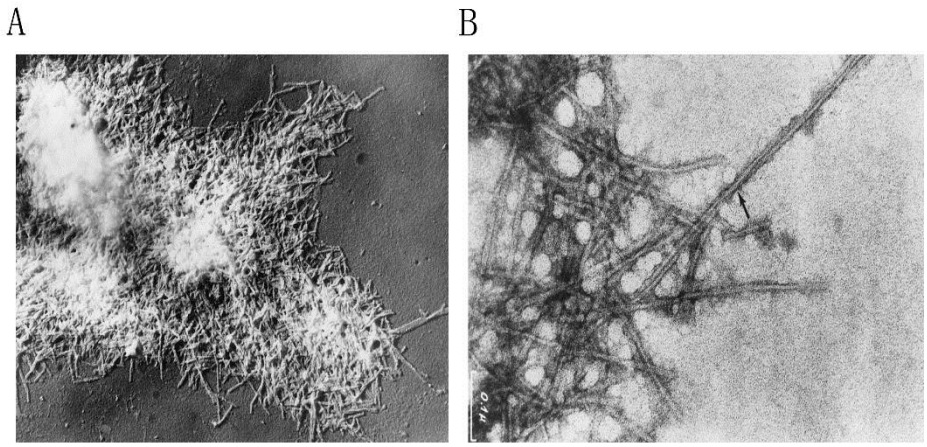

Figure 1.16. Structures of Amyloid fibrils from human amyloidotic spleen *in vitro*. (A) Amyloid fibrils isolated by homogenization in physiological saline followed by sucrose gradient centrifugation. (B) Sucrose gradient fraction negatively stained with uranyl acetate. Adapted from Ref. (Sipe & Cohen 2000) and original figure from The Journal of Cell Biology, 1967, Vol. 33, pp. 679–708.

1.3.1 Prions

Prions are amyloid fibrils produced from oligomerization of specific proteins, which thought to be the cause of the transmissible spongiform encephalopathies (TSEs). Prions are involved in many neurodegenerative diseases such as Parkinson's disease, Alzheimer's disease and Huntington's disease (Knowles et al. 2014). A detailed list of known prion diseases is shown in Table 1.6. Briefly, Prion diseases can be categorised into two groups, neurodegenerative ones and non-neuropathic ones. The former occurs in the brain and the later aggregates amyloid fibrils in other tissues.

Table 1.6. Human diseases induced by prions.

Disease	Aggregating protein or peptide	Number of residues
Neurodegenerative diseases		
Alzheimer's disease	Amyloid β peptide	40-42
Amyotrophic lateral sclerosis	Superoxide dismutase 1	153
Familial British dementia	ABri	23

Familial Danish dementia	ADan	23
Frontotemporal dementia with Parkinsonism	Tau	352–441
Hereditary dentatorubral-pallidoluysian atrophy	Atrophin-1 with polyQ expansion	1185
Huntington's disease	Huntingtin with polyQ expansion	3144
Parkinson's disease and Dementia with Lewy bodies	α-Synuclein	140
Spinocerebellar ataxias	Ataxins with polyQ expansion	816
Spinocerebellar ataxia 17	TATA box-binding protein with polyQ expansion	919
Spongiform encephalopathies	Prion protein or fragments thereof	253
Non-neuropathic systemic amyloidoses		
AA amyloidosis and Familial Mediterranean fever	Fragments of serum amyloid A protein	76–104
AL amyloidosis	Immunoglobulin light chains or fragments	~90
Aortic medial amyloidosis	Medin	50
ApoAI amyloidosis	N-terminal fragments of apolipoprotein AI	80-93
ApoAII amyloidosis	N-terminal fragment of apolipoprotein AII	98
ApoAIV amyloidosis	N-terminal fragment of apolipoprotein AIV	~70
Atrial amyloidosis	Atrial natriuretic factor	28
Calcifying epithelial odontogenic tumors	Unknown	~46
Cataract	γ-Crystallins	Variable
Corneal amylodosis associated with trichiasis	Lactoferrin	692
Cutaneous lichen amyloidosis	Keratins	Variable

Familial amyloidotic polyneuropathy	Mutants of transthyretin	127
Fibrinogen amyloidosis	Variants of fibrinogen α-chain	27-81
Finnish hereditary amyloidosis	Fragments of gelsolin mutants	71
Hemodialysis-related amyloidosis	β2-microglobulin	99
Hereditary cerebral haemorrhage with amyloidosis	Mutants of amyloid β peptide	40 or 42
Hereditary lattice corneal dystrophy	Mainly C-terminal fragments of kerato-epithelin	50-200
Icelandic hereditary cerebral amyloid angiopathy	Mutant of cystatin C	120
Inclusion-body myositis	Amyloid βpeptide	40 or 42
Injection-localized amyloidosis	Insulin	21 + 30
Lysozyme amyloidosis	Mutants of lysozyme	130
Medullary carcinoma of the thyroid	Calcitonin	32
Pituitary prolactinoma	Prolactin	199
Pulmonary alveolar proteinosis	Lung surfactant protein C	35
Senile systemic amyloidosis	Wild-type transthyretin Mutants	127
Type II diabetes	Amylin, also called islet amyloid polypeptide (IAPP)	37

Adapted from Ref. (Chiti & Dobson 2006)

With the development of microscopy technology, the structures of amyloid fibrils have been determined by transmission electron microscopy (TEM) or atomic force microscopy (AFM). Each fibril typically consists of 2-6 protofilaments, 2-5 nm in diameter, wraped around each other to form a 7-13 nm width fibril (Figure 1.17) (Serpell et al. 2000; Sacchettini & Kelly 2002). The β-rich amyloid fibril binds specific dyes such as thioflavin T (ThT) and Congo red (CR) (Nilsson 2004). Protofilaments of different prions do not share obvious sequence identity and conservation (Table 1.6), but form a highly conserved fibril structure (Figure 1.17). Although prions share the same structure, not all prions are pathogenic or harmful for the organism. For example,

the curlin in *E.coli* colonizes inert surfaces and regulates binding to host proteins (Chapman et al. 2002); [*URE3*] in yeast helps adaptation in a low-nitrogen environment by promoting the uptake of poor nitrogen sources (Chien et al. 2004); [PSI^+] in yeast facilitates the readthrough of translation to resist stressful environments and promotes evolution (Fitzpatrick et al. 2011). The intralumenal domain of Pmel17 in human forms inside melanosomes, fibrous striations upon which melanin granules form (Berson et al. 2003). These examples indicate that highly ordered prions, even in higher organisms, can be physiologically useful for specific and specialized biological functions. Interestingly, recent work even used amyloid fibrils as a nano material to store valuable proteins basing on the highly ordered structure (Zhou et al. 2015).

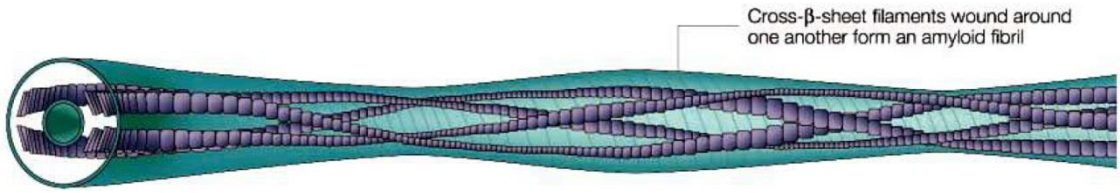

Figure 1.17. The structural model of an amyloid fibril. Adapted from Ref. (Sacchettini & Kelly 2002).

1.3.2 Yeast prions

In 1965, Cox described the first prion in *S. cerevisia* and named [PSI^+] (COX 1965). However, Cox did not identify many [PSI^+] traits until after many years of effort. In 1994, Wicker correctly established prion hypothesis and yeast prion models, [PSI^+] and [*URE3*] (Wickner 1994). After that, yeast became a widely used model and has been used to investigate the mechanism of prion formation. There are now 11 prions confirmed to be present in yeast (Table 1.7).

Table 1.7. Yeast prion with specific funtions

Prion	Protein	Normal Function	Function of the resulting amyloid fibril
[*GAR*$^+$]	Pma1+Std1	plasma membrane P2-type ATPase , pumps proton; control expression of glucose-regulated gene	Resistant to glucose-associated repression
[*ISP*$^+$]	Sfp1	Global transcriptional regulator	Anti-suppressor of certain sup35 mutations
[*MCA*$^+$]	Mca1	Ca^{2+}-dependent cysteine protease	Unknown
[*MOD*$^+$]	Mod5	tRNA isopentenyl transferase	Unknown
[*MOT3*$^+$]	Mot3	Transcriptional repressor	Derepress transcription of anaerobic genes and change CWI
[*OCT*$^+$]	Cyc8	General transcriptional co-repressor	Derepress transcription
[*PSI*$^+$]	Sup35	Translation termination factor eRF3	mRNA readthrough and increased nonsense suppressor phenotype
[*RNQ*$^+$]/ [*PIN*$^+$]	Rnq1	Protein template factor	Promotes propagation of [*PSI*$^+$] and other prions
[*SWI*$^+$]	Swi1	Regulates transcription by chromatin remodeling	Poor growth on glycerol, raffinose and galactoose carbon sources
[*URE3*]	Ure2	Nitrogen catabolite repression transcriptional regulator	Promotion survival on poor nitrogen sources by derepression of nitrogen catabolism enzmes and transporters
[β]	yscB	death in stationary phase, failure in meiosis	Inhibition of degradation of cellular proteins under nitrogen starvation

Adapted from (Wickner et al. 2009) and https://en.wikipedia.org/wiki/Fungal_prion

1.3.2.1 [*PSI*$^+$] prion

[*PSI*$^+$] is the aggregation form of the translation termination factor eRF3, Sup35. In [*psi*$^-$] yeast cells, Sup35 protein is in a soluble state and interacts with Sup45 (Class Ⅰ release factor eRF1) to terminate translation when mRNA carrying stop codons enters the A site of the ribosome. However, Sup35 in the [*PSI*$^+$] state cannot form the termination complex with Sup45. Thus there is no functional translation termination complex to release the nascent polypeptide from the ribosome in [*PSI*$^+$] cells. This results in readthrough of protein translation and enhancement of several nonsense repression, which leads to development of new phenotypes which could permit adaptation during various environments (Figure 1.18) (Fitzpatrick et al. 2011; Wickner et al. 2004). The [*PSI*$^+$] phenotype is heritable as Sup35 in the self-seeding monomeric prion state adapting the same state (Figure 1.18). And [*PSI*$^+$] can be passed from mother cell to daughter during mitosis (Tuite & Cox 2003).

Sup35 is comprised of three domains: N-terminus domain (residues 1-123), which are enriched in a high proportion of uncharged polar amino acids (S, T, N, Q, Y) and involved with the PrD (prion forming domain) of Sup35 (King & Diaz-Avalos 2004; Ter-Avanesyan et al. 1994; Glover et al. 1997). The M (middle) region (residues 124-253) are highly charged and conformationally flexible, this assists in maintaining Sup35 protein solubility and enabling the prion to stabilize in the soluble non-prion state (Liu et al. 2002). The C (C-terminal) domain (residues 254-685) is a GTPase essential for translation termination activity (Figure 1.19A) (Stansfield et al. 1995). The minimal prion forming domain (PrD) of Sup35 extends from residue 1 to residue 97 and was distinct in the QN rich (QNR) sub-region and oligopeptide repeat region (OPR) (Figure 1.19B and C). Moreover, the oligopeptide repeat of the Sup35 PrD is similar with the PrP octapeptide repeat. The former contains five imperfect regions of an octapeptide sequence YQQYNPQGG resembling and the later which has a PHGGGWGQ repeat (Figure 1.19D). Both of them have a G-G-aromatic motif which might play a crucial role in prion aggregations (Gazit 2002).

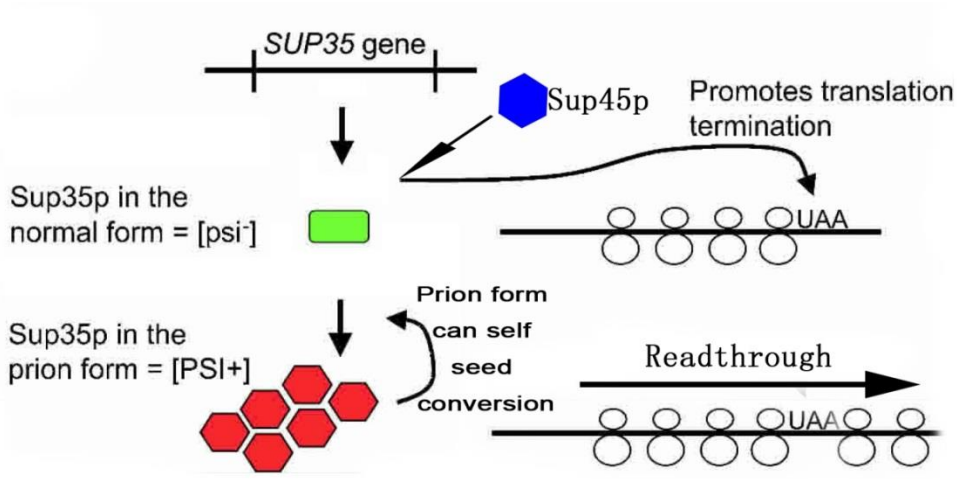

Figure 1.18. Functions of Sup35 [*psi*$^-$] and [*PSI*$^+$] prion. Adapted from Ref. (Wickner et al. 2004) with minor amendment.

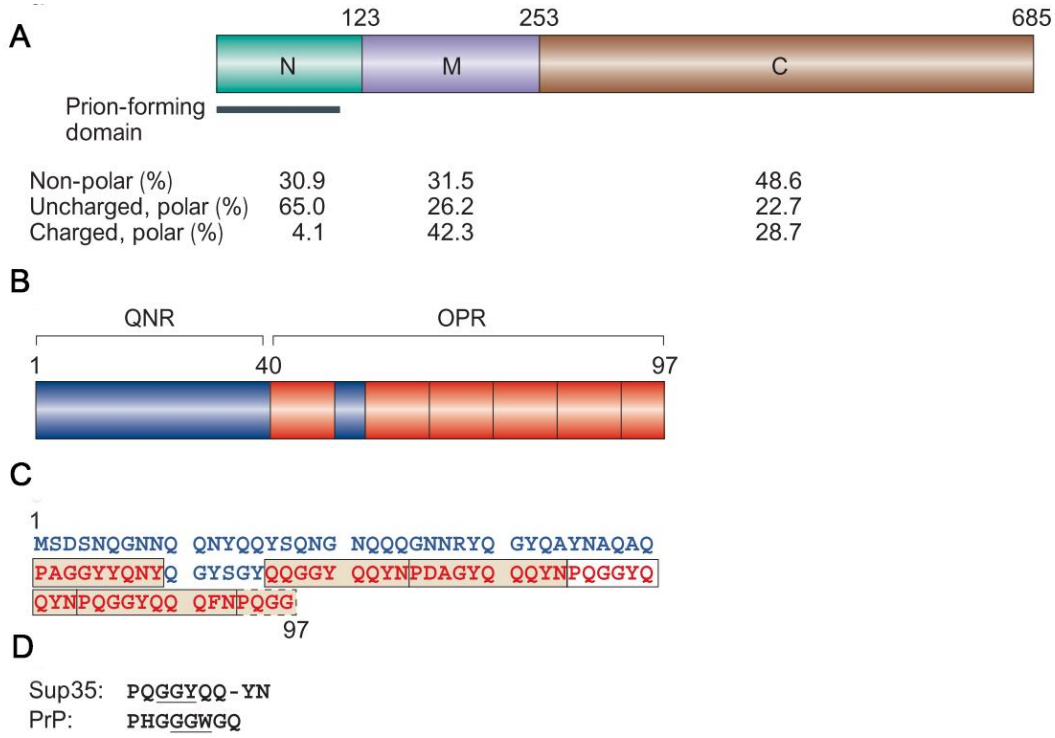

Figure 1.19. Schematic diagram of the Sup35 protein. (A) Assignment of three domains of the Sup35 protein. The N-terminus domain, the middle domain and the C-terminal domain. (B) The minimal prion forming domain (PrD) of Sup35 extends from residue 1 to residue 97 and was distinct to the QN rich (QNR) sub-region and oligopeptide repeat region (OPR). (C) The sequence of Sup35 PrD. The region is rich in asparagine (N) and glutamine (Q) highlighted in red. The boxed sequences are the complete oligopeptide repeats in the OPR region, whereas the part repeat is identified by the dotted box. (D) The oligopeptide repeat of the Sup35 PrD is similar to the PrP octarepeat. The underlined G-G-aromatic motif may play a crucial role in both Sup35 and PrP aggregation. Adapted from Ref. (Tuite & Cox 2003).

1.3.2.2 [*PSI*$^+$] prion assessment

As shown in Section 1.3.2, yeast has been established as a classic model to investigate prions *in vivo*. As well as the safety aspect of the yeast model, prion phonotype can be easily screened based on colony colour. In a strain containing a prion suppressible nonsense mutation in either the *ADE1* or *ADE2* gene, [*PSI*$^+$] cells are white on YPD and grow on synthetic media without adenine (-ADE); conversely, [*psi*$^-$] cells are red on YPD and cannot grow on -ADE. The handy and convenient screen method is caused by a coloured by-product of adenine biosynthesis (COX 1965). Briefly, the yeast adenine biosynthesis pathway consists of seven processes which convert P-ribosyl-PP (PRPP) to adenine monophosphate (Figure 1.20). The *ADE* genes encode seven enzymes involved in the catalytic pathway. The laboratory strains we used are with aberrant stop codons in *ADE1* or *ADE2* genes which are N-succinyl-5-aminoimidazole-4-carboxamide ribotide synthetase and Phospho-ribosylaminoimidazole carboxylase respectively. In [*PSI*$^+$] cells, since Sup35 mainly exists as a prion state, there is no functional Sup35 to terminate translation. As a result, *ADE1* or *ADE2* genes can be expressed functionally and cells grow on adenine lacking medium. However, in [*psi*$^-$] cells, mutations in *ADE1* or *ADE2* genes interrupt step 6 or step 7 of the adenine biosynthesis pathway, thus inducing an accumulation of AIR product. Finally, AIRs are abundantly accumulated in vacuoles and form red pigment which is secreted out of the cell (Shorter & Lindquist 2005). This method is still the most widely used and rapid way to assess the yeast prion *in vivo*.

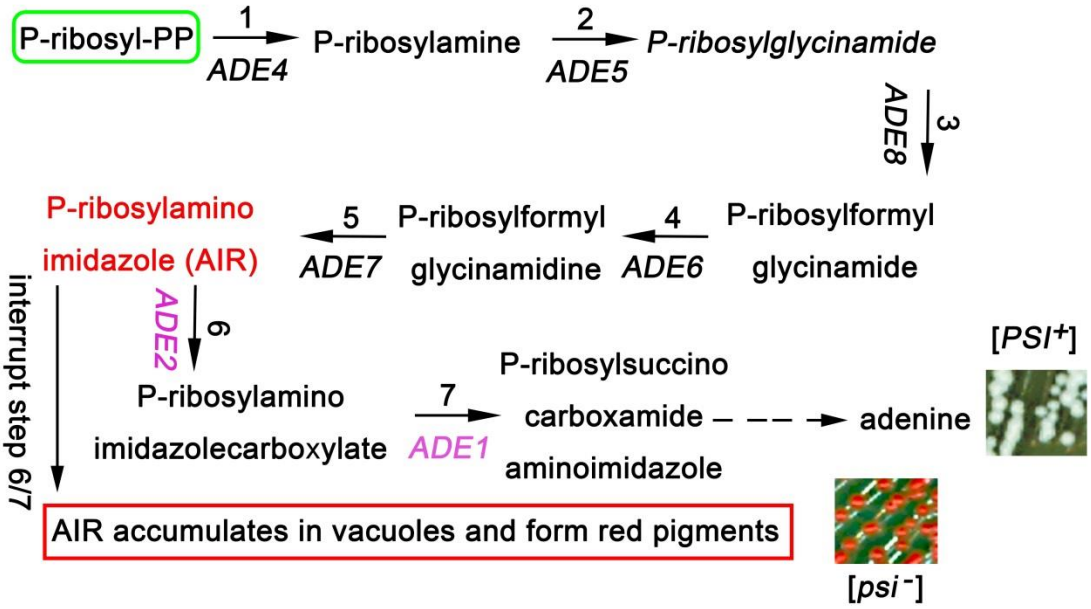

Figure 1.20. The adenine biosynthesis pathway in *S. cerevisiae*.

1.3.3 Mechanisms of amyloid fibril formation

The aggregation of amyloid fibrils is a complex process regulated by self-seeding and several molecular chaperones. However, the formation of prions from various species shares the same process and mechanism. In Figure 1.21A, a classic model of mammalian prion aggregation has been shown. The seeded-polymerization model suggests infectious PrP^{Sc} oligomers act as seeds that interact with monomers of PrP^{C} and convert normal cellular PrP^{C} to PrP^{Sc}. Then PrP^{Sc} oligomers further assemble into higher-molecular-weight fibrils, which do not have any infectious potential. The new seeds were generated by degrading amyloid fibrils into fragments with the assistance of molecular chaperones (Tuite & Cox 2003).

In yeast, either [*PSI*$^{+}$] or [*URE3*] have similar aggregation processes with that of mammalian cells (Figure 1.21B). Briefly, Sup35 or Ure2 form transient oligomeric intermediates. Then oligomer seeds convert their conformation to highly ordered β-sheets and assemble into the higher-molecular-weight fibrils. The whole process is regulated by molecular chaperones such as HSP104, HSP70 and HSP40 (Tuite & Cox 2003). The detailed roles of molecular chaperones in prion propagation will be discussed in the next section.

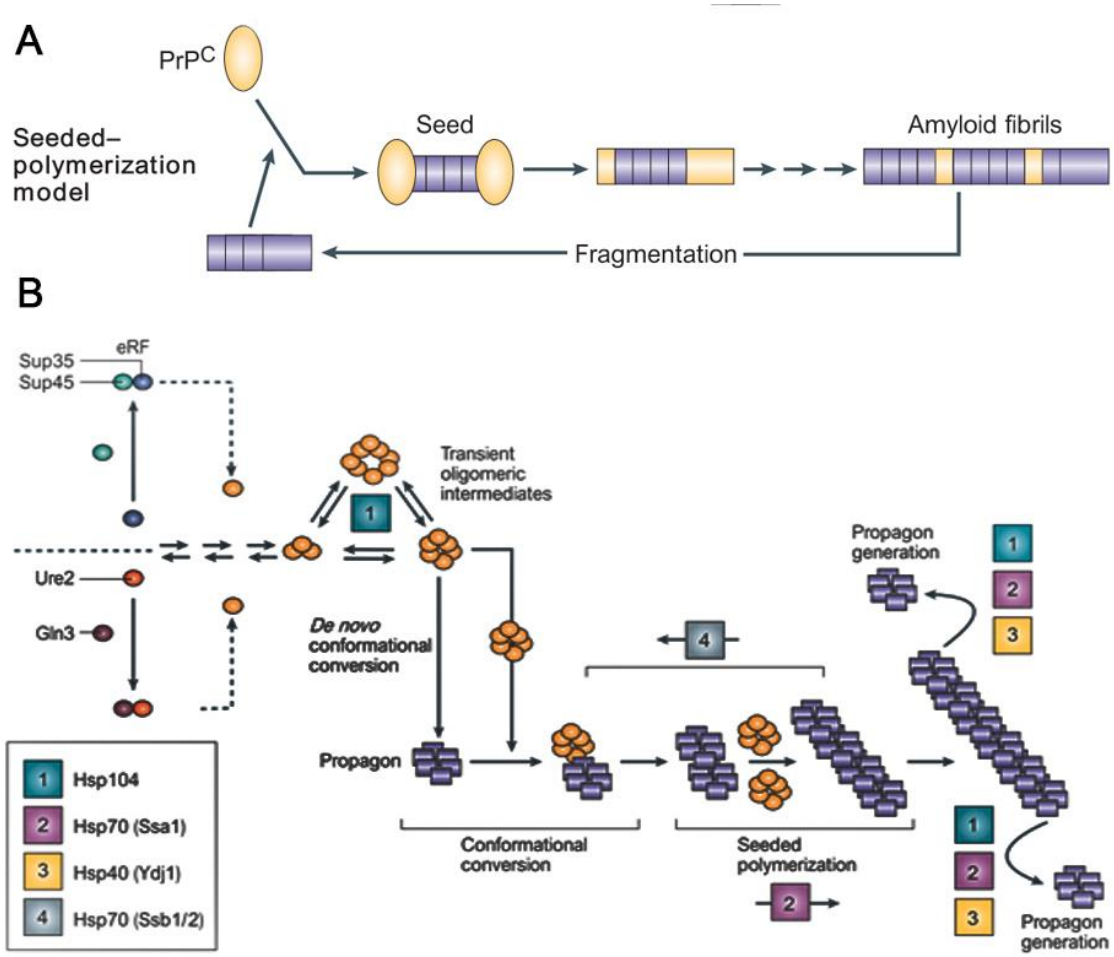

Figure 1.21. Aggregation reaction network. (A) The aggregation process of mammalian prions; (B) The formation of yeast prions. Prion state is shown in orange circles and seeds are shown in blue squares. Adapted from Ref. (Tuite & Cox 2003).

1.3.4 Molecular chaperones in prion regulation

Molecular chaperones play crucial roles in regulating the aggregation of amyloid fibrils (Figure 1.21 and Table 1.8). HSP104 is one of the protein-remodeling factors and is necessary to maintain [*PSI*$^{+}$] and [*URE3*] prions as a deletion of HSP104 eliminates both prions. The presence of 5 mM guanidium chloride (GdnHCl) cures prions by inhibiting ATPase activity of HSP104 (Jung & Masison 2001). Overexpression of HSP104 did not affect [*URE3*] but cured [*PSI*$^{+}$] prions. One of the explanations for this division is that HSP104 fragments [*PSI*$^{+}$] prions to fragmentation without an infectious endpoint. Nevertheless, the endpoint of [*URE3*] fragmentation is infective prion fibrils (Shorter & Lindquist 2006). The N-terminal of HSP104 is critical for prion-

disaggregase activity (Sweeny & Shorter 2015). Furthermore, HSP104 confers tolerance to diverse thermal and chemical stresses by recovering natively folded protein from disordered aggregates harbouring denatured proteins and by disassembling aggregated structures harbouring functional proteins (Wallace et al. 2015; Sanchez & Lindquist 1990; Dawn A. Parsell et al. 1994; Glover & Lindquist 1998).

HSP70 machinery has been demonstrated on the regulation of prion propagation (Perrett & Jones 2008; Glover & Lindquist 1998; Shorter & Lindquist 2008; Walter et al. 2011). The actual roles of HSP104 in regulating protein misfolding and cellular stress responses are part of the HSP70 machinery. Except HSP104, HSP40 and NEF which are the other two important chaperones in the machinery. The solubilisation of prions affected by HSP70 machinery is in an ATP-dependent manner (Gao et al. 2015). HSP40 stimulated ATP activity of HSP70 and delivered substrates to HSP70; NEFs stimulated ADP release and ATP rebinding of HSP70 (Bukau & Horwich 1998). HSP70-HSP40-NEFs machinery powerfully disaggregate α-Synuclein fibrils *in vitro* into shorter fibrils or monomers (Gao et al. 2015).

There are two cytosolic HSP70 subfamilies (Ssa and Ssb) which influence [PSI^+] propagation (Allen 2004; Jones et al. 2004; Jung et al. 2000). The Ssa subfamily has four members (Ssa1-4) and plays a crucial role in protein folding, translocation and refolding denatured protein so that at least one of them is necessary for viability (Werner-Washburne et al. 1987; Albanèse et al. 2006). High levels of Ssa1 or Ssb1 cure weak [PSI^+], as do high levels of the HSP40s, Sis1 and Ydj1. However, strong [PSI^+] variants are largely unaffected by these treatments (Kryndushkin et al. 2002; Kushnirov et al. 2000).

A recent report showed that yeast sHSP, HSP26 and HSP42, assist the HSP70 network to control [PSI^+] propagation. Briefly, HSP42 prevents conformational rearrangements of molten oligomers that benefit from seeds and de novo prionogenesis and collaborate with HSP70 to attenuate self-templating. Relatively, HSP26 prevents self-templating upon binding assembled prions. sHSP binding destabilizes Sup35 prions and promotes their disaggregation by HSP104, HSP70, and HSP40. In yeast, overexpression of HSP26 or HSP42 inhibits [PSI^+] propagation and promotes [PSI^+]-curing by

overexpressing HSP104 (Duennwald et al. 2012). This mechanism is conserved in the depolymerisation of α-Synuclein fibrils as well (Duennwald et al. 2012).

In addition to chaperones of HSP70, the interdomain communication of HSP70 plays a crucial role in the regulation of prion propagation. There are a lot of mutations impairing [PSI^+] that have been indicated at NBD and SBD, and previous research has shown that some of the second-site suppressors of the SBD mutant (such as second-site suppressors of L483W) are located in NBD which suggest that prion propagation is related with interdomain communication (Jones & Masison 2003). L483W is the classic SBD mutant having identified and characterized impairing [PSI^+] by reducing the number of seeds (Jung et al., 2000; Song et al., 2005). Deletion of nucleotide exchange factors (NEFs) Fes1 or Sse1 increases [PSI^+] which implies that L483W enhances substrate binding affinity, and our previous steered molecular dynamics simulations support this hypothesis (Jung et al. 2000; Jones et al. 2004; Xu et al. 2013). However, early research suggests that L483W has weakened substrate-binding activity to a small peptide substrate (Needham & Masison 2008). The reasons for this discrepancy may be from the size of the peptide and Ssa1 model (Xu et al. 2013).

Table 1.8. Roles of molecular chaperones in yeast prion propagation.

Molecular chaperones	Cellular function	Effects on prion propagation when	
		overexpressed	deleted
HSP104	Protein disaggregation and stress tolerance	Efficiently cures [PSI^+] but not [*URE3*]or [PIN^+]/[RNQ^+]	Cures all known naturally occurring yeast prions
Ssa1-4	Protein folding and stress tolerance. Bind to denatured proteins and prevent aggregation. Also involved in aspects of protein translocation and translation	Can cure some variants of [PSI^+] when co-chaperones co-expressed. Can counteract the [PSI^+] curing effect of HSP104 overexpression. Ssa1 can cure [*URE3*] while	Deletion of all 4 Ssa members is lethal, constitutes an essential gene family

		Ssa2 cannot	
Ssb1/2	Ribosome associated. Aid in folding of newly synthesized proteins	Can cure some weak variants of [*PSI*$^+$]	Ten-fold increase in spontaneous appearance of [*PSI*$^+$]in a [*PIN*$^+$] background
HSP40 (Ydj1, Sis1, Apj1)	Delivers peptide substrates and stimulates ATPase activity of their relevant HSP70 partner. Sis1 is involved in translation initiation	Ydj1 efficiently cures [*URE3*] but not [*PSI*$^+$]. All three can cure artificial [*PSI*$^+$] variants	No effects of *YDJ1* or *APJ1* deletion. *SIS1* is essential
HSP110 (Sse1/2)	Nucleotide exchange factor for HSP70 (Ssa and Ssb)	Efficiently cures [*URE3*]	Reduced efficiency of propagation for some [*PSI*$^+$] variants. Cures [*URE3*]
Fes1	Nucleotide exchange factor for HSP70 (Ssa)	No reported effects Reduced	Reduced efficiency of propagation for some [*PSI*$^+$] variants. Cures [*URE3*]
Sti1	Aids in the HSP70-HSP90 protein folding cycle. Sti1 bridges HSP70 to HSP90 and regulates ATPase activity of both proteins	Cures artificial [*PSI*$^+$] and weakens wild type variant	Reduced stability of [*URE3*]

Adapted from Ref. (Perrett & Jones 2008).

1.4 Aims and objectives of this study

As mentioned above, many human neurodegenerative diseases such as Alzheimer's, Parkinson's and the prion disease Creutzfeldt-Jacob Disease (CJD) share a common link in that the causative protein agent has aggregated into a structure termed amyloid and formed fibres that are intimately linked to the pathology of the disease. A key player in influencing amyloid formation is the Heat Shock Protein 70 (HSP70) chaperone machinery. Moreover, HSP70 is also a key player in the heat shock response. However,

due to the lack of a complete crystal structure of HSP70, it remains unclear how the allosteric HSP70 (especially allosteric SBD) and PTMs of HSP70 directly effects the heat shock response and [PSI^{+}] inheritance.

The main aim of this work is to obtain a clear understanding of how the SBD of HSP70 and PTM regulate amyloid and respond to heat shock stress, and to determine whether this information is conserved in mammalian cells. This can potentially be used for the design of novel therapeutics for neurodegenerative diseases based on targeting molecular chaperones. Therefore, in this study our key research questions are:

1) Do HSP70 SBD mutants that alter prion propagation and HSR do so through the same mechanism or are there multiple ways?
2) Are mutants located in the HSP70 SBD involved in interdomain communication through the same or a different mechanism?
3) Do PTMs of HSP70 alter prion propagation and HSR through the same or a different mechanism?
4) Can we use this information to help predict the types of HSP70-targeted drugs that may be new potential therapeutics for neurodegenerative amyloid diseases?

In order to answer these questions, I will use the well-established yeast system as a model for amyloid formation and HSR investigation. A combination of computational biology, genetics, structural biology, biochemistry and molecular biology, will be utilized in this work. Due to the high degree of conservation in the HSP70 chaperone system our findings will be directly applicable to mammalian amyloid diseases and HSR and will aid in the future design of therapeutics that target this chaperone machinery.

CHAPTER TWO

MATERIALS AND METHODS

2.1 Plasmids used in this study

Yeast shuttle vectors and *E.coli* expression vectors were employed in this study and listed in Table 2.1. Ssa1 mutations in this study generated by random mutagenesis (previous work from Sarah A. Cusack) or site-directed mutagenesis (SDM) listed in Table 2.2. All the *SSA* genes and their mutations are under the *SSA2* promoter unless otherwise stated.

Table 2.1. Vectors in this study

Plasmid	Description	Source
pRS315	Centromeric *Saccharomyces cerevisiae* shuttle vector - Amp and *LEU2* selection	(Sikorski & Hieter 1989)
pC210-Ssa1	pRS315 carrying *SSA1* under *SSA2* promoter - Amp and *LEU2* selection	Yeast Genetics Lab
pC210-Ssa2	pRS315 carrying *SSA2* under *SSA2* promoter - Amp and LEU2 selection	Yeast Genetics Lab
pC210-Ssa3	pRS315 carrying *SSA3* under *SSA2* promoter - Amp and *LEU2* selection	Yeast Genetics Lab
pC210-Ssa4	pRS315 carrying *SSA4* under *SSA2* promoter - Amp and *LEU2* selection	A gift from D.C. Masison
pC210-Ssa1-flag	pRS315 carrying N-terminal flag tagged *SSA1* under *SSA2* promoter - Amp and *LEU2* selection	This study
pC210-Ssa1-6His	pRS315 carrying N-terminal 6*His tagged *SSA1* under *SSA2* promoter - Amp and *LEU2* selection	Yeast Genetics Lab
pJ120	pRS315 carrying *SSA1* with 500bp 5' and 3' flanking regions - Amp and *LEU2* selection	(Jung et al. 2000)
Ssa1 2-642	pET28a-Smt3 carrying *SSA1* (2-642) - Kanamycin selection	This study
Ssa1 ΔAΔC88	pET28a-Smt3 carrying *SSA1* (382-554) - Kanamycin selection	(Hu, 2015)
pDCM90	*URA3*-based single-copy plasmid containing a thermolabile bacterial luciferase- Amp selection	A gift from D.C. Masison
HSE-lacZ	pUP41carrying *lacZ* under HSE - Amp and *URA3* selection	A gift from M. Mollapour
pET28a-Smt3	*E.coli* expression vector with Kanamycin selection	(Zheng et al. 2012)
Hsc70	*pCMV* carrying HaloTag-*HSC70* (with His and flag tag) – Amp selection	(Truman et al. 2012)

Table 2.2. Mutation plasmids in this study

Plasmid	Description	Source
F475S-pJ120	F475S introduced by random mutagenesis into pJ120	Yeast Genetics Lab
F475S- pC210-Ssa1	F475S introduced by SDM into pC210-Ssa1	This study
F475S- pC210-Ssa2	F475S introduced by SDM into pC210-Ssa2	Yeast Genetics Lab
F475S- pC210-Ssa4	F475S introduced by SDM into pC210-Ssa4	Yeast Genetics Lab
L483W-pC210-Ssa1	L483W introduced by SDM into pC210-Ssa1	Yeast Genetics Lab
L483A-pC210-Ssa1	L483A introduced by SDM into pC210-Ssa1	Yeast Genetics Lab
L483H-pC210-Ssa1	L483H introduced by SDM into pC210-Ssa1	Yeast Genetics Lab
A394V-pC210-Ssa1	A394V introduced by SDM into pC210-Ssa1	This study
F475A- pC210-Ssa1	F475A introduced by SDM into pC210-Ssa1	This study
F475C- pC210-Ssa1	F475C introduced by SDM into pC210-Ssa1	This study
F475W- pC210-Ssa1	F475W introduced by SDM into pC210-Ssa1	This study
F475Y- pC210-Ssa1	F475Y introduced by SDM into pC210-Ssa1	This study
A394/F475S- pC210-Ssa1	A394V/F475S introduced by SDM into pC210-Ssa1	This study
P433S/F475S- pC210-Ssa1	P433S/F475S introduced by SDM into pC210-Ssa1	This study
V477I/F475S- pC210-Ssa1	V477I/F475S introduced by SDM into pC210-Ssa1	This study
F475S-pC210-Ssa1-flag	F475S introduced by SDM into pC210-Ssa1-flag	This study
L483W-pC210-Ssa1-flag	L483W introduced by SDM into	This study

	pC210-Ssa1-flag	
L483A-pC210-Ssa1-flag	L483A introduced by SDM pC210-Ssa1-flag	This study
L483H-pC210-Ssa1-flag	L483H introduced by SDM into pC210-Ssa1-flag	This study
V393A-pC210-Ssa1	V393A introduced by SDM into pC210-Ssa1	This study
I417A-pC210-Ssa1	I417A introduced by SDM into pC210-Ssa1	This study
D476A-pC210-Ssa1	D476A introduced by SDM into pC210-Ssa1	This study
D478A-pC210-Ssa1	D478A introduced by SDM into pC210-Ssa1	This study
N480A-pC210-Ssa1	N480A introduced by SDM into pC210-Ssa1	This study
I482A-pC210-Ssa1	I482A introduced by SDM into pC210-Ssa1	This study
N484A-pC210-Ssa1	N484A introduced by SDM into pC210-Ssa1	This study
D503A-pC210-Ssa1	D503A introduced by SDM into pC210-Ssa1	This study
K504A-pC210-Ssa1	K504A introduced by SDM into pC210-Ssa1	This study
I512A-pC210-Ssa1	I512A introduced by SDM into pC210-Ssa1	This study
I533A-pC210-Ssa1	I533A introduced by SDM into pC210-Ssa1	This study
K86Q-pC210-Ssa1	K86Q introduced by SDM into pC210-Ssa1	Yeast Genetics Lab
K86R-pC210-Ssa1	K86R introduced by SDM into pC210-Ssa1	Yeast Genetics Lab
K185Q-pC210-Ssa1	K185Q introduced by SDM into pC210-Ssa1	Yeast Genetics Lab
K185R-pC210-Ssa1	K185R introduced by SDM into pC210-Ssa1	Yeast Genetics Lab

K354Q-pC210-Ssa1	K354Q introduced by SDM into pC210-Ssa1	Yeast Genetics Lab
K354R-pC210-Ssa1	K354R introduced by SDM into pC210-Ssa1	Yeast Genetics Lab
K562Q-pC210-Ssa1	K562Q introduced by SDM into pC210-Ssa1	Yeast Genetics Lab
K562R-pC210-Ssa1	K562R introduced by SDM into pC210-Ssa1	Yeast Genetics Lab
K86Q/K185Q-pC210-Ssa1	K86Q/K185Q introduced by SDM into pC210-Ssa1	Yeast Genetics Lab
K86R/K185R-pC210-Ssa1	K86R/K185R introduced by SDM into pC210-Ssa1	Yeast Genetics Lab
K86Q/K185Q/K354Q-pC210-Ssa1	K86Q/K185Q/K354Q introduced by SDM into pC210- Ssa1	Yeast Genetics Lab
K86R/K185R/K354R -pC210-Ssa1	K86R/K185R/K354R introduced by SDM into pC210-Ssa1	Yeast Genetics Lab
K86Q/K185Q/K354Q/K562Q -pC210-Ssa1 (4Q)	K86Q/K185Q/K354Q/K562Q introduced by SDM into pC210-Ssa1	Yeast Genetics Lab
K86R/K185R/K354R/K562R-pC210-Ssa1 (4R)	K86R/K185R/K354R/K562R introduced by SDM into pC210-Ssa1	Yeast Genetics Lab
K86Q/K185Q/K354Q/K562Q -pC210-Ssa1-6His (4Q-6His)	K86Q/K185Q/K354Q/K562Q introduced by SDM into pC210-Ssa1-6His	This study
K86R/K185R/K354R/K562R-pC210-Ssa1-6His (4R-6His)	K86R/K185R/K354R/K562R introduced by SDM into pC210-Ssa1-6His	This study
K86Q/K185Q/K354Q/K562Q -pC210-Ssa1-flag (4Q-flag)	K86Q/K185Q/K354Q/K562Q introduced by SDM into pC210-Ssa1-flag	This study
K86R/K185R/K354R/K562R-pC210-Ssa1-flag (4R-flag)	K86R/K185R/K354R/K562R introduced by SDM into pC210-Ssa1-flag	This study
K106R-pC210-Ssa1	K106R introduced by SDM into pC210-Ssa1	This study
K523R-pC210-Ssa1	K523R introduced by SDM into pC210-Ssa1	This study

K106R/K523R-pC210-Ssa1	K106R/K523R introduced by SDM into pC210-Ssa1	This study
F475S-ΔAΔC88	F475S introduced by SDM into pET28a-Smt3-Ssa1 ΔAΔC88	This study
L483W-ΔAΔC88	L483W introduced by SDM into pET28a-Smt3-Ssa1 ΔAΔC88	This study
L483A-ΔAΔC88	L483A introduced by SDM into pET28a-Smt3-Ssa1 ΔAΔC88	This study
L483H-ΔAΔC88	L483H introduced by SDM into pET28a-Smt3-Ssa1 ΔAΔC88	This study
A394V/F475S-ΔAΔC88	A394V/F475S introduced by SDM into pET28a-Smt3-Ssa1 ΔAΔC88	This study
P433S/F475S-ΔAΔC88	P433S/F475S introduced by SDM into pET28a-Smt3-Ssa1 ΔAΔC88	This study
V477I/F475S-ΔAΔC88	V477I/F475S introduced by SDM into pET28a-Smt3-Ssa1 ΔAΔC88	This study
F475A-ΔAΔC88	F475A introduced by SDM into pET28a-Smt3-Ssa1 ΔAΔC88	This study
F475C-ΔAΔC88	F475C introduced by SDM into pET28a-Smt3-Ssa1 ΔAΔC88	This study
F475W-ΔAΔC88	F475W introduced by SDM into pET28a-Smt3-Ssa1 ΔAΔC88	This study
F475Y-ΔAΔC88	F475Y introduced by SDM into pET28a-Smt3-Ssa1 ΔAΔC88	This study
F475S- Ssa1 2-642	F475S introduced by SDM into pET28a-Smt3-Ssa1 2-642	This study
L483W- Ssa1 2-642	L483W introduced by SDM into pET28a-Smt3-Ssa1 2-642	This study
L483A- Ssa1 2-642	L483A introduced by SDM into pET28a-Smt3-Ssa1 2-642	This study
L483H- Ssa1 2-642	L483H introduced by SDM into pET28a-Smt3-Ssa1 2-642	This study
A394V/F475S- Ssa1 2-642	A394V/F475S introduced by SDM into pET28a-Smt3-Ssa1 2-642	This study
P433S/F475S- Ssa1 2-642	P433S/F475S introduced by SDM into pET28a-Smt3-Ssa1 2-642	This study

V477I/F475S- Ssa1 2-642	V477I/F475S introduced by SDM into pET28a-Smt3-Ssa1 2-642	This study
F475A- Ssa1 2-642	F475A introduced by SDM into pET28a-Smt3-Ssa1 2-642	This study
F475C- Ssa1 2-642	F475C introduced by SDM into pET28a-Smt3-Ssa1 2-642	This study
F475W- Ssa1 2-642	F475W introduced by SDM into pET28a-Smt3-Ssa1 2-642	This study
F475Y- Ssa1 2-642	F475Y introduced by SDM into pET28a-Smt3-Ssa1 2-642	This study
F478S-Hsc70	F478S introduced by SDM into Hsc70	This study
K88Q/K187Q/K357Q/K567Q -Hsc70 (4Q-Hsc70)	K88Q/K187Q/K357Q/K567Q introduced by SDM into Hsc70	This study
K88R/K187R/K357R/K567R- Hsc70 (4R-Hsc70)	K88R/K187R/K357R/K567R introduced by SDM into Hsc70	This study

2.2 *E.coli* and *S. cerevisiae* strains in this study

Bacterial strains DH5α and Top10 were used to amplify plasmids. Full-length and truncation Ssa1 and mutations were transformed and expressed into BL21-CodonPlus (DE3)-RIL. C41 (DE3) was used for Ydj1 purification. More details of those strains have been shown in Table 2.3. *S. cerevisiae* strains used in this study have been listed in Table 2.4. For long term storage, yeast strains were stored in liquid YPD containing 15% glycerol at -70℃.

Table 2.3. *E.coli* strains

Strain	Genotype	Usage
DH5α	F-Φ80*lac*ZΔM15 Δ(*lac*ZYA-*arg*F) U169 *rec*A1 *end*A1 *hsd*R17 (rK-, mK+) *pho*A *sup*E44 λ- *thi*-1 *gyr*A96 *rel*A1	Plasmid amplification
Top10	F- *mcr*A Δ(*mrr-hsd*RMS-*mcr*BC) Φ80*lac*ZΔM15 Δ*lac*X74 *rec*A1 *ara*D139 Δ(*ara leu*) 7697 *gal*U *gal*K *rps*L (StrR) *end*A1 *nup*G	Plasmid amplification
C41 (DE3)	F^- *ompT hsdSB* ($r_B^-m_B^-$) *gal dcm* (DE3)	Protein expression
BL21-CodonPlus (DE3)-RIL	B F- *ompT hsdS* ($r_B^-m_B^-$) dcm^+ Tet^r *gal* λ(DE3) *endA* Hte [*argU ileY leuW* Cam^r]	Protein expression

Table 2.4. *S. cerevisiae* strains

Strain	Genotype	Source
G402	*MATa ade2-1 SUQ5 kar1-1 his3 leu2 lys2 trp1 ura3 ssa1::KanMX, ssa2::HIS3, ssa3::TRP1, ssa4::URA3*-1f/pRDW10	A gift from D.C. Masison
Ssa1	*MATa ade2-1 SUQ5 kar1-1 his3 leu2 lys2 trp1 ura3 ssa1::KanMX, ssa2::HIS3, ssa3::TRP1, ssa4::URA3*-1f/pC210-Ssa1	Yeast Genetics Lab
Ssa2	*MATa ade2-1 SUQ5 kar1-1 his3 leu2 lys2 trp1 ura3 ssa1::KanMX, ssa2::HIS3, ssa3::TRP1, ssa4::URA3*-1f/pC210-Ssa2	Yeast Genetics Lab
Ssa4	*MATa ade2-1 SUQ5 kar1-1 his3 leu2 lys2 trp1 ura3 ssa1::KanMX, ssa2::HIS3, ssa3::TRP1, ssa4::URA3*-1f/pC210-Ssa4	Yeast Genetics Lab
L483W	*MATa ade2-1 SUQ5 kar1-1 his3 leu2 lys2 trp1 ura3 ssa1::KanMX, ssa2::HIS3, ssa3::TRP1, ssa4::URA3*-1f/pC210-Ssa1-L483W	Yeast Genetics Lab
L483A	*MATa ade2-1 SUQ5 kar1-1 his3 leu2 lys2 trp1 ura3 ssa1::KanMX, ssa2::HIS3, ssa3::TRP1, ssa4::URA3*-1f/pC210-Ssa1-L483A	Yeast Genetics Lab

L483H	*MATa ade2-1 SUQ5 kar1-1 his3 leu2 lys2 trp1 ura3 ssa1::KanMX, ssa2::HIS3, ssa3::TRP1, ssa4::URA3*-1f/pC210-Ssa1-L483H	Yeast Genetics Lab
F475S	*MATa ade2-1 SUQ5 kar1-1 his3 leu2 lys2 trp1 ura3 ssa1::KanMX, ssa2::HIS3, ssa3::TRP1, ssa4::URA3*-1f/pC210-Ssa1-F475S	This study
A394V/F475S	*MATa ade2-1 SUQ5 kar1-1 his3 leu2 lys2 trp1 ura3 ssa1::KanMX, ssa2::HIS3, ssa3::TRP1, ssa4::URA3*-1f/pC210-Ssa1-A394V/F475S	This study
P433S/F475S	*MATa ade2-1 SUQ5 kar1-1 his3 leu2 lys2 trp1 ura3 ssa1::KanMX, ssa2::HIS3, ssa3::TRP1, ssa4::URA3*-1f/pC210-Ssa1-P433S/F475S	This study
V477I/F475S	*MATa ade2-1 SUQ5 kar1-1 his3 leu2 lys2 trp1 ura3 ssa1::KanMX, ssa2::HIS3, ssa3::TRP1, ssa4::URA3*-1f/pC210-Ssa1-V477I/F475S	This study
F475A	*MATa ade2-1 SUQ5 kar1-1 his3 leu2 lys2 trp1 ura3 ssa1::KanMX, ssa2::HIS3, ssa3::TRP1, ssa4::URA3*-1f/pC210-Ssa1-F475A	This study
F475C	*MATa ade2-1 SUQ5 kar1-1 his3 leu2 lys2 trp1 ura3 ssa1::KanMX, ssa2::HIS3, ssa3::TRP1, ssa4::URA3*-1f/pC210-Ssa1-F475C	This study
F475Y	*MATa ade2-1 SUQ5 kar1-1 his3 leu2 lys2 trp1 ura3 ssa1::KanMX, ssa2::HIS3, ssa3::TRP1, ssa4::URA3*-1f/pC210-Ssa1-F475Y	This study
Ssa1-6His	*MATa ade2-1 SUQ5 kar1-1 his3 leu2 lys2 trp1 ura3 ssa1::KanMX, ssa2::HIS3, ssa3::TRP1, ssa4::URA3*-1f/pC210-Ssa1-6His	This study
Ssa1-flag	*MATa ade2-1 SUQ5 kar1-1 his3 leu2 lys2 trp1 ura3 ssa1::KanMX, ssa2::HIS3, ssa3::TRP1, ssa4::URA3*-1f/pC210-Ssa1-flag	This study
L483W-flag	*MATa ade2-1 SUQ5 kar1-1 his3 leu2 lys2 trp1 ura3 ssa1::KanMX, ssa2::HIS3, ssa3::TRP1, ssa4::URA3*-1f/pC210-Ssa1-L483W-flag	This study
L483A-flag	*MATa ade2-1 SUQ5 kar1-1 his3 leu2 lys2 trp1 ura3 ssa1::KanMX, ssa2::HIS3, ssa3::TRP1, ssa4::URA3*-1f/pC210-Ssa1-L483A-flag	This study

L483H-flag	*MATa ade2-1 SUQ5 kar1-1 his3 leu2 lys2 trp1 ura3 ssa1::KanMX, ssa2::HIS3, ssa3::TRP1, ssa4::URA3*-1f/pC210-Ssa1-L483H-flag	This study
F475S-flag	*MATa ade2-1 SUQ5 kar1-1 his3 leu2 lys2 trp1 ura3 ssa1::KanMX, ssa2::HIS3, ssa3::TRP1, ssa4::URA3*-1f/pC210-Ssa1-F475S-flag	This study
pJ120	*MATa ade2-1 SUQ5 kar1-1 his3 leu2 lys2 trp1 ura3 ssa1::KanMX, ssa2::HIS3, ssa3::TRP1, ssa4::URA3*-1f/pJ120-Ssa1	This study
pJ120-F475S	*MATa ade2-1 SUQ5 kar1-1 his3 leu2 lys2 trp1 ura3 ssa1::KanMX, ssa2::HIS3, ssa3::TRP1, ssa4::URA3*-1f/pJ120-Ssa1-F475S	This study
A394V	*MATa ade2-1 SUQ5 kar1-1 his3 leu2 lys2 trp1 ura3 ssa1::KanMX, ssa2::HIS3, ssa3::TRP1, ssa4::URA3*-1f/pC210-Ssa1-A394V	This study
V393A	*MATa ade2-1 SUQ5 kar1-1 his3 leu2 lys2 trp1 ura3 ssa1::KanMX, ssa2::HIS3, ssa3::TRP1, ssa4::URA3*-1f/pC210-Ssa-V393A	This study
I417A	*MATa ade2-1 SUQ5 kar1-1 his3 leu2 lys2 trp1 ura3 ssa1::KanMX, ssa2::HIS3, ssa3::TRP1, ssa4::URA3*-1f/pC210-Ssa1-I417A	This study
D478A	*MATa ade2-1 SUQ5 kar1-1 his3 leu2 lys2 trp1 ura3 ssa1::KanMX, ssa2::HIS3, ssa3::TRP1, ssa4::URA3*-1f/pC210-Ssa1-D478A	This study
N480A	*MATa ade2-1 SUQ5 kar1-1 his3 leu2 lys2 trp1 ura3 ssa1::KanMX, ssa2::HIS3, ssa3::TRP1, ssa4::URA3*-1f/pC210-Ssa1-N480A	This study
I482A	*MATa ade2-1 SUQ5 kar1-1 his3 leu2 lys2 trp1 ura3 ssa1::KanMX, ssa2::HIS3, ssa3::TRP1, ssa4::URA3*-1f/pC210-Ssa1-I482A	This study
N484A	*MATa ade2-1 SUQ5 kar1-1 his3 leu2 lys2 trp1 ura3 ssa1::KanMX, ssa2::HIS3, ssa3::TRP1, ssa4::URA3*-1f/pC210-Ssa1-N484A	This study
D503A	*MATa ade2-1 SUQ5 kar1-1 his3 leu2 lys2 trp1 ura3 ssa1::KanMX, ssa2::HIS3, ssa3::TRP1, ssa4::URA3*-1f/pC210-Ssa1-D503A	This study

K504A	*MATa ade2-1 SUQ5 kar1-1 his3 leu2 lys2 trp1 ura3 ssa1::KanMX, ssa2::HIS3, ssa3::TRP1, ssa4::URA3*-1f/pC210-Ssa1-K504A	This study
I512A	*MATa ade2-1 SUQ5 kar1-1 his3 leu2 lys2 trp1 ura3 ssa1::KanMX, ssa2::HIS3, ssa3::TRP1, ssa4::URA3*-1f/pC210-Ssa1-I512A	This study
I533A	*MATa ade2-1 SUQ5 kar1-1 his3 leu2 lys2 trp1 ura3 ssa1::KanMX, ssa2::HIS3, ssa3::TRP1, ssa4::URA3*-1f/pC210-Ssa1-I533A	This study
K86Q	*MATa ade2-1 SUQ5 kar1-1 his3 leu2 lys2 trp1 ura3 ssa1::KanMX, ssa2::HIS3, ssa3::TRP1, ssa4::URA3*-1f/pC210-Ssa1-K86Q	Yeast Genetics Lab
K86R	*MATa ade2-1 SUQ5 kar1-1 his3 leu2 lys2 trp1 ura3 ssa1::KanMX, ssa2::HIS3, ssa3::TRP1, ssa4::URA3*-1f/pC210-Ssa1-K86R	Yeast Genetics Lab
K185Q	*MATa ade2-1 SUQ5 kar1-1 his3 leu2 lys2 trp1 ura3 ssa1::KanMX, ssa2::HIS3, ssa3::TRP1, ssa4::URA3*-1f/pC210-Ssa1-K185Q	Yeast Genetics Lab
K185R	*MATa ade2-1 SUQ5 kar1-1 his3 leu2 lys2 trp1 ura3 ssa1::KanMX, ssa2::HIS3, ssa3::TRP1, ssa4::URA3*-1f/pC210-Ssa1-K185R	Yeast Genetics Lab
K354Q	*MATa ade2-1 SUQ5 kar1-1 his3 leu2 lys2 trp1 ura3 ssa1::KanMX, ssa2::HIS3, ssa3::TRP1, ssa4::URA3*-1f/pC210-Ssa1-K354Q	Yeast Genetics Lab
K354R	*MATa ade2-1 SUQ5 kar1-1 his3 leu2 lys2 trp1 ura3 ssa1::KanMX, ssa2::HIS3, ssa3::TRP1, ssa4::URA3*-1f/pC210-Ssa1-K354R	Yeast Genetics Lab
K562Q	*MATa ade2-1 SUQ5 kar1-1 his3 leu2 lys2 trp1 ura3 ssa1::KanMX, ssa2::HIS3, ssa3::TRP1, ssa4::URA3*-1f/pC210-Ssa1-K562Q	Yeast Genetics Lab
K562R	*MATa ade2-1 SUQ5 kar1-1 his3 leu2 lys2 trp1 ura3 ssa1::KanMX, ssa2::HIS3, ssa3::TRP1, ssa4::URA3*-1f/pC210-Ssa1-K562R	Yeast Genetics Lab
K86Q/K185Q	*MATa ade2-1 SUQ5 kar1-1 his3 leu2 lys2 trp1 ura3 ssa1::KanMX, ssa2::HIS3, ssa3::TRP1, ssa4::URA3*-1f/pC210-Ssa1-K86Q/K185Q	Yeast Genetics Lab

K86R/K185R	*MATa ade2-1 SUQ5 kar1-1 his3 leu2 lys2 trp1 ura3 ssa1::KanMX, ssa2::HIS3, ssa3::TRP1, ssa4::URA3*-1f/pC210-Ssa1-K86R/K185R	Yeast Genetics Lab
K86Q/K185Q /K354Q	*MATa ade2-1 SUQ5 kar1-1 his3 leu2 lys2 trp1 ura3 ssa1::KanMX, ssa2::HIS3, ssa3::TRP1, ssa4::URA3*-1f/pC210-Ssa1-K86Q/K185Q/K354Q	Yeast Genetics Lab
K86R/K185R /K354R	*MATa ade2-1 SUQ5 kar1-1 his3 leu2 lys2 trp1 ura3 ssa1::KanMX, ssa2::HIS3, ssa3::TRP1, ssa4::URA3*-1f/pC210-Ssa1-K86R/K185R/K354R	Yeast Genetics Lab
K86Q/K185Q/K354Q/K562Q (4Q)	*MATa ade2-1 SUQ5 kar1-1 his3 leu2 lys2 trp1 ura3 ssa1::KanMX, ssa2::HIS3, ssa3::TRP1, ssa4::URA3*-1f/pC210-Ssa1-4Q	Yeast Genetics Lab
K86R/K185R/K354R/K562R (4R)	*MATa ade2-1 SUQ5 kar1-1 his3 leu2 lys2 trp1 ura3 ssa1::KanMX, ssa2::HIS3, ssa3::TRP1, ssa4::URA3*-1f/pC210-Ssa1-4R	Yeast Genetics Lab
K86Q/K185Q/K354Q/K562Q-6His (4Q-6His)	*MATa ade2-1 SUQ5 kar1-1 his3 leu2 lys2 trp1 ura3 ssa1::KanMX, ssa2::HIS3, ssa3::TRP1, ssa4::URA3*-1f/pC210-Ssa1-4Q-6His	This study
K86R/K185R/K354R/K562R-6His (4R-6His)	*MATa ade2-1 SUQ5 kar1-1 his3 leu2 lys2 trp1 ura3 ssa1::KanMX, ssa2::HIS3, ssa3::TRP1, ssa4::URA3*-1f/pC210-Ssa1-4R-6His	This study
K86Q/K185Q/K354Q/K562Q-flag (4Q-flag)	*MATa ade2-1 SUQ5 kar1-1 his3 leu2 lys2 trp1 ura3 ssa1::KanMX, ssa2::HIS3, ssa3::TRP1, ssa4::URA3*-1f/pC210-Ssa1-4Q-flag	This study
K86R/K185R/K354R/K562R-flag (4R-flag)	*MATa ade2-1 SUQ5 kar1-1 his3 leu2 lys2 trp1 ura3 ssa1::KanMX, ssa2::HIS3, ssa3::TRP1, ssa4::URA3*-1f/pC210-Ssa1-4R-flag	This study
K106R	*MATa ade2-1 SUQ5 kar1-1 his3 leu2 lys2 trp1 ura3 ssa1::KanMX, ssa2::HIS3, ssa3::TRP1, ssa4::URA3*-1f/pC210-Ssa1-K106R	This study
K523R	*MATa ade2-1 SUQ5 kar1-1 his3 leu2 lys2 trp1 ura3 ssa1::KanMX, ssa2::HIS3, ssa3::TRP1, ssa4::URA3*-1f/pC210-Ssa1-K523R	This study
K106R/K523R	*MATa ade2-1 SUQ5 kar1-1 his3 leu2 lys2 trp1 ura3 ssa1::KanMX, ssa2::HIS3, ssa3::TRP1, ssa4::URA3*-1f/pC210-Ssa1-K106R/K523R	This study

Ssa1+pDCM90	*MATa ade2-1 SUQ5 kar1-1 his3 leu2 lys2 trp1 ura3 ssa1::KanMX, ssa2::HIS3, ssa3::TRP1, ssa4::URA3*-1f/pC210-Ssa1+pDCM90	This study
F475S+pDCM90	*MATa ade2-1 SUQ5 kar1-1 his3 leu2 lys2 trp1 ura3 ssa1::KanMX, ssa2::HIS3, ssa3::TRP1, ssa4::URA3*-1f/pC210-F475S+pDCM90	This study
L483W+pDCM90	*MATa ade2-1 SUQ5 kar1-1 his3 leu2 lys2 trp1 ura3 ssa1::KanMX, ssa2::HIS3, ssa3::TRP1, ssa4::URA3*-1f/pC210-L483W+pDCM90	This study
L483A+pDCM90	*MATa ade2-1 SUQ5 kar1-1 his3 leu2 lys2 trp1 ura3 ssa1::KanMX, ssa2::HIS3, ssa3::TRP1, ssa4::URA3*-1f/pC210-L483A+pDCM90	This study
L483H+pDCM90	*MATa ade2-1 SUQ5 kar1-1 his3 leu2 lys2 trp1 ura3 ssa1::KanMX, ssa2::HIS3, ssa3::TRP1, ssa4::URA3*-1f/pC210-L483H+pDCM90	This study
F475A+pDCM90	*MATa ade2-1 SUQ5 kar1-1 his3 leu2 lys2 trp1 ura3 ssa1::KanMX, ssa2::HIS3, ssa3::TRP1, ssa4::URA3*-1f/pC210-F475A+pDCM90	This study
F475C+pDCM90	*MATa ade2-1 SUQ5 kar1-1 his3 leu2 lys2 trp1 ura3 ssa1::KanMX, ssa2::HIS3, ssa3::TRP1, ssa4::URA3*-1f/pC210-F475C+pDCM90	This study
F475Y+pDCM90	*MATa ade2-1 SUQ5 kar1-1 his3 leu2 lys2 trp1 ura3 ssa1::KanMX, ssa2::HIS3, ssa3::TRP1, ssa4::URA3*-1f/pC210-F475Y+pDCM90	This study
4Q+pDCM90	*MATa ade2-1 SUQ5 kar1-1 his3 leu2 lys2 trp1 ura3 ssa1::KanMX, ssa2::HIS3, ssa3::TRP1, ssa4::URA3*-1f/pC210-4Q+pDCM90	This study
4R+pDCM90	*MATa ade2-1 SUQ5 kar1-1 his3 leu2 lys2 trp1 ura3 ssa1::KanMX, ssa2::HIS3, ssa3::TRP1, ssa4::URA3*-1f/pC210-4R+pDCM90	This study
pC210+HSE	*MATa ade2-1 SUQ5 kar1-1 his3 leu2 lys2 trp1 ura3 ssa1::KanMX, ssa2::HIS3, ssa3::TRP1, ssa4::URA3*-1f/pC210+HSE-lacZ	This study
F475S+HSE	*MATa ade2-1 SUQ5 kar1-1 his3 leu2 lys2 trp1 ura3 ssa1::KanMX, ssa2::HIS3, ssa3::TRP1, ssa4::URA3*-1f/pC210-F475S+HSE-lacZ	This study

4Q+HSE	*MATa ade2-1 SUQ5 kar1-1 his3 leu2 lys2 trp1 ura3 ssa1::KanMX, ssa2::HIS3, ssa3::TRP1, ssa4::URA3*-1f/pC210-4Q+HSE-lacZ	This study
4R+HSE	*MATa ade2-1 SUQ5 kar1-1 his3 leu2 lys2 trp1 ura3 ssa1::KanMX, ssa2::HIS3, ssa3::TRP1, ssa4::URA3*-1f/pC210-4R+HSE-lacZ	This study
MH272	*MATa ssa1*Δ*::trp1 ssa2::HisG ssa3::HisG ssa4::HisG* (*ssa1-4*) [YCPlac33 SSA1]	(Jaiswal et al. 2011)
MH272-pC210	*MATa ssa1*Δ*::trp1 ssa2::HisG ssa3::HisG ssa4::HisG* (*ssa1-4*)/pC210-Ssa1	This study
MH272-pC210-flag	*MATa ssa1*Δ*::trp1 ssa2::HisG ssa3::HisG ssa4::HisG* (*ssa1-4*)/pC210-Ssa1-flag	This study
MH272-4Q	*MATa ssa1*Δ*::trp1 ssa2::HisG ssa3::HisG ssa4::HisG* (*ssa1-4*) /pC210-Ssa1-4Q	This study
MH272-4R	*MATa ssa1*Δ*::trp1 ssa2::HisG ssa3::HisG ssa4::HisG* (*ssa1-4*) /pC210-Sssa1-4R	This study
ΔHAT1	*MATa ssa1*Δ*::trp1 ssa2::HisG ssa3::HisG ssa4::HisG* (*ssa1-4*) *HAT1::kanMX4* [YCPlac33 SSA1]	This study
ΔHAT1-pC210	*MATa ssa1*Δ*::trp1 ssa2::HisG ssa3::HisG ssa4::HisG* (*ssa1-4*) *HAT1::kanMX4*/pC210-Ssa1-flag	This study
BY4741-F475S	*MATa his3Δ1; leu2Δ0; met15Δ0; ura3Δ0*/pC210-Ssa1-F475S-flag	This study
ΔPEP4-F475S	BY4741; *MATa; ura3Δ0; leu2Δ0; his3Δ1; met15Δ0; YPL154c::kanMX4*/pC210-Ssa1-F475S-flag	This study
ΔUFD2-F475S	BY4741; *MATa; ura3Δ0; leu2Δ0; his3Δ1; met15Δ0; YDL190c::kanMX4*/pC210-Ssaa1-F475S-flag	This study
ΔUBI4-F475S	BY4741; *MATa; ura3Δ0; leu2Δ0; his3Δ1; met15Δ0; YLL039c::kanMX4*/pC210-Ssa1-F475S-flag	This study
BY4741-pC210	*MATa his3Δ1; leu2Δ0; met15Δ0; ura3Δ0*/pC210-Ssa1-flag	This study
ΔPEP4- pC210	BY4741; *MATa; ura3Δ0; leu2Δ0; his3Δ1; met15Δ0; YPL154c::kanMX4*/pC210-Ssa1-flag	This study
BY4741-4Q	*MATa his3Δ1; leu2Δ0; met15Δ0; ura3Δ0*/pC210-4Q-flag	This study
ΔPEP4-4Q	BY4741; *MATa; ura3Δ0; leu2Δ0; his3Δ1; met15Δ0; YPL154c::kanMX4*/pC210-4Q-flag	This study

BY4741-4R	*MATa his3Δ1; leu2Δ0; met15Δ0; ura3Δ0*/pC210-4R-flag	This study
ΔPEP4-4R	BY4741; *MATa; ura3Δ0; leu2Δ0; his3Δ1; met15Δ0; YPL154c::kanMX4*/pC210-4R-flag	This study
BY4741	*MATa his3Δ1; leu2Δ0; met15Δ0; ura3Δ0*	Yeast Genetic Lab
YNL330c (RPD3)	BY4741; *MATa;his3D1;leu2D0;met15D0;ura3D0;YNL330c::kanMX4*	EUROSCARF
YPL001w (HAT1)	BY4741; *MATa;his3D1;leu2D0;met15D0;ura3D0;YPL001w::kanMX4*	EUROSCARF
ΔPEP4	BY4741; *MATa; ura3Δ0; leu2Δ0; his3Δ1; met15Δ0; YPL154c::kanMX4*	EUROSCARF
ΔUFD2	BY4741; *MATa; ura3Δ0; leu2Δ0; his3Δ1; met15Δ0; YDL190c::kanMX4*	EUROSCARF
ΔUBI4	BY4741; *MATa; ura3Δ0; leu2Δ0; his3Δ1; met15Δ0; YLL039c::kanMX4*	EUROSCARF

Mutations introduced in Ssa1 except the extra statements.

2.3 Sterilisation technique

Materials, such as tips and Eppendorf tubes, solid and liquid media used in this study were autoclaved at 121 ℃ for 15 min unless otherwise stated. Any solutions unsuitable for autoclaving were filtered using a 0.22 μm membrane filter (Millipore). The workplace and laminar flow cabinet was wiped with 70 % (v/v) ethanol before use.

2.4 Growth media

Chemicals used in this study were ordered from Sigma-Aldrich (Ireland) unless otherwise stated. Growth media components purchased from Becton Dickinson (BD). Growth media components were weighed accurately and adjusted to volume with distilled water (dH_2O). Growth media was autoclaved as mentioned in Section 2.2 unless otherwise stated. Liquid media was stored at room temperature (RT) or 4 ℃. Solid agar plates were stored at 4 ℃ and some of them only can be prepared fresh for use.

2.4.1 Bacterial growth media

LB (Luria Broth) was used in *E.coli* transformation of molecular experiments such as molecular cloning, SDM and plasmid amplification. To culture most of the expression strains 2YT was used. M9 with isotopes was used to express Ssa1 truncation mutations for NMR.

LB (Luria Broth), 1 L

Luria-Bertani broth (Sigma)	25 g
Bacto agar (for solid media)	20 g

LB-Ampicillin, 1 L

LB media was prepared as above. After autoclaving, the media was allowed to cool to approximately 60 ℃, and then 1 ml of 100 mg/ml ampicillin stock solution was supplemented to get a final concentration of 100 μg/ml. The 100 mg/ml ampicillin stock solution was prepared by dissolving 1 g of ampicillin to a final volume of 10 ml with dH_2O. This solution was then sterilised using a 0.22 μm filter and 1 ml was aliquoted into sterile Eppendorf tubes and stored at -20 °C.

LB-Kanamycin, 1 L

LB media was prepared as above. After autoclaving, the media was allowed to cool to approximately 60 ℃, and then 1 ml of 50 mg/ml kanamycin stock solution was supplemented to get a final concentration of 50 μg/ml. The 50 mg/ml kanamycin stock solution was prepared by dissolving 0.5 g kanamycin to a final volume of 10 ml with dH_2O. This solution was then sterilised using a 0.22 μm filter and 1ml was aliquoted into sterile Eppendorf tubes and stored at -20 °C.

2YT, 1 L

Yeast extract (Oxoid Ltd., Hampshire, England) (1 %, w/v)	10 g
Tryptone (Oxoid Ltd., Hampshire, England) (1.6 %, w/v)	16 g
NaCl (0.5 %, w/v)	5 g

After autoclaving, ampicillin or kanamycin was supplemented to get a final concentration of 100 μg/ml or 50 μg/ml as mentioned above.

M9-^{15}N, 500 ml

$Na_2HPO_4 \cdot 12H_2O$	8.55 g
KH_2PO_4	1.5 g
NaCl	0.25 g
$^{15}NH_4Cl$	0.5 g

The above components were dissolved in deionized water to get a final volume of 493 ml. After autoclaving, the media was complemented by adding 6.25 ml 40 % (w/v) D-Glucose stock solution and 1 ml $MgSO_4$ stock solution (1 M). D-Glucose stock solution and 1 M $MgSO_4$ stock solution was prepared in deionized water and autoclaved separately.

M9-^{15}N^{13}C, 500 ml

$Na_2HPO_4 \cdot 12H_2O$	8.55 g
KH_2PO_4	1.5 g
NaCl	0.25 g
$^{15}NH_4Cl$	0.5 g

The above components were dissolved in deionized water to get a final volume of 489 ml. After autoclaving, media was complemented by adding 10 ml ^{13}C-Glucose stock solution (0.75 g/10ml) and 1 ml $MgSO_4$ stock solution (1 M). ^{13}C-Glucose stock solution and 1 M $MgSO_4$ stock solution was prepared in deionized water and autoclaved separately.

2.4.2 Yeast growth media

Yeast growth media used in this study was prepared as mentioned in the yeast handbook (Amberg *et al*., 2005) unless otherwise stated.

YPD (Yeast Peptone Dextrose), 1 L

Bacto-yeast extract (1 %, w/v)	10 g
Bacto-peptone (2 %, w/v)	20 g
D-Glucose (2 %, w/v)	20 g
Bacto-agar (2 %, w/v) (for solid media)	20 g

YPD with 3 mM Gdn-HCl (guanidine hydrochloride), 1 L

Solid YPD was prepared and let cool to approximately 60 ℃ after autoclaving. Gdn-HCl stock solution (10 ml) was added to 990 ml of YPD to get a final concentration of 3 mM. The 300 mM Gdn-HCl stock solution was prepared by dissolving 1.45 g Gdn-HCl into 50 ml dH_2O, then filter sterilised. The Gdn-HCl stock solution can be stored at 4 ℃.

YPD with Sorbitol, 1 L

The components of 1 L YPD were autoclaved in a final volume of 500 ml with dH_2O. Sorbitol (182 g) was dissolved in dH_2O in a final volume of 500 ml and filter to sterilise. Mixed 500 ml of YPD components and 500 ml sorbitol solution together to get a final concentration of 1 M sorbitol in 1 L of YPD.

YPD-G418, 100 ml

Solid YPD was prepared and let cool to approximately 60 ℃ after autoclaving. Geneticin (20 mg) was dissolved in 0.5 ml of sterile water and added to 100 ml YPD to get a final concentration of 200 μg/ml. After gently mixing, media was poured into petri dishes and stored at 4 ℃ for no longer than three days.

Synthetic Complete (SC) media, 1 L

Yeast nitrogen base without amino acids (1 %) (Sigma)	6.7 g
Dropout mix (0.2 %) (Table 2.5)	2 g
D-Glucose (2 %)	20 g
Bacto-agar (2 %) (for solid media)	20 g

pH was adjusted to 6.0-6.5 by adding 4 ml of 1 M NaOH. Media was then supplemented using the following amino acids (Table 2.6).

Table 2.5. Components of dropout mix

Amino acid	Quantity
Alanine	2 g
Aminobenzoic acid	2 g
Arginine	2 g

Aspartic acid	2 g
Asparagine	2 g
Cysteine	2 g
Glutamic acid	2 g
Glutamine	2 g
Glycine	2 g
Inositol	2 g
Isoleucine	2 g
Lysine	2 g
Methionine	2 g
Phenylalanine	2 g
Proline	2 g
Serine	2 g
Threonine	2 g
Tyrosine	2 g
Valine	2 g

The components were ground in a mortar and stored at RT.

Table 2.6. Supplemented amino acids into 1 L SC media

Amino acid	Stock solution (g/50 ml)*	Volume of stock solution in 1 L SC (ml)	Final concentration in SC media (μg/ml)
Adenine	0.1	10	20
Histidine	0.5	2	20
Leucine	0.5	10	100
Tryptophan	0.5	2	20
Uracil	0.1	10	20

*Amino acid stock solutions were prepared by weighing the appropriate quantity of amino acid and dissolved to a final volume of 50 ml with dH_2O. Solutions were then filter sterilised and stored at 4 ℃.

SC-5-FOA (5-fluoro-orotic acid), 1 L

Yeast nitrogen base without amino acid (1 %) (Sigma)	6.7 g
Dropout mix (0.2 %) (Table 2.5)	2 g
D-Glucose (2 %)	20 g
Uracil	50 mg

The above components and 1 g of 5-FOA were added to a final volume of 500 ml with dH_2O and dissolved by stirring, then filter sterilised. Amino acid stock solutions were then supplemented according to Table 2.6. Agar (20 g) was brought to a final volume of 500 ml with dH_2O and autoclaved. The autoclaved agar was then cooled to approximately 60-80 ℃ and mixed with the filtered components to get a final volume of 1 L. The final concentration of 5-FOA was 1 mg/ml. The mixture was poured into sterile petri dishes and stored at 4 ℃.

SC-H_2O_2

SC media was prepared as described before supplemented with amino acids. After autoclaving, media was cooled to approximately 60 ℃ and supplemented with 9.8 M H_2O_2 (30 % H_2O_2) to get the required concentrations (Table 2.7). Plates with H_2O_2 were either used immediately or stored at 4 ℃ for 3 days.

Table 2.7. Volume of 9.8 M H_2O_2 supplemented into 50 ml SC media

Finally concentration (mM)	Volume of 9.8 M H_2O_2 (µl)
0	0
1	5
2	10
3	15
4	20
5	25

YPD-SDS

YPD solid medium was prepared as described before. After autoclaving, media was cooled to approximately 60-80 ℃ and 1 % SDS was supplemented to get the required concentrations (Table 2.8). Plates with SDS were either used immediately or stored at 4 ℃.

Table 2.8. Volume of 1 % SDS supplemented with 50 ml YPD media

Finally concentration (%, m/v)	Volume of 1 % SDS (ml)
0	0
0.005	0.25
0.01	0.5
0.015	0.75
0.02	1

SC-0.1 % Proline, 250 ml

Yeast nitrogen base without amino acid and ammonium sulphate (BD) (1 %)	1.675 g
Dropout mix (0.2 %) (Table 2.5)	0.5 g
D-Glucose (2 %)	5 g
Proline (0.1 %)	0.25 g

The pH was adjusted to 5.5-6.0 by adding 2 ml of 1 M NaOH slowly with stirring. The required amino acids were then added into the media based on the selection required per strain (Table 2.6). Media was then filtered and stored at RT.

2.5 Bacterial and yeast culture conditions

2.5.1 Bacterial culture conditions

LB agar plates with/without selection were cultured at 37 ℃ overnight (B series, Binder incubator, Mason Technology) to grow single colonies. For liquid culturing, LB and 2YT, a single colony was picked from the overnight plate and inoculated into 5 ml of the appropriate bacterial media. Liquid media was incubated at 37 ℃ overnight or for a specific time with 200 rpm shaking (Innova 44, Orbital Shaker, New Brunswick Scientific, UK).

2.5.2 Yeast culture conditions

Agar plates were incubated at 30 ℃ for 2-3 days (BD series Binder incubator, Mason Technology) to get a single colony. For liquid culturing, a single colony was picked from the agar plate and inoculated into 5 ml of the appropriate yeast media. Liquid media was incubated at 30 ℃ overnight with 200 rpm shaking (Innova 44, Orbital

Shaker, New Brunswick Scientific, UK). Overnight cultures were then ready for further treatments.

2.6 Preparation and transformation of *E.coli* competent cells

The *E.coli* transformation used in this study is described by (Chung & Miller 1988) with minor modifications.

2.6.1 Solutions

TSB (Transformation stock buffer), 10 ml

50 % PEG (w/v)	2 ml to get a final concentration of 10 % (w/v)
DMSO	50 µl to get a final concentration of 0.5 % (v/v)
50 % Glycerol (v/v)	2 ml to get a final concentration of 10 % (v/v)
1 M $MgCl_2$ and $MgSO_4$	100 µl to get a final concentration of 10 mM
LB	5.85 ml to adjust a final volume of 10 ml

With the exception of DMSO, the other solutions were autoclaved before use.

5×KCM (K^+-Ca^{2+}-Mg^{2+} enhancer), 50 ml

KCl	1.86 g to get a final concentration of 0.5 M
$CaCl_2 \cdot 2H_2O$	1.103 g to get a final concentration of 0.15 M
$MgCl \cdot 6H_2O$	2.55 g to get a final concentration of 0.25 M

The above components were dissolved in deionized water to get a final volume of 50 ml. The KCM solution was then sterilised using a 0.2 µm filter and aliquoted into a 1.5 ml sterile Eppendorf tubes and stored at -20 °C.

2.6.2 Preparation of competent *E.coli* cells

LB (5 ml) was inoculated with a single colony and cultured overnight at 37 °C, 200 rpm. The next day, 500 µl overnight culture was inoculated into 50 ml of fresh LB media (1:100) and continued to grow at 37 °C, 200 rpm until an OD_{600} of 0.4-0.6 was achieved (This process normally needs about 3 h). Cells were harvested by centrifugation at 4000 rpm for 10 min at 4 °C (Centrifuge 5810R, Eppendorf). The supernatant was removed as complete as possible. Cells were resuspended into 5 ml of TSB solution

(culture:TSB=10:1) and kept on ice for 10 min. Competent cells were then transferred to pre-chilled 1.5ml Eppendorf tubes in 100 µl aliquots, and stored at -70 °C.

2.6.3 Transformation of competent *E.coli* cells

DNA 0.5-2 µl was mixed with 10 µl 5×KCM solution and adjusted to 50 µl with sterile water. DNA mixture was vortexed briefly and kept on ice. Competent cells were defrosted rapidly and 50 µl of competent cells were then applied to the DNA mixture. The Eppendorf tube with DNA and competent cells were incubated for 20 min on ice and another 10 min at RT. After incubation, 500 µl of fresh LB was added into the Eppendorf tube and incubated at 37 °C static for 45-60 min. Cells were collected by a brief centrifugation at 5000 rpm, 1 min. Around 450 µl supernatant was discarded and cells were resuspended into the rest of the supernatant. Cells were then spread on a plate with appropriated selections. Water and a positive vector were employed as controls. Plates were cultured at 37 °C static overnight.

2.6.4 Fast transformation of competent *E.coli* cells

Fast transformation only can be used to transform highly effective plasmid DNA. DNA (0.1-0.5 µl) was mixed with 10 µl 5×KCM solution and then adjusted to 50 µl with sterile water. Vortexed DNA mixture briefly and kept on ice. Defrosted competent cells rapidly and applied 50 µl competent cells into DNA mixture. The Eppendorf tube with DNA and competent cells were then incubated for 5 min on ice. After incubation, cells were immediately spread on selection plates and then incubated at 37 °C overnight.

2.7 Preparation and transformation of yeast competent cells

The yeast transformation method used in this study is described by (Gietz & Schiestl 2008) with minor modifications.

2.7.1 Solutions

1 M LiAc (Lithium acetate):	5.1 g LiAc dissolved into deionized water to 50 ml finally.
100 mM LiAc:	1 ml of 1 M LiAc applied into 9 ml deionized water.

50 % PEG (w/v)	25 g PEG-6000 dissolved into deionized water to 50 ml final volume.
10 mM Tris/ 1mM EDTA, pH 7.5	23.6 mg Tris base, 127 mg Tris-HCl and 2.92 g EDTA were dissolved into deionized water, and the final volume was adjusted to 100 ml.
Carrier DNA (2 mg/ml)	200 mg of salmon sperm DNA was dissolved into 10 mM Tris/ 1mM EDTA buffer to get a final volume of 100 ml.
Plasmid DNA	The DNA concentration was calculated by a Nanodrop spectrophotometer (Mason Technology), and then diluted 1 μg of total DNA into 50 μl sterile water.

With the exception of carrier DNA and plasmid DNA, the other solutions were autoclaved and stored at RT. Carrier DNA was dissolved and denatured by incubating at 100 °C and then aliquoted into Eppendorf tubes. The aliquots were stored at -20 °C.

2.7.2 Preparation of yeast competent cells

A single colony was inoculated into 5 ml of the appropriate media and cultured overnight at 30°C, 200 rpm. The next day, yeast cultures were diluted and recultured into 50 ml of same media starting at OD_{600} of 0.2. After OD_{600} reached 0.6-0.8, cells were harvested by centrifugation at 2500 rpm for 10 min. Supernatant was discarded and cell pellet washed with 25 ml of sterile dH_2O and centrifuged again. The supernatant was removed as complete as possible. The cell pellet was resuspended in 1 ml of 100 mM LiAc and stood on ice for several minutes. Cells were collected by a table top centrifuge (Centrifuge 5415D, Eppendorf AG, Hamburg) at 13200 rpm for several seconds and resuspended in 500 μl of 100 mM LiAc. The competent yeast cells could be used immediately or stored at 4 °C for 5-7 days.

2.7.3 Transformation of yeast competent cells

50% PEG	240 μl
1M LiAc	36 μl
Carrier DNA	25 μl
Plasmid DNA	50 μl

50 µl competent yeast cells were aliquoted into 1.5ml sterile tubes. Then the competent cells were pelleted at 13200 rpm for several seconds to remove LiAc solution. After that, the solutions listed above were added to the top of the cell pellet in order. DNA mixture was vortexed briefly and incubated for 30 min at 30 °C. After incubation, the mixture was heat shocked at 42 °C for 25 min. Cells were collected by a brief centrifugation at 13000 rpm, 15 s. Supernatant was discarded and cells were resuspended into 150 µl of sterile water. Cells were plated on plates with the appropriate selection. Water and a positive vector (such as pRS315 for Lue selection) were employed as controls. Plates were incubated at 30 °C for 2-3 days.

2.8 DNA recombination

In this study, DNA recombination was used to introduce 6×His tag or flag tag into pC210 plasmids and to subclone specific gene or mutation into the other vectors.

2.8.1 PCR (Polymerase Chain Reaction)

The PCR was performed following the standard manual of Q5 High-Fidelity DNA Polymerase (NEB) with minor modifications. PCR reactions were performed in a PTC-200 Peltier Thermal Cycler (MJ Research) described as following, primers have been listed in Table 2.9.

PCR Mixture (25 µl)	**PCR Cycle**
5×reaction buffer 5 µl	Step1: 98 °C 1 min
Template DNA 0.5 µl (100-800 ng/µl)	Step2: 98 °C 30 s
Forward primer 1 µl (10 ng/µl)	Step3: 55 °C 30 s
Reverse primer 1 µl (10 ng/µl)	Step4: 72 °C 2 Kb per min
10 µM dNTP mix 0.5 µl	Step5: go to step2, 35 times
Q5 High-Fidelity DNA polymerase 0.5 µl	Step6: 72 °C 5 min
ddH_2O 16.5 µl	Step7: 4 °C hold

Table 2.9. Primers of cloning

Primer	Sequence
SA1-Flag-Ned1-F	5'GAATTCCATATG*GACTACAAGGACGATGATGACAAG*ATGTCAAAAGCTGTCGGTAT 3'
SA1-6His-Ned1-F	5'GAATTCCATATG*CATCACCATCACCATCAC*ATGTCAAAAGCTGTCGGTAT 3'
SA1-Nde1-F	5' TTTATACATATGTCAAAAGCTGTCGGTATTGATT 3'
SA1-Sph1-R	5' GACAAAGCATGCTTAATCAACTTCTTCAACG 3'
*^F-2Ssa1-BamH1	5' GGGAATTCGGATCCAAAGCTGTCGGTAT 3'
*R-642Ssa1-Xho1	5' CCGCTCGAGTTAATCAACTTCTTCAAC 3'

*primers were used to subclone *SSA1* (2-642) to pET28a-Smt3 vector. ^ *SSA1* forward primer was designed from the third residue since there is an extra Serine left after Ulp1cleaving (Zheng et al. 2012) and the second residue is Serine in Ssa1. The rest was used to recombine *SSA1* or its mutations into pC210 vector.

2.8.2 DNA separation by agarose gel

0.8 % or 1 % agarose gel was used in this study by adding 0.24 g or 0.3 g of agarose to 30 ml of 1×TAE buffer. 50×TAE buffer was prepared by dissolved 242 g of tris base, 100 ml of 0.5 EDTA solution and 57.1 ml glacial acetic acid with deionized water to get a final volume of 1 L (pH 8.0). Agarose solution was microwaved for 1-2 min until dissolved completely. Agarose gel was allowed to cool to 50 °C before supplementing with 2 µl of ethidium bromide. The gel was poured in a gel castle with a comb. After setting, DNA samples were loaded containing loading buffer and run in 1×TAE buffer at 100 V for 30-60 min. The gel was then visualised using Snygene INGenius BioImager (Mason Technology).

2.8.3 PCR purification

PCR product was purified using the PCR Purification kit (Qiagen) to remove the influence of PCR reaction buffers to further process. The procedure followed the standard manual exactly with the only exception of the final flow through being placed back onto the column and centrifuged again to increase DNA concentration.

2.8.4 Double restriction digestion

All restriction enzymes were purchased from NEB. A typical double restriction digestion was performed as following:

Digestion Mixture (50 µl)

10×reaction buffer	5 µl
restriction enzyme A	2 µl
restriction enzyme B	2 µl
Plasmid DNA or PCR products (1.5 µg DNA totally)	41 µl

The reaction system was incubated at 37 °C for 3 h. If restriction enzymes used in one system have different incubation temperatures, one of the two restriction enzymes was added and incubated at its optimal temperature. After incubation of first restriction enzyme, the second one was then added and incubated for another 2-3 h.

2.8.5 Gel Extraction

In order to isolation target DNA fragments effectively, 1 % agarose gel was run at 80 V for 1 h in this study. After running the gel, gel extraction was carried out following the manual of the Gel Extraction kit (Qiagen) with minor modification. Briefly, DNA fragments were excised from gel under a UV Trans-illuminator. Excised gel was dissolved in buffer for at least 15 min at 55 °C. To promote the binding activity of DNA fragments with the column, dissolved DNA-gel solution was placed on ice for 1-2 min before binding with the column, and the FT of DNA-gel mixture was replaced back onto the column and centrifuged again to increase DNA binding. After washing the gel was dissolved in buffer once and wash buffer twice, the column was centrifuged for another 2 min to remove any residual buffer completely. Finally, DNA fragments were eluted in 30 µl of deionized water (replaced back once and incubated at 55 ℃ for 1-2 min if required). DNA elution was quantified and stored at -20 ℃.

2.8.6 T4 ligation of vector and target DNA

T4 ligase used in this study was purchased from NEB. A typical T4 ligase system was prepared as following. The reaction system was incubated at 16 °C overnight in a PTC-200 Peltier Thermal Cycler (MJ Research).

T4 ligation system (10 µl)

10×reaction buffer	1 µl
T4 ligase	0.5 µl
vector insert	8.5 µl (vector: insert=1:3~10, *molar ratio)

*molar ratio was calculated according to the rough MW of DNA fragment and the concentration of DNA fragment.

2.9 Site-directed mutagenesis (SDM)

QuickChange Site-Directed Mutagenesis Kit (Agilent) was used in this study to introduce mutations in plasmids. The SDM performed following the standard manual with minor modifications. PCR reaction was performed in a Thermal Cycler as described below; primers have been listed in Table 2.10.

PCR Mixture (25 µl)	**PCR Cycle**
10×reaction buffer 2.5 µl	Step1: 95 °C 1 min
Plasmid DNA 0.5 µl (80 ng/µl)	Step2: 95 °C 30 s
Forward primer 1 µl (10 ng/µl)	Step3: 55 °C 1 min
Reverse primer 1 µl (10 ng/µl)	Step4: 68 °C 1Kb per min
dNTP mix 0.5 µl	Step5: go to step2, 16 times
Pfu Turbo DNA polymerase 0.5 µl	Step6: 68 °C 10 min
ddH_2O 19 µl	Step7: 4 °C hold

After PCR reaction, 1 µl *Dpn*1 restriction enzyme was added into 25 µl PCR product directly and then incubated at 37 °C for 2 h to digest the template DNA.The PCR product (5 µl) was transformed into the competent *E.coli* strain Top10. Two colonies were picked randomly from the plates next day and the plasmid DNA was extracted as

described in the following section. The concentration and quality of plasmids were calculated by the Nanodrop Spectrophotometer and agarose gel. Plasmid DNA was sent to LGC for sequencing.

Table 2.10. PCR primers for SDM

Primer	Sequence
A394V	F 5’ TGTCGTTCCATTATCCTTGGGTATTGAAACT 3’
	R 5’ ATGGAACGACATCCAACAACAATAGATCTTGA 3’
P433S	F 5’ ACCAATCAGGTGTCTTGATTCAAGTCTTTG 3’
	R 5’ ACACCTGATTGGTTATCAGCATAAGTGGAA 3’
V477I	F 5’ CGATATCGACTCTAACGGTATTTTGAATGTTTCC 3’
	R 5’ GTCGATATCGGAAGTGACTTCAATTTGTGGG 3’
F475S	F 5’ AGTCACTTCCGATGTCGACTCTAACGGTATTTTG 3’
	R 5’ GTCGACATCGGAAGTGACTTCAATTTGTGGG 3’
F475W	F 5' TTGAAGTCACTTGGGATGTCGACTCTAACGGTATT 3'
	R 5' GTCGACATCCCAAGTGACTTCAATTTGTGGGACAC 3'
F475Y	F 5' TTGAAGTCACTTACGATGTCGACTCTAACGGTATT 3'
	R 5' GTCGACATCGTAAGTGACTTCAATTTGTGGGA 3'
F475C	F 5' TTGAAGTCACTTGCGATGTCGACTCTAACGGTATT 3'
	R 5' GTCGACATCGCAAGTGACTTCAATTTGTGGGA 3'
F475A	F 5' TTGAAGTCACTGCCGATGTCGACTCTAACGGTATT 3'
	R 5' GTCGACATCGGCAGTGACTTCAATTTGTGGGA 3'
L483W	F 5’ GTATTTGGAATGTTTCCGCCGTCGAAAAGGGT 3’
	R 5’ CGGAAACATTCCAAATACCGTTAGAGTCGACATCG 3’
L483A	F 5’ GTATTGCGAATGTTTCCGCCGTCGAAAAGGGT 3’
	R 5’ CGGAAACATTCGCAATACCGTTAGAGTCGACATCG 3’
L483H	F 5’ GGTATTCATAATGTTTCCGCCGTCGAAAAGGGT 3’
	R 5’ GCGGAAACATTATGAATACCGTTAGAGTCGACATCG 3’
V393A	F 5’ GTTGTTGGATGCCGCTCCATTATCCTTGGGTATTG 3’
	R 5’ GATAATGGAGCGGCATCCAACAACAATAGATCTTGAGTCT 3’
I417A	F 5’ ACTCTACCGCTCCAACAAAGAAGTCCGAGATCTTTTCC 3’
	R 5’ CTTTGTTGGAGCGGTAGAGTTTCTTGGAATCAACTTGG 3’

D476A	F 5’ GAAGTCACTTTCGCTGTCGACTCTAACGGTATTTTGAATGT 3’
	R 5’ GAGTCGACAGCGAAAGTGACTTCAATTTGTGGGACAC 3’
D478A	F 5’ CACTTTCGATGTCGCCTCTAACGGTATTTTGAATGTTTCC 3’
	R 5’ CCGTTAGAGGCGACATCGAAAGTGACTTCAATTTGTGGGA 3’
N480A	F 5’ ATGTCGACTCTGCCGGTATTTTGAATGTTTCCGCCG 3’
	R 5’ TCAAAATACCGGCAGAGTCGACATCGAAAGTGACTTC 3’
I482A	F 5’ CTCTAACGGTGCTTTGAATGTTTCCGCCGTCGA 3’
	R 5’ GGAAACATTCAAAGCACCGTTAGAGTCGACATCGAAAG 3’
N484A	F 5’ CTCTAACGGTATTTTGGCTGTTTCCGCCGTCGA 3’
	R 5’ GGCGGAAACAGCCAAAATACCGTTAGAGTCGACATC 3’
D503A	F 5’ CTATTACCAACGCCAAGGGTAGATTGTCCAAGGAAGATATC 3’
	R 5’ GGACAATCTACCCTTGGCGTTGGTAATAGTGATCTTGTTAG 3’
K504A	F 5’ CTATTACCAACGACGCGGGTAGATTGTCCAAGGAAGATATC 3’
	R 5’ GGACAATCTACCCGCGTCGTTGGTAATAGTGATCTTGTTAG 3’
I512A	F 5’ CCAAGGAAGATGCCGAAAAGATGGTTGCTGAAGC 3’
	R 5’ CCATCTTTTCGGCATCTTCCTTGGACAATCTACCCTT 3’
I533A	F 5’ GAATCTCAAAGAGCTGCTTCCAAGAACCAATTGGAATCC 3’
	R 5’ TCTTGGAAGCAGCTCTTTGAGATTCCTTTTCATCTTCTTC 3’
K106R	F 5’ CAAGTTGAATTTAGGGGTGAAACCAAGAACTTTACC 3’
	R 5’ CTTGGTTTCACCCCTAAATTCAACTTGAATTTGTG 3’
K523R	F 5’ GCCGAAAAATTCAGGGAAGAAGATGAAAAGGAATCTCA 3’
	R 5’ CATCTTCTTCCCTGAATTTTTCGGCTTCAGCAAC 3’
F478S	F 5’ TTGAAGTCACTTCTGACATTGATGCCAATGGTATACTC 3’
	5’ CATCAATGTCAGAAGTGACTTCAATCTGAGGAACACC 3’
K88Q	5’ CAGTCTGATATGCAACATTGGCCCTTTATGGTGGTG 3’
	R 5’ GCCAATGTTGCATATCAGACTGGACAACAGCATCA 3’
K187Q	F 5’ CGGCTTAGACCAAAAGGTTGGAGCAGAAAGAAACG 3’
	R 5’ GCTCCAACCTTTTGGTCTAAGCCGTAAGCAATAGCAG 3’
K357Q	F 5’ TCTTCAATGGACAAGAACTGAATAAGAGCATCAACCCTG 3’
	R 5’ ATTCAGTTCTTGTCCATTGAAGAAGTCTTGGAGAAGCTTC 3’
K567Q	F 5’ ACGATGAGGACCAACAGAAGATTCTGGACAAGTGTAAT 3’
	R 5’ CAGAATCTTCTGTTGGTCCTCATCGTTAATCTTGCCTT 3’

K88R	F 5’ CAGTCTGATATGAGACATTGGCCCTTTATGGTGGTG 3’
	R 5’ GCCAATGTCTCATATCAGACTGGACAACAGCATCA 3’
K187R	F 5’ CGGCTTAGACAGAAAGGTTGGAGCAGAAAGAAACGTG 3’
	R 5’ GCTCCAACCTTTCTGTCTAAGCCGTAAGCAATAGCAG 3’
K357R	F 5’ TCTTCAATGGAAGAGAACTGAATAAGAGCATCAACCCTG 3’
	R 5’ ATTCAGTTCTCTTCCATTGAAGAAGTCTTGGAGAAGCTTC 3’
K567R	F 5’ ACGATGAGGACAGACAGAAGATTCTGGACAAGTGTAAT 3’
	R 5’ CAGAATCTTCTGTCTGTCCTCATCGTTAATCTTGCCTT 3’

The codons underlined are the sites of SDM. F represents forward primer. R represents reverse primer.

2.10 Extraction of plasmid DNA from *E.coli*

Extraction of plasmid DNA was performed using the miniprep kit (Qiagen) following the manual with minor modification. Briefly, the overnight culture was centrifuged to collect cells at 4000 rpm for 5 min. The cell pellet was resuspended in 250 µl resuspension buffer with RNase. Then 250 µl of lysis buffer was applied into the same Eppendorf tube and incubated for less than 5 min at RT. After incubation, 350 µl of neutralising buffer was added into the Eppendorf tube to precipitate proteins and genome DNA. The supernatant with plasmid DNA was separated from proteins by centrifugation for 10 mins at 13000 rpm. The supernatant was then transferred into a DNA binding column and centrifuged again at 13000 rpm, 1 min. Flow-through (FT) was discarded and the column was washed with 750 µl of wash buffer containing 70 % ethanol twice. After washing, the column was centrifuged for another 2 min to remove wash buffer completely. Finally, plasmid DNA was eluted in 50 µl of elution buffer and stored at -20 ℃.

2.11 DNA sequencing

DNA sequencing sample was prepared by mixing 4 µl of plasmid, 5 µl of primer and 6 µl of sterile deionized water together. The amount of plasmid in 4 µl is approximately 1000 ng-2000 ng. The concentration of primer is around 6 pmol/µl. Roughly, 10 µl of 100 µM stock primer was diluted into 160 µl deionized water to prepare sequencing primer. Then the mixture was sent to LGC (https://shop.lgcgenomics.com/) and results

were analysed by NCBI blast tool (http://blast.ncbi.nlm.nih.gov/Blast.cgi). The sequencing primers used in this study were listed in Table 2.11.

Table 2.11. DNA sequencing primer

Primer	Oligonucleotide
*Sp1-New-R	5' CTATCCGAAAAGGAAGACATC 3' (binding position after *Sph*1 site)
*Sp1-R	5' CTCATTATACCCAGATCA 3'(binding position before *Sph*1 site)
*Sp2-R	5' CTTTTCGACGGCGGAAAC 3'
*Sp3-R	5' CATCGACTTGAGATTTG3'
*Sp4-R	5' CAGCGTCATTGACCTTGGC 3'
*Sp5-SA2Prom-F	5' TATATAAGCCGCAATTGGG 3' (binding with *SSA2* promotor)
*Sp6-F	5' GGTCTTGGGTAAGATG 3'
*Sp7-F	5' CAGATCTACTTTGGACCC 3'
*Sp8-F	5' CACAAATTGAAGTCAC 3'
^SUMO-F	5´ AGATTCTTGTACGACGGTATTAG 3´
^T7-R	5´ TAGTTATTGCTCAGCGGTGG 3´
$^{+}$CMV-F	5' CGGTGGGAGGTCTATATAAGC 3'
$^{+}$T7tag-F	5' TGGTATGGCTAGCATGACTGG 3'
$^{+}$Hsc70-FM	5' CTCAGCGTCAGGCTACCAAAG 3'
$^{+}$bGH-R	5' GTCAAGGAAGGCACGGGG 3'

Primers with * were used to sequence pC210 plasmid. ^ was used for pET28a-Smt3, *E.coli* expression vector. $^{+}$ was suitable to sequence HaloTag-*HSC70*.

2.12 Plasmid shuffle technique

In order to express the Ssa1 mutation as the only Ssa source in cells, the plasmid shuffle technique was performed as a previous description (Loovers et al. 2007). The yeast strains containing pRDW10 with the uracil marker (*URA3*) and *SSA1* was used to prepare competent cells. Then another plasmid with Ssa1 mutant was transformed into competent cell and grew on selection media. After 2-3 days incubation, four colonies were picked randomly and streaked onto SC media with 5-FOA which is toxic to *URA3* cells and hence selects for cells that lost the pRDW10 vector. Finally, colonies grew on SC-5-FOA were ones with Ssa1 mutation as only Ssa source and restreaked onto YPD.

2.13 Isolation of yeast genomic DNA

The solutions used in genomic DNA isolation were listed following:

1 M Sorbitol/100 mM EDTA	9.11 g Sorbitol and 1.46 g EDTA was dissolved in deionized water to a final volume of 50 ml. pH was adjusted to 8.0 and stored at RT.
5 mg/ml Zymolase	50 mg Zymolase was dissolved in deionized water to a total volume of 10 ml and stored at -20 ^{0}C.
1 M Tris base/100 mM EDTA	6.05g Tris base and 1.46 g EDTA was dissolved in deionized water to a 50 ml volume and stored at 4 ^{0}C.
10 % (w/v) SDS	5 g SDS was dissolved in deionized water to a total volume of 50 ml and stored at RT.
5 M Potassium Acetate (KAc)	24.54 g KAc was dissolved in deionized water to a total volume of 50 ml and stored at RT.

S. cerevisiae strain was cultured in 2 ml YPD at 30 ^{0}C with shaking overnight. Cells were harvested at 2500 rpm for 5 min, washed with 5 ml deionized water and pelleted again. Cells were resuspended in 150 µl of 1 M sorbitol/100 mM EDTA and transformed into a sterile 1.5 ml Eppendorf tube. 12 µl of 5 mg/ml zymolyase was added to the tube and incubated for 1 h at 37 ^{0}C to weaken the cell wall. Cells were collected at 13000 rpm for several seconds and resuspended in 150 µl of 1 M Tris/100 mM EDTA. 10 µl of 10 % SDS solution was added and incubated mixture at 65 ^{0}C for 0.5 h. KAc (60 µl, 5 M) was added and subsequently incubated on ice for 1 h. Proteins were removed by centrifuge at 13000 rpm for 10 min and supernatant was transferred to a new Eppendorf tube. Isopropanol (195 µl) was added and then incubated at RT for 5 min to precipitate DNA. The sample was centrifuged at 13000 rpm for 1 min to pellet DNA. The supernatant was removed and the pellet was dried briefly and dissolved in 30-50 µl of dH_2O. Genomic DNA was stored at -20 ^{0}C.

2.14 Deletion of genes in yeast

BY4741 knockout strains used in this study were ordered from EUROSCARF (http://www.euroscarf.de/search.php?name=Order). MH272 knockout strains were made in this study basing on homologous recombination technique. Briefly, the

knockout cassette was created by PCR from the BY4741 knockout strain directly. There were around 100-500 bp upstream (+) and downstream (-) regions flanked *KanMX*. The knockout primers were designed as following:

HAT1-KO-F	5' TGGCAAATTCTACCAGTCGTTCTTGGAATACC 3'	+400 bp
HAT1-KO-R	5' CGCTTTAGAACCGCTACCATGGTGTGTCA 3'	-450 bp
RPD3-KO-F	5' CTGAACTGAATCATTATGAAGCGGTGAGAGC 3'	+300 bp
RPD3-KO-R	5' GCTTTATCAACAGCGGTGGGACGAGACG 3’	-300 bp
RPD3-KO-F-2	5' ATGCTCTCTGCTCAGATGCAATGCTTAACGCC 3'	+500 bp
RPD3-KO-R-2	5' TGCAATTAGAAGAGAGTGAATCAGATGAGGATAGGG 3’	-500 bp
RPD3-KO-F-3	5' TTTATTTACTTACCCTCCCCGGCTCATAGTATC 3'	+170 bp
RPD3-KO-R-3	5' TTCGAAACGTATGGGACGCGGTTGATG 3’	-190 bp

The knockout cassette with *KanMX* and overhangs was amplified from genomic DNA of BY4741 knockout strains by PCR. The purified PCR product was then transformed into MH272 competent cells. Transformed yeast cells were incubated in 2 ml of fresh YPD overnight with shaking. The next day, cells were collected by briefly centrifuging and plated on YPD-G418 media for 2-3 days incubation at 30 °C. Colony PCR was used to test positive knockout.

2.15 Colony PCR

Colony PCR is an effective way to test positive colony after subcloning and knockout.

PCR Mixture (25 µl)

5× MyTaq reaction buffer 5 µl

ddH_2O with cells 1 µl

Forward primer 1 µl (10 ng/µl)

Reverse primer 1 µl (10 ng/µl)

MyTaq DNA polymerase 0.5 µl

ddH_2O 16.5 µl

PCR Cycle

Step1: 95 °C 5 min

Step2: 95 °C 45 s

Step3: 55 °C 30 s

Step4: 72 °C 1 Kb per min

Step5: go to step2, 35 times

Step6: 72 °C 10 min

Step7: 4 °C hold

2.15.1 Bacteria colony PCR

A single colony was picked from the agar plate and transferred into 10 µl of sterile ddH_2O as the DNA template. The corresponding DNA sequencing primers were used for colony PCR. Bacteria colony PCR was carried out as above and a 0.8 % agarose gel was used to run and visualise the PCR product.

2.15.2 Yeast colony PCR

A single yeast colony was picked from a freshly incubated agar plate and transferred to 10 µl of sterile ddH_2O as the DNA template. In order to increase the genomic DNA yield, 10 µl of sterile ddH_2O can be used instead of 20 mM NaOH and 0.2 % SDS solution. Primers were used to the amplify knockout cassette (Section 2.13) and to bind with *KanMX* (Table 2.12). PCR was carried out as above and a 0.8 % agarose gel was used to run and visualise PCR product.

Table 2.12. Primers of knockout test

Primer	Sequence	Size
KanMX4-R	5'GTCTGACCATCTCATCTGTAACATCAT TGGCAAC 3'	Around 587bp from start codon
KanMX4-F	5'TTCTCACCGGATTCAGTCGTCACTCAT GG 3'	Around 490bp from stop codon

2.16 Yeast growth assays

2.16.1 Thermotolerance assay

Mild heat shock

Single colonies were inoculated and cultured in 5 ml of YPD or SC selective media at 30 °C, 200 rpm overnight. The next morning, yeast cultures were diluted into 6 ml of same media to reach an OD_{600} of 0.2. Cells were cultured reaching an OD_{600} of 0.5. And then a 1/5 serial dilution was carried out for each strain in a 96-well plate under sterile conditions. Briefly, 200 µl of culture was added into A1 of the plate. A2-A6 was filled with 160 µl of fresh media. Dispensed 40 µl of cultures from A1 to A6 in order. Following the serial dilution, cells were plated onto YPD plates or other appropriate selective plates using a flamed cell replicator under sterile conditions. Finally, plates were incubated in 30 °C, 37 °C and 39 °C incubators respectively for 2 days.

Extreme temperature

Single colonies were inoculated and cultured in 5 ml of YPD or SC selective media at 30 °C, 200 rpm overnight. The next day, yeast cultures were diluted in 7 ml of the same media to reach an OD_{600} of 0.2. Cells were cultured until reaching an OD_{600} of 0.5. A 1 ml aliquot was immediately transferred to a 1.5 ml Eppendorf tube and placed on ice. Subsequently, 0.5 ml volumes of aliquots were maintained at 47 ºC, 200 rpm shaking for 5, 10, 15, 20, 25, 30 and 40 min respectively. As described above, a 1/5 serial dilution of the aliquots of each time point were carried out. Finally, YPD plates with spotted cells were incubated in 30 °C incubator for 2 days.

2.16.2 Acquired thermotolerance assay

Single colonies were inoculated and cultured in 5 ml of YPD or SC selective media at 30 °C, 200 rpm overnight. The next day, yeast cultures were diluted in 7 ml of the same media to reach an OD_{600} of 0.2. Cells were cultured until reaching an OD_{600} of 0.4. A 1 ml aliquot was immediately transferred to a 1.5 ml Eppendorf tube and placed on ice. The rest of the culture was heat shocked at 39 ℃ with shaking for 1 h to induce Hsp104. Subsequently, 0.5 ml volumes of cell aliquots were maintained at 47 ºC (G402 background) or 50 ºC (MH272 background) shaking incubator at 200 rpm for 0, 10, 20, 30 and 40 min respectively. As described above, a 1/5 serial dilution of the aliquots of each time point were carried out. Finally, YPD and YPD-3 mM Gdn-HCl plates with spotted cells were incubated in 30 °C incubator for 2 days.

2.16.3 Growth assay under oxidant stress

H_2O_2 was used as an oxidative stress inducer in this study. Single colonies were inoculated and cultured in 5 ml of YPD or SC selective media at 30 °C, 200 rpm overnight. The next day, yeast cultures were diluted in 7 ml of the same media to reach an OD_{600} of 0.2. Cells were cultured until reaching an OD_{600} of 0.5. A 1/5 serial dilution was carried out for each strain in a 96-well plate under sterile conditions. Following serial dilution, cells were spotted onto SC-H_2O_2 (0 mM, 1 mM, 2 mM, 3 mM, 4 mM and 5 mM) using a cell replicator under sterile conditions. Finally, plates were incubated at 30 °C for 2 days.

2.16.4 Growth assay under cell well damaging agent

SDS was used as cell well damaging agent in this study. Single yeast colonies were inoculated and cultured in 5 ml of YPD at 30 °C with shaking overnight. The next morning, the yeast cultures were diluted in 6 ml of fresh media at an OD_{600} of 0.2. Cells were cultured until reaching an OD_{600} of 0.5. A 1/5 serial dilution was carried out for each strain in a 96-well plate under sterile conditions. Following serial dilution, cells were plated onto YPD with different concentration of SDS (0, 0.005 %, 0.01 %, 0.015 % and 0.02 %) using a cell replicator under sterile conditions. Finally, plates were incubated in a 30 °C incubator for 2 days.

2.17 Luciferase refolding assay

Luciferase refolding was employed to calculate the refolding activity of Hsp70 machinery as described by (Parsell et al. 1994) with minor modification. Prior to the assay, the pDCM90 plasmid was transformed into yeast strains. Strains containing pDCM90 were grown in 5 ml of SC media without uracil (SC-URA) at 30 ºC shaking overnight and three biological replicates for each strain were prepared. Cultures were diluted in 7 ml of fresh SC-URA to an OD_{600} of 0.2. Diluted cultures were incubated at 37 ºC shaking for 0.5 h to induce the expression of heat shock proteins. After 37 ºC incubation, the luciferase activity of each strain was measured in triplicate for each of the three biological replicates by immediately adding 200 µl of culture to 10 µl of decanal (Sigma) in 5 ml rohren tubes (Starstedt) in a FB 12 Luminometer (Berthold Detection Systems) at RT. This luciferase activity was used as 100 % activity. The rest of cells were incubated at 45 ºC with shaking for 1 h to denature luciferase. The final concentration of 10 µg/ml Cycloheximide (Sigma) was added into the culture to prevent protein synthesis after 50 min incubation at 45 ºC. Following, a further 10 min incubation was continued at 45 ºC with shaking. After 1 h denaturation, luciferase activity was measured as mentioned above. 1 ml volumes of cell aliquots were incubated at 25 ºC for 15, 30, 45 and 60 min respectively to refold luciferase. Luciferase refolding activity was measured as described for each time point. Finally, the luciferase refolding activity of the Hsp70 machinery at each time point was calculated as a percentage of the 100 % activity.

2.18 Protein extraction of yeast cells

Yeast strains were cultured overnight in 5 ml YPD or selective media. The next morning, cells were diluted in 25 ml of same media to an OD_{600} of 0.2 and incubated until an OD_{600} of 0.6-0.8 was reached. Cells were harvested by centrifugation at 4 ºC (10 min, 2500 rpm). Cells were washed by sterile dH_2O and pelleted again by centrifugation. Pellets were resuspended in 750 µl Y cell lysis reagent (Sigma, C4482) and transferred to pre-chilled 2 ml microcentrifuge tubes (Sigma). Y cell lysis reagent was supplemented with the appropriate Protease Inhibitor Cocktail (Sigma, P8215, 3 µl/sample normally) and 10 mM DTT. 0.5 mm soda lime glass beads were added into tubes and then additional lysis reagent was added to remove as much air as possible. Cells were then bead-beaten using a mini-beater (Biospec products) at frequency 30 Hz for 20 s and chilled on ice for at least 1 min. This was repeated 10 times and tubes were then centrifuged at 13000 rpm for 10 min at 4 ºC. Supernatants were centrifuged again at 4 ºC, 13000 rpm for 10 min to obtain clarified lysates. Finally, supernatants were transferred to pre-chilled 1.5 ml microfuge tubes and stored at -20 ºC (long-term storage at -70 ºC).

2.19 Protein assay

In this study, two kinds of protein assay (Bradford assay and BCA assay) were employed to measure the protein concentration. The former was normally used to measure the concentration of cell lysate. BCA can be used to measure purified protein and cell lysate with a low concentration of DTT.

2.19.1 Bradford assay

BSA standards were prepared as descriptions in Table 2.13. Standards and samples were triplicated and quadruplicated to decrease the error. 2 µl of protein/standard sample was applied into a well of the 96-well plate and then 200 µl of Bradford reagent (Bio-rad) was mixed with sample thoroughly. The 96-well plate was incubated at RT for 30 min. After incubation, the plate was measured OD_{595} on a SpectraMax M3e (Molecular Devices, USA).

Table 2.13. Preparation of diluted BSA standards

Concentration (mg/ml)	Volume of source BSA (μl)	Volumes of diluent (μl)
2	40 (2 mg/ml)	0
1.5	45 (2 mg/ml)	15
1	40 (2 mg/ml)	40
0.75	20 (1.5 mg/ml)	20
0.5	40 (1 mg/ml)	40
0.25	40 (0.5mg/ml)	40
0.125	40 (0.25mg/ml)	40
0.025	10 (0.125mg/ml)	40
0	0	40

2.19.2 BCA protein assay

BSA standards were prepared as descriptions in Table 2.13. Standards and samples were triplicated and quadruplicated to decrease the error. 10 μl of protein/standard sample was applied into a well of the 96-well plate and then 200 μl of mixed BCA reagent (buffer A: buffer B=50:1, Thermo) was added to each well. The 96-well plate was incubated at 37 ºC for 30 min. After incubation, the plate was measured OD_{562} on a SpectraMax M3e (Molecular Devices, USA).

2.20 Sodium Dodecyl sulphate-Poly acrylamide gel electrophoresis (SDS-PAGE)

SDS-PAGE was used to separate and test protein in this study according to protein size. The chemical reagents used in this study were purchased from Sigma unless otherwise stated.

2.20.1 Preparation of SDS-PAGE

SDS-PAGE gels 12.5 % and 15 % were prepared in this study using 1 mm Bio-Rad glass plates and 10-well or 15-well combs having at most 44 μl or 26 μl sample capacity respectively. The compositions of running gel and stacking gel have been listed in Tables 2.1 and 2.15 respectively. A 12.5 % gel was used to separate cell lysates and

purified Ssa1 proteins. A 15 % gel was used to check Ssa1 truncation mutants and purified Ydj1. Gels were sealed in a casting frame of glass plates and a Biorad Gel Cassette. The running gel was prepared first as described in Table 2.14 by adding reagents in a 50 ml tube. TEMED can be added just before casting the gel. The mixture was gently mixed several times before being pipetted into the glass-plates cassette to roughly 70 % capacity of glass plates. Finally, 1 ml of 100 % isopropanol or water was layered on top of the running gel to ensure a smooth levelled surface. Isopropanol or water was discarded after the running gel set. Subsequently, the stacking gel was mixed in a fresh tube as described in Table 2.15 and pipetted onto the top of the running gel to 100 % capacity of the plates. A comb was inserted into the stacking gel gently and allowed to set by standing static for 0.5 h. The comb was removed from the gel carefully and was ready for use immediately or stored in 1×running buffer for several days at 4 ºC.

Table 2.14. Composition of running gel

Reagents	Volume for 12.5 % gel	Volume for 15 % gel	Storage
*4× running gel buffer	2.5 ml	2.5 ml	RT
Deionized water	3.3 ml	2.45 ml	RT
Protogel	4.15 ml	5 ml	RT
^10% AP	100 µl	100 µl	-20 ºC
TEMED	10 µl	10 µl	RT

*4× running gel buffer was prepared by dissolving 34.57 g Tris base and 4 g SDS in deionized water to a final volume of 500 ml, pH8.0.

^10 % AP (w/v) was prepared by dissolving 5 g ammonium persulfate in deionized water to a final volume of 50 ml.

Table 2.15. Compositions of stacking gel

Reagents	Volume	Storage
*2× stacking gel buffer	1.25 ml	RT
Deionized water	0.825 ml	RT
Protogel	400 µl	RT
10 % AP	25 µl	-20 ºC
TEMED	2.5 µl	RT

*2× stacking gel buffer was prepared by dissolving 15 g Tris base and 0.2 g SDS in deionized water to a final volume of 500 ml, pH 8.0.

2.20.2 Sample preparation and SDS-PAGE running

The 6×protein sample loading buffer was prepared as described in Table 2.16. An appropriate amount of proteins (10 µg of cell lysates or 5 µg purified protein) were mixed with the required amount of 6× protein sample loading buffer and boiled at 100 °C for 10-20 min in a water bath or digital dry bath. The prepared gels were then assembled in the gel running frames and placed into the electrophoresis tank (Biorad) which was filled with 1× protein running buffer (diluted from 10× protein running buffer, Table 2.16) to an appropriate level. After boiling, protein samples were briefly centrifuged to collect condensates and then loaded into the lanes of the gel. Protein ladder 10-250 kDa was purchased from Fermentas, Life Sciences. The gels were then run in 1× protein running buffer at 100 V for 15-30 min until slim bands can be seen in the gels. Voltage was then increased to 200 V and kept running until bromophenol blue run out of the gels.

Table 2.16. 6× protein loading buffer

Reagents	Volume
SDS	3 g
DTT	0.385 g
Bromophenol blue	3.6 mg
glycerol	30 ml
2× stacking gel buffer	Adjust to 50 ml

Table 2.17. 10× running buffer

Reagents	Amount	Concentration
Tris base	30 g	250 mM
Glycine	144 g	1.92 M
SDS	10 g	1 % (w/v)
dH_2O	Adjust to 1 L, RT storage	

2.20.3 Coomassie blue staining

Following SDS-PAGE, gels can be stained by coomassie brilliant blue (Serva). Briefly, the gel was transferred into a stained box with Coomassie Blue Dye and incubated for 30 min on a shaker.The gel was then destained by shaking in destaining solution. The staining and destaining processes can be done at RT or by microwaving solutions for several seconds to increase efficiency. Coomassie Blue Dye and the destaining solution were prepared as following.

Comassie Blue Dye	30 % Methanol, 10 % Acetic Acid, 0.1 % Comassie brilliant blue and 60 % dH_2O
Destaining solution	10 % Ethanol, 10 % Acetic acid and 80 % dH_2O

2.21 Western blot (WB)

Western blot was used to detect specific proteins in this study. Before using western blot, the cell lysates, protein samples and SDS-PAGE were prepared as mentioned in the corresponding sections.

2.21.1 Solutions for WB

Chemical reagents were purchased from Sigma to prepare WB solutions. Skim milk (Marvel) purchased from supermarket.

10×Transfer buffer	30.3 g Tris base and 144 g glycine dissolved in deionized water to a final volume of 1 L; stored at 4 ºC.
1×Transfer buffer	100 ml 10×transfer buffer, 200 ml methanol and 700 ml deionized water; stored at 4 ºC.
10×TBS, pH 7.5	63.5 g Tris-HCl, 11.8 g Tris base and 87.66 g NaCl dissolved into deionized water to a final volume of 1 L; stored at 4 ºC.
TBST, 0.1 % (v/v)	0.1 ml Tween20 into 100 ml of 1×TBS
Blocking Buffer	5 % skim milk in TBST, eg. 2.5 g skim milk dissolved in a final volume of 50 ml TBST.

2.21.2 Electrotransfer

SDS-PAGE was performed as described in the previous section. Meanwhile, 6 filter papers and a polyvinylidene fluoride (PVDF) membrane cut according to gel size were prepared (normally 7.8×5 cm). PVDF membrane was soaked in pure methanol for 1 min before use. Then, filter papers, PVDF and two pieces of sponge were equilibrated in 1×transfer buffer until use. After running SDS-PAGE, glass plates were separated carefully and the gel was washed in 1×transfer buffer. A transfer case was then created in order as following: the black side of case—sponge—3 filter papers—gel—PVDF—3 filter papers—sponge —the red side of the case. The case was carefully closed and squeezed to make sure that there were no air bubbles between the gel and PVDF membrane, the case were then put in a transfer tank filled with 1×transfer buffer. The PVDF membrane should always be between the gel and positive electrode. The transfer was run at 100V for 1.5 h on ice.

2.21.3 Ponceau S staining

In order to check if the transfer worked well, PVDF membrane can be stained by Ponceau S 2-3 min and then rinsed by dH_2O. Ponceau S can be removed by washing in TBST several times. If protein bands are seen on the PVDF membrane after transfer this step can be skipped.

2.21.4 Blocking and antibody incubations

The membrane was transferred to 5 % skim milk in TBST for 1 h shaking at RT. Primary antibody was diluted in 10 ml of TBST with 5 % skim milk as mentioned in Table 2.18. The PVDF membrane was incubated with the primary antibody overnight shaking at 4 ºC. The next day, the PVDF membrane was washed with 5 ml TBST for 5 min at RT and repeated three times. After washing, the PVDF membrane was incubated in 10 ml of TBST with 5 % skim milk for 10 min. Subsequently, the secondary antibody was supplemented and incubated for 1 h at RT on a shaker. Finally, the membrane was washed for 5 min with TBST three times at RT.

Table 2.18. Antibodies list

Antibody Name	Origin	Source	Dilution
SPA-822 (Hsp/c70)	Mouse	Stressgen (Victoria, BC, Canada)	1/2000
Hsp104	Rabbit	John Glover (University of Toronto)	1/150,000
Hsp26	Rabbit	Johannes Buchner (Technische Universität München)	1/4000
Hsp40 (Ydj1)	Mouse	StressMarq (Cat: SMC-166D)	1/2000
Sup35	Rabbit	Mick Tuite (University of Kent)	1/2000
Anti-His	Mouse	BioLegend (Cat: 652502)	1/3000
Anti-Flag M2	Mouse	SIGMA (Cat: F1804)	1/1000
GAPDH	Mouse	Proteintech (Cat: 60004-I-Ig)	1/5000
HRP anti-rabbit IgG	Donkey	BioLegend (Cat: 406401)	1/1000-5000
HRP anti-mouse IgG	Goat	BioLegend (Cat: 405306)	1/2000-5000

2.21.5 Chemiluminescence and visualization

In this study, Clarity™ Western ECL Blotting Substrate (Bio-rad) was used for chemiluminescence. The PVDF membrane was kept moist in TBST buffer while preparing the substrate mixture. Substrates in the kit were mixed freshly in a 1:1 ratio. For a 7×8.5 cm membrane, a 1.5 ml mixture was enough to cover the whole surface of the membrane. The PVDF membrane was placed protein side up on a clear film and ECL mixture was pipetted on top of the PVDF membrane. Visualization of the membrane was carried out in the Syngene Image Station (G:BOX Chemi systems, SYNGENE).

Visualization of the membrane can also be done by developing X-ray film in a dark room. Briefly, the chemiluminescent membrane was wrapped in preservative film and placed on an X-ray cassette. X-ray film was placed on top of the membrane and the cassette was shut for varying times (2-10 min). Film was immediately transferred to the developer solution (7 ml Kodak developer and 30 ml dH_2O) for several seconds until

signals were seen. Film was then fixed in fixer solution (7 ml Kodak fixing solution and 30 ml dH_2O) for approximately 30 s. Developed film was washed by dH_2O and allowed to dry.

2.21.6 Membrane stripping

In order to probe multiple target proteins on the same membrane, The PVDF membrane was stripped by incubating with 0.2 M NaOH for 5 min. Before stripping, the membrane was washed in dH_2O twice. After stripping, remaining NaOH should be removed by washing with water and TBST immediately. The stripped membrane can be blocked in blocking buffer and probed with other antibodies.

2.22 Co-Immunoprecipitation (Co-IP)

Co-IP performed in this study following the standard manual using 50% Anti-Flag M2 Magnetic Beads (Sigma) with minor modification.

2.22.1 Solutions of Co-IP

Yeast cell lysis reagent (Sigma)

Complemented with the protease inhibitor cocktail (5 µl/sample).

10×TBS: 50 mM Tris-HCl, 150 mM NaCl, pH7.5 (RT)

Tris-HCl (63.5 g), Tris base (11.8 g) and NaCl (87.66 g) was dissolved in deionized water to a final volume of 1 L; stored at 4 ºC.

Elution buffer of 3×Flag peptide

a) The 3×Flag peptide was dissolved in 0.5 M Tris-HCl and 1 M NaCl, pH 7.5 to get a final concentration of 25 µg/µl. This was then split into 5 µl per tube and stored at -20 ºC.
b) One tube was diluted 5 fold with deionized water to prepare a 3×Flag containing 5 µg/ul of 3×Flag peptide.
c) For elution, 3 µl of 5 µg/µl stock was added to 97 µl of 1×TBS to reach a final concentration of 150 ng/µl.

Cleaning buffer: 0.1 M glycine-HCl, pH 3.0

Cleaning buffer (50 ml) was prepared by dissolving 0.3754 g of glycine in 45 ml of deionized water, then adjusted pH to 3.0. The volume was made up to 50 ml and finally and stored at 4 ºC.

Storage buffer: 50 % glycerol in 1×TBS containing 0.02 % sodium azide.

Storage buffer (50 ml) was prepared by autoclaving 25 ml of glycerol and 25 ml of 2×TBS mixture which was then dissolved in 0.01 g of NaN_3. Storage buffer was stored at -20 ºC and in 1 ml aliquot.

2.22.2 Cell lysate preparation

Flag-tagged *SSA1* and mutations were transformed into appropriate yeast backgrounds. After culturing, cell lysates were prepared as mentioned before with more protease inhibitor cocktail. The concentration of fresh cell lysates was measured by BCA assay.

2.22.3 Protein binding

Gently resuspended beads by wide tips to make sure the volume of beads was even. Beads (50 µl-100 µl) were placed into siliconized tubes. Tubes were placed on a magnetic separator to remove storage buffer using narrow tips. Equilibrated beads were washed with 5 volumes of TBS four times. After final washing, TBS was discarded completely and then protein lysate containing 300 µg of protein was incubated with the equilibrated beads overnight on a gentle roller at 4 ºC. A magnetic stirring system was not used.

2.22.4 Washing

The following day, supernatant was discarded by placing the tubes on the magnetic separator. 10-fold beads volume of TBS was used to remove all of the non-specifically bound proteins. Washing was repeated 4 times on ice.

2.22.5 Competitive elution

Three volumes of 3×Flag peptides were added to each sample and incubated on a rotator for 1 h at 4 ºC. After incubation, beads were separated by plating on magnetic

separator, and then the supernatant was collected in a fresh tube. Centrifuged the supernatant at 1300 rpm for 10 minutes at 4 ºC and transferred clarified supernatant into another tube. Co-IP proteins can be stored at -80 ºC directly or prepared running sample with 6×protein loading buffer. 25 µl of Co-IP elution were analysed by western blotting.

2.22.6 Recycle and storage

Beads were cleaned immediately after use by washing with a 3 fold volume of 0.1 M glycine-HCl, pH 3.0. Beads were equilibrated in TBS until the effluent was at neutral pH. Beads were collected on a magnetic separator after cleaning and then stored beads in 1 beads volume of storage buffer.

2.23 Degradation assay

Proteasome and vacuole provide two pathways which breakdown different classes of proteins in yeast. Normally, short-lived proteins are degraded in proteasome pathway which is inhibited by MG132. However, long-lived proteins are more often degraded by vacuolar proteases which could be blocked by PMSF (Lee & Goldberg 1996). In order to investigate that whether Ssa1 could be degraded in those pathways, chemical inhibitors and proteases knockout strains were employed in this study.

2.23.1 Chemical inhibitors

MG132 and PMSF, two classic protease inhibitors, were purchased from Sigma. Firstly, strains were cultured in 6 ml SC media overnight at 30 ºC with shaking. The following morning, overnight cultures were diluted in 25 ml of SC media to an OD_{600} of 0.2 and triplets were prepared for each strain. Cultures were incubated until OD_{600} reached 0.5. Cells were harvested by centrifuge at 2500 rpm for 10 min and then cell pellets were resuspended in 20 ml of fresh SC with 0.003 % SDS. MG132 and PMSF were complemented respectively in SC-0.003 % SDS as described in Table 2.19 to get a working concentration. As a control, the same amount of DMSO was added into another SC-0.003 % SDS media. Triplicates of each strain were cultured at 30 ºC with shaking for another 2 h. Protein extraction protocol and WB were performed as described in previous sections.

Table 2.19. Complemented components of SC-0.1 % Proline

Reagent	Preparation	Volume (μl) of stock solution in 1ml media	Working concentration
10 mM MG132	5 mg in 1.05 ml DMSO	7.5 μl	75 μM
200 mM PMSF	35 mg in 1ml DMSO	*5 μl	1 mM
1 % SDS (w/v)	5 g in a final volum of 50 ml deionized water	3 μl	0.003 %

*the volume of PMSF stock solution was made to a final volume of 7.5 μl by adding DMSO (7.5 μl /ml).

2.23.2 Degradation under heat shock

Strains were cultured in 6 ml YPD media overnight at 30 ºC with shaking. The following morning, overnight cultures were diluted in 25 ml YPD media to an OD_{600} of 0.2 and triplets were prepared for each strain. Cultures were incubated until OD_{600} of 0.5 reached. Triplicates were treated as in Table 2.20. Cells were pelleted by centrifugation at 2500 rpm for 10 min at 4 ºC. Protein extraction, Co-IP and WB were performed one after another to investigate the degradation of Ssa1 and its mutations. In order to evaluate the viability of strains after heat shock, cultures were diluted to an OD_{600} of 0.5 after heat-shock incubation, and then 1/5 serial dilutions were carried out and the cells were spotted onto YPD plates and incubated for 2 days at 30 ℃.

Table 2.20. Degradation assay under heat shock

Number of triplicates	Temperature	Incubation time	*Final OD_{600}
No.1	30 ºC	2-3 h	around 0.9
No.2	39 ºC	2 h	around 0.9
No.3	39 ºC	3 h	more than 1

All cultures were shaking at 200rpm. *Final OD_{600} listed here from WT.

2.23.3 Degradation under the stress of misfolding proteins

L-Azetidine-2-carboxylic acid (AZC), an analogue of L-Proline, induces misfolding of proteins *in vivo* to mimic heat shock condition (Shichiri et al. 2001). In this assay, the Flag-tagged Ssa1 was cultured in 6 ml SC media overnight at 30 ºC with shaking. The following morning, the overnight culture was diluted into duplicates of 25 ml SC media and 25 ml SC media with 300 μg/ml AZC (Sigma) to an OD_{600} of 0.2. Cultures were incubated until an OD_{600} 0.4 was reached. One of the duplicates of 25 ml SC media was placed in 39 ºC shaking incubator for 2 h heat shock and while the remaining cultures were kept in a 30 ºC shaking incubator until OD_{600} reached 0.5-0.7. Cells were harvested by centrifugation at 2500 rpm for 10 min. Protein extraction, Co-IP and WB were performed one after another to investigate the degradation of Ssa1 under misfolding-proteins stress.

2.23.4 Degradation assay in proteases-knockout backgrounds

Flag-tagged Ssa1 and its mutations were transformed into BY4741, ΔPEP4, ΔUFD2 and ΔUBI4 backgrounds. Strains were cultured in 6ml SC media without Leucine overnight at 30 ºC with shaking. The following morning, overnight culture diluted into duplicates of 25 ml same media to an OD_{600} of 0.2. Cultures were incubated until OD_{600} reached 0.5. One of the duplicates was heat shocked at 42 ºC for 2 h shaking. The other maintained culturing at 30 ºC for 2 h. Cells were pelleted by centrifuge at 2500 rpm for 10 min at 4 ºC. Protein extraction, Co-IP and WB were performed one after another to investigate the degradation of Ssa1 and its mutations. In order to evaluate the viability of each strain after heat shock, cultures were diluted to an OD_{600} of 0.5 after heat-shock incubated, and then 1/5 serial dilutions were carried out and the cells were spotted onto SC-Leu plates and incubated for 2 days at 30 ℃.

2.24 β-Galactosidase assay

This method involves use of a crude protein extract (Rose & Botsten 1983) and suitable for assessment at different growth condition or different genetic backgrounds. The chemical reagents used in this assay were purchased from Sigma except extra statements. Before assay, a plasmid with *lacZ* under HSE regulation was transformed into appropriate strains. As HSF1 binding with HSE and activating the gene expression

under it, the β-Galactosidase assay was employed to indirectly calculate activity of the HSF1 *in vivo*.

2.24.1 Solutions

All chemical reagents were purchased from Sigma. And solutions prepared as following.

Assay buffer

$Na_2HPO_4 \cdot 7H_2O$ (1.61 g), $NaH_2PO_4 \cdot H_2O$ (0.55g), KCl (0.075 g), $MgSO_4 \cdot 7H_2O$ (0.0246 g) and 270 µl of β-mercaptoethanol were dissolved in deionized water to a final volume of 100 ml, pH 7.0. Buffer was stored at 4 ℃.

Start solution

ONPG (4 mg/ml) in assay buffer and stored at -20 ℃.

Stop solution

Na_2CO_3 (10.6 g) dissolved with deionized water to a final volume of 100 ml. Final concentration was 1 M and stored at 4 ℃.

2.24.2 Calculation of the lacZ activity

Strains were cultured in 5 ml of SC-Leu overnight and re-cultured in 25 ml of the same media from an OD_{600} of 0.2 to an OD_{600} of 0.6-0.8. Triplicates were prepared for each strain. Cells were pelleted by centrifugation at 4 ℃, 2500 rpm, 10 min. Cells were washed with 25 ml deionized water and collected again. Cell pellets were stored at -70 ℃ for use later. Cell extraction was performed as previously described in Y lysis buffer with 1 mM DTT and inhibitor cocktail (3 µl/sample). Following extraction, BCA assay was carried out to measure the concentration of yeast cell lysate.

The amount of protein (20 µg) was diluted in 100 µl lysis buffer and mixed with 900 µl assay buffer thoroughly. Mixture was incubated in a 28 ℃ water bath for 5 min. After incubation, 200 µl start solution was applied to the mixture to initiate the reaction. The mixture was incubated at 28 ℃ water bath for around 30 min or until a yellow colour

develops. The reaction was stopped by adding 500 µl of 1 M Na_2CO_3 solution.. The mixture was measured at OD_{420} with triplicates for each.

2.24.3 Expression of the activity

The activity of lacZ was expressed in the following formula:

$$\text{Activity of lacZ} = \frac{OD420 \times 1.7}{0.0045 \times P \times T}$$

OD_{420} is the optical density of the product o-nitrophenol at 420 nm. Corrected factor 1.7 is the reaction volume. The factor 0.0045 is the OD of a 1 nmol/ml solution of the product. P is the amount of protein lysate in mg. T is reaction time in minute. The specific activity of lacZ is expressed as nmoles/min/mg of lysate protein.

2.25 Expression and purification of the full-length Ssa1

2.25.1 Solutions

MCAC-0 (Metal-Chelate Affinity Chromatography): 50 mM Tris-HCl, 300 mM NaCl, pH7.5

Dissolved 6.35 g Tris-HCl, 1.18 g Tris base and 17.5 g NaCl in deionized water to a final volume of 1 L and stored at 4 ℃.

MCAC-1000: 50 mM Tris-HCl, 300 mM NaCl, 1 M imidazole, pH7.5

Dissolved 6.35 g Tris-HCl, 1.18 g Tris base, 17.5 g NaCl and 68.08 g imidazole in deionized water to a final volume of 1 L. Solution was filtered if required and stored at 4 ℃.

MCAC-10: 50 mM Tris-HCl, 300 mM NaCl, 10 mM imidazole, 3 mM 2-Mercaptoethanol, pH7.5

MCAC-1000 (1 ml) was diluted in 99 ml of MCAC-0 and complemented with 20 µl of 2-Mercaptoethanol.

MCAC-20: 50 mM Tris-HCl, 300 mM NaCl, 20 mM imidazole, 3 mM 2-Mercaptoethanol, pH7.5

MCAC-1000 (2 ml) diluted in 98 ml MCAC-0 and complemented with 20 µl of 2-Mercaptoethanol.

MCAC-60: 50 mM Tris-HCl, 300 mM NaCl, 60 mM imidazole, 3 mM 2-Mercaptoethanol, pH7.5

MCAC-1000 (6 ml) diluted in 94ml MCAC-0 and complemented with 20µl 2-Mercaptoethanol.

MCAC-200: 50 mM Tris-HCl, 300 mM NaCl, 200 mM imidazole, 3 mM 2-Mercaptoethanol, pH7.5

MCAC-1000 (20 ml) diluted in 80 ml MCAC-0 and complemented with 20 µl 2-Mercaptoethanol.

Protease inhibitor cocktail (Roche, EDTA-free) solution

One pill of inhibitor cocktail tablet was dissolved with 1 ml of deionized water and aliquoted 100 µl into Eppendorf tubes and stored at -80 ℃.

10×Gel filtration buffer: 500 mM Tris-HCl, 1 M KCl, 50 mM $MgCl_2$, pH7.5

Tris-HCl (63.5 g) was dissolved, Tris base (11.8 g), KCl (74.55 g) and $MgCl_2$ (10.165 g) in deionized water to a final volume of 1 L. Solution was filtered if required and stored at 4 ℃.

1×Gel filtration buffer: 50 mM Tris-HCl, 100 mM KCl, 5 mM $MgCl_2$, pH7.5

100 ml 10×Gel filtration buffer was diluted in 900 ml of deionized water. Vacuum filtration was performed to remove dissolved oxygen and tiny impurities before use.

2.25.2 Protein expression

Full-length Ssa1 (2-642) and the corresponding mutations were constructed in a pET28a-Smt3 vector containing 6×His and a Smt3 tag (Zheng et al. 2012). Plasmids were transformed into BL21-CodonPlus (DE3)-RIL competent cells. A single colony was picked from a fresh transformation plate and inoculated in 4 ml of 2YT-Kanamycin.

E.coli cells were grown at 37 ℃ with 200 rpm shaking overnight. The following morning, 4 ml of the overnight culture was inoculated to 1 L 2YT-Kanamycin and grown in the same conditions for several hours until an OD_{600} of 0.8 was reached. After incubation, target proteins were induced by adding IPTG to a final concentration of 200 μM and incubated at 16 ℃ for 16 h in a shaking incubator. Cells were collected by centrifugation at 4000 rpm for 0.5 h at 4 ℃. Cell pellets were washed by MCAC-0 buffer and pelleted again by centrifugation. Cell pellets were either used immediately or stored at -80 ℃.

2.25.3 Protein extraction and Ni-affinity purification

The *E.coli* pellet was thawed and resuspended in 40 ml of MCAC-10 complemented with 100 μl protease inhibitor cocktail. Cells were disrupted by a high-pressure homogenizer (JNBIO-JN3000) at 1000-1200 KPa for 3-5 times at 4 ℃. The high-pressure homogenizer was washed with deionized water for several times and rinsed with 10 ml MCAC-10 before use. After disruption, homogenizer was rinsed once by 5 ml MCAC-10 and collected with cell lysate together. Cells lysate was then centrifuged at 16000 rpm for 30 min at 4 ℃ to get clarified supernatant. Meanwhile, a Ni affinity column (GE Healthcare) was washed with at least 10 agarose bead volumes of deionized water and MCAC-10 successively. The supernatant was then run through the Ni affinity column around 1 ml/min on ice. The column was then washed again at least 5 agarose bead volumes of MCAC-10 and at least 100 ml MCAC-60 to remove non-specific binding. Following washing, proteins were eluted by MCAC-200. Then the elution proteins were concentrated by an Amicon Pro Purification System, 30 kDa (Millipore) at 4 ℃ and diluted in MCAC-0 to get a final imidazole concentration of 15-20 mM. The diluted product was incubated with 100 μl of purified Ulp1 at 4 ℃ for at least 1 h. Meanwhile, a fresh Ni affinity column (GE Healthcare) was washed with at least 10 agarose bead volumes of deionized water and MCAC-20 successively. After Ulp1 digestion, product got through Ni affinity column again to remove 6×His-Smt3 tag, 6×His-Ulp1 and non-cleaved proteins. Flow-through was collected and stored on ice for further purification. Ni affinity agarose beads could be recycled by washing with deionized water, 2 % SDS and 0.1 M EDTA. After recycling, agarose beads were washed with water (200-300 ml) and stored in 0.2 M $NiCl_2$ at 4 ℃.

2.25.4 Gel Filtration

The protein product was further purified by gel filtration chromatography (Superdex 200, GE Healthcare) in 50 mM Tris (pH 7.5), 100 mM KCl and 5 mM $MgCl_2$ buffer using ÄKTA system (GE Healthcare). Briefly, gel filtration column was washed by half column volume of vacuumed deionized water and equilibrated by 1.2 column volume of the 1×gel filtration buffer. Meanwhile, the flow-through was collected from the second run of Ni affinity column and concentrated by an Amicon Pro Purification System, 30 kDa (Millipore) at 4 ℃ to get a final volume of 1-2 ml. The concentrated protein product was injected into the equilibrated column and run in the gel filtration buffer (1 ml/min, alarm pressure 0.5 MPa, absorbance 260 nm and 280 nm). The target protein was collected at around 70-80 ml after protein loading and applied to a 12.5 % SDS-PAGE gel to calculate the purity. The gel filtration column could be cleaned by washing with half a column volume of deionized water and 1.2 column volumes of vacuumed 20 % ethanol. The recycled gel filtration column was stored at 4 ℃.

2.26 Expression and purification of the Ssa1 truncation mutations

2.26.1 Solutions

MCAC-0: 50 mM Tris-HCl, 200 mM NaCl, pH8.0

Tris-HCl (4.44 g) , Tris base (2.65 g) and NaCl (11.67 g) was dissolved in deionized water to a final volume of 1 L and stored at 4 ℃.

MCAC-1000: 50 mM Tris-HCl, 200 mM NaCl, 1 M imidazole, pH8.0

Tris-HCl (4.44 g), Tris base (2.65 g), NaCl (11.67 g) and imidazole (68.08 g) was dissolved in deionized water to a final volume of 1 L. Solution was filtered if required and stored at 4 ℃.

MCAC-20: 50 mM Tris-HCl, 200 mM NaCl, 20 mM imidazole, pH8.0

MCAC-1000 (2 ml) diluted into 98 ml MCAC-0 and stored at 4 ℃.

MCAC-30: 50 mM Tris-HCl, 200 mM NaCl, 30 mM imidazole, pH8.0

MCAC-1000 (3 ml) was diluted in 97 ml of MCAC-0 and stored at 4 ℃.

MCAC-300: 50 mM Tris-HCl, 200 mM NaCl, 300 mM imidazole, pH8.0

MCAC-1000 (30 ml) diluted in 70 ml of MCAC-0 and stored at 4 ℃.

Protease inhibitor cocktail (Roche, EDTA-free) solution

One pill of inhibitor cocktail tablet dissolved in 1 ml deionized water and aliquoted 100 µl into Eppendorf tubes and stored at -80 ℃.

4×Gel filtration buffer: 200 mM Na-phosphate, 200 mM NaCl, pH 7.0

$Na_2HPO_4 \cdot 12H_2O$ (87.386 g), $NaH_2PO_4 \cdot 2H_2O$ (24.338 g) and NaCl (23.376 g) in deionized water to a final volume of 2 L. Solution was filtered if required and stored at 4 ℃.

1×Gel filtration buffer: 50 mM Na-phosphate, 50 mM NaCl, pH 7.0

100 ml of 10×Gel filtration buffer was diluted in 300 ml of deionized water. Vacuum filtration was performed to remove dissolved oxygen and tiny impurities before use.

2.26.2 Protein expression

Ssa1 truncation mutant of SBD (382-554) (Hu et al. 2015) and corresponding other mutations were constructed into a pET28a-Smt3 vector containing 6×His and a Smt3 tag (Zheng et al. 2012). The plasmids were transformed in BL21-CodonPlus (DE3)-RIL competent cells. A single colony was picked from fresh transformation plate and inoculated in 4 ml 2YT-Kanamycin. *E.coli* cells were grown at 37 ℃ with 200 rpm shaking overnight. The following morning, 4 ml of overnight culture was inoculated in 1 L of 2YT- Kanamycin and grown in the same conditions for several hours until an OD_{600} of 0.8 was reached. For NMR, 500 ml M9 minimal medium containing ^{15}N-NH_4Cl or ^{15}N-NH_4Cl/^{13}C-glucose was used. After incubation, target proteins were induced by adding IPTG to get a final concentration of 500 µM and incubated at 18 ℃ for 40 h in a shaking incubator. Cells were collected by centrifugation at 4000 rpm for 0.5 h at 4 ℃. Cell pellets were washed by MCAC-0 buffer and pelleted again by centrifugation. Cell pellets could be used immediately or stored at -80 ℃.

2.26.3 Protein extraction and Ni-affinity purification

Protein extraction was performed as described in Section 2.25.3. Ni affinity column (GE Healthcare) was washed with at least 10 agarose bead volumes of deionized water and MCAC-0 successively. After centrifugation, the supernatant was run through Ni affinity column for around 1ml/min on ice. The column was then washed with at least 100 ml MCAC-30 to remove non-specific binding. Following washing, proteins were eluted by MCAC-300.

2.26.4 Dialysis

Dialysis membrane (Spectra/Por, MWCO 3000) was boiled in deionized water for 10 min and cooled by changing deionized water. One side of the membrane was snapped by a clean clip, and the MCAC-300 elution was collected and transferred to the treated dialysis membrane (Spectra/Por, MWCO 3000). The other side of the membrane was sealed with another clean clip and the dialysis bag was immersed in 400 ml of MCAC-20. Dialysis was performed at 4 ℃ stirring for 2-3 h, and then 400 ml fresh MCAC-20 buffer was replaced before being left at 4 ℃ stirring overnight.

2.26.5 Gel filtration

After dialysis, the protein product was transferred to a tube and incubated with 100 μl of purified Ulp1 at 4 ℃ for at least 1 h. Meanwhile, a fresh Ni affinity column (GE Healthcare) was washed with at least 10 agarose bead volumes of deionized water and MCAC-20 successively. After Ulp1 digestion, the protein product went through the fresh Ni affinity column to remove the 6×His-Smt3 tag, 6×His-Ulp1 and non-cleaved proteins. The flow-through was collected and concentrated by an Amicon Pro Purification System, 10 kDa (Millipore) at 4 ℃ to get a final volume of 2-3 ml. The gel filtration column (Superdex 75, GE Healthcare) was washed by half a column volume of vacuumed deionized water and equilibrated with 1.2 column volume of the gel filtration buffer (50mM Na-phosphate buffer with 50mM NaCl, pH 7.0). The concentrated protein product was injected into the equilibrated column and run in the gel filtration buffer (1ml/min, alarm pressure 0.5 MPa, absorbance 220 nm, 260 nm and 280 nm). The target protein was collected at around 55-70 ml after protein loading and

applied to a 15 % SDS-PAGE gel to calculate the purity. The gel filtration column was recycled and stored previously described.

2.27 Ydj1 expression and purification

2.27.1 Solutions

MCAC-0: 50 mM Tris-HCl, 300 mM NaCl, pH8.4

Tris-HCl (2.64 g), Tris base (4.03 g) and NaCl (17.5 g) was dissolved in deionized water to a final volume of 1 L and stored at 4 ℃.

MCAC-1000: 50mM Tris-HCl, 300 mM NaCl, 1 M imidazole, pH8.4

Tris-HCl (2.64 g), Tris base (4.03 g) and NaCl (17.5 g) and 68.08 g imidazole was dissolved in deionized water to a final volume of 1 L. Solution was filtered if required and stored at 4 ℃.

MCAC-10: 50 mM Tris-HCl, 300 mM NaCl, 10 mM imidazole, pH8.4

MCAC-1000 (1 ml) diluted into 99 ml MCAC-0.

MCAC-70: 50 mM Tris-HCl, 300 mM NaCl, 70 mM imidazole, pH8.4

MCAC-1000 (7 ml) diluted into 93 ml MCAC-0.

MCAC-200: 50 mM Tris-HCl, 300 mM NaCl, 200 mM imidazole, pH8.4

MCAC-1000 (20 ml) diluted into 80 ml MCAC-0.

Protease inhibitor cocktail (Roche, EDTA-free) solution

One pill of inhibitor cocktail tablet was dissolved in 1 ml deionized water and aliquoted 100 µl into Eppendorf tubes and stored at -80 ℃.

10×Gel filtration buffer: 500 mM Tris-HCl, 1 M KCl, 50 mM $MgCl_2$, pH7.5

Tris-HCl (63.5 g), Tris base (11.8 g), KCl (74.55 g) and $MgCl_2$ (10.165 g) was dissolved in deionized water to a final volume of 1 L. Solution was filtered if required and stored at 4 ℃.

1×Gel filtration buffer: 50 mM Tris-HCl, 100 mM KCl, 5 mM $MgCl_2$, pH7.5

100 ml 10×Gel filtration buffer was diluted in 900 ml of deionized water. Vacuum filtration was performed to remove dissolved oxygen and tiny impurities before use.

2.27.2 Protein expression

Ydj1 was constructed in a mini-pRSETa vector containing 6×His tag. The plasmid was transformed into C41 competent cells. A single colony was picked from a fresh transformation plate and inoculated in 4 ml 2YT-Amp. *E.coli* cells were grown at 37 ℃ with 200 rpm shaking overnight. The following morning, 4 ml overnight cultures were inoculated in 1 L 2YT-Amp and grown at the same conditions for several hours until an OD_{600} of 0.8 is reached. After incubation, target proteins were induced by adding IPTG to get a final concentration of 200 μM and incubated at 16 ℃ for 16 h in a shaking incubator. Cells were collected by centrifugation at 4000 rpm for 0.5 h at 4 ℃. Cell pellets were washed with MCAC-0 buffer and pelleted again by centrifugation. Cell pellets could be used immediately or stored at -80 ℃.

2.27.3 Protein extraction and Ni-affinity purification

Protein extraction was performed exactly as described in Section 2.25.3. Ni affinity column (GE Healthcare) was washed with at least 10 agarose bead volumes of deionized water and MCAC-10 successively. After centrifugation, the supernatant was run through Ni affinity column around 1 ml/min on ice. The column was then washed with 50 ml MCAC-10 and at least 100 ml MCAC-70 to remove non-specific binding. Following washing, proteins were eluted by MCAC-200.

2.27.4 Gel filtration

The flow-through was collected in MCAC-200 elution and concentrated using an Amicon Pro Purification System, 10 kDa (Millipore) at 4 ℃ to get a final volume of 1 ml. Protein was further purified by using gel filtration chromatography (Superdex 200, GE Healthcare, 24 ml). For more details see Section 2.25.4.

2.28 ATPase assay

ATPase activity was measured based on colorimetric determination of inorganic Na-phosphate using malachite green as a previous described (Chang et al. 2008). Briefly, 10 µl of 2 µM Ssa1 (50 mM Tris pH 7.5, 100 mM KCl, 5 mM $MgCl_2$ and 1 mM DTT) or standards (Table 2.21, from 0-150 µM) mixed with 2 mM ATP equally into each well of a 96-well plate, and then incubated at 30 ℃ for 5 h. If Ydj1 or peptide (ALLLSAPRR) required, 8 µM and 400 µM were reached respectively in a total volume of 10 µl Ssa1 protein solution. After incubation, 80 µl of malachite green reagent was added to each well. Stock solutions of malachite green (0.081 %, w/v), polyvinyl alcohol (2.3 %, w/v), and ammonium heptamolybdate tetrahydrate (2.85 %, w/v in 3 M HCl) were prepared, and mixed in the ratio of 1:1:1 to prepare the malachite green reagent (Table 2.22). Following the malachite green reagent, 10 µl 34 % (w/v) sodium citrate was added to stop the non-enzymatic hydrolysis of ATP. The samples were mixed thoroughly and incubated at 30 ℃ for 30 min before measuring OD_{620} on a SpectraMax M3e (Molecular Devices, USA).

Table 2.21. Preparation of Na-phosphate standards

Concentration of phosphate radical	Volume of source Na-phosphate (µl)	^Volumes of diluent (µl)
5 mM	100 (*50 mM)	900
500 µM	100 (5 mM)	900
200 µM	400 (500 µM)	600
150 µM	300 (500 µM)	700
100 µM	200 (500 µM)	800
75 µM	500 (150 µM)	500
50 µM	500 (100 µM)	500
25 µM	500 (50 µM)	500
10 µM	200 (50 µM)	800
5 µM	500 (10 µM)	500
0 µM	0	1000

* 50 mM Na-phosphate buffer is the 1×gel filtration buffer from Section 2.26.1.

^ Diluent buffer is the 1×gel filtration buffer from Section 2.25.1.

Table 2.22. Components of the malachite green reagent

Name	Final concentration (w/v)	Preparation	Ratio
Malachite green	0.081 %	40.2 mg in 50 ml deionized water	1
Polyvinyl alcohol	1.15 %	575 mg in 50 ml deionized water	1
Ammonium heptamolybdate tetrahydrate-HCl	2.85 % in 3 M HCl	1.425 g $(NH_4)_6Mo_7O_{24}\cdot 4H_20$ and 12.5 ml concentrated HCl dissolved with deionized water to a 50ml volume	1

2.29 Circular dichroism spectroscopy

CD spectroscopy is dichroism involving circularly polarized light to measure the secondary structure of proteins. The α-helix structure absorbs at 208nm and 222nm while β-sheets have significant absorbance at 215-217nm. Disordered structure normally has the biggest absorbance before 200nm. The CD spectra of full-length Ssa1 and mutation proteins were obtained in 50 mM Tris (pH 7.5), 100 mM KCl and 5 mM $MgCl_2$ at a protein concentration of 3 μM using Chirascan Plus CD spectrometer (Applied Photophysics, UK). Spectra were measured from 260 nm to 200 nm in a 0.1mm path-length thermostatted quartz cuvette. The temperature was controlled using an extra Peltier device. The truncation mutants at a protein concentration of 10 μM were measured in 50 mM phosphate buffer (pH 7.0) with 50 mM NaCl at the same conditions.

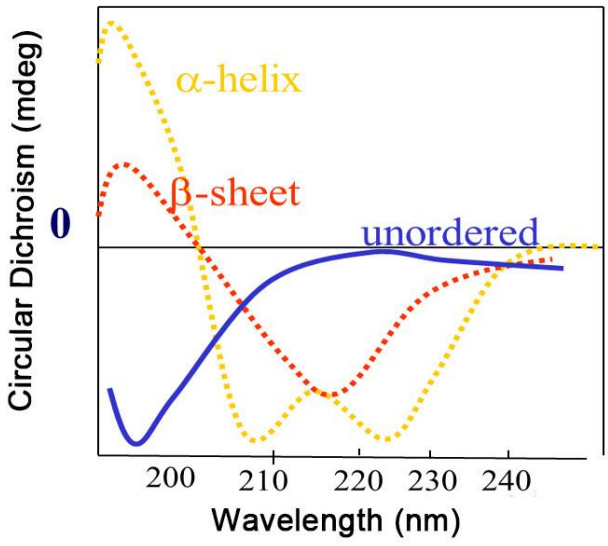

Figure 2.1. CD spectroscopy to detect the secondary structure of proteins.

2.30 Size exclusion chromatography (SEC)

The oligomeric state of SBD truncation mutants was roughly calculated by SEC (Superdex 75, 24 ml, GE Healthcare) in 50 mM Na-phosphate buffer (pH 7.0) with 50 mM NaCl at room temperature according to the Figure 2.1. Briefly, the gel filtration column was washed by 12 ml vacuumed deionized water and equilibrated with 30 ml of gel filtration buffer (50 mM Na-phosphate buffer and 50 mM NaCl, pH 7.0). Protein sample (100 µl; 50 µM) was injected into the equilibrated column and run in gel filtration buffer (0.5 ml/min, alarm pressure 1.5 MPa, absorbance 220nm, 260 nm and 280 nm). The gel filtration column was then cleaned and stored as previously described. More details of reproducibility and durability can be seen in the Data File of Superdex 75 (https://www.gelifesciences.com).

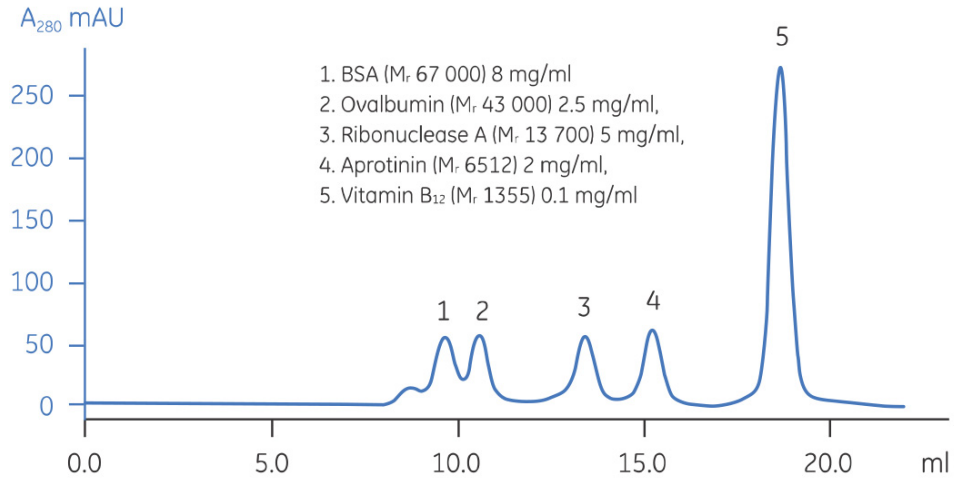

Figure 2.2. Comparison of the protein separation on Superdex 75. Buffer was 0.05 M phosphate with 0.15 M NaCl, pH 7.0. Flow rate was 0.4ml/min, room temperature. Adapted from the Data File of Superdex 75.

2.31 MALDI-TOF

In order to detect the molecular weight of the F475S truncation mutant, protein was passed through C18 ziptip to remove salt and then mixed with a SA matrix. MALDI-TOF was performed on a MALDI-TOF AXIMA-CFR Plus（KRATOS Analytical, Shimadzu Corporation, Japan). MALDI-TOF was performed at the Institute of Biophysics Core Facilities, Institute of Biophysics, Chinese Academy of Sciences, China, and assisted by Lili Niu.

2.32 Intrinsic fluorescence

The intrinsic fluorescence spectra of wide-type Ssa1 and mutations were measured on a Hitachi F-4500. Briefly, a quartz cuvette was washed with deionized water and rinsed with gel filtration buffer (50 mM Tris, 100 mM KCl and 5 mM $MgCl_2$, pH 7.5). Protein sample (600 μl; 2 μM) was excited at 280 nm and emitted from 290 nm to 400 nm at room temperature in the quartz cuvette. Scan speed was 240 nm/min. Each sample was scanned twice.

2.33 NMR spectroscopy

Nuclear magnetic resonance (NMR) is a powerful technique to obtain physical, chemical, and structural information of molecules in solution and in their solid state based on absorbance and re-emission of electromagnetic radiation when nuclei are in a magnetic field. The strength of the magnetic field and the magnetic properties of the isotopes determine the specific resonance frequency. NMR spectroscopy was employed in this study to investigate conformational changes of the SBD truncation of the Ssa1 induced by mutants and heat shock.

2.33.1 2D ^{1}H-^{15}N HSQC spectrum

^{15}N labelled Ssa1 truncation mutations were expressed in M9 minimal medium containing ^{15}N-NH_4Cl and purified as described in Section 2.26. After purification, 15 % SDS-PAGE was applied to check the purity and the BCA assay was performed to quantify the protein concentrations. The monomeric/oligomeric state of the SBD truncation mutants were calculated by SEC (Superdex 75, 24 ml, GE Healthcare) as the described in Section 2.30. Purified proteins were concentrated by an Amicon Pro Purification System, 10 kDa to get a final concentration of 300-400 μM. NMR samples were prepared in 50 mM Na-phosphate buffer (pH 7.0) containing 50 mM NaCl, 0.02 % NaN_3, 5 mM EDTA, 10 % D_2O and protease inhibitor (Table 2.23). NMR experiments were performed at 30 ℃, 37 ℃ and 39 ℃ on a Varian INOVA 600 MHz spectrometer equipped with a triple-resonance cryo probe under the assisting of Dr. Huiwen Wu (Institute of Biophysics, Chinese Academy of Sciences, China). More details as described in Ref. (Hu et al. 2015).

Table 2.23. Preparation of NMR samples

Solution	Preparation of stock solution	Volume (μl)	Final concentration
Protein solution (300-400 μM)	Concentrated protein was centrifuged at 14000 rpm for 10 min before use	450	250-400 μM
Protease inhibitor cocktail	1 table dissolved in 0.5ml 50 mM Na-phosphate buffer (pH 7.0)	5	1 table/50 ml
2 % NaN_3	20 mg dissolved in 1ml deionized water	5	0.02 % (w/v)
0.5 M EDTA	1.46 g dissolved to 50 mM Na-phosphate buffer (pH 8.0) to a 10 ml volume	5	5 mM
D_2O	-	52	10 % (v/v)

2.33.2 3D ^{1}H-^{15}N-^{13}C HSQC-NOESY spectrum

^{15}N-^{13}C labelled L483W of the Ssa1 truncation mutation was expressed in M9 minimal medium containing ^{15}N-NH_4Cl and ^{13}C-glucose and purified as descriptions in Section 2.26. After purification, 15 % SDS-PAGE was applied to check the purity and BCA assay was performed to quantify the protein concentration. The monomeric/oligomeric state of SBD truncation mutant was calculated by SEC (Superdex 75, 24 ml, GE Healthcare) as described in Section 2.30. The stability of L483W truncation mutant was assessed by incubating at 35 ℃, 37 ℃ and 39 ℃ respectively for 48 h.

As L483W truncation mutant has weaker signals in 50 mM Na-phosphate buffer than that of WT, concentrated protein was dialysed into *20 mM Na-phosphate buffer (pH7.0, with 1 mM DTT) for 4 h as the described in Section 2.26.4. NMR samples were prepared as in Table 2.23 in 20 mM Na-phosphate buffer (pH 7.0) containing 0.02 % NaN_3, 5 mM EDTA, 10 % D_2O, the protease inhibitor and 10 mM DTT (extra 9 mM DTT was complemented after dialysis). NMR experiments were performed at 35 ℃ on a Varian INOVA 600 MHz spectrometer equipped with a triple-resonance cryo probe under the assisting of Dr. Weibin Gong (Institute of Biophysics, Chinese Academy of Sciences, China). After collection of the 3D spectrum, the sample was respectively titrated back to 50 mM Na-phosphate buffer (pH 7.0) and 50 mM NaCl using stock

solution in Table 2.24 to keep the same buffer used as WT sample (Hu et al. 2015). During titrations 2D spectrums were collected at 35 ℃ and 30 ℃.

Table 2.24. Stock solution of titration

Solution	Preparation of stock solution	Volume (μl)	Final concentration
5 M NaCl	2.922 g NaCl dissolved to deionized water to a 10ml	5.2	50 mM
1 M Na-phosphate buffer (pH 7.0)	2.185 g $Na_2HPO_4 \cdot 12H_2O$ and 0.608 g $NaH_2PO_4 \cdot 2H_2O$ dissolved to deionized water to a 10 ml	16	50 mM

*20 mM Na-phosphate buffer containing 1 mM DTT was prepared by dissolving 4.37 g $Na_2HPO_4 \cdot 12H_2O$, 1.22 g $NaH_2PO_4 \cdot 2H_2O$ and 0.15425 g DTT to 1 L deionized water.

2.34 Molecular dynamics (MD)

Molecular dynamics is a computational method to simulate the physical movements of atoms in molecules based on Newton's equations of motion developed in the 1950s. It has been wildly applied in theoretical physics, chemistry, materials science and structural biology. In computational biology, MD has been used to investigate the motions of proteins and nucleic acids, interactions of biological macromolecules, protein folding and unfolding. In this study, MD was employed to investigate the conformational changes induced by mutations and heat shock using the SBD model (Xu et al. 2013).

2.34.1 Model construction

In this study, DnaK SBD complex with NRLLTG peptide (PDB code: 1Q5L) (Stevens et al. 2003) was downloaded from RCSB database as the WT model. The other SBD mutations were constructed using Swiss-Pdb Viewer (Guex & Peitsch 1997) basing on the WT structure. After modelling, all of the mutation models were subjected to Procheck analysis.

2.34.2 Molecular dynamics simulation

MDs were performed using the GROMACS 4.5.7 and 4.6 packages (Van Der Spoel et al. 2005) as previously described (Xu et al., 2013). Briefly, there are 6 steps for MD and all MDs were performed on the ICHEC (Ireland's High-Performance Computing Centre).

1) Topology generation

Topology file was prepared by running pdb2gmx programme and the united-atom GROMOS96 43A1 had been chosen when force field was asked.

pdb2gmx_d -ignh -f input.pdb -o output.gro -p output.top -water spce

2) Box definition and protein solvation

A cubic box was defined and solvated protein with SPC water:

editconf_d -f output.gro -o newbox.gro -bt cubic -d 1.0 -c -princ

genbox_d -cp newbox.gro -cs spc216.gro -o b_em.gro -p output.top

3) Neutralization

If the solvated system contains a charged protein, the Na^+ or Cl^- was used to neutralize the system. If the solvated system was neutralized already, ignore this step and go to step 4 directly. em.mdp required has been shown in step4.

grompp_d -f em.mdp -c b_em.gro -p output.top -o em.tpr

genion_d -s em.tpr -o ion.gro -nn/-np -random

The molecular numbers of different compounds in the output.top should be changed after neutralization.

4) Energy Minimization

This step arranges atoms where the net inter-atomic force on each atom is acceptably close to zero. em.mdp and em.pbs scripts have shown following:

em.mdp script

```
;       File 'em.mdp' was generated
;       By user: linan
;       At date: Fri Oct 08 09:30:17 2013
;
title = em
cpp = /usr/bin/cpp ; the c pre-processor
define = -DFLEXIBLE
```

```
constraints = none
integrator = cg
dt =0.002 ; ps !
nsteps = 10000
nstlist = 10
ns_type = grid
rlist = 1.0
coulombtype = PME
rcoulomb = 1.0
vdwtype = cut-off
rvdw = 1.0
fourierspacing = 0.12
fourier_nx = 0
fourier_ny = 0
fourier_nz = 0
pme_order = 4
ewald_rtol = 1e-5
optimize_fft = yes
emtol = 15.0
emstep = 0.01
niter = 20
fcstep = 0
nstcgsteep = 1000
nbfgscorr = 10
```

em.pbs script

```
#!/bin/bash
#PBS -N em
#PBS -j oe
#PBS -A nuim01
#PBS -r n
#PBS -l nodes=4:ppn=12
#PBS -l walltime=00:05:00
#PBS -m bea
#PBS -M linan.xu.2014@nuim.ie
#PBS -V

module load gromacs/4.6

# go to work dir
cd $PBS_O_WORKDIR

# pre-process the input for start

# grompp_mpi_d -f grompp.mdp -p topol.top -c conf.gro -o water.tpr
grompp_mpi_d -f em.mdp -p output.top -c neutralized.gro -o em.tpr

# start the md

# mpiexec mdrun_mpi_d -s water.tpr -o water.trr -c water.out -g water.log
mpiexec mdrun_mpi_d -s em.tpr -o em.trr -c em.out -g em.log
```

5) Equilibration

This step is to equilibrate MD system containing proteins in water. pr.mdp and pr.pbs scripts as shown in the following text:

pr.mdp script

```
;       File 'pr.mdp' was generated
;       By user: linan
;       At date: Fri Oct 08 09:39:10 2013
;

title               = pr
cpp                 = cpp
define                      = -DPOSRES
integrator          = md
tinit               = 0
dt                  = 0.002
nsteps              = 500000
init_step           = 0
comm-mode           = Linear
nstcomm             = 10
bd-fric             = 0
ld-seed             = 1993
nstxout             = 50000
nstvout             = 50000
nstfout             = 0
nstcalcenergy       = 10
nstcheckpoint       = 1000
nstlog              = 5000
nstenergy           = 5000
nstxtcout           = 0
xtc-precision       = 1000
energygrps          = Protein non-Protein
nstlist             = 10
ns-type             = Grid
pbc                 = xyz
rlist               = 1
coulombtype         = PME
rcoulomb-switch     = 0
rcoulomb            = 1
epsilon_r           = 1
epsilon_rf          = 1
vdw-type            = Cut-off
rvdw-switch         = 0
rvdw                = 1
DispCorr            = EnerPres
fourierspacing      = 0.12
fourier_nx          = 0
fourier_ny          = 0
fourier_nz          = 0
pme_order           = 4
ewald_rtol          = 1e-5
ewald_geometry      = 3d
epsilon_surface     = 0
```

optimize_fft = yes
tcoupl = V-rescale
tc-grps = Protein non-Protein
tau-t = 0.1 0.1
ref-t = 303 303
Pcoupl = Berendsen
Pcoupltype = Isotropic
tau-p = 1
compressibility = 4.5e-5
ref-p = 1
refcoord_scaling = all
gen-vel = yes
gen-temp = 300
gen-seed = 173529
constraints = all-bonds
constraint-algorithm = Lincs
unconstrained-start = no
shake-tol = 0.0001
lincs-order = 4
lincs-iter = 1
lincs-warnangle = 30
morse = no
nstdisreout = 100
orire = no
orire-fc = 0
orire-tau = 0
nstorireout = 100
dihre = No
dihre-fc = 1000
dihre-tau = 0
nstdihreout = 100
free-energy = no
init-lambda = 0
delta-lambda = 0
sc-alpha = 0
sc-power = 0
sc-sigma = 0.3

pr.pbs script

```
#!/bin/bash
#PBS -N pr
#PBS -j oe
#PBS -A nuim01
#PBS -r n
#PBS -l nodes=4:ppn=12
#PBS -l walltime=01:00:00
#PBS -m bea
#PBS -M linan.xu.2014@nuim.ie
#PBS -V

module load gromacs/4.6

# go to work dir
```

```
cd $PBS_O_WORKDIR

# pre-process the input for start

# grompp_mpi_d -f grompp.mdp -p topol.top -c conf.gro -o water.tpr
grompp_mpi_d -f pr.mdp -p output.top -c em.out.gro -o pr.tpr

# start the md

# mpiexec mdrun_mpi_d -s water.tpr -o water.trr -c water.out -g water.log
mpiexec mdrun_mpi_d -s pr.tpr -o pr.trr -c pr.out -g pr.log
```

6) MD

The linear constraint solver (LINCS) method (Hess et al. 1997) was used to constrain bond lengths, allowing an integration step of 2 fs. Electrostatic interactions were calculated using the particle mesh Ewald algorithm with a distance cutoff of 9 Å (Essmann et al. 1995; Darden et al. 1993). The Lennard-Jones potential was used for describing the short-range attractive and repulsive dispersion interactions with a 10 Å cutoff. The temperature and pressure were coupled using V-rescale and Parrinello-Rahman algorithm respectively. After equilibration several independent simulations were carried out over a 20 ns period at 303 K, 310 K and 312 K respectively, pH 7.0 and 1 bar pressure. The coordinate trajectories were saved every 1 ps for subsequent data analysis.

md.pbs script

```
#!/bin/bash
#PBS -N md
#PBS -j oe
#PBS -A nuim01
#PBS -r n
#PBS -l nodes=4:ppn=12
#PBS -l walltime=12:00:00
#PBS -m bea
#PBS -M linan.xu.2014@nuim.ie
#PBS -V

module load gromacs/4.6

# go to work dir
cd $PBS_O_WORKDIR

# pre-process the input for start

# grompp_mpi_d -f grompp.mdp -p topol.top -c conf.gro -o water.tpr
grompp_mpi_d -f md.mdp -p output.top -c pr.out.gro -o 20ns.tpr
```

```
# start the md

# mpiexec mdrun_mpi_d -s water.tpr -o water.trr -c water.out -g water.log
mpiexec mdrun_mpi_d -s 20ns.tpr -o 20ns.trr -c 20ns.out -g 20ns.log
```

2.34.3 Analysis of trajectories

After MDs, data was analysed using applications of the GROMACS package (Table 2.25). All structural images were produced by the VMD programme (Humphrey et al. 1996).

Table 2.25. GROMACS applications used in this study

Analysis	Command
Index	*make_ndx -f md.gro -o md.ndx*
RMSD	*g_rms -f 20ns.trr -s pr.tpr -o rmsd.xvg*
RMSF	*g_rmsf -f 20ns.trr -s 20ns.tpr -o rmsf.xvg –res*
Secondary structure	*do_dssp -f 20ns.trr -s 20ns.tpr -o ss.xpm -dt 25*
Trajectory	*trjconv -f 20ns.trr -s 20ns.tpr -o md.pdb -dt 1000 -sep*
Distance	*g_dist -f 20ns.trr -s 20ns.tpr -n md.ndx -o dist.xvg*
Gyration radius	*g_gyrate -f 20ns.trr -s 20ns.tpr -n md.ndx -o gyr.xvg*
	g_hbond -f 20ns.trr -s 20ns.tpr -n md.ndx -num hb.xvg
Hydrogen bond	*g_hbond -f 20ns.trr -s 20ns,tpr -n md.ndx -hbm hb.xpm -dt 50*
	g_hbond -f 20ns.trr -s 20ns,tpr -n md.ndx -hbn hbn.ndx -dt 50

CHAPTER THREE

A NOVEL SBD MUTATION F475S ALTERS PRION PROPAGATION AND THERMOTOLERANCE

3.1 SBD mutants of Hsp70

Hsp70 is a highly conserved 70 KDa protein found in all species that assists protein folding, refolding and protects cells from different stresses (Tyedmers et al. 2010). Structurally, Hsp70 is comprised of two domains: N-terminal 45 KDa nucleotide binding domain (NBD) and C-terminal 25 KDa substrate-binding domain (SBD) (Morshauser et al. 1985; Zhu et al. 1996; Mayer & Kityk 2015). From a cell stress perspective, heat shock proteins, especially Hsp70s, are critical for the response to extracellular stresses such as heat shock and oxidative stress. From a therapeutics perspective, Hsp70 is a potential drug design target in many neurodegenerative diseases such as α-synuclein (α-Syn) in Parkinson's disease, β-amyloid (Ab) and Tau in Alzheimer's disease, tauopathies, and polyglutamine-expanded huntingtin in Huntington's disease (Knowles et al. 2014; Gao et al. 2015; Sweeny & Shorter 2015; Tyedmers et al. 2010).

Saccharomyces cerevisiae is a well-established model organism for the study of both stress response and prion propagation. *S. cerevisiae* has four cytosolic Hsp70s of the Ssa family, and expression of at least one of them is essential for growth. Ssa1 is one of two constitutively expressed Ssa Hsp70s. In conjunction with another chaperone Hsp104 and a co-chaperone Hsp40, Hsp70 modulates the disaggregation of denatured proteins within the yeast cells. The Hsp40 co-chaperone is responsible for stimulating Hsp70's ATPase activity and regulating substrate binding. A variety of genetics and biochemical studies in yeast have identified the Hsp70 chaperone machinery as a key modulator of prion propagation and many mutations of Hsp70 (Ssa1) have been isolated that impair propagation of tyeast prions [PSI^{+}] and [*URE3*] (Jones & Masison 2003). However, most of the mutants that impair prion propagation are located in NBD, and detailed biochemical analysis for these mutants has yet to be carried out.

In order to identify SBD mutants that alter prion propagation, a modified random mutagenesis strategy was employed (details see Sarah A. Cusack' thesis, 2010). This screen identified four novel SBD mutations, V439I, F475S, M515I and S545F, and two previously characterized mutants G481D (Loovers et al. 2007) and L483W (Jones et al. 2004; Needham & Masison 2008; Xu et al. 2013). Among the new mutants, F475S exhibited the strongest prion-impairing effects and also a temperature sensitivity

phenotype. In this chapter, I assessed in detail the biochemical and molecular changes within the F475S mutant, and also three second-site suppressors of this mutation, in terms of temperature sensitivity (identified by Dr. Sarah A. Cusack) (Figure 3.1). Additionally, the importance of the Phe475 residue was further investigated through creation of an array of targeted amino acid subsitutions at this site followed by genetic and biochemical analysis.

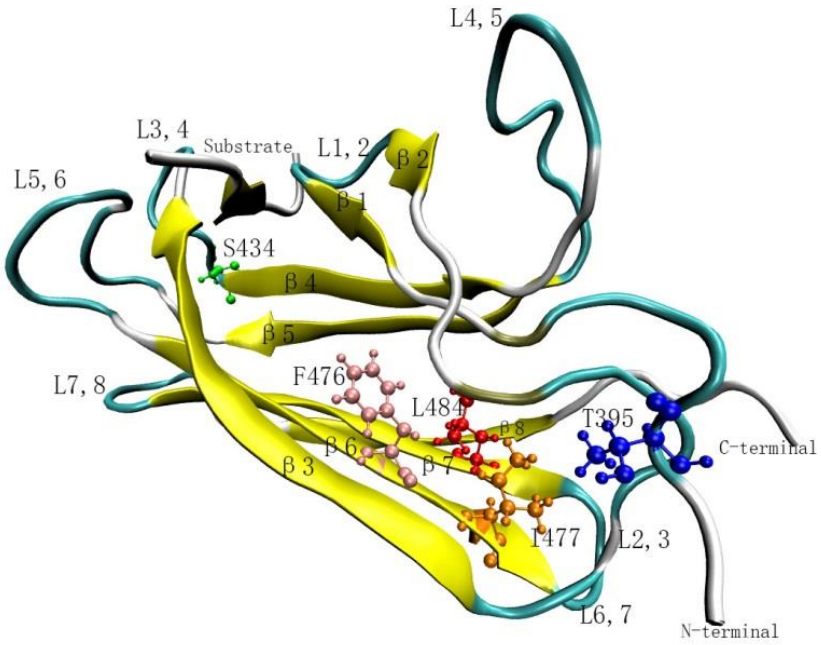

Figure 3.1. Locations of Phe475 and second-site suppressors on the DnaK structure. Ribbon schematic representations of the Protein Data Bank structure 1Q5L. The *E.coli* amino acid residue numbers are homologous to those of the Ssa1 mutations assessed. Phe475 in Ssa1 is homologous to Phe476 in DnaK. Three second-site suppressors, A394V, P433S and V477I in Ssa1, are shown in Thr395, Ser434 and Ile477 in DnaK respectively.

3.2 F475S impairs [*PSI*$^+$] propagation

To assess [*PSI*$^+$] propagation in F475S, the plasmid pC210 carrying F475S and second-site suppressors were transformed into the G402 background. The pRS315 with WT was removed by growing on the medium containing 5-FOA. The prion phenotype was assessed on YPD and -ADE at 30℃ or RT. As previous research has illuminated the

importance of SBD mutant L483W in impairment of [*PSI*$^{+}$] propagation (Jones & Masison 2003; Xu et al. 2013), L483W was employed in this section as a control for a prion-impairing Hsp70 mutant. As shown in Figure 3.2, L483W is [*psi*$^{-}$] (red colonies on YPD and no growth on -ADE) as previously reported, and F475S is also [*psi*$^{-}$]. Furthermore, three F475S second-site suppressors do not alter impairment of prion phenotype induced by F475S. Considering that residues 483 and residue 475 are adjacent (Figure 3.1), it was presumed that F475S and L483W may share a similar mechanism in relation to impairment of prion propagation.

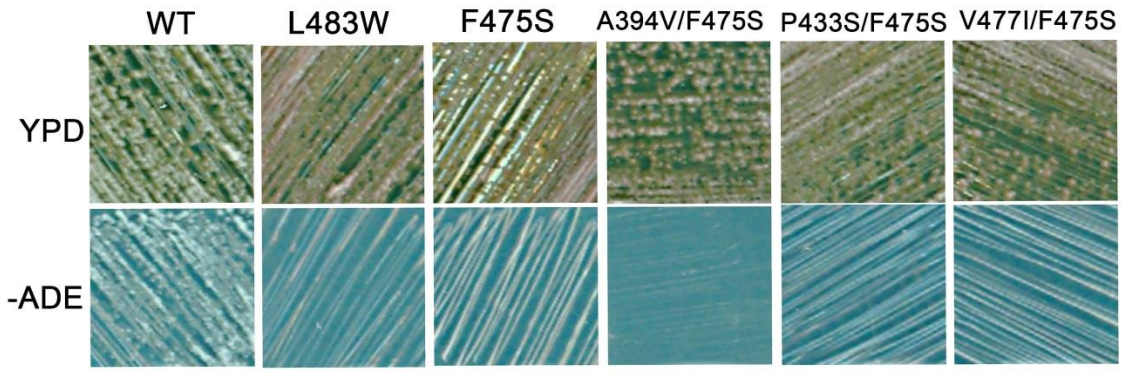

Figure 3.2. Assessment of F475S and three second-site suppressors on [*PSI*$^{+}$] phenotype. A single colony was streaked on YPD and –ADE plates. Plates were incubated at 30℃ (or all incubated at RT to promote the growth of [*PSI*$^{+}$] cells). As described in the introduction, [*psi*$^{-}$] cells were red colonies on YPD and lethal on -ADE plates; [*PSI*$^{+}$] cells were white colonies on YPD and grew on –ADE plates.

3.3 F475S causes a temperature sensitivity phenotype

Heat shock results in the unfolding of protein, misfolding of protein and loss of membrane integrity by increasing the fluidity of membranes and can lead to cell death (scchoffl 1999, wahid 2007, Kamada et al., 1995). Hsp70 is a critical chaperone to response heat shock in all species. Therefore, I assessed the temperature sensitivity of F475S and second-site suppressors. As shown in Figure 3.3, F475S slightly affected the growth on YPD at 30℃. Moreover, it was clearly sensitive at 37℃ and lethal at 39℃ on YPD plates. Three second-site suppressors did not alter prion phenotype (Figure 3.2), but rescued the temperature sensitivity induced by F475S to varying degrees (Figure 3.3). Particularly A394V, exhibited the best restoration of thermotolerance to Ssa1.

Considering that elevated temperature weakened the cell well (Kamada et al. 1995) and maintenance of osmotic stress decreased damage due to heat shock (Gunasekera et al. 2008), we repeated temperature sensitivity tests using YPD supplemented with 1M sorbitol to maintain osmotic balance of cells under heat shock. As previous reports, 1M sorbitol obviously increased the cells survival at elevated temperatures. However, 1M sorbitol did not significantly increase thermotolerance of those mutants compared with that of WT, which implied that temperature sensitivity of F475S didn't cause a deficiency of the cell well. Therefore, there must be other reasons causing temperature sensitivity of F475S variant.

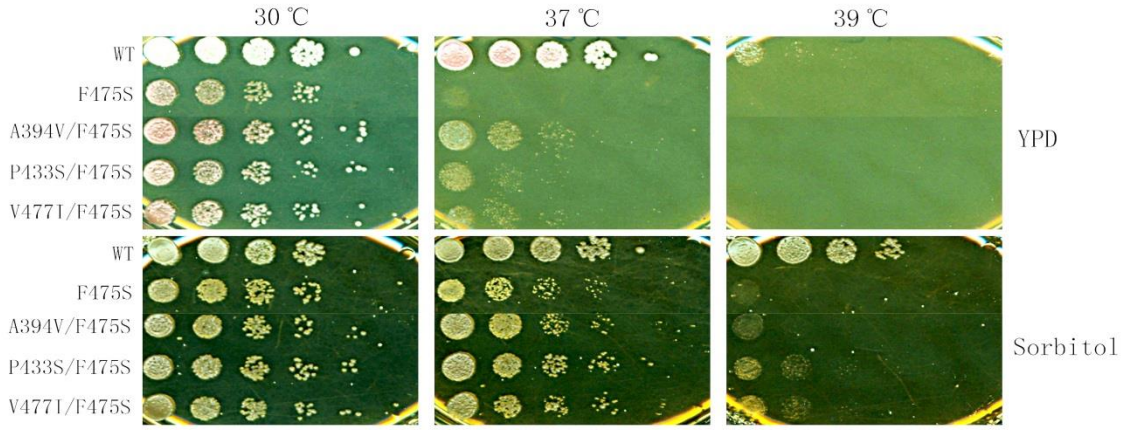

Figure 3.3. Growth assay of the F475S and three second-site suppressors at elevated temperatures. Fresh cultures were spotted on YPD and YPD containing 1M sorbitol as the description in the growth assay method.

3.4 Assessment of acquired thermotolerance

The thermotolerance of yeast cells is regulated by a group of heat shock proteins (Lindquist & Craig 1988; Morimoto 1998), and Hsp104 is a key component in yeast to ensure cell survival at high temperature (Jones & Tuite 2005). To assess the contribution of Hsp104 with Hsp70 mutations, cells containing appropriate mutant as sole Ssa source were plated on YPD medium and YPD containing 3 mM Gdn-HCl, which inhibits *in vivo* activity of Hsp104 (Jung & Masison 2001). As shown in Figure 3.4, F475S and second-site suppressors exhibit decreased acquired thermotolerance compared to wide-type Ssa1 on YPD. Acquired thermotolerance was reduced for all of those strains on 3 mM Gdn-HCl plates compared to YPD. This suggested that Hsp104 is

not a major contributor to the thermotolerance phentoypes exhibited by these mutants. Moreover, recovery of second-site suppresssors temperature sensitivity could be observed on YPD and YPD containing 3 mM Gdn-HCl plates as well, but it may be still irrelevant with the contribution of the Hsp104.

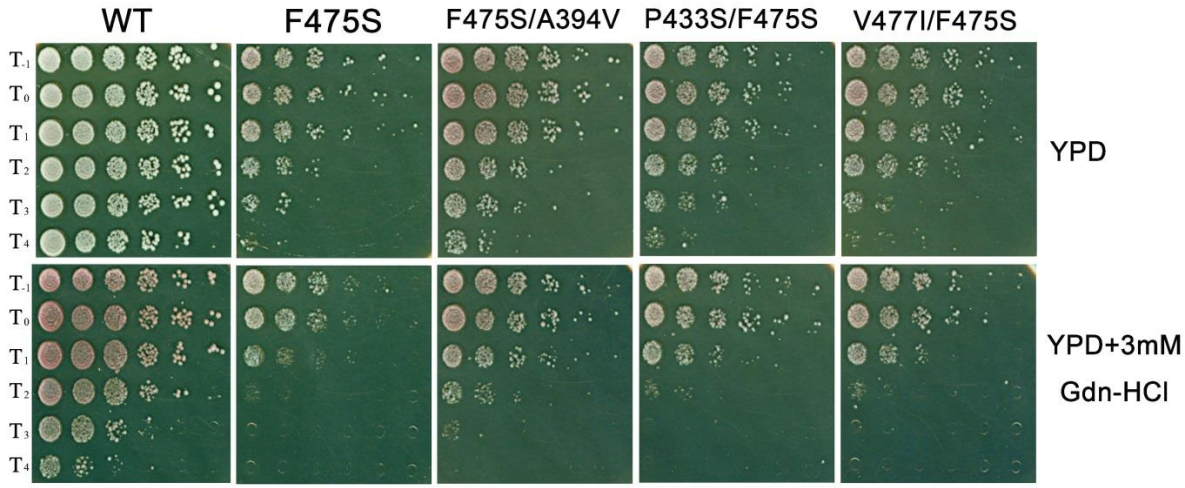

Figure 3.4. Acquired thermotolerance assay of the F475S and second-site suppressors. The fresh cultures were incubated at 39℃ for 1h to induce the expression of Hsp104 *in vivo*. Then cultures were moved to 47℃ incubator for a time course (T_0-T_4 mean 0, 10, 20, 30 and 40 minutes respectively). T_{-1} means cultures before 39℃ incubation. Cells were spotted on YPD and YPD containing 3mM Gdn-HCl after a 1/5 dilution.

3.5 Assessment of F475S to response other stresses

Previous reports have shown that Hsp70 is a sensor for the regulation of the oxidative stress and may be related to cell-wall damage also (Wang et al. 2012; Hasin et al. 2014). In addition to differences in heat shock in the Ssa1 mutants, it was also observed differences in response to cell-wall damage reagent SDS and oxidative reagent H_2O_2 (Figure 3.5). Cells expressing those mutations as only Ssa source are sensitive to both SDS and H_2O_2, suggesting that F475S may alter the basal structure and function of the Ssa1 so that cells have serious deficiencies in response to common stresses. Interestingly, second-site suppressors did not rescue the deficiency of F475S under SDS and H_2O_2 stresses, implying that those three suppressors may be specific to recover the temperature sensitivity of F475S.

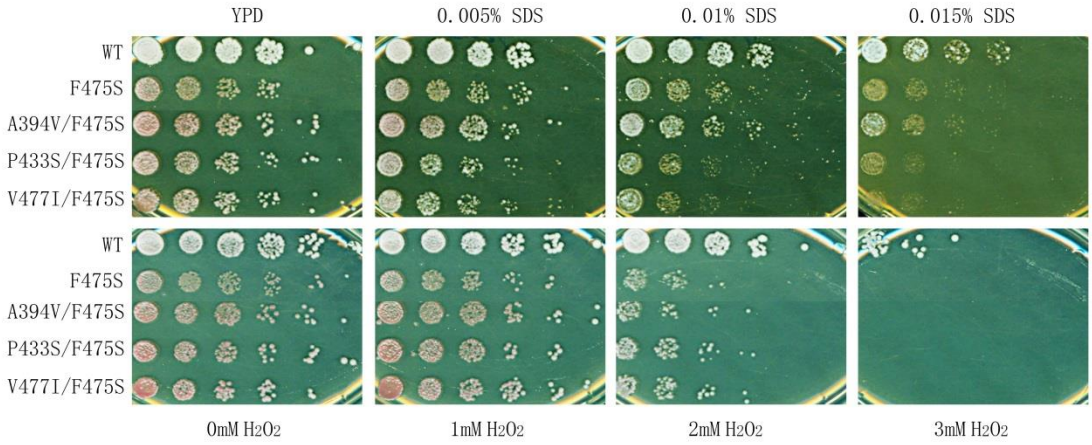

Figure 3.5. Growth assay of F475S under other stresses. YPD and SC medium were complemented with cell-wall damage reagent SDS and oxidant reagent H_2O_2 respectively to achieve required concentrations. Fresh cultures were spotted on those plates as the description in growth assay section and incubated for 2 days at 30℃.

3.6 The structural stability of the SBD mutants

After the growth assay under various stresses, it was considered that F475S may alter the basal structure and function of the Ssa1. In order to gain insight to whether F475S causes conformational changes of the SBD, MD was employed in this study based on the DnaK model I constructed previously (Xu et al. 2013). Following simulations, the structural stability of mutants was assessed by calculation of the root-mean-square deviation (RMSD) of the protein Cα atoms. The RMSD profiles indicated that the F476S (homolog F475S in Ssa1) disturbed the structural stability of the SBD at 30℃, 37℃ and 39℃, but WT and L484W (homolog L483W in Ssa1) only disturbed SBD at 39℃ with much less disturbance than F476S (Figure 3.6 and Table 3.1), which provides a possible explanation for the temperature sensitivity of F475S. Furthermore, P434S rescued the stability of F476S at 30℃ and 37℃, but the other two second-site suppressors did not (Figure 3.6 and Table 3.1). Interestingly, when the structural stability of models was further assessed by B-factor (so called Temperature Factor), all those three second-site suppressors recovered the B-factor to that of WT level, which might explain why they rescued the temperature sensitivity of F475S. Taking all together, the disturbance of SBD causes the temperature sensitivity of the F475S mutation. However, the impairment of [PSI^+] propagation may not be related to the stability of the SBD as L483W has a relatively stable SBD at 30℃.

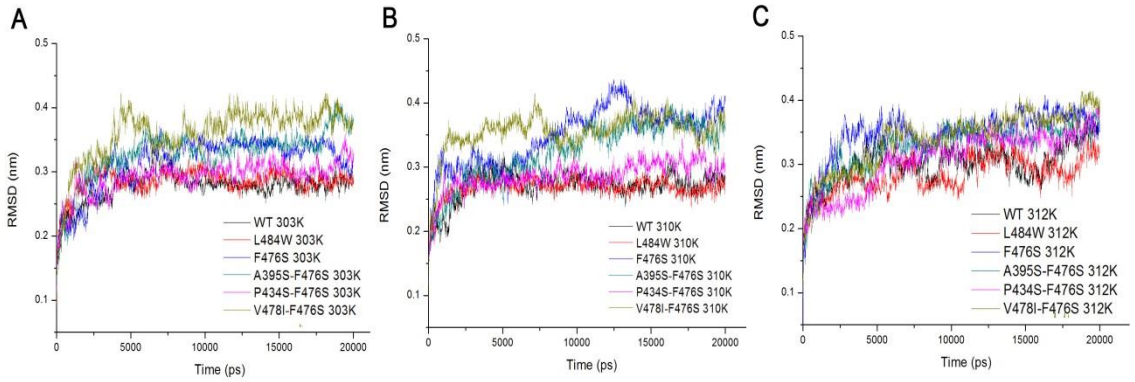

Figure 3.6. RMSDs as a function of the simulation time. (A) RMSDs profiles at 303K (30℃); (B) RMSDs profiles at 310K (37℃); and (C) RMSDs profiles at 312K (39℃). RMSDs were calculated by g_rms program basing on the Cα atoms of the protein.

Table 3.1. The average of RMSD and B-factor during MD

	Temperature	RMSD	B-factor
WT	303K	0.2806	95.0739
	310K	0.2745	54.1728
	312K	0.3135	279.6299
L484W	303K	0.2869	78.0420
	310K	0.2688	78.1810
	312K	0.2998	226.6345
F476S	303K	0.3371	154.9818
	310K	0.3832	152.3284
	312K	0.3663	377.1160
A395V/F476S	303K	0.3472	68.3210
	310K	0.3603	74.0806
	312K	0.3498	99.1044
P434S/F476S	303K	0.3060	67.9695
	310K	0.2984	55.9856
	312K	0.3409	65.5230
V478I/F476S	303K	0.3835	67.3077
	310K	0.3653	66.4143
	312K	0.3704	81.6397

The average of the RMSDs and B-factor was calculated during 20ns simulation.

3.7 F475S remains in the monomeric state of SBD

To further investigate the SBD disturbance induced by F475S, I employed an *E.coli* expression system to express and purify SBD truncation mutant (382-554) (Hu et al. 2015). After purification, I firstly detected the monomeric or oligomeric state of F475S truncation protein using size exclusion chromatography (SEC). F475S truncation protein displayed decreasing exclusion volume around where the dimer or oligomer should be compared to where monomer WT is located (Figure 3.7A). However, the molecular weight of F475S truncation protein was still monomeric (around 18.8KDa) (Figure 3.7B), suggesting that the decreased exclusion volume might be caused by the unfolding of F475S truncation protein, not dimerization or oligomerization. Thus, the F475S mutant still maintains monomeric state *in vitro* but with an unfolded secondary structure perhaps, which is consistent with MD conclusion in Figure 3.6A. P433S/F475S and V477I/F475S had a very similar monomeric state with F475S protein, however, B-factor did show a recovery of stability. Actually, a slight recovery was observed from unfolded monomer to folded monomer at 12 ml in Figure 3.7A. However, the recovery is too small to be significant. Therefore, it was thought that the conformational changes recovered by P433S and V477I existed, but perhaps are too slight to see due to technical limitations of the SEC. Interestingly, A394V significantly recovered the exclusion volume of F475S protein to the monomeric state of WT (around 12 ml), which implied that A394V rescued the unfolding caused by F475S variant to folded monomeric state with good secondary structure formation (Figure 3.7A).

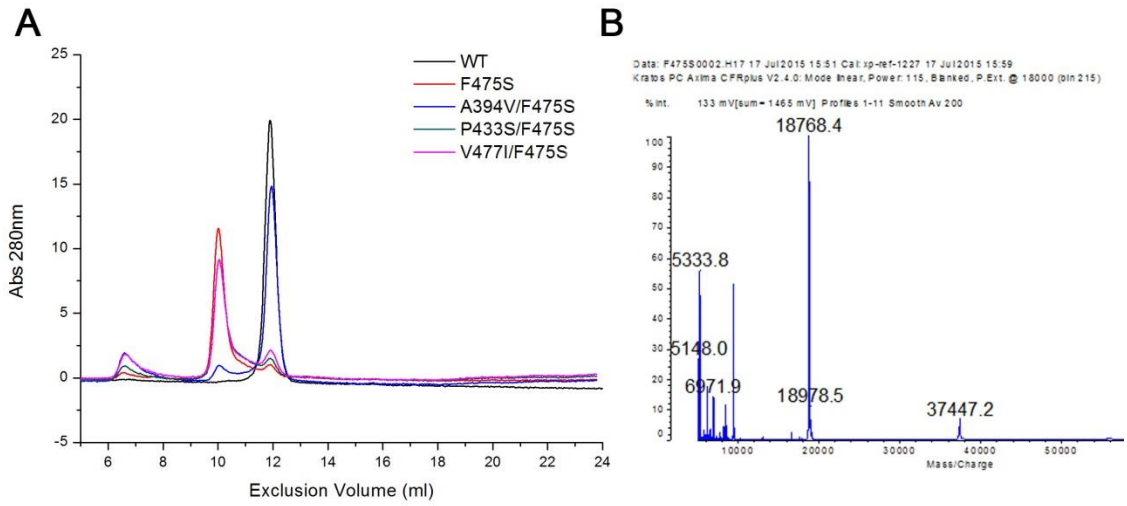

Figure 3.7. The monomeric state of F475S mutation. (A) The SEC at RT; (B) Molecular weight of F475S truncation mutant assessed by MALDI-TOF.

3.8 Secondary structure analysis of CD spectroscopy

CD spectroscopy is dichroism involving circularly polarized light to measure the secondary structure of proteins. The α-helix structure absorbs at 208nm and 222nm while β-sheets have significant absorbance at 215-217nm. Disordered structure normally has the biggest absorbance before 200nm. To confirm the disturbance of F475S variant in SBD truncation protein, I employed CD spectroscopy to provide insight into the secondary structure of F475S truncation protein. As the SBD truncation mutant contains the SBDβ and a part of the α-helical lid, CD spectroscopy showed a mixed α-β wild-type protein (Figure 3.8A). Significantly, F475S variant displayed a clearly reduced absorbance at 215-217nm (β-sheet), 208nm and 222nm (α-helix), but larger absorbance before 200nm (disordered structure), which suggested there were gross alterations of secondary structure in F475S truncation protein no matter if at optimal or elevated temperatures (Figure 3.8A and B), which is in aggreement with MD and SEC results (Figure 3.6, Table 3.1 and Figure 3.7). L483W only had slight changes compared to WT at 30 ℃, but with temperatures elevation, the content of α-helix and β-sheets gradually declined, suggesting the conformational changes induced by L483W really existed at high temperatures (Figure 3.8B). Although previous reports had not found L483W is sensitive at 37℃ (Jones & Masison 2003), it was predicted that the temperature sensitivity of L483W may be observed at a higher temperature, such as 39℃. The significant differences were observed in L484W simulations at elevated temperature, which may be caused by limited simulation time.

Moreover, P433S and V477I displayed a slight increase in absorbance around 200nm-205nm, suggesting that the P433S and V477I might rescue temperature sensitivity of F475S by maintaining the secondary structure of SBDβ to some degree (Figure 3.8A). Interestingly, A394V recovered the secondary structure of F475S truncation protein to almost that of WT level (Figure 3.8A) and which was also observed in SEC Figure 3.7A. Indeed, A394V/F475S has consistently been the best at suppressing temperature sensitivity induced by F475S variant of all three second-site suppressors (Figure 3.3 and 3.4). Considering Valine 394 is located in the linker, it was speculated that residue 394 not only improves the secondary structure of the SBDβ, but also may be involved in inter-domain communication in full-length Ssa1.

Taking these results together, F475S clearly disrupts the native secondary structure of the SBD. This disturbance of SBD is one of the reasons that alter thermotolerance of Ssa1 *in vivo*. It was predicted that unfolded SBD would be further degraded easily.

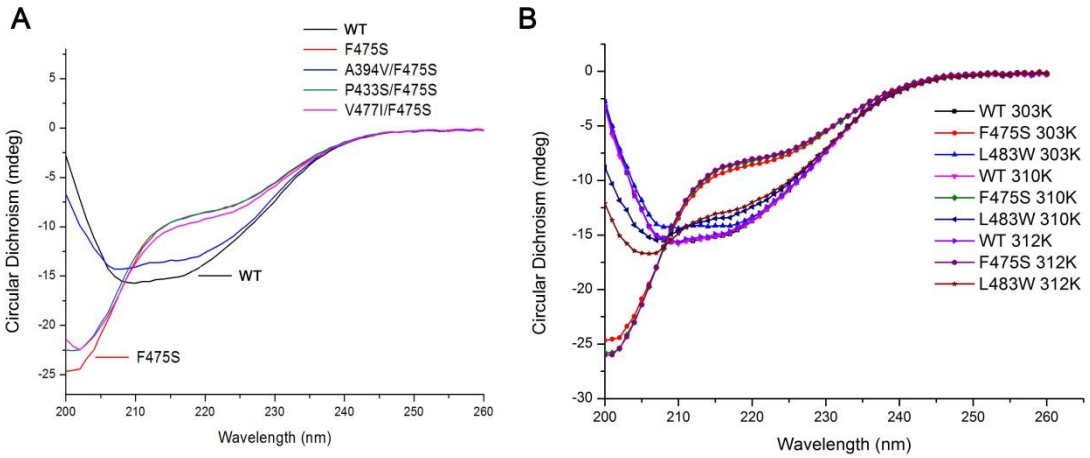

Figure 3.8. CD spectroscopy analysis of SBD truncation mutations. (A) CD spectroscopy of SBD truncation mutants at 30℃; (B) CD spectroscopy of SBD truncation mutants at elevated temperatures. The temperature was precisely controlled by an extra digital module and a plugin device.

3.9 SBD degradation assays by SEC

To directly investigate SBD degradation, I incubated SBD truncation proteins at 30℃ and allowed them to pass through a 24 ml Superdex 75 column. After 12 h incubation, unfolded F475S and second-site suppressors were markedly degraded as judged by large absorbance decreases to varying degrees (Figure 3.7A and Figure 3.9A). After 24 h incubation, almost all of proteins containing F475S and second-site suppressor mutations had been degraded to small pieces (Figure 3.9B). Furthermore, A394V/F475S showed an increased absorbance around 10 ml after 12 h incubation which suggested that the A394V/F475S also tends to form disordered structure to some extent. Although A394V/F475S tends to exhibit similar characters with WT (Figure 3.7A and Figure 3.8A), it is still not as stable as WT after 24 h incubation (Figure 3.9B). Therefore, unfolded SBD is degarded more easily and may directly cause the temperature sensitivity of cells expressing these mutants. I speculated the degradation of the F475S SBD truncation protein would be enhanced by higher temperature.

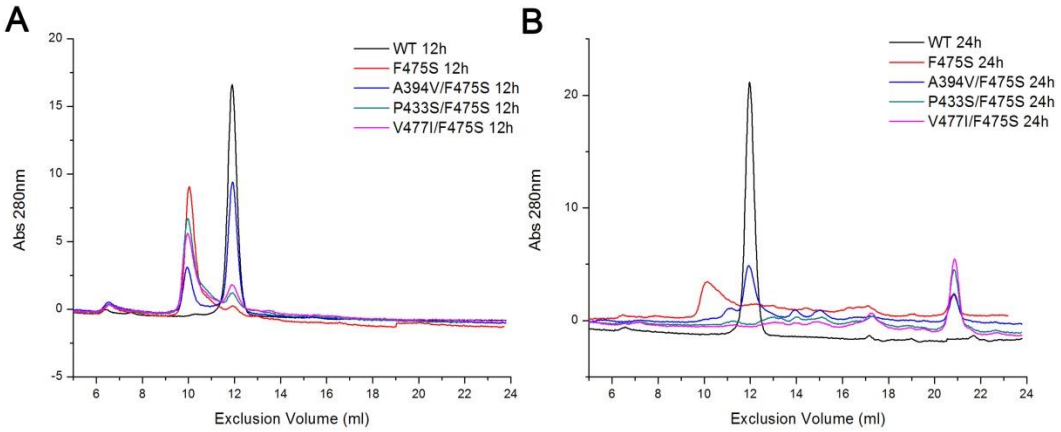

Figure 3.9. SBD degradation assays by SEC. (A) The SEC after 12 h incubation; (B) The SEC after 24 h incubation. Purified SBD truncation mutations were incubated at 30 ℃. 100 μl of 50 μM protein was loaded into a 24 ml Superdex 75 column.

3.10 Conformational changes of the SBD caused by F475S

To discover the conformational changes of the SBD induced by F475S mutant, MD and NMR both were employed in this section. First of all, root-mean-square fluctuations (RMSF) of backbone atoms were used to measure the residue fluctuation. F476S (F475S in Ssa1) mutant induced significant fluctuations for almost all of residues during a 20 ns simulation, suggesting large conformational changes of the SBD (Figure 3.10A). Moreover, 2D ^{1}H-^{15}N HSQC spectrum of F475S truncation protein also came to this conclusion as a lot of peaks disappeared compared to that of WT (Figure 3.10B). The signal attenuation of the NMR strongly supported the disordered secondary structure of F475S truncation protein and suggested that significant conformation changes did happen in SBD.

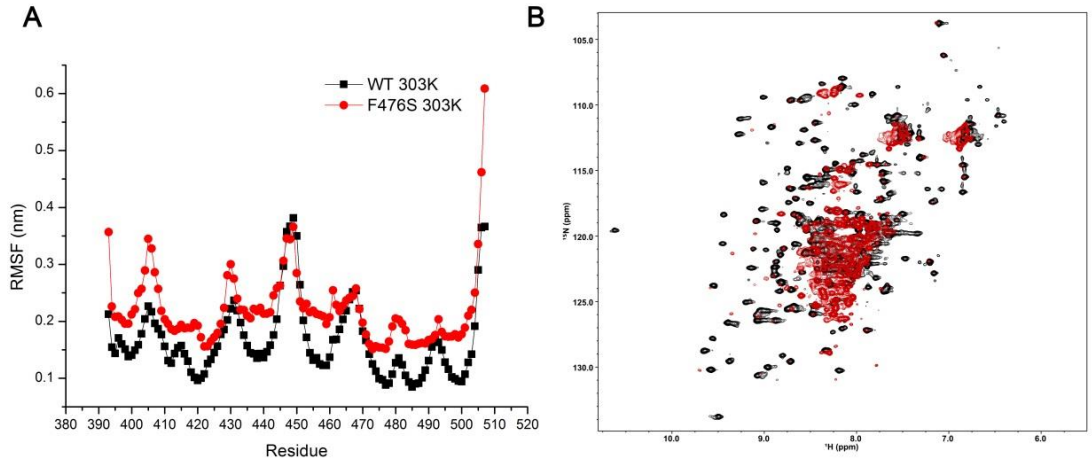

Figure 3.10. Conformational changes of the SBD induced by F475S. (A) RMSFs of backbone atoms during the simulations at 30 ℃ (303K); (B) 2D ^{1}H-^{15}N HSQC spectrum of WT (black) and F475S (red) at 30 ℃.

3.11 Second-site suppressors recover conformational changes of F475S

To further investigate the conformation changes of SBD mutations, we carried out NMR analysis for second-site suppressors and all spectra were scanned at optimal and elevated temperatures to observe the effects of second-site suppressors and heat shock. 2D ^{1}H-^{15}N HSQC spectrum of F475S displayed significant signal attenuation at all temperatures, compared to WT (Figure 3.11 A and B). Importantly, A394V, P433S and V477I all enhanced the NMR signal intensity of F475S at 30 ℃, with A394V again exhibiting the most dramatic effects (Figure 3.11C-E). However, 2D ^{1}H-^{15}N HSQC spectrum of A394V/F475S did display significant peaks changes compared to WT at 30 ℃ (Figure 3.11F), suggesting A394V/F475S also harbours an altered intrinsic SBD structure. With temperature increasing, the peak signal attenuation can be observed for second-site suppressors, particularly P433S/F475S and V477I/F475S, which explained why second-site suppressors were more sensitive than WT at elevated temperatures. Taking all together, second-site suppressors rescue the conformational changes of F475S to varying degrees, and elevated temperature accelerated conformational changes of the SBD.

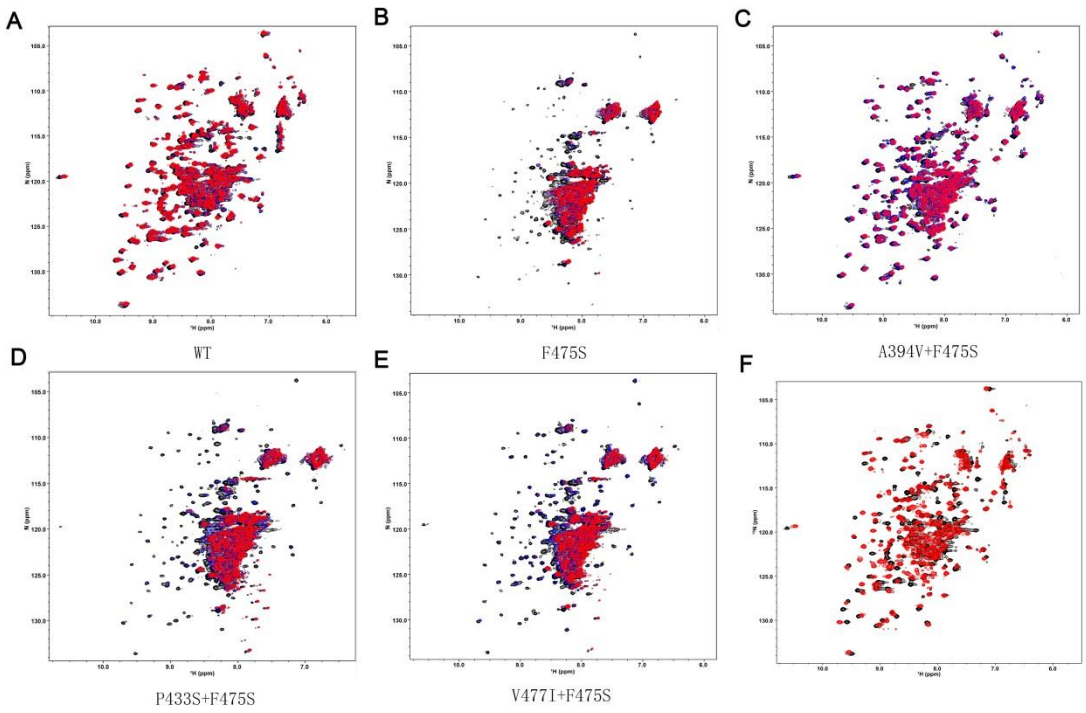

Figure 3.11. Second-site suppressors recovered conformational changes of F475S. 2D ^{1}H-^{15}N HSQC spectrum of SBD mutants were scanned at 30 ℃ (black), 37 ℃ (blue) and 39 ℃ (red) respectively; (A) WT; (B) F475S; (C) A394V/F475S; (D) P433S/F475S; (E) V477I/F475S. (F) 2D ^{1}H-^{15}N HSQC spectrum of WT (black) and A394V/F475S (red) at 30 ℃.

3.12 Extension of the hydrophobic core of F475S

Recent research suggested that binding of the central hydrophobic residues requires an expansion of the substrate binding pocket as compared to the ATP-bound state, leading to an overall reorganization of the SBDβ (Mayer & Kityk 2015; Kityk et al. 2015), which may be trigged by the β5/β7/β8 hydrophobic core (Zhuravleva & Gierasch 2015). Based on the position of F475S variant (Figure 3.1), it was predicted that F475S mutation might alter the conformation of the SBDβ by disrupting the hydrophobic core and therefore decreasing the stability of the substrate-binding pocket. In order to investigate this hypothesis, I calculated the radius of gyration of three highly conserved residues (Leu454, Leu484 and Ile501 in DnaK) in the hydrophobic core by MDs. Figure 3.12A showed that F476S and well-characterised L484W, both had an extended hydrophobic core at 30 ℃, especially F476S. Further MD analysis displayed that F476S mutant caused a more significant perturbation over all three hydrophobic core residues (Figure 3.12D), but L484W mainly caused a side-chain shift of Trp484 (Figure 3.12C).

The extended degree of the hydrophobic core is in line with the SBD stability and the viability of cells under heat shock.

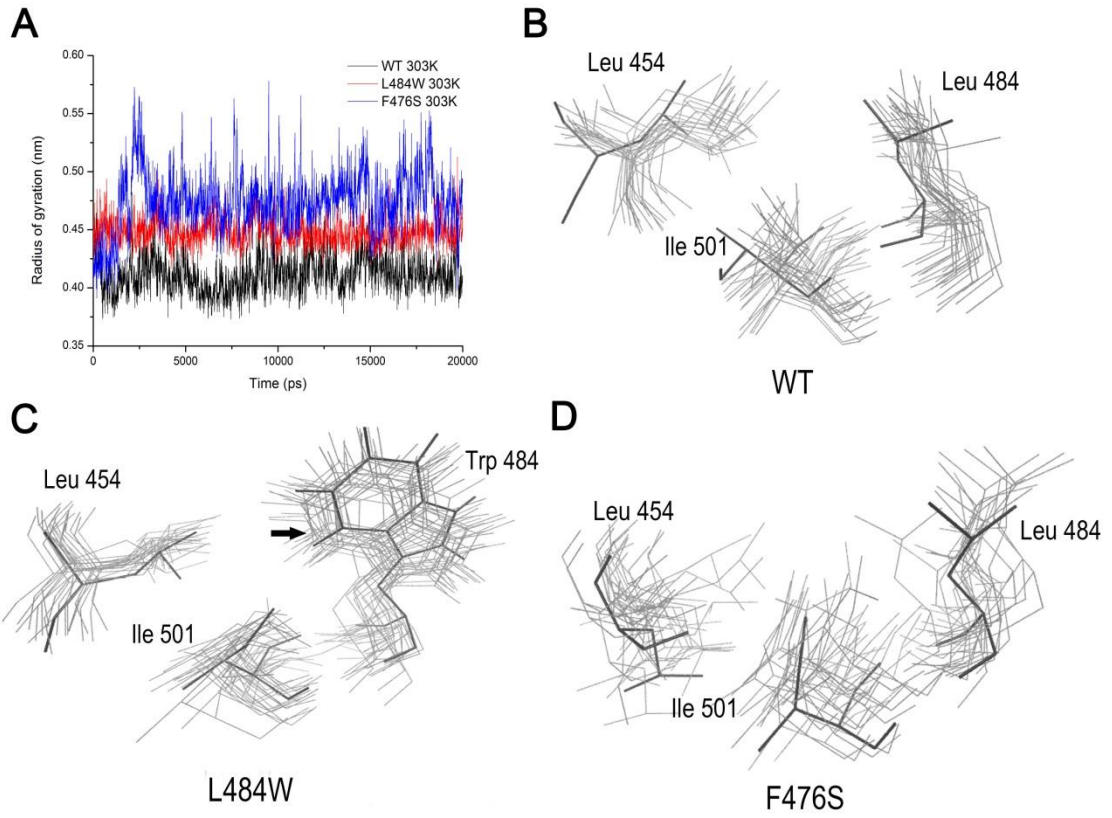

Figure 3.12. Extension of the hydrophobic core during simulations. (A) The radius of gyration as a function of simulation time at 30 ℃. (B) Superposition of three highly conserved residues (Leu454, Leu484 and Ile501 in DnaK) snapshots in the WT hydrophobic core; (C) Superposition of three highly conserved residues snapshots in the L484W hydrophobic core; (D) Superposition of three highly conserved residues snapshots in the F476S hydrophobic core.

3.13 Extension of the hydrophobic core under heat shock

To investigate if the extension of the hydrophobic core is a common occurence for WT under heat-shock conditions, I calculated the radius of gyration of three highly conserved residues by MDs. Figure 3.13A showed that extended hydrophobic core did happen to WT but only at 39 ℃. Then, in order to further verify the conclusion from MDs, I calculated NMR chemical shift perturbation (CSP) of WT SBD truncation mutant between 30 ℃ and 39 ℃ (Figure 3.13B) and mapped conformational changes of residues based on CSPs in Figure 3.13D. At 39 ℃, two of the three hydrophobic core

residues, Leu453 and Ile500, displayed obvious CSPs (Figure 3.13B) and peaks of all those three shifted in different directions with elevated temperatures (Figure 3.13C), suggesting that conformational changes happened for/around them. Furthermore, the other residues next to those three hydrophobic core residues also induced significant CSPs (Leu452, Ile482, Thr499 and Thr501; Figure 3.13B), which also supports the idea of an extended hydrophobic core at elevated temperatures. Finally, it was found that the linker, β5 and β8 have the most significant CSPs (Figure 3.13B and D). In addition, L12, L23, L45, L56, β3 and β7 also have several residues with significant CSPs (Figure 3.13B and D) suggesting conformational changes happens in those regions also.

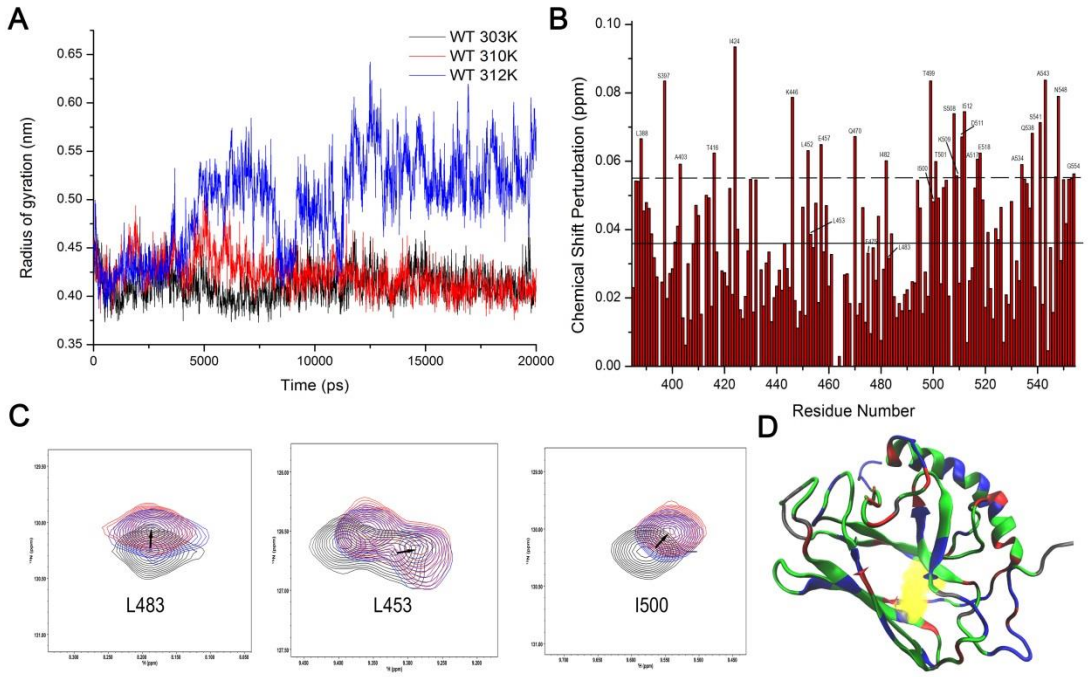

Figure 3.13. Extension of the hydrophobic core under heat shock. (A) The radius of gyration of three highly conserved residues (Leu454, Leu484 and Ile501 in DnaK) of WT as a function of simulation time at elevated temperatures. (B) CSPs Histogram of WT between 30 ℃ and 39 ℃. The Solid line showed the average of CSPs; the dotted line showed the average plus SD. (C) Peak displacement pattern of three highly conserved residues in the hydrophobic core of WT at elevated temperatures. 30 ℃, 37 ℃ and 39 ℃ are represented black, blue and red respectively. (D) Mapping all of the allosteric residues between 30 ℃ and 39 ℃ onto the DnaK structure (PDB: 1BPR) (Wang et al. 1998). Unassigned residues are showed in gray; CSP of residue less than is showed in green; CSP more than average but less than average plus SD is showed in blue; significant CSPs (more than average plus SD) are showed in red.

3.14 The hydrophobic core triggers SBD allostery under heat shock

Recent research reported that the β5/β7/β8 hydrophobic core is a central hub for the SBD allosteric network (Zhuravleva & Gierasch 2015), which is in line with the extension of the hydrophobic core I found in F475S and WT at elevated temperatures (section 3.12 and 3.13). In this section, I aimed to identify the regions with significant conformational changes caused by F475S variant based upon CSPs of NMR. As shown in Figure 3.14, F475S disturbed the hydrophobic core of the SBD at 30℃, like MD had predicted (Figure 3.12 A and D), and the disturbance of the residues was extended from the hydrophobic core to the whole SBD with increased temperature (Figure 3.14). Taking all together, the hydrophobic core triggered conformational changes of the SBD and F475S variant accelerated the disturbance of the hydrophobic core. Unfortunately, the 3D structure of F475S mutant cannot be obtained due to the dramatic reduction in signal attenuation.

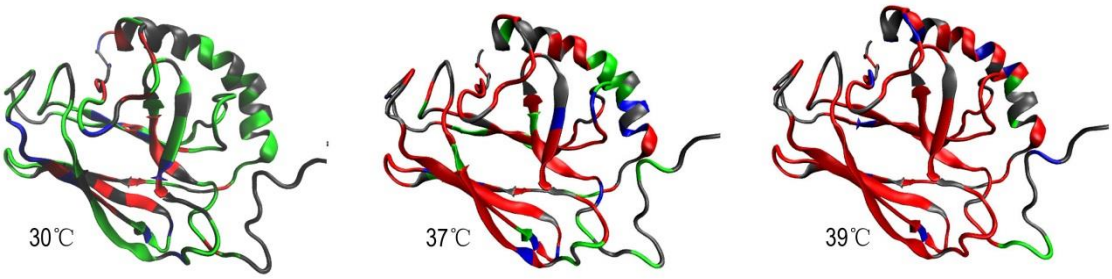

Figure 3.14. Conformational changes of F475S compared to that of WT at 30 ℃, 37 ℃ and 39 ℃ respectively on DnaK model. Gray: residues that cannot be assigned in NMR spectra. Green: CSP is less than 0.5 peak width. Blue: CSP is between 0.5 and 1.0. Red: CSP is more than 1.0 peak width.

3.15 Assessment of β-sheet content using MD

Considering the unfolding of the SBD mentioned in earlier sections, the β-sheets with significant CSPs were further analysed by MDs. As shown in Figure 3.15A, the content of β-sheets of WT can be maintained very well even at 39 ℃. L484W and F476S both displayed slight decreases in β-sheets content at elevated temperatures (Figure 3.15A) which is basically in line with CD results in an earlier section (Figure 3.8). Further β-sheet unfolding assessment indicated that L484W unfolded β3, only at 30 ℃ during sectors of the simulation (Figure 3.15B). In contrast, F476S disturbed more sheets

included β3, β5 and β6 (Figure 3.15B) and for prolonged perios of the simulation. Therefore, the unfolding of β-sheets induced by L483W and F475S appears to occur in different ways and to varying degrees.

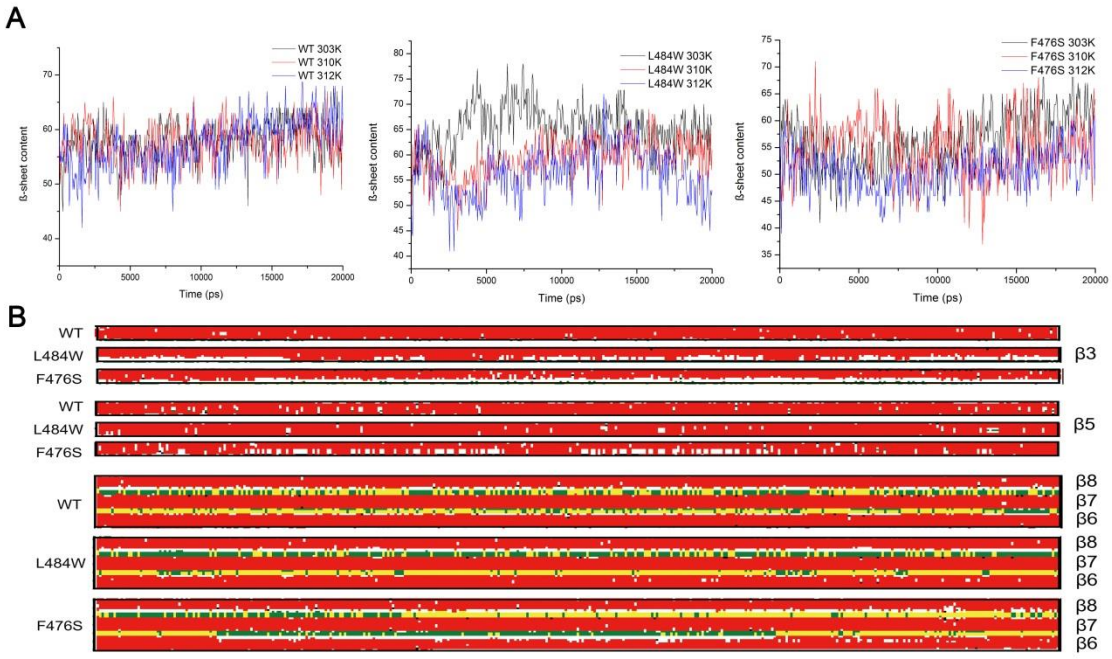

Figure 3.15. Assessment of the secondary structure of β-sheets. (A) The content of β-sheets as a function of simulation time at elevated temperatures. (B) The content of β-sheet patterns for sheets with significant CSPs. The existing of β-sheet was shown in red; coil is in white; bend is in green and turn is in yellow.

3.16 A structurally conserved β6-β7 region

F475S and L483W are located in the β6-β7 region which is one of the most conserved regions in SBD. Therefore, I wanted to know whether L483W and F475S mutants directly disturb residues within this region. Figure 3.16 showed the distance between β6 and β7 during simulations. Clearly, L484W and F476S both did not cause significant changes in the distance between β6 and β7 (Figure 3.16A), and this distance was not affected by elevated temperatures also (Figure 3.16B). As the β6 region of F476S seemed to unfold to a limited degree Figure 3.15B, it was predicted that the β6 was still close to β7 even following partial unfolding. Therefore, the disturbed β6-β7 region must exert effects through a series of both short-range and long-range interactions to affect the hydrophobic core.

As the long-range interactions are too complicated to decipher, I simply calculated the hydrogen bonds between residue 476 and the other residues to further investigate the short-range interactions (Table 3.2). The Phe476N:His422O is the most important hydrogen bond in all the mutants. It formed between β3 and β6 and weakened approximately 15%-20% by SBD mutations. However, a few side-chain hydrogen bonds between β3 and β6 were supplemented after Serine replacement (upright-letter hydrogen bonds in Table 3.2). Moreover, I found a hydrogen bond between residue 476 and loop 2,3, Ser476OG:Leu411O, which might be related to inter-domain communication. I speculate some hydrogen bonds contributed to the short-range interactions that regulate conformational changes of the SBD. Regarding the long-range interactions, although there is no data to support directly, I speculate that the three second-site suppressor residues imply the pathway of long-range regulation in SBD allostery to some degree.

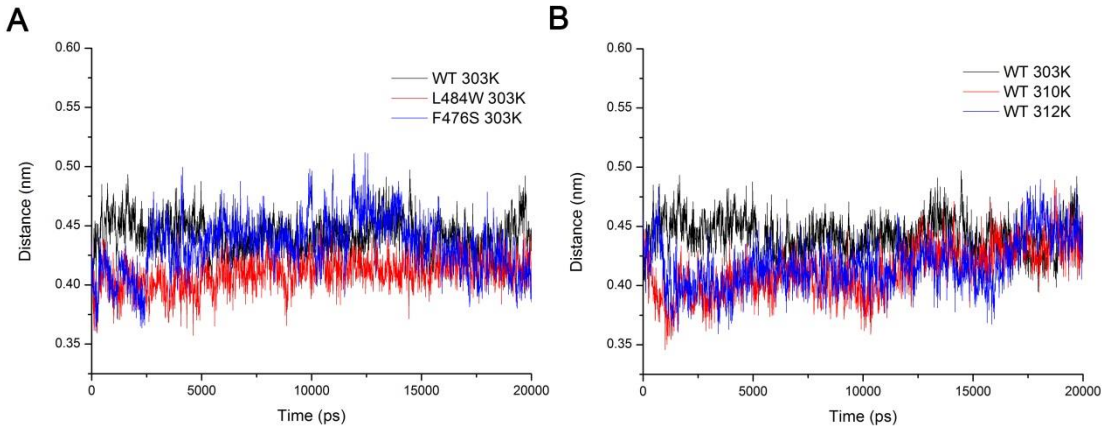

Figure 3.16. Distances between β6 and β7 as a function of simulation time. (A) The β6-β7 distance in SBD mutations; (B) β6-β7 distance of WT at elevated temperatures.

Table 3.2. Hydrogen bonds of residue 476 and other residues

	Temperature	Hydrogen Bonds of Residue 476 and Others	
		Average	Hydrogen bonds (lifetime, %)
WT	303K	0.9002	**Phe476N:His422O (92.5%)**
	310K	0.8962	**Phe476N:His422O (96.0%)**
	312K	0.8104	**Phe476N:His422O (79.5%)**
	303K	0.6527	**Phe476N:His422O (72.0%)**

L484W	310K	0.9261	**Phe476N:His422O (89.5%)**
	312K	0.8263	**Phe476N:His422O (85.5%)**
	303K	1.2395	**Ser476N:His422O (78.0%)**; Ser476OG:Leu411O (5%); Ser476OG:His422O (7.5%); Ser476OG:Gln424OE1 (5.5%)
F476S	310K	1.5250	**Ser476N:His422O (77.0%)**; Ser476OG:Thr420OG1 (16.0%); Ser476OG:Thr420O (31.0%); Ser476OG:His422ND1 (9.5%)
	312K	1.1756	**Ser476N:His422O (61.0%)**; Ser476OG:Leu411O (25.0%); *Ser476OG:Val474O (5%)*; *Ser476N:Val474O (6.5%)*
	303K	1.1936	**Ser476N:His422O (72.5%)**; Ser476OG:Leu411O (5.0%); Ser476OG:Thr420OG1(7.5%); Ser476OG:Thr420O(6.5%)
A395V/F476S	310K	1.4451	**Ser476N:His422O (78.0%)**; Ser476OG:Leu411O (24.0%); Ser476OG:His422O (5.5%); Ser476OG:Gln424OE1 (14.0%); *Ser476OG:Val474O (6.0%)*
	312K	1.7705	**Ser476N:His422O (89%)**;Ser476OG:Thr420OG1 (55.5%); Ser476OG:Thr420O (6.5%)
P434S/F476S	303K	0.9780	**Ser476N:His422O (81%)**
	310K	1.2754	**Ser476N:His422O (84%);** Ser476OG:His422O (11.0%)
	312K	1.2116	**Ser476N:His422O (81.5%)** ; Ser476OG:His422O (11.0%)
V478I/F476S	303K	1.7106	**Ser476N:His422O (80.5%)**; Ser476OG:Thr420O (30.0%); Ser476OG:Leu411O (14.5%)
	310K	1.0499	**Ser476N:His422O (84.5%)**; Ser476OG:His422O (5.0%)

312K	1.3673	**Ser476N:His422O (75.0%)**; Ser476OG:Gln424OE1 (15.0%); Ser476OG:Leu411O(16.0%)

Note: bold means backbone hydrogen bonds between β3 and β6. The normally upright letters mean side-chain hydrogen bonds between β3 and β6. The italics mean those hydrogen bonds are not located in β3 and β6. The underline letters mean hydrogen bonds between residue 476 and Loop 23 which are related to ATPase regulation.

3.17 Secondary structure analysis of the full-length Ssa1 proteins

As the predicted changes within F475S variant were drawn utilising a truncated version of the SBD, I also assessed changes in full-length Ssa1 protein. Therefore, I expressed and purified the full-length wild-type protein and SBD mutations. CD spectra revealed that there were several differences in the secondary structure of F475S protein in comparison to that of WT. Briefly, absorbance differences are focused on 208nm, 222nm (α-helix) and 215-217nm (β-sheets). F475S variant clearly showed decreased absorbance at 215-217nm which suggested the decreased level of β-sheet formation also occurs in the SBD of full-length protein as well as the truncated protein (Figure 3.17A). Interestingly, A394V/F475S had a similar absorbance at 215-217nm compared to WT, but in contrast P433S/F475S and V477I/F475S, had reduced absorbance at 215-217nm, suggesting that the secondary structure of SBD has not been recovered in these mutants (Figure 3.17A). Moreover, the mutants displayed modified absorbance at 208nm and 222nm compared to WT, which implies that significant conformational changes occurred to α-helical regions also. Considering there are two α-helical rich regions in full-length Ssa1, NBD and SBDα, we cannot distinguish between which of these regions is the one most affected. Apart from F475S variant, CD spectra of the WT and second-site suppressors did not display significant changes at elevated temperature (Figure 3.17 B and C), suggesting that the restoration of secondary structure of full-length Ssa1 under heat shock may be responsible for the recovery of temperature sensitivity of F475S.

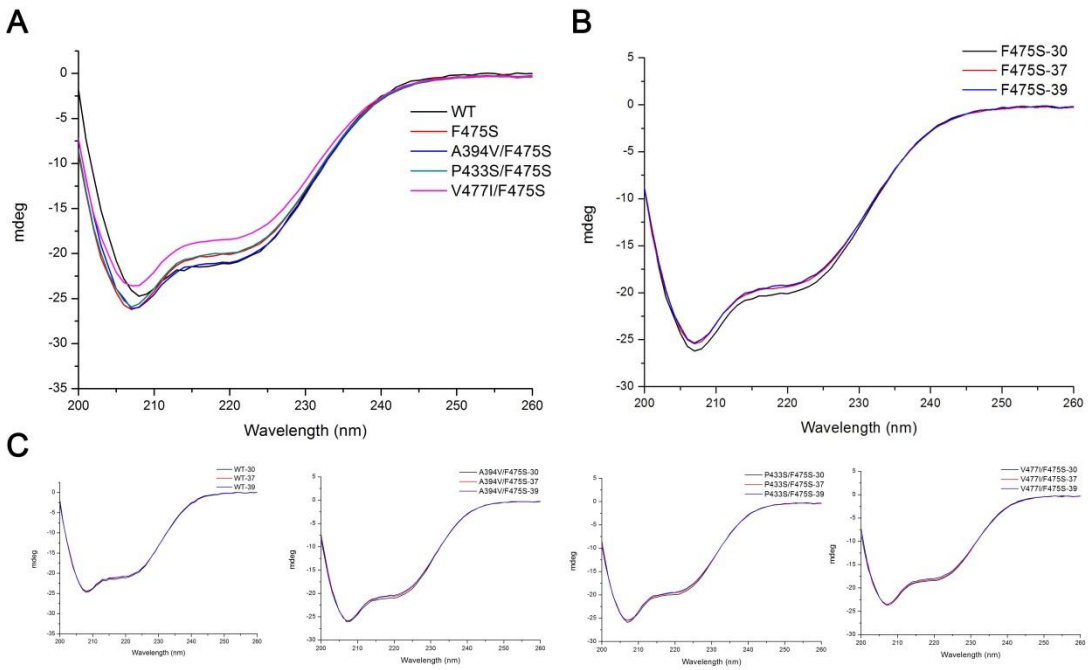

Figure 3.17. Secondary structure monitored by far-UV CD spectra for full-length Ssa1. (A) CD spectra scanned at 30℃; (B) CD spectra of F475S scanned at elevated temperatures; (C) CD spectra of WT and second-site suppressors scanned at elevated temperatures. The temperature was controlled precisely by an extra digital module and a plugin device.

3.18 Intrinsic Fluorescence of full-length F475S mutants

As there are two main α-helix areas in full-length Ssa1, NBD and SBDα, we cannot deduce which α-helix region is affected by F475S Figure 3.17A. Fortunately, there is only one tryptophan located in the SBDα, which can be used to monitor the conformational changes of the SBDα. It was found that F475S and V477I/F475S caused a slight increase in intrinsic fluorescence intensity, suggesting that F475S caused slight conformational changes in the SBDα, such as slight rearrangement or opening or closing of the SBDα. However, distinctions of the intrinsic fluorescence intensity were too small to explain significant influences in CDs (Figure 3.17A). Therefore, it was speculated that the absorbance differences of CD spectra at 208nm and 222nm are caused mainly by conformation changes located in the NBD. In another words, F475S might influence inter-domain communication of the full-length Ssa1.

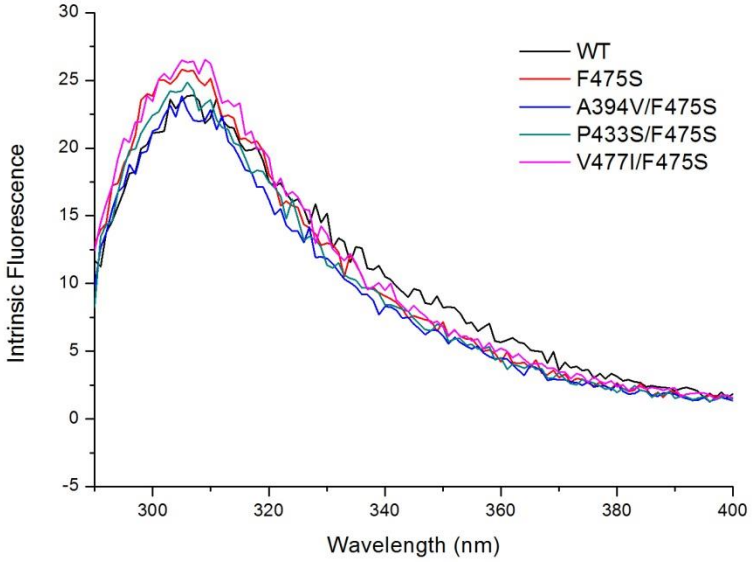

Figure 3.18. Intrinsic Fluorescence for full-length F475S mutants. Intrinsic fluorescence was scanned at RT.

3.19 F475S abolishes the SBD repression to ATPase activity of NBD

To investigate the inter-domain communication and conformation changes of the α-helix in NBD, I assessed the basal ATP hydrolysis of Ssa1 mutants at optimal and elevated temperatures (Figure 3.19A). F475S and second-side suppressors all increased intrinsic ATPase activity to varying degrees, compared to WT (roughly F475S: 6 fold; A394V/F475S: 4 fold; P433S/F475S: 6 fold; V477I/F475S: 6 fold). Furthermore, the basal ATP hydrolysis rate can be enhanced by elevated temperatures, but F475S mutants cannot be stimulated by peptide or Ydj1. One possible explanation for loss of Ydj1 and peptide stimulated ATPase activity is that mutants adopt a conformation that mimics the co-chaperone-stimulated state so that ATPase activity is not further stimulated since the Hsp70 is already activated. Alternatively, the affinity to Ydj1 and peptide might be decreased. Regarding increasing of the basal ATPase rate by SBD mutants and heat shock, it has been known that the SBD acts as a brake on NBD's ATPase activity and that the free NBD with the linker domain attached has a higher activity than full-length Hsp70 (O'Brien & McKay 1993). It is thought that the ATPase inhibition from SBD requires docking of NBD with SBD (Kityk et al. 2015). Therefore, the elevated basal ATPase rate by SBD mutants (especially F475S) and heat shock

(more significantly) suggests that losing important contacts between NBD and SBD prevents the inhibition of ATP hydrolysis. In another words, the F475S destabilizes the interface between NBD and SBD and results in a equilibrium shift towards the undocking state, which allows NBD subdomains to rotate to a degree where the catalytic residues in the ATPase active center reach the optimal position for γ-phosphate cleavage (Mayer & Kityk 2015). As a consequence, Ssa1 mutant's inability to implement SBD inhibition of ATP hydrolysis may directly cause disequilibrium of ATP and ADP states and influence substrate binding and co-chaperone interactions. Previous analysis confirmed that increasing ATPase activity by overexpressing Sti1 or decreasing ADP release by deleting the NEF Fes1, weakens [*PSI*$^{+}$] phenotype (Jones et al. 2004). It is likely that the increase of ATPase activity of F475S may be one of the reasons for impairing [*PSI*$^{+}$] propagation.

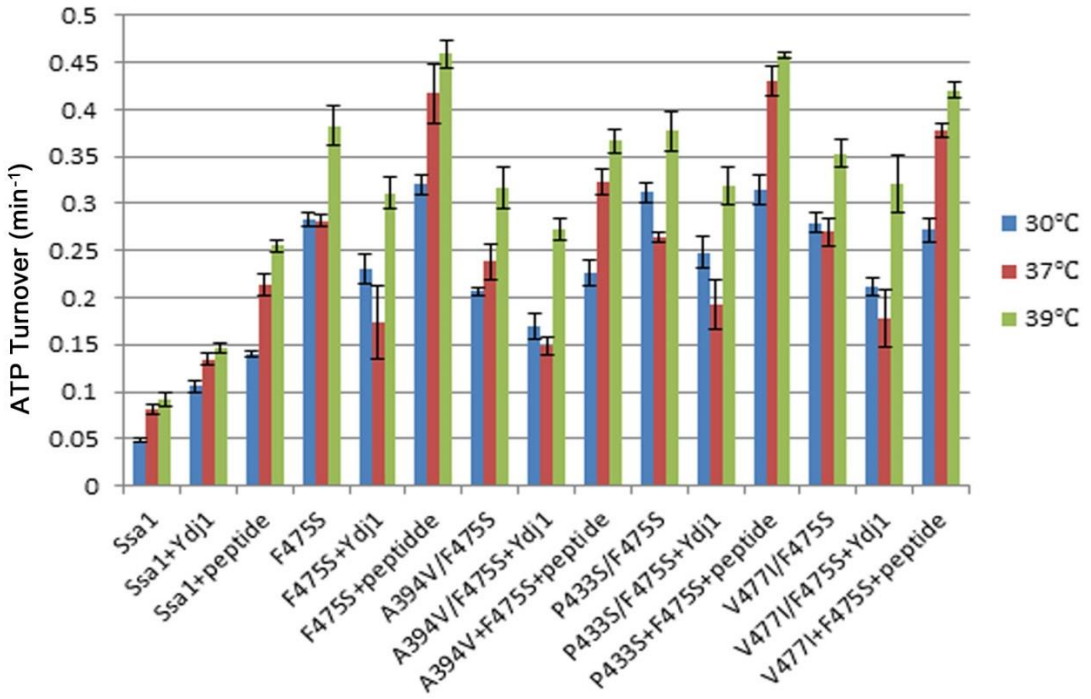

Figure 3.19. The ATPase activity of the mutants with or without Ydj1 or peptide at elevated temperatures. The unit of the ATP turnover rate is min^{-1}.

3.20 Assessment of highly conserved residue 475 of Ssa1

Phe475 is highly conserved in the Ssa family, *E.coli* DnaK and Human Hsp/c70. The F475S mutant has shown a significant disturbance in the SBD, implying residue 475

plays a crucial role in maintaining the structure and function of Hsp70. In order to further investigate the importance of residue 475 and the mechanism of how F475S exerts effect, I designed and assessed other amino acid substitutions at this site (Table 3.3). It was found that decreasing the size of amino acid side chain of residue 475, such as Alanine (slight sensitivity at 39 ℃) and Serine, results in temperature sensitivity and [PSI^+] impairment (Figure 3.20A, B and C). Increasing size of side chain of residue 475 larger than Cysteine, no matter whether it is polar or nonpolar (Tyrosine and Phenylalanine), thermotolerance and [PSI^+] can be maintained (Figure 3.20A, B and C). However, if the side chain size is increased too much by introducing tryptophan, Ssa1 will lose intrinsic function and fails to support cell survival (Table 3.3). Considering the contribution of residue 475 in forming the hydrophobic pocket, it was speculated that an appropriately sized side-chain is necessary to maintain the functional confirmation of the substrate-binding pocket. Too small side chain may be not enough to fill the cavity around residue 475 and if side chain is too large this may distort the local secondary structure too much due to steric hindrance.

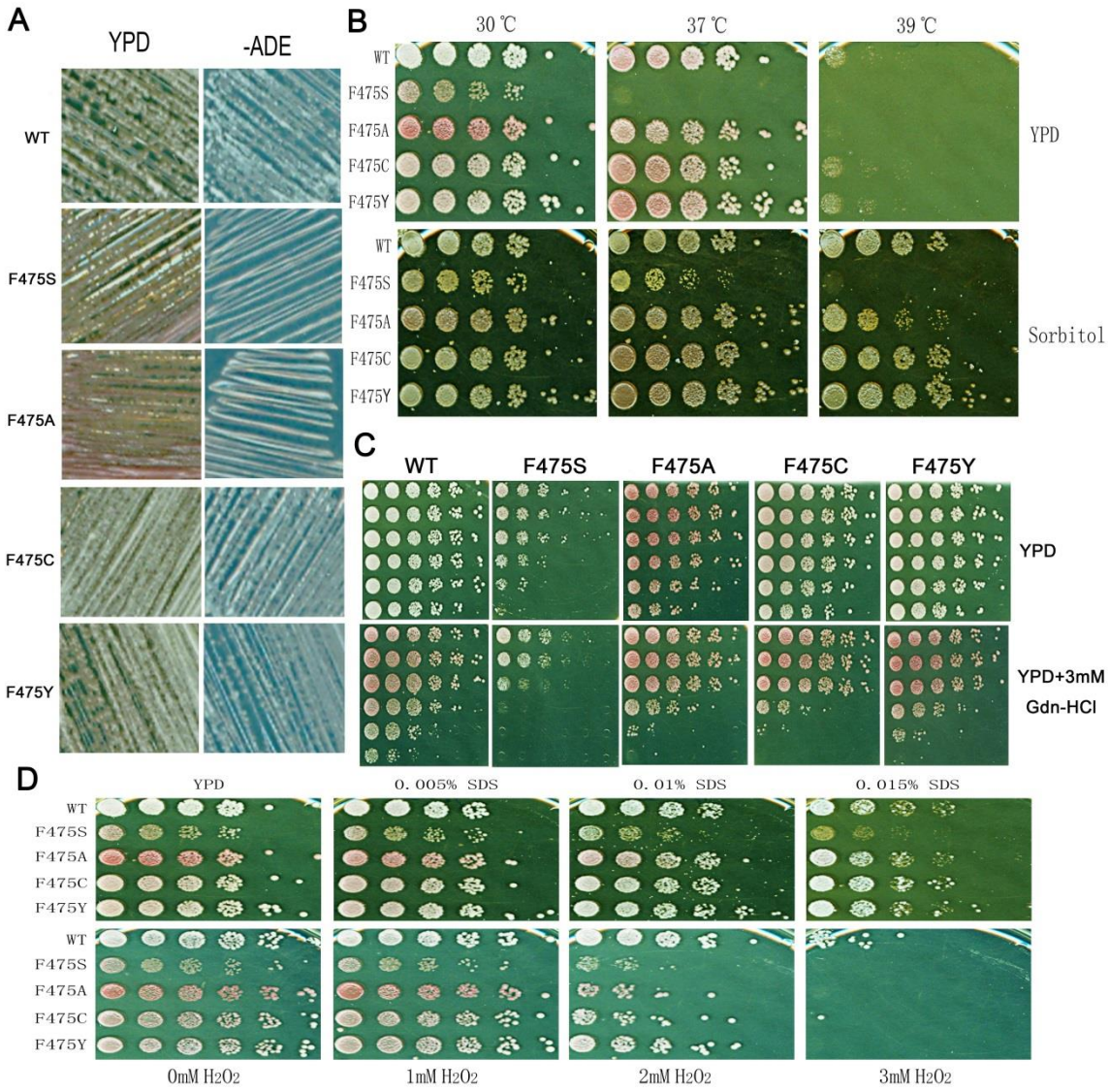

Figure 3.20. Phenotypes of different Phe475 substitution mutations. (A) Assessments of [*PSI*$^+$] propagation; (B) Effects of elevated temperatures on 475 mutations; (C) Acquired thermotolerance assays on 475 mutations; (D) Assessments of 475 mutations under stresses of SDS and H_2O_2.

Table 3.3. Property of Phe475 mutations

Amino Acid on Residue 475	Size of the Side Chain	Polar/Nonpolar (+/-)	[*PSI*$^+$]/[*psi*$^-$]	Temperature Sensitive
Phe	+	-	+	N
Ser	--	+	-	Y
Ala	---	-	-	Y
Cys	-	+	+	N
Trp	+++	-	NA	NA
Tyr	++	+	+	N

3.21 Degradation assay of SBD truncation with Phe475 substitutions

To further assess the relationship between SBD degradation and unfolded SBD, I purified SBD truncation with Phe475 substitutions and incubated them at 30 ℃ independently. Following incubation, samples were passed through a 24 ml Superdex 75 column one by one. As shown in Figure 3.21A, F475A, F475C and F475Y maintained the monomeric state similar to WT, but the lethal mutant F475W had the biggest absorbance difference compared to WT, and F475S also showed significant change. This implies that F475W induced complicated conformational changes in the SBD. As F475S caused the unfolding of the SBD, it was considered that F475W resulted in a similar, but markedly increased effect. Following incubation, F475C and F475Y showed similar stability to WT (Figure 3.21C and Figure 3.9). Although F475A also had similar characteristics with WT at short incubation (5h), following longer incubation (12h and 24h) it it does exhibit instability compared to WT. Interestingly, the degradation of the F475W did happen after 12h incubation (F3.21B). Therefore, new mutations at residue 475 further highlight the crucial role of this residue in maintaining the stability of the SBD and also further enhance the proposal that the instability of the SBD is the primary cause of the temperature sensitivity of cells expressing these mutants.

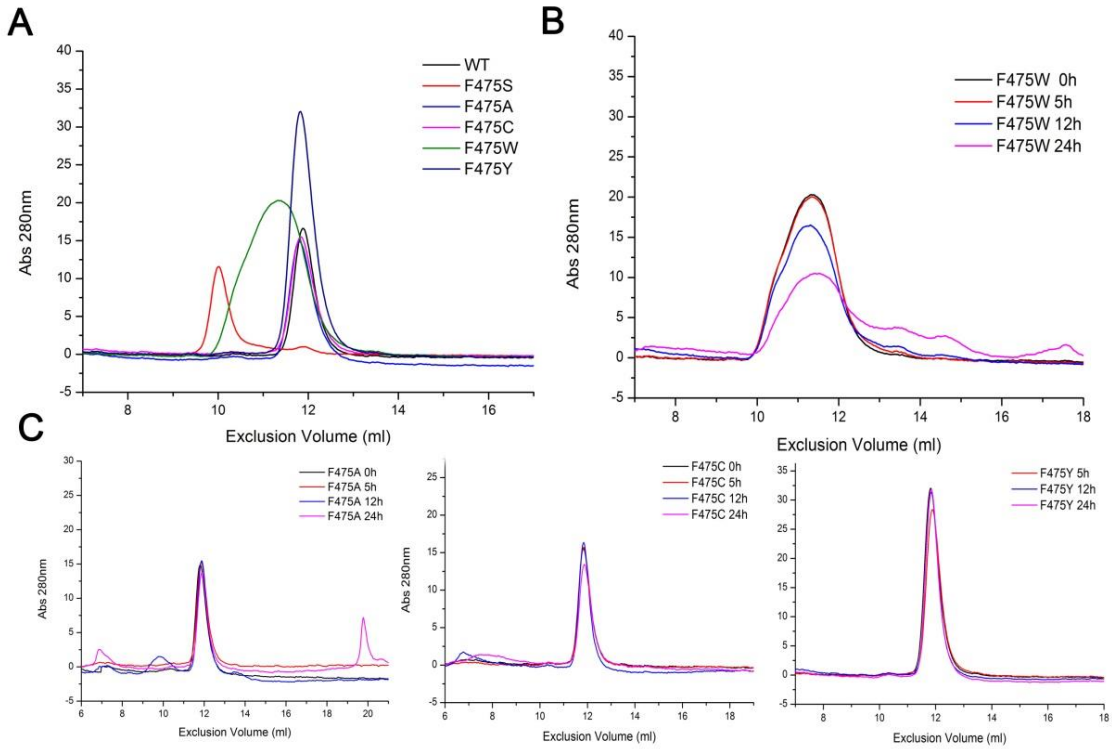

Figure 3.21. SBD degradation assay by SEC. (A) Comparative analysis of the Phe475 substitutions on the stability of the SBD; (B) The SEC assays of F475W after 24 h incubation. (C) SEC assays of F475A/C/Y after 24 h incubation. Purified SBD truncation mutations were incubated at 30 ℃. 100 µl of 50 µM protein was loaded into a 24 ml Superdex 75 column.

3.22 Secondary structure analysis of the SBD truncation with Phe475 substitutions

In this section, it was assessed the secondary structure of the truncated SBD with Phe475 substitutions (F475A, F475C, F475S F475W, F475Y) using CD. CD spectra revealed similar findings to ealrier CD results. Briefly, F475S and F475W truncation proteins showed reduced absorbance at 215-217nm which suggested β-sheets are unfolding in SBD truncation proteins (Figure 3.22A). However, F475A/C/Y displayed similar CD profiles as obtained for WT (Figure 3.22A). All Phe475 substitutions displayed increased disordered structure at elevated temperatures (Figure 3.22 B and C), especially F475W and F475A, which is consistent with growth deficiency under normal or heat-shock conditions (Figure 3.22B, C, Figure 3.20B, C and Table 3.3).

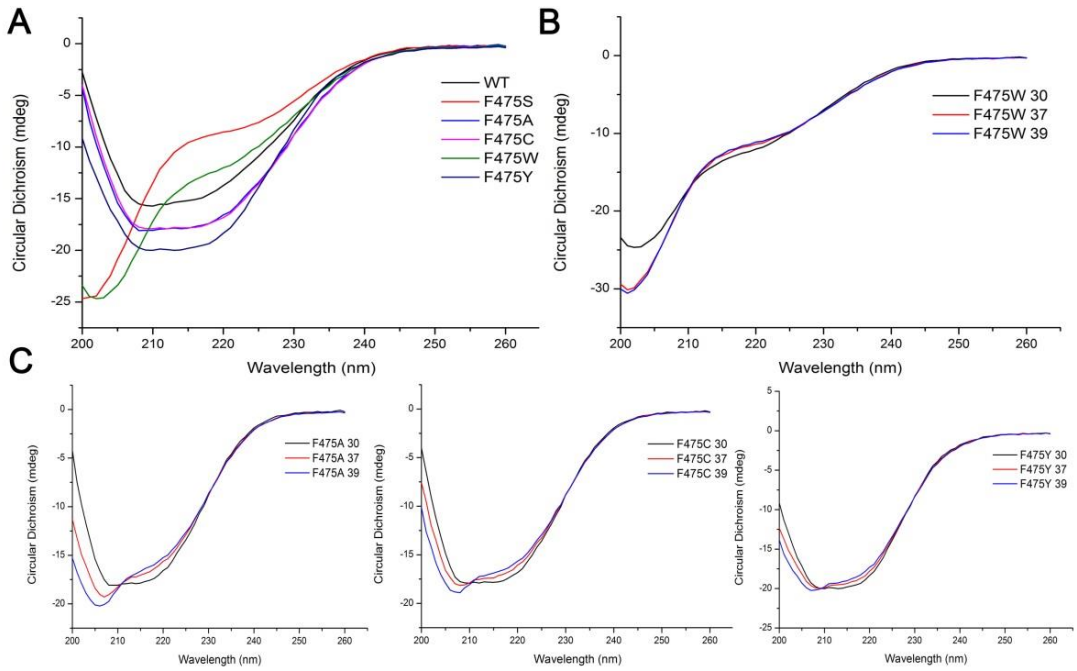

Figure 3.22. Secondary structure monitored by far-UV CD spectra for the SBD truncation mutations at residue 475. (A) CD spectra scanned at 30 ℃; (B) CD spectra of F475W scanned at elevated temperatures; (C) CD spectra of F475A, F475C and F475Y scanned at elevated temperatures. The temperature was controlled by an extra digital module and a plugin device.

3.23 Secondary structure analysis of the full-length Ssa1 mutations

As the instability of the Phe475 substitutions was observed from the SBD truncation model, I wanted to see what kind of effects may occur in the full-length Ssa1 proteins. Therefore, I expressed and purified the full-length Ssa1 protein harbouring Phe475 substitutions. CD spectra revealed that F475S and F475W had similar characteristics in the full-length protein as for truncated SBD. Briefly, the absorbance around 208nm, 222nm (α-helix) and 215-217nm (β-sheets) had the largest changes. F475W/S variants obviously showed a decreased absorbance at 215-217nm which implied loss of β-sheets in SBDβ (Figure 3.23A). Additionally, F475A/C/Y had similar CD profiles and absorbance at 215-217nm decreased compared to WT, revealing that the content of β-sheets was reduced in full-length proteins. Most of the mutants gave the variant absorbance at 208nm and 222nm compared to WT, which implies the conformational changes happened to α-helix regions to some degree. Considering F475S and second-site suppressors mainly affected the α-helix regions in NBD, it was considered that the

substitutions on residue 475 had the same manner too. In another words, Phe475 substitutions influenced the inter-domain communication between NBD and SBD.

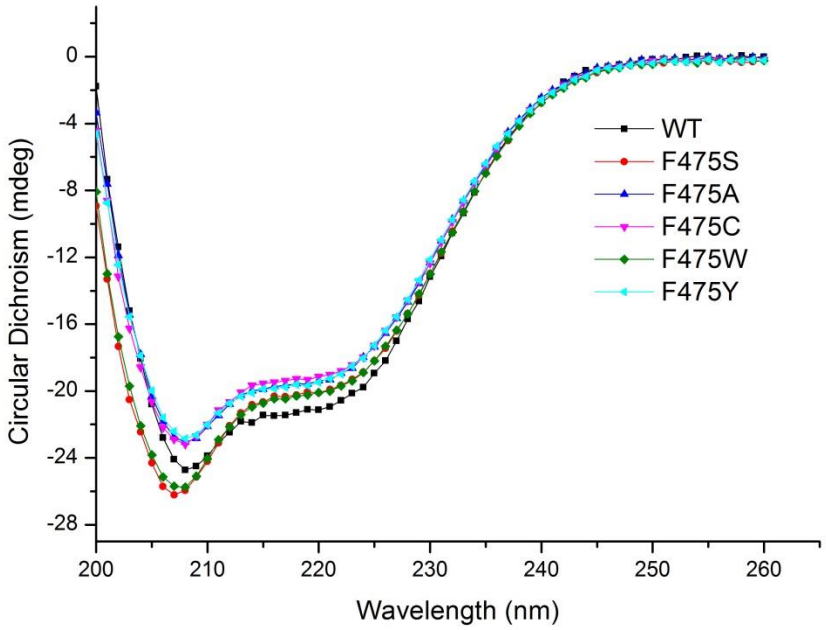

Figure 3.23. Secondary structure monitored by far-UV CD spectra for the full-length Ssa1 mutations on the residue 475. CD spectra were scanned at 30 ℃.

3.24 ATPase activity of the full-length Ssa1 with Phe475 substitutions

To investigate the NBD conformational changes induced by mutations on residue 475, I assessed the basal ATP hydrolysis of the full-length Ssa1 with these Phe475 substitutions at optimal and elevated temperatures (Figure 3.24A). Similar to F475S, F475W significantly increased ATPase activity at 30℃ (F475W: 4 fold; F475S: 6 fold) (Figure 3.24 and Figure 3.19). Furthermore, the basal ATP hydrolysis rate of F475W is hardly stimulated by peptide or Ydj1. One possible explanation for the losing of Ydj1 and peptide stimulated ATPase activities is that those mutants adopt a conformation that mimics the co-chaperone-stimulated state so that ATPase activity is not further stimulated since the Hsp70 are already activated. Alternatively, the affinity to Ydj1 and peptide might be decreased. By contrast, F475A has a small effect on basal ATPase activity and F475C/Y are similar to WT. However, F475C/Y still showed a deficiency in ATPase activity under peptide stimulation, which may be related to the secondary

structure changes in Figure 3.23. The elevated basal ATPase rate by SBD mutants (especially F475W and F475S) and heat shock (more significantly) implied that the loss of contacts between NBD and SBD prevents the inhibition of ATP hydrolysis. In another words, SBD mutations F475W/S (perhaps F475A as well) affect interface stabilization resulting in an equilibrium shift to the undocking state, which allows NBD subdomains to rotate to a degree where the catalytic residues in the ATPase active center reach the optimal position for γ-phosphate cleavage (Mayer & Kityk 2015). As a consequence, the SBD inhibition to ATP hydrolysis of the NBD is abolished. Such a disruption of inter-domain contacts might directly influence the equilibrium of ATP and ADP and even substrate binding and co-chaperones interactions.

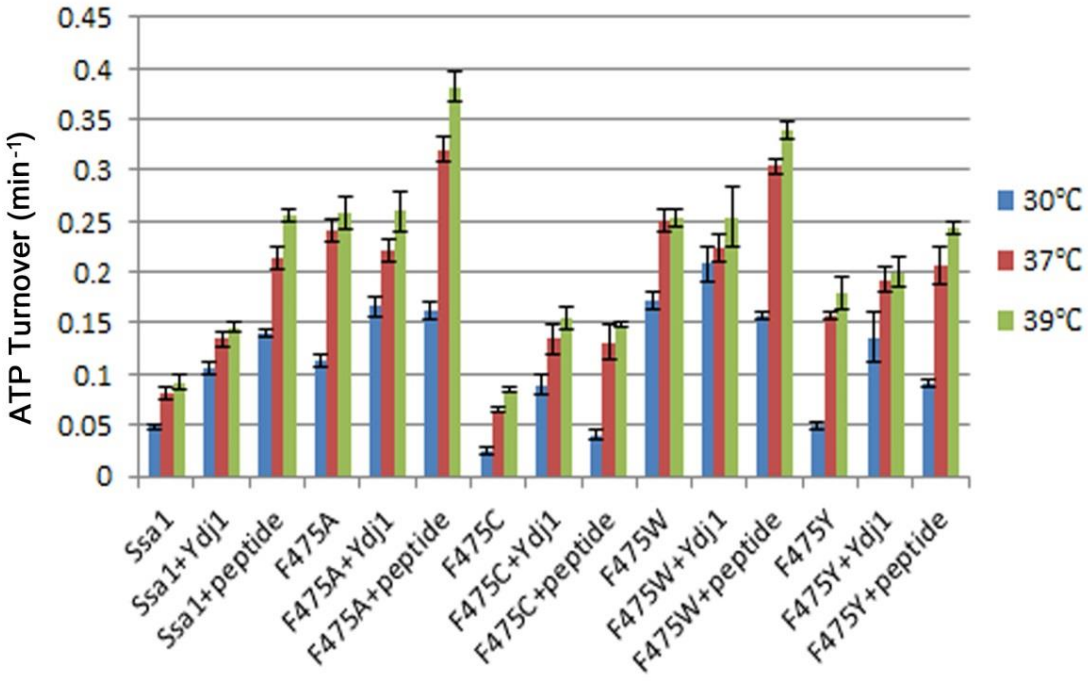

Figure 3.24. The ATPase activity of the Phe475 mutants with or without Ydj1 or peptide stimulation at elevated temperatures.

3.25 Luciferase refolding assay of mutations at residue 475

The Hsp70/Hsp40/Hsp104 machinery plays an essential role in prion propagation and thermotolerance. A major function of Hsp70 machinery is refolding proteins that have become dentatured due to heat stress. Because the inherent ATPase activity of F475S variant was accelerated and refractory to the addition of the peptide and Hsp40 co-

chaperone, it was predicted that the F475S would be unable to refold denatured luciferase. To assess this I assayed luciferase refolding activity for F475S variant and the other mutations at residue 475. Unsurprisingly, F475S displayed a deficiency in luciferase refolding, as expected. More interestingly, both [*psi*$^-$] mutations (F475S and F475A) lost or had clearly reduced ability to refold denatured luciferase (Figure 3.25). One explanation is that the deficiency of refolding activity of the Hsp70 machinery accelerates the accumulation of amorphous aggregation, but decreases the formation of organized fibers so that dramatically reduces the number of prion seeds *in vivo*. Moreover, as the accumulation of amorphous aggregation, cells may be more sensitive to response heat shock and other stresses.

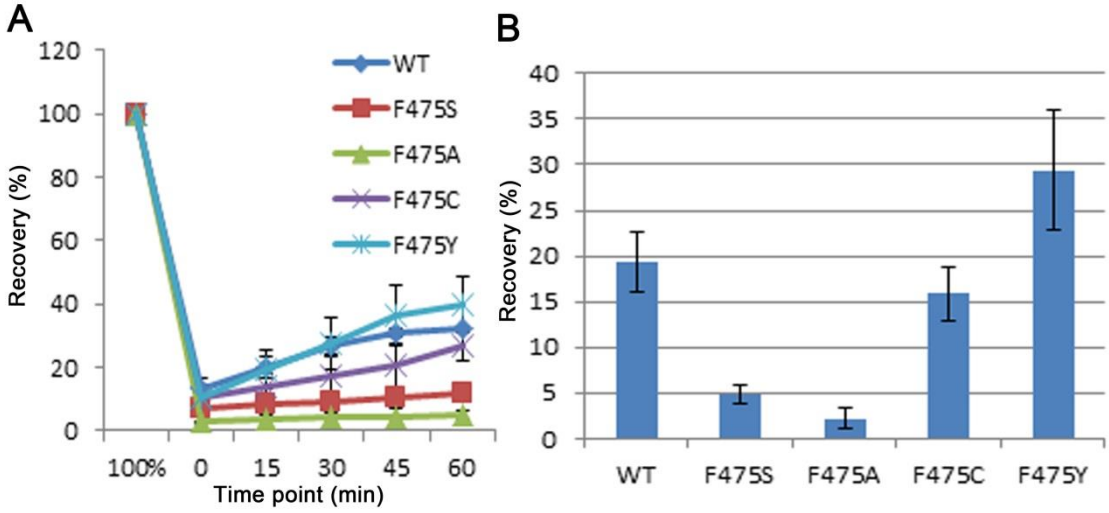

Figure 3.25. Luciferase refolding activity of mutations at residue 475. (A) Luciferase refolding profiles during a 60 min time course; (B) Luciferase recovery rate at 1 h. Fresh cultures were shifted to 37 ℃ for 30 min before 45 ℃ denaturation for 1 h. Denatured luciferase cultures were recovered at 25 ℃ for a 1 h period. Cycloheximide was added to prevent protein synthesis during the recovery period.

3.26 Basal expression level of the Hsp70-Hsp40-Hsp104 machinery

Previous reports showed that Hsp70 levels are significantly elevated under heat shock (Gunasekera et al. 2008). In addition to Hsp70, cytoplasmic chaperones such as Hsp110, Hsp90, Hsp70, Hsp40 and small Hsps, mitochondrial chaperones such as Hsp10 and Hsp60 can be induced under heat shock as well (Tan et al. 2015). Therefore, to further characterize SBD mutants, I tested the intracellular expression level of main members

of Hsp70 machinery (Ssa1, co-chaperones Ydj1 and Hsp104) using Western blotting. Figure 3.26 shows that Hsp104 was expressed at similar levels in WT and all mutants, and suggests this is not a contributing factor to thermotolerance deficiencies in these mutants, which is in line with the conclusion from Figure 3.4. The expression levels of Ydj1 did not show any significant changes either. However, there are obvious differences (F475S, second-site suppressors and F475C) in Ssa1 expression level (Figure 3.26). The expression levels of Ssa1 in F475S and other mutations were lower than that of WT. One possible reason is that unfolded SBDβ (Figure 3.8) is degraded, by the ubiquitin pathway or other degradation system, and this is the major reason why cells are temperature sensitive. However, A394V/F475S and V477I/F475S did not recover the temperature sensitivity of F475S by simply increasing Ssa1 level, and a small amount of Ssa1 F475C is enough to maintain the normal cellular functions of Ssa1. Thus, I considered that there are multiple effects induced by F475S, such as expression level, inter-domain communication, interactome changes and perhaps other functions of the Ssa1 which are also altered. Taken together, possible explanations for observed phenotypes include: 1) SBD disturbance by F475S variant causes multiple effects and one of these is greatly decreased protein level of Ssa1; 2) P433S/F475S rescued the temperature sensitivity of F475S by stabilizing SBD and increasing protein level; 3) Considering the locations of A394V/F475S and V477I/F475S, they may rescue F475S disturbance through altering inter-domain communication and other functions of Ssa1 rather than increasing protein level; 4) impairment of [PSI^{+}] propagation caused by F475 mutations is independent from the protein level of Ssa1.

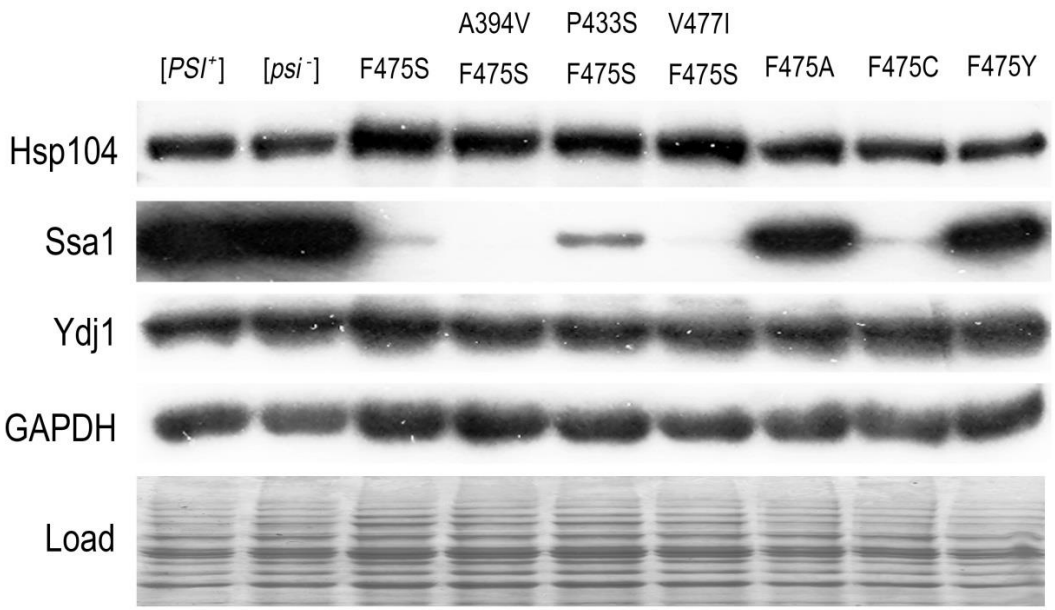

Figure 3.26. Chaperones abundance of the Hsp70 machinery. Western bolting was performed to assess the expression levels of Hsp104, Ssa1 and Ydj1. GAPDH and a stained SDS-PAGE ran under the same conditions were used as loading controls.

3.27 Assessments of FLAG-tagged F475S mutant

In order to investigate the interaction changes between F475S mutant and Ssa1 binding partners *in vivo*, I constructed N-terminally tagged Ssa1 and F475S versions in pC210 vector. Previously we have demonstrated that incorporating a 6×His tag at the N-terminal region of L483W and F475S can cause the protein to be non-functional *in vivo* (Sarah A. Cusack' thesis, 2010), therefore I fused a smaller FLAG tag to the N-terminal of Ssa1 and F475S in this work. Prior to performing a Co-IP I assessed the affect of FLAG-tagging on SSa1 and F475S *in vivo* function (Figure 3.27). The prion assessment showed that FLAG-tagged F475S did not alter the [*psi*$^-$] phenotype (Figure 3.27 A). Although FLAG-tagged Ssa1 are slightly more sensitive to elevated temperatures and acquired thermotolerance assay compared to non-tagged Ssa1, the temperature sensitivity of the F475S variant was maintained well (Figure 3.27 B and C). Furthermore, FLAG tag hardly influenced the activity of F475S in response other stresses such as SDS and H_2O_2 (Figure 3.27 D and E). Therefore, it was concluded that fusing N-terminal FLAG tag did not significantly alter the function of F475S mutation *in vivo*, and it can be used for further investigations.

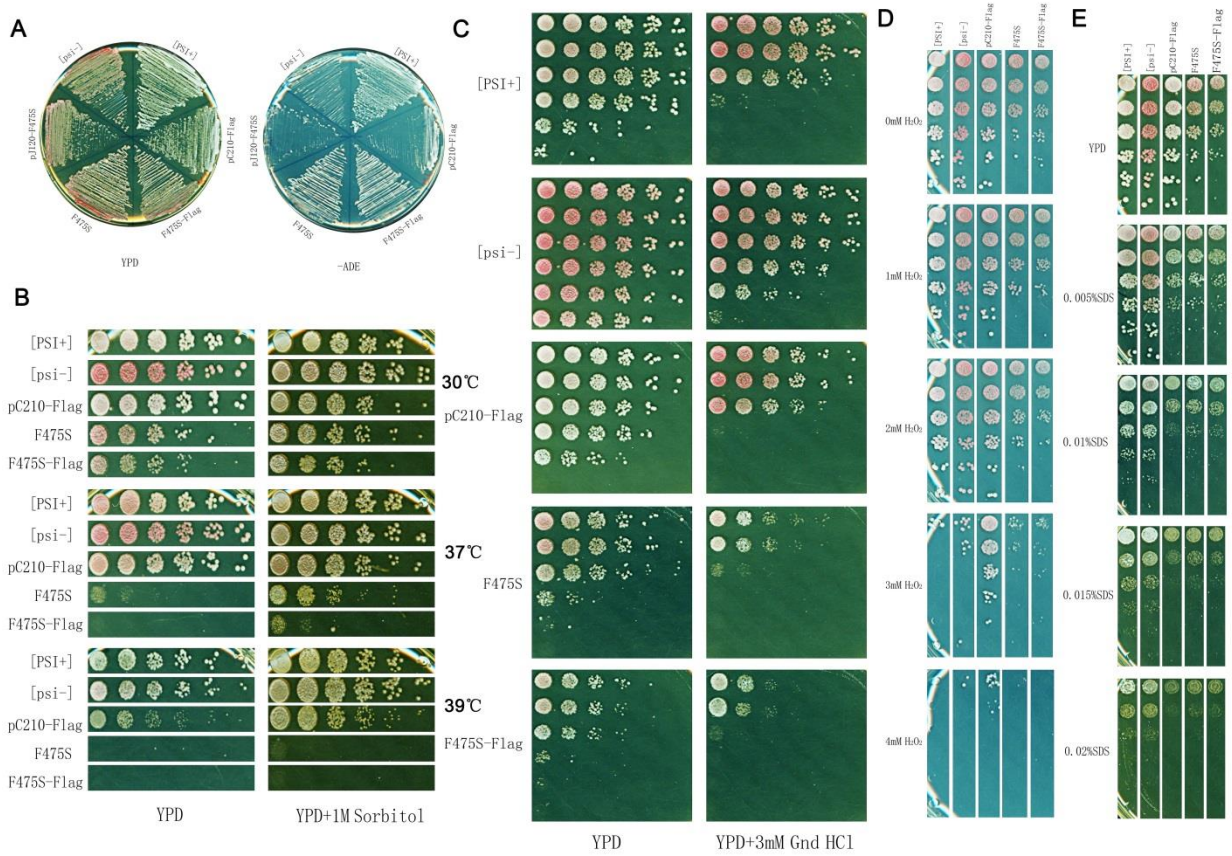

Figure 3.27. Phenotypical analysis of FLAG-tagged F475S mutation. (A) Assessment of [*PSI*$^+$] propagation in FLAG-tagged Ssa1 and F475S; (B) Effects of elevated temperatures in FLAG-tagged Ssa1 and F475S; (C) Acquired thermotolerance in FLAG-tagged Ssa1 and F475S; (D) Comparative growth assessments of FLAG-tagged F475S in response to cell-wall damaging agent SDS; (E) Comparative growth assessments of FLAG-tagged F475S in response to oxidative stress agent H_2O_2.

3.28 Co-IP analysis of interactions between Ssa1 and binding partners

To identify Ssa1 binding partners influenced by the F475S mutation, I cultured cells with FLAG-tagged WT or F475S as sole Ssa source and purified the FLAG-Ssa1 interactomes using Anti-FLAG M2 magnetic beads and compared them by WB. First of all, I checked the cross reaction of the Anti-FLAG M2 magnetic beads and whole proteins in the G402 background. As shown in Figure 3.28A, no signal can be seen in non-tagged samples, suggesting Anti-FLAG M2 magnetic beads have great specific binding in this study. Surprisingly, there were several obvious bands around 40-50 KDa from FLAG-F475S sample, and they were hard to be seen in FLAG-WT sample. As I fused FLAG tag to the N-terminal of Ssa1 and the size of the NBD is around 44 KDa (Figure 1.6), the degradation bands of the FLAG-F475S suggested that *in vivo* the SBD

is readily degraded in F475S and results in production of N-terminal NBD fragments. To directly test Ssa1 interactions with common co-chaperone binding partners, Co-IP samples were probed with antibodies against Hsp104, Ydj1, Hsp26 and Sup35. Western blotting indicated that the F475S variant slightly enhanced binding with Hsp104 and Hsp26. Previous reports showed that Hsp26 impaired [*PSI*$^+$] prion propagation by inhibiting self-templating and preventing conformational rearrangements of molten oligomers in yeast (Duennwald et al. 2012) and overexpression of Hsp104 cured [*PSI*$^+$] prion (Shorter & Lindquist 2006; Chernoff et al. 1995). Therefore, the impairment of [*PSI*$^+$] prion propagation by F475S may be influenced by increasing the affinity of Ssa1 for Hsp104 and Hsp26. Although Ydj1 is important to regulate [*PSI*$^+$] prion, I did not see any difference here. Interestingly, F475S variant hardly bound with Sup35, which may also contribute to the inability to propagate the prion.

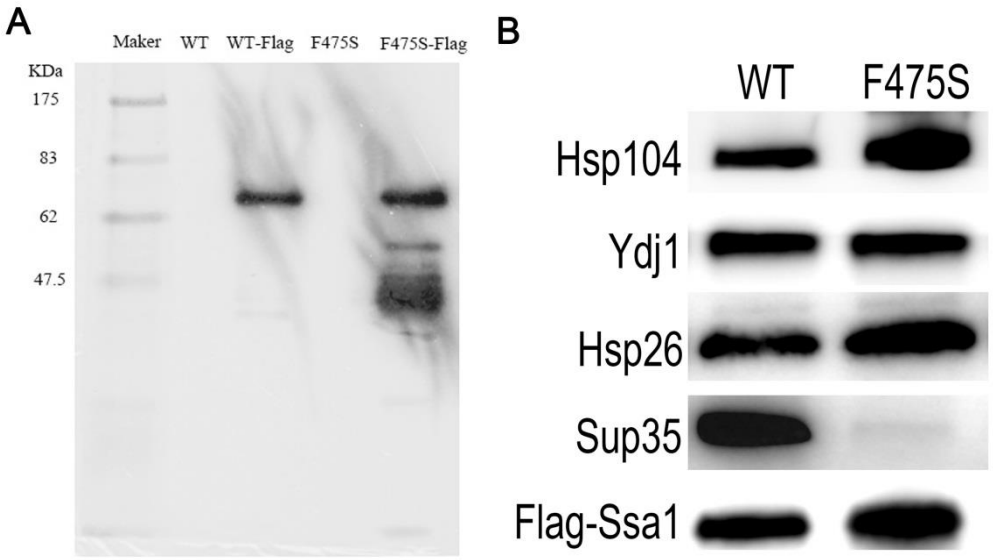

Figure 3.28. F475S alters the Ssa1 interactions with clients. (A) Ssa1 was pulled down from cells with or without the FLAG tag and probed for Anti-FLAG M2. (B) FLAG-tagged Ssa1 was pulled down from WT and F475S cells and probed for Hsp104, Ydj1, Hsp26 and Sup35. FLAG-Ssa1 was used as loading control.

3.29 Assessment of F475S mutation within the Ssa Family

Phe475 is conserved throughout the whole Ssa family. To assess functional conservation of this residue we created F475S in the other Ssa family members, Ssa2,

Ssa3 and Ssa4. Unfortunately, Ssa3^{F475S} is lethal when the sole Ssa source in cells, which underscores the importance of this residue. Perhaps the structural changes induced in the SBD are not tolerated as well in Ssa3 and hence a non-functional protein is produced? Interestingly, Ssa2 ^{F475S} and Ssa4 ^{F475S} both impaired [*PSI*$^{+}$] propagation and caused a temperature-sensitive phenotype in a similar manner to Ssa1 ^{F475S} (Figure 3.29 A and B). Therefore, we drew the conclusion that the Phe475 residue is functionally important across the whole Ssa family and introduction of F475S has similar functional consequences for Hsp70s.

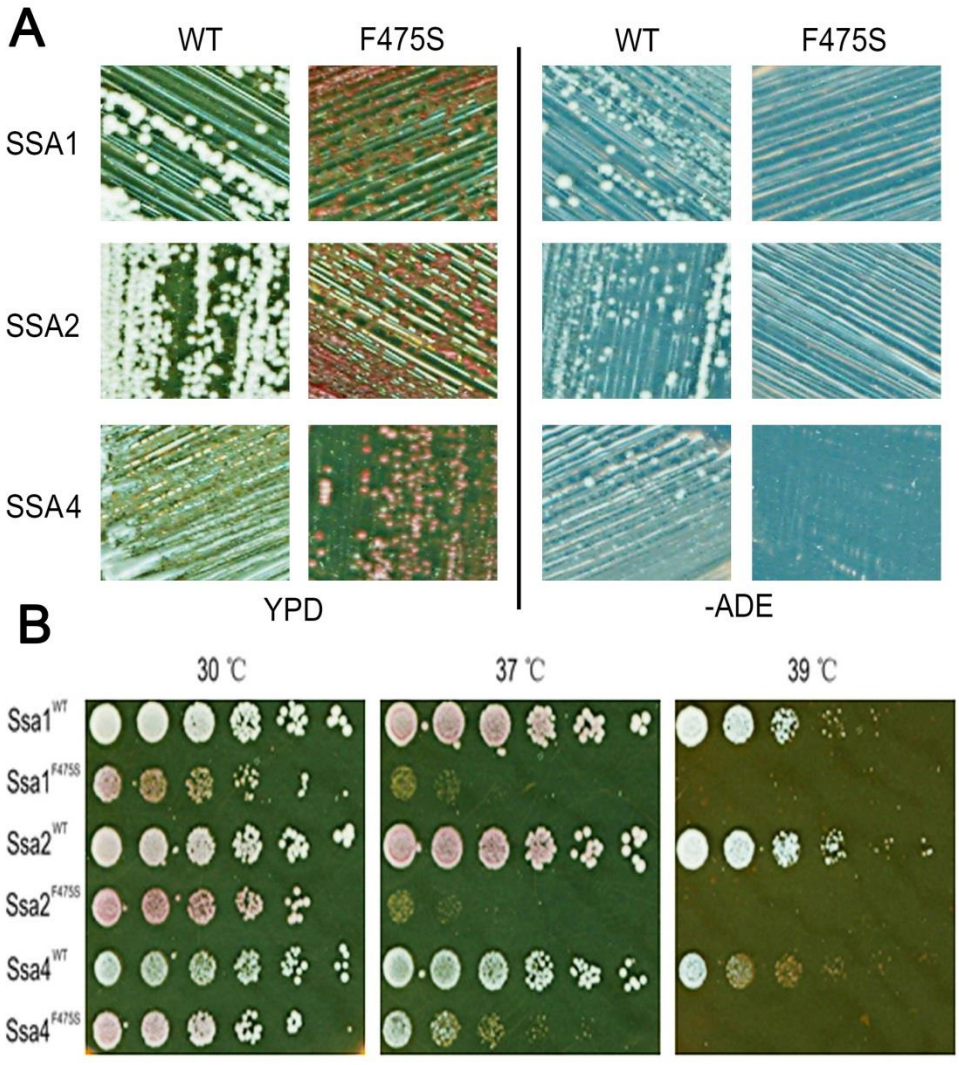

Figure 3.29. Conservation of the F475S mutant in the Ssa family. (A) [*PSI*$^{+}$] propagation in F475S variants of Ssa2 and Ssa4; (B) Growth assay at elevated temperatures for the F475S variants in the Ssa family.

3.30 Chapter conclusion

In this chapter we illuminate that the highly conserved residue 475 plays a crucial in the structure and function of the Hsp70. Structurally, Phe475 is located in a conserved β6-β7 region which is highly conserved in the Ssa family, and across species such as in *E.coli* DnaK and human Hsp/c70. The F475S variant, which was isolated from a random mutagenesis strategy, displayed deficiencies in [PSI^+] propagation and temperature sensitivity. It was found that introduction of smaller amino acid side chains at residue 475, such as alanine and serine, resulted in temperature sensitivity and [PSI^+] impairment. When the side chain of residue 475 is larger than Cysteine, no matter if it is polar or nonpolar (tyrosine and phenylalanine), thermotolerance and [PSI^+] can be maintained. However, there is a limit to side-chain size as if too large, such as tryptophan, Ssa1 will lose intrinsic function and fail to support cell viability. Considering the contribution of residue 475 in forming the hydrophobic pocket, it was speculated that a correctly sized side-chain at this site is necessary to maintain the integrity of the substrate-binding pocket.

We also isolated three second-site suppressors, A394V/F475S, P433S/F475S and V477I/F475S, all of them supressed, to varying degrees, only the temperature sensitivity phenotype. From structural biology aspects, F475S variant disturbed the stability of the SBD which appears related to the temperature sensitivity. Moreover, second-site suppressors rescued the temperature sensitivity by stabilizing the SBD to varying extents. F475S variant accelerated the disturbance of the hydrophobic core and thus triggered conformational changes of the SBD. After SBD disruption, F475S variant altered inter-domain communication between the NBD and SBD. Finally, disruption of the SBD structure abolished repression of ATP hydrolysis of the NBD, reduced protein refolding activity and enhanced interactions with Hsp104 and Hsp26 but decreased the interactions with Sup35. The degradation of the SBD results in reduced abundance of Ssa1 in cells, and the specific SBD degradation had been observed *in vitro* and *in vivo* directly.

Taken together, the disruption and degradation of the SBD are the definitive reasons for causing the temperature sensitivity of cells. Moreover, the increased ATPase activity and interactions with Hsp104 and Hsp26 and the decreased refolding activity and

interaction with Sup35 may be related to impairment of [*PSI*$^{+}$] propagation. Finally, I surmise that degradation of the SBD is meaningful for wild-type Ssa1 under specific conditions or to regulate specific cellular activity. Considering WT protein, at elevated temperatures, looked similar to F475S in terms of protein degradation, it was speculated that SBD degradation may be related to heat shock response of Hsp70. This hypothesis is investigated further in Chapter 5.

CHAPTER FOUR

SBD ALLOSTERY MEDIATES HEAT SHOCK RESPONSE AND PRION PROPAGATION

4.1 A classic SBD mutant L483W of Ssa1

A variety of genetic and biochemical studies in yeast have identified many mutations of Hsp70 (Ssa1) that impair propagation of the yeast prions [PSI^+] or influence cell growth activity (Jones & Masison 2003; Loovers et al. 2007; Needham et al. 2015a) (Figure 4.1). L483W variant of Ssa1 has been characterized impairing [PSI^+] propagation by reducing the number of "seeds" (Jung et al., 2000; Song et al., 2005). Deletion of nucleotide exchange factors (NEFs) Fes1 or Sse1 increases [PSI^+] which implied that L483W enhanced substrate binding affinity, indeed our previous steered molecular dynamics simulations support this hypothesis (Jung et al. 2000; Jones et al. 2004; Xu et al. 2013). However, earlier research suggests that L483W has weakened substrate-binding activity to a small peptide substrate (Needham & Masison 2008). The reasons for this discrepancy may be the peptide size or Ssa1 model used (Xu et al. 2013). In addition to L483W, most of the mutations impairing [PSI^+] are located in the NBD and some of the second-site suppressors of L483W are also located in NBD, which implied that prion propagation is related to inter-domain communication (Jones & Masison 2003).

There is a bidirectional allosteric intramolecular regulation between NBD and SBD. Briefly, ATP binding and hydrolysis of the NBD regulate the substrate capture by the SBD, and substrate binding of the SBD increases ATP hydrolysis (Mayer & Kityk 2015). Compared with DnaK-ADP state, DnaK-ATP state is more compact. Moreover, the lid completely detached from the substrate-binding pocket and docked onto one side of the NBD; and also the linker is buried into the cleft of the NBD to steer the SBD docking onto another side of the NBD (Kityk et al. 2012; Bertelsen et al. 2009). Several residues which are part of the NBD and SBD interface have been reported such as Arg151, Arg167, Asp326, Asp393, Lys414, Asp481 (residue numbers in DnaK) (Kityk et al. 2012; Kityk et al. 2015). Therefore, the stability of the interface plays a critical role in allosteric regulation and intramolecular communication in Hsp70. In particular, Asp481 and Lys414 which contact the NBD subdomain IA and IIA respectively as a clamp to fix the NBD and SBD interaction in the ATP state and strongly decreas basal ATPase activity without stimulation of substrate and Hsp40 (Kityk et al. 2015). A recent study has shown Leu484 and another residue Asp481 in DnaK (homologous to Leu483 and Asn480 in Ssa1) play critical roles in the regulation of signal transduction

from the SBD to the NBD (Kityk et al. 2015). However, although these mutants have been characterized extensively, their structural and functional analysis is severely lacking and in cases where such data exists this has not been informative from a functional point of view. It thus remains unclear whether the allosteric SBD have direct effects on heat shock response and [*PSI*$^+$] inheritance. In this chapter, I address these issues and define the direct effects of the allosteric SBD and components of the Hsp70 machinery to regulate heat shock response and [*PSI*$^+$] prion propagation.

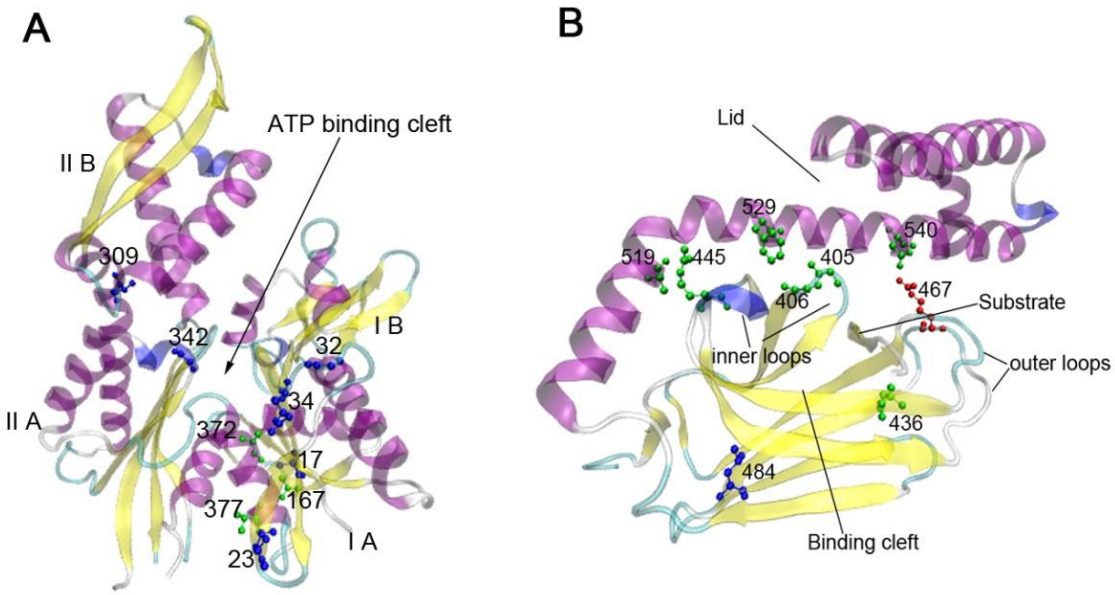

Figure 4.1. Locations of SSA1 mutations on the DnaK structure. (A) Locations of NBD mutations in the DnaK structure. Ribbon schematic representations of the Protein Data Bank structures 1DKG. (B) Locations of SBD mutations in the DnaK structure. Ribbon schematic representations of the Protein Data Bank structures 1DKZ. The *E. coli* amino acid residue numbers homologous to those of the SSA1 mutations had been assessed. Residues identified as forward mutations are blue and those identified as suppressing mutations are green. The red residue forms an important salt bridge with the α-helical lid.

4.2 Impairment of [*PSI*$^+$] propagation

[*PSI*$^+$] phenotype can be assessed based on the colour of colonies on YPD and survival on synthesis medium without Adenine (-ADE). [*PSI*$^+$] cells are white on YPD and can grow well on -ADE. [*psi*$^-$] cells present red colonies on YPD and cannot survive on -ADE plates. When [*PSI*$^+$] cells are in a "weak" state, cells display pink colonies on

YPD and grow slowly on -ADE plates. As shown in Figure 4.2, L483W variant was [*psi*$^-$] as the only Ssa source in the G402 cells (Jones & Masison 2003). There were two predicted mutations at residue 483, L483A and L483H, using steered molecular dynamics (SMD) simulations (Xu et al. 2013). L483A cells were [*PSI*$^+$] phenotype and L483H displayed red colonies on YPD as [*psi*$^-$] cells (Figure 4.2A). However, L483A seems to grow better on -ADE compared to WT, implying [*PSI*$^+$] prion is much stronger in L483A cells (Figure 4.2A). L483H cells displayed red colonies on YPD, but can grow slowly on -ADE after an extra 2 days incubation at RT, suggesting L483H cells are in a very weak [*PSI*$^+$] prion state (Figure 4.2A). To further investigate whether a weak [*PSI*$^+$] prion existed at RT in the L483H variant, I inoculated cells from a single colony on YPD and –ADE plates and then incubated them at RT for 5-7 days. As shown in Figure 4.2B, L483H cells grew slightly on -ADE plates, but L483W cells did not. Therefore, it is possible that L483A cells are [*PSI*$^+$] and even slightly stronger than that of WT; the L483H variant impairs [*PSI*$^+$] prion propagation like L483W variant but still retains a few weakened [*PSI*$^+$] prion *in vivo*.

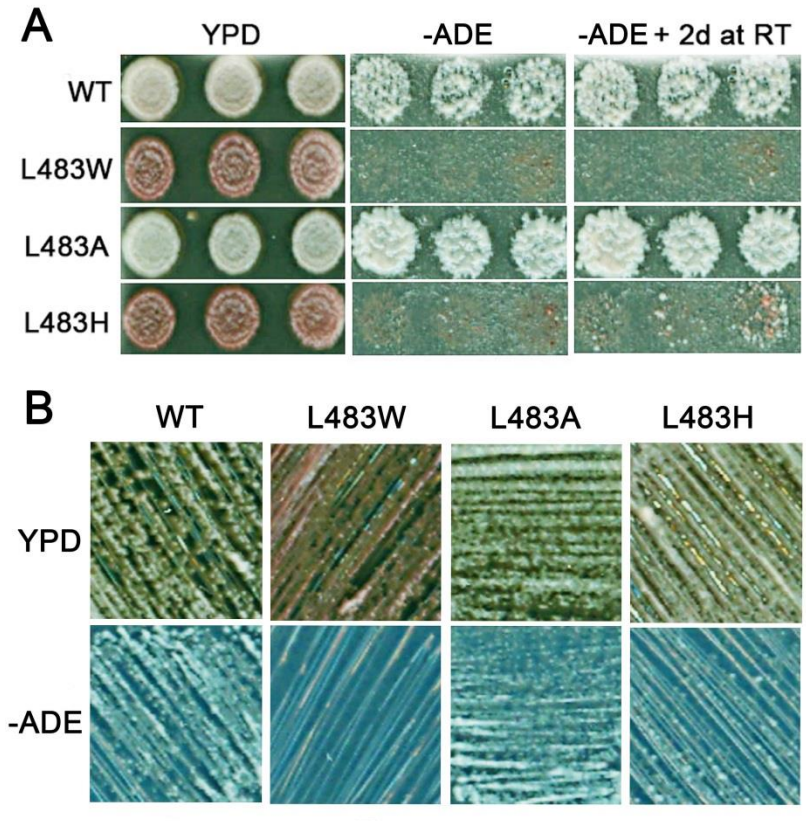

Figure 4.2. Assessments of Leu483 variants on [*PSI*$^+$] propagation. (A) [*PSI*$^+$] propagation assay at 30 ℃. Fresh cultures (OD_{600} of 0.5) were spotted on YPD plates and incubated at 30 ℃

for 2 days. After incubation, the dots on YPD were duplicated on -ADE plates and incubated at 30 ℃ for 2 days plus extra 2d incubation at RT. (B) [*PSI*$^{+}$] propagation assay at RT. Single colonies were striped on YPD and -ADE plates which were then incubated at RT for 5-7 days. As described in the Introduction, [*psi*$^{-}$] cells were red colonies on YPD and lethal on -ADE plates; [*PSI*$^{+}$] cells were white colonies on YPD and viable on -ADE plates.

4.3 L483W increases the temperature sensitivity of cells

Comparative growth analysis showed that L483A, L483H and L483W cells were not sensitive at 30 ℃ and 37 ℃ (Figure 4.3), indeed the same conclusion of L483W variant has been reported before (Jones & Masison 2003). In Section 3.8, I found that the content of α-helix and β-sheets of L483W mutation gradually declined with elevated temperature, suggesting the conformational changes induced by L483W variant existed at higher temperatures (Figure 3.8B). Consequently, it was predicted that the temperature sensitivity of L483W cells may be observed at a higher temperature. To prove the hypothesis, all the mutants at residue 483 were spotted on YPD and incubated at 39 ℃ (Figure 4.3). Interestingly, both L483W and L483H were sensitive at 39 ℃ on YPD, which further proves that disruption of SBD involving in heat shock response. Considering that elevated temperature weakened the cell wall (Kamada et al. 1995) and maintenance of osmotic stress decreased damage from heat shock (Gunasekera et al. 2008), I spotted those cells on YPD complemented with 1M sorbitol. As previous reports, 1 M sorbitol obviously increased the cells survival at elevated temperatures. However, L483W and L483H still displayed significant sensitivity at 39 ℃ on YPD with 1 M sorbitol (Figure 4.3), which implied that temperature sensitivity of L483W and L483H variants wasn't caused by the deficiency of the cell wall. Therefore, the disturbance of SBD and maybe more functional changes of Ssa1 result in the temperature sensitivity of L483W/H cells.

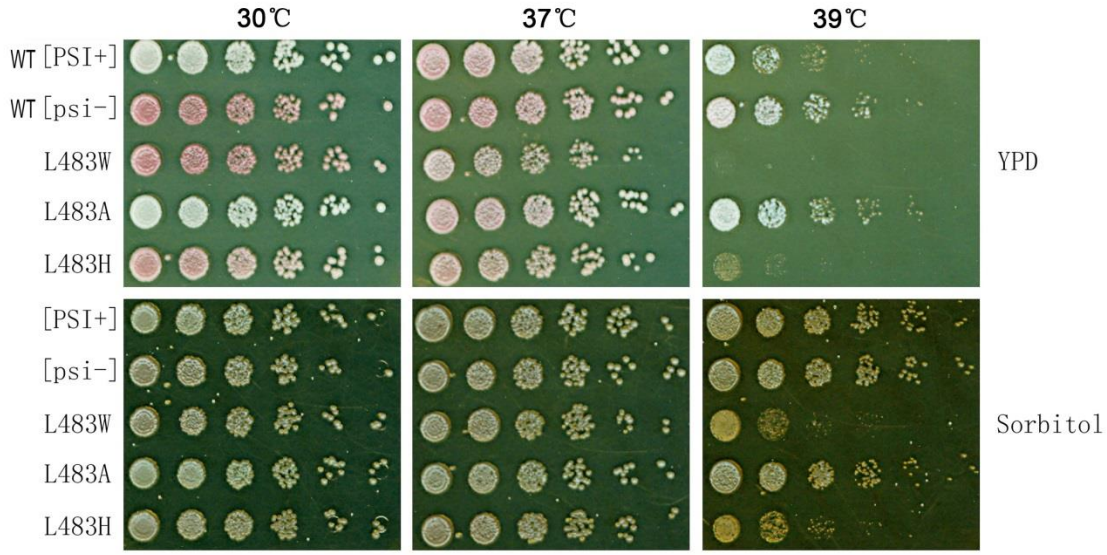

Figure 4.3. Growth assay of the mutations at Ssa1 residue 483 at elevated temperatures. Fresh cultures were spotted on YPD and YPD containing 1 M sorbitol as the description in the section of the growth assay (Section 2.15).

4.4 Acquired thermotolerance of Ssa1 Leu483 mutations

To assess the contribution of Hsp104 in association with Hsp70 mutations, cells containing appropriate mutation as the sole Ssa source were cultured and plated on YPD medium and YPD containing 3 mM Gdn-HCl which inhibits *in vivo* activity of Hsp104 (Jung & Masison 2001). As shown in Figure 4.4, both L483W and L483H decreased acquired thermotolerance compared to WT Ssa1 on YPD, which is line with their temperature sensitivity at 39 ℃. The L483A variant is the only one which maintained acquired thermotolerance like that of WT on YPD plates (Figure 4.4). Acquired thermotolerance was reduced for all of those strains on YPD plates containing 3 mM Gdn-HCl compared to that on YPD plates, and L483W and L483H mutations displayed a much more similar survival with that of WT and L483A variant compared to that on YPD plates (Figure 4.4). All of the above suggested that Hsp104 may be contributing to the decreasing of thermotolerance of the L483W and L483H variants. I hypothesize that the interactions between L483W/H variant and Hsp104 have been changed.

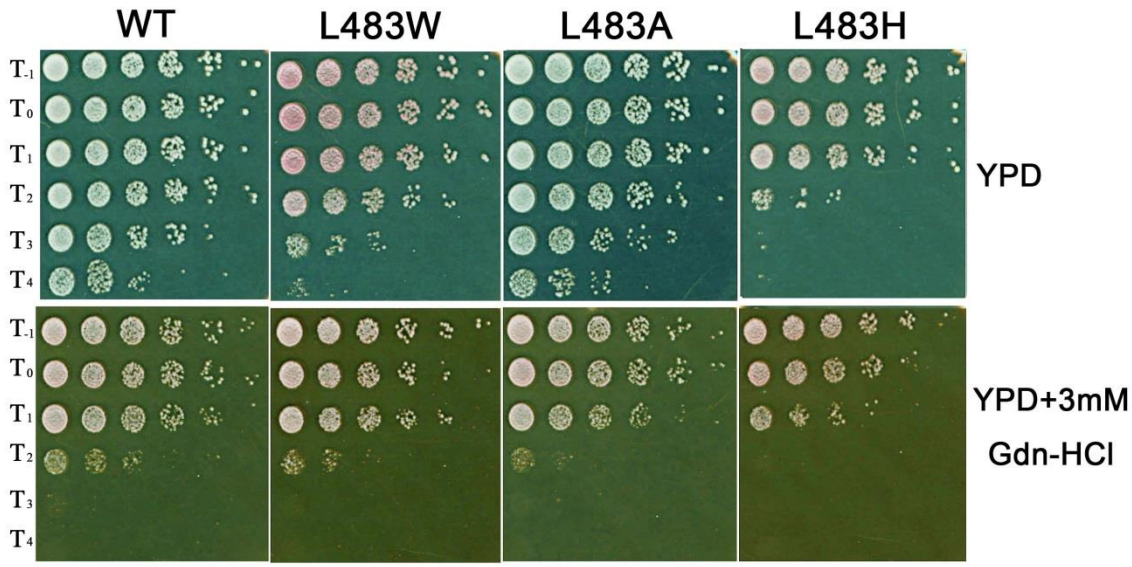

Figure 4.4. Acquired thermotolerance assay of mutations on the residue 483. Fresh cultures were incubated at 39 ℃ for 1 h to induce expression of Hsp104 *in vivo*. Then cultures were moved to 47 ℃ incubator for a time course (T_0-T_4 mean 0, 10, 20, 30 and 40 min respectively). T_{-1} means cultures before 39 ℃ incubation. Cells were spotted on YPD plates and YPD containing 3mM Gdn-HCl after a 1/5 dilution.

4.5 Investigation of Ssa1 Leu483 mutants in response to other stresses

In order to further investigate the ability of Leu483 mutations of Ssa1 to respond stresses, I observed the growth of cells under the cell wall damaging reagent SDS and oxidant reagent H_2O_2. As shown in Figure 4.5, cells expressing L483W, L483A and L483H mutations respectively as only Ssa source were not sensitive to SDS, but sensitive to H_2O_2, implying that L483W variant did not significantly alter basal structure and function of the Ssa1 like F475S variant did. Interestingly, although the L483A variant and WT both are [PSI^+] and have similar tolerance under heat shock, they did not respond similarly under H_2O_2 stress, implying that L483A variant still causes conformational changes in Ssa1 protein and Ssa1 may have different or separated ways to respond various stresses.

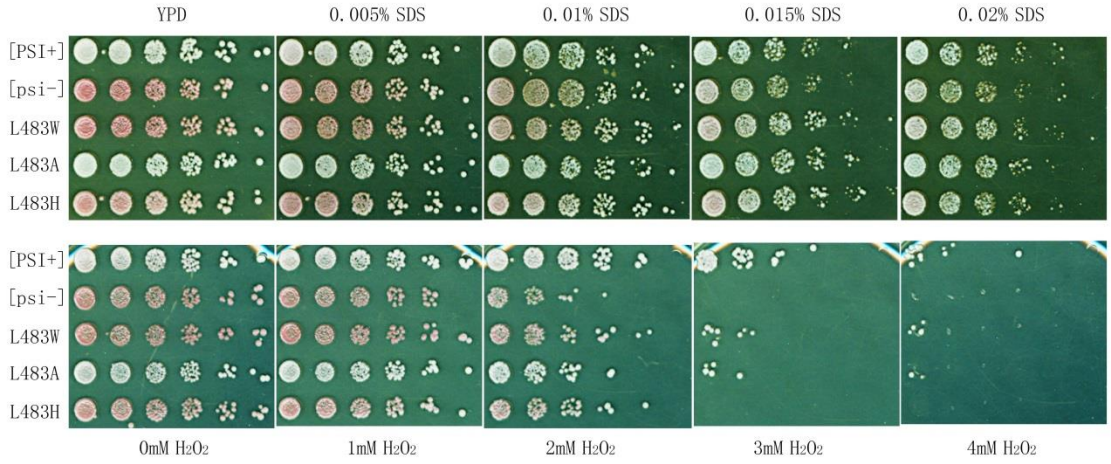

Figure 4.5. Growth assays of Ssa1 Leu483 mutations under other stress. YPD and SC medium were complemented with cell-wall damaging reagent SDS and oxidant reagent H_2O_2, respectively, to achieve required concentrations. Fresh cultures were spotted on those plates as the description in growth assay section and incubated for 2 days at 30 ℃.

4.6 The structural stability of the SBD after Leu483 mutation

In Chapter 3, it was found that the temperature sensitivity of the F475S variant resulted in the disruption of SBD. To discover the stability of the SBD after Leu483 mutations, molecular dynamic simulation (MD) was employed in this section. After simulations, the structural stability of those mutations was assessed by calculation of the RMSD of the protein Cα atoms and RMSF of the backbone of the protein. The RMSD profiles indicated that L484W (homologous to L483W in Ssa1) did not disturb the structural stability of the SBD during short-time simulation at 30 ℃ (Figure 4.6A), but all three Leu483 mutations brought a lot of residue-backbone fluctuations on the RMSF profiles (Figure 4.6B). It implied that Leu483 mutations might induce conformational changes. However, the SBD disturbance cannot see in L483W simulations at 30 ℃ because L483W variant maintains cell growth better than F475S variant, especially at 30 ℃. As simulations at higher temperatures have not been done, it is not clear whether the disturbance of SBD L483W and L483H variants happens at elevated temperatures, or occurs due to the complications associated with the native physiological environment.

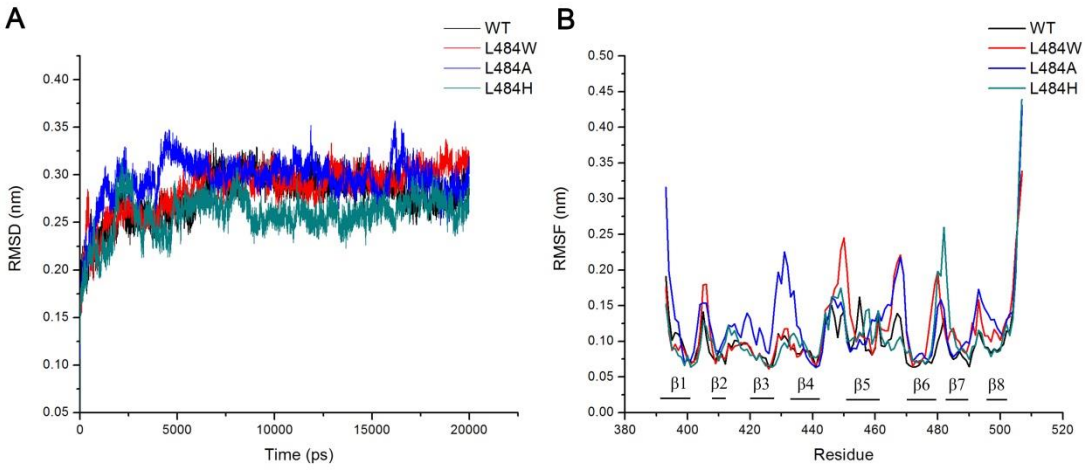

Figure 4.6. The structural stability of the SBD on Leu483 mutations. (A) RMSDs profile as a function of simulation time at 303K (30 ℃). RMSDs were calculated by the g_rms program basing on the Cα atoms of the protein. (B) RMSFs of backbone atoms during the simulations at 30 ℃. RMSFs were calculated by the g_rmsf program.

4.7 Assessments of the SBD stability by SEC

To further investigate the SBD stability induced by mutations at residue 483 of Ssa1, I expressed and purified SBD truncation mutation (382-554). After purification, I firstly detected the monomeric state of Leu483 variants using SEC. Obviously, L483W and L483A variants displayed similar profiles like WT, suggesting they maintained monomeric state well *in vitro* (Figure 4.7A and B). However, except a main absorbance at the monomeric region, L483H eluted around 12 ml which is where the unfolded monomer F475S should be (Figure 4.7A and B). After 24 h incubation at 30 ℃, L483W and L483A variants retained stability of the SBD well (Figure 4.7 C-E). Interestingly, L483H had a few monomeric proteins transformed to unfolded proteins (12 ml), and degraded fragments could be seen easily after 24 h incubation. Thus, partially unfolded L483H variant is degraded more easily than the others and it directly caused the temperature sensitivity of L483H cells. I did not detect L483W degradation here and speculate that it may occur at elevated temperatures.

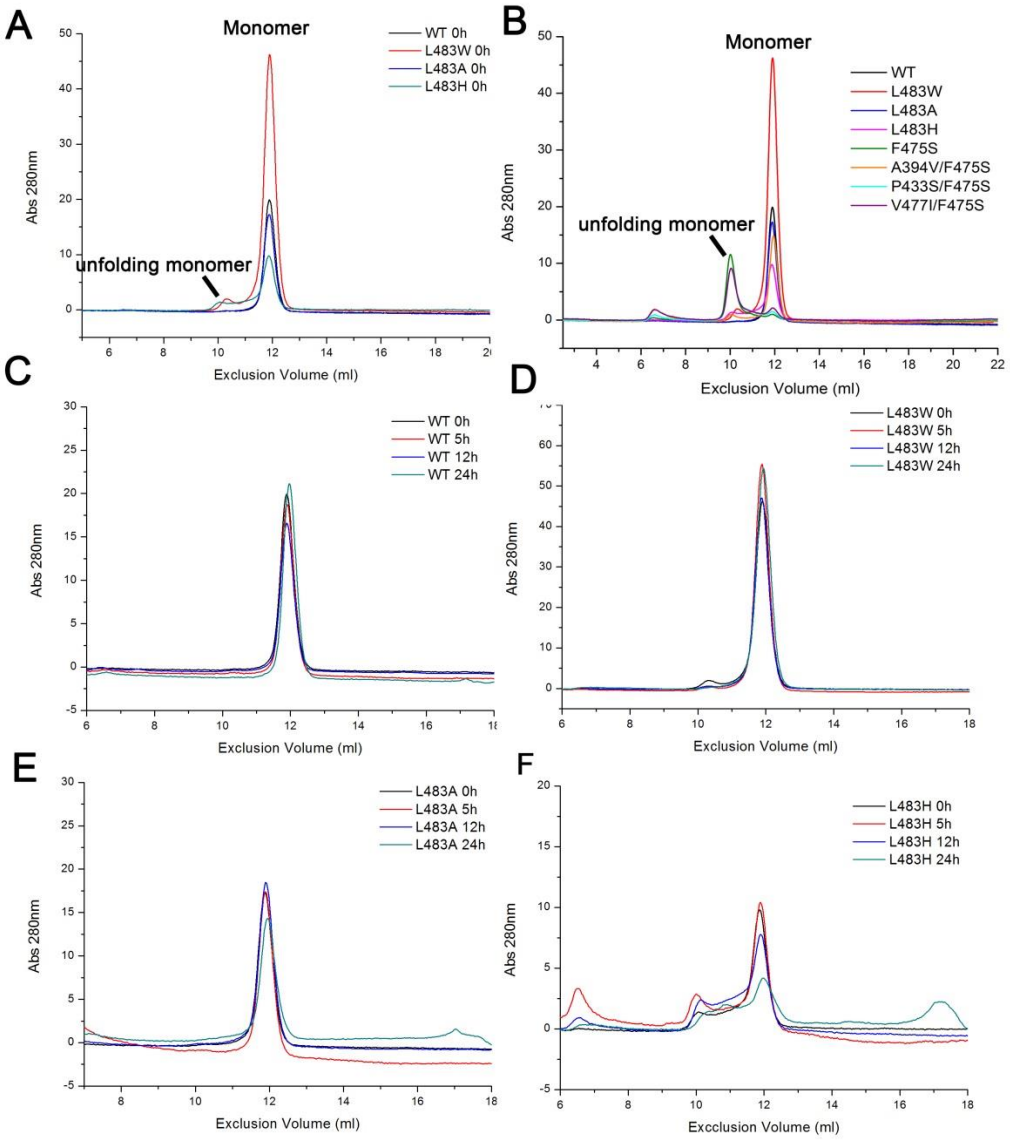

Figure 4.7. Assessments of the SBD stability by SEC. (A) The monomeric state of Leu483 mutations. (B) The monomer or unfolded monomer of Leu483 mutations. (C) WT SBD degradation assays by SEC after 30 ℃ incubation. (D) L483W SBD degradation assays by SEC after 30 ℃ incubations. The dramatic absorbance was caused by the extra Tryptophan at residue 483. (E) L483A SBD degradation assays by SEC after 30 ℃ incubation. (F) L483H SBD degradation assays by SEC after 30 ℃ incubation.

4.8 Secondary structure analysis of CD spectroscopy

To test the disturbance of Leu483 variants in the SBD, I employed CD spectroscopy to gain insight the secondary structure of the protein. CD spectra revealed L483W and L483H variants obviously showed a decreasing absorbance at 215-217nm which suggested the β-sheets unfolding occurred in SBD truncation proteins (Figure 4.8A).

Moreover, L483A had almost the same CD profile as WT, implying L483A variant maintained secondary structure of the SBD better than the others (Figure 4.8A). The content of β-sheets in SBD is consistent with growth deficiency under heat-shock conditions (Figure 4.3 and Figure 4.4). WT kept the secondary structure of the SBD well at elevated temperatures (Figure 4.8B). However, L483W and L483H mutations displayed increasingly disordered structure at elevated temperatures, especially for the L483H variant. Interestingly, L483A variant also displayed the disruption under elevated temperatures (Figure 4.8D), but was not sensitive at 39℃. One of the possible reasons is that SBD disturbance of L483A variant can be recovered by NBD or binding partners. Taking all together, residue 483 is highly conserved and sensitive in SBD. Any replacement at this site will bring conformational changes to some degree. Although mutants like L483A maintains most of the characteristics of WT (Figure 4.2, Figure 4.3, Figure 4.4, Figure 4.7A and Figure 4.8A), it still induces a few conformational changes in SBD.

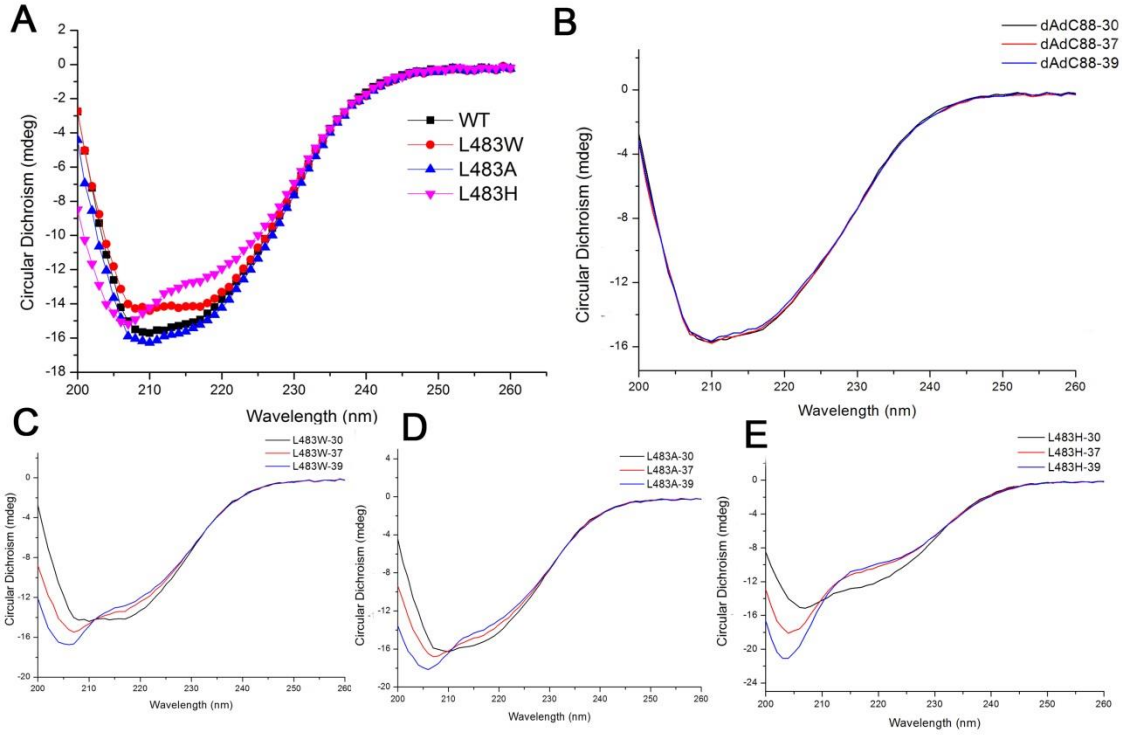

Figure 4.8. Secondary structure monitored by far-UV CD spectra for the SBD truncation mutations on the reside 483. (A) CD spectra scanned at 30 ℃; (B) CD spectra of WT scanned at elevated temperatures; (C) CD spectra of L483W at elevated temperatures; (D) CD spectra of L483A at elevated temperatures; (E) CD spectra of L483H at elevated temperatures. The temperature was exactly controlling by an extra digital module and a plugin device.

4.9 Conformational changes of Leu483 mutations

To further investigate the conformation changes caused by SBD mutations, we carried out NMR analysis of Leu483 mutations and all spectra were scanned at optimal or elevated temperatures to detect effects induced by mutations and heat shock. 2D ^{1}H-^{15}N HSQC spectrum of L483W and L483H displayed significant peak walking at 30 ℃, but L483A only had a few residue shifts compared to that of WT (Figure 4.9A). This suggested that all three variants caused conformational changes in SBD, but that L483W and L483H disturbed SBD more than L483A variant. Remarkably, the peak walking and signal attenuation can be observed for both L483W and L483H variants with increasing temperature, especially at 39 ℃ but not for in the L483A variant (Figure 4.9B), which explains the temperature sensitivity of L483W and L483H cells (Figure 4.3 and Figure 4.4).

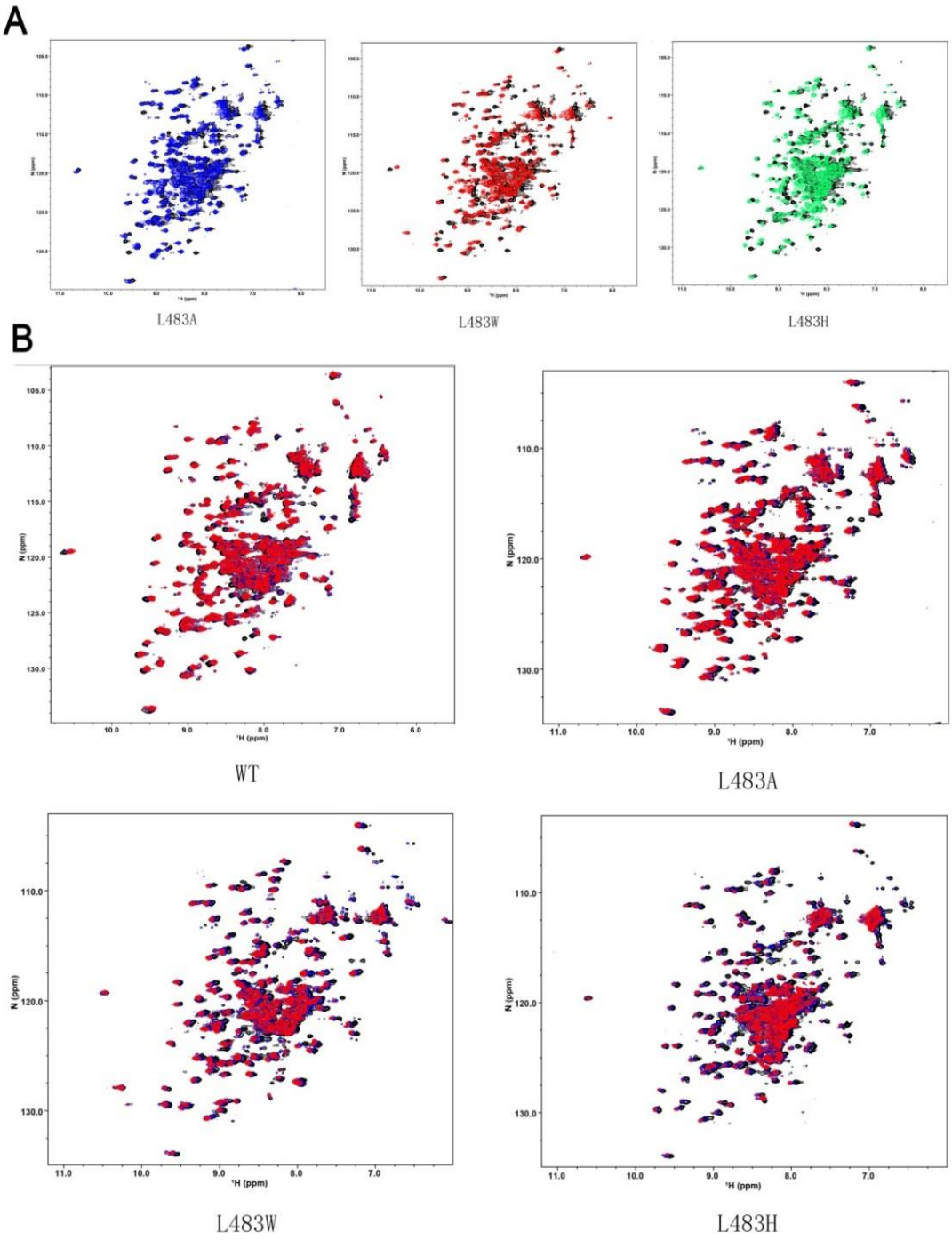

Figure 4.9. Conformational changes of Leu483 mutations. (A) 2D ^{1}H-^{15}N HSQC spectrum of Ssa1 L483A (blue), L483W (red) and L483H (green) were compared to that of WT (black) at 30 ℃ respectively; (B) 2D ^{1}H-^{15}N HSQC spectrum at 30 ℃ (black), 37 ℃ (blue) and 39 ℃ (red) for WT, L483A, L483W and L483H, respectively.

4.10 The stability of the arch structure of Leu483 mutations

Previous reports have shown that the arch structure formed by residues Met404 and Ala429 located in substrate-binding loops plays crucial role of peptide binding (Pellecchia et al., 2000; Stevens et al., 2003; Zhu et al., 1996) and L484W formed a tighter arch than WT to enhance affinity to peptide binding (Xu et al. 2013). In order to confirm the conclusion, I calculated the distance between Met404 and Ala429 during 20 ns simulations. The tighter arches could still be seen for L484W and L484H variants (Figure 4.10A). It was that WT and L484A more readily drift Ala429 far away from Met404, but L484W and L484H prefer to maintain or extend Ala429 to Met404 (Figure 4.10B) to form tight arch structure. These findings are in line with that the L484W and L483H enhanced the interactions with peptide due to the formation of tighter binding loops (Xu et al. 2013).

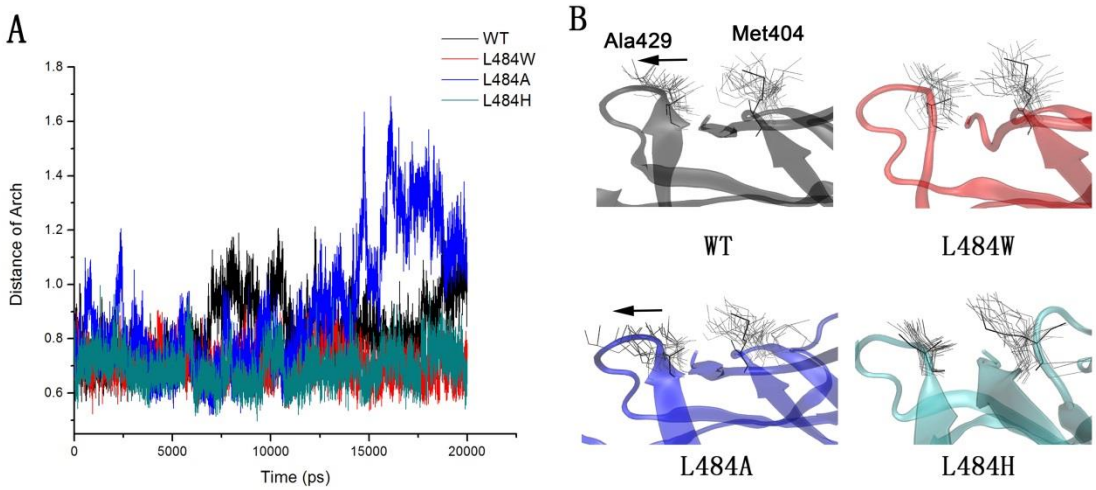

Figure 4.10. The stability of the arch structure of Leu483 mutations. (A) The width of the arch structure as a function of simulation time. (B) Superposition of the arch structure snapshots for WT, L484W, L484A and L484H variants respectively. DnaK models were used for MDs at 30 ℃. Snapshots were collected for every ns.

4.11 The flexibility of the backbone and side chain of residue 483

Any conformational effects of a mutation must occur at the residue itself and then radiate it to the whole protein. To assess the effects of Leu483 mutations, I employed MD again to calculate the conformational changes on backbone atoms and the side chain of residue 484 (homologous to the residue 483 in Ssa1) using DnaK SBD models.

The Ramachandran plot was originally developed in 1963 and used to visualize energetically allowed regions for the backbone of the protein residues. Figure 4.11A illustrates the distribution of the backbone dihedral angle of the residue 484. The backbone of Ala484, Trp484 and His484 distributed in the favoured region of β-sheets during simulations, suggesting that there were no significant conformational changes happening in the backbone of residue 484 and β-sheets could be still maintained around it. Furthermore, I calculated the side-chain fluctuation of residue 484 through RMSDs. Figure 4.11B displays that the side chain of Trp484 and His484 was disturbed much more than that of Leu484 and Ala484, which demonstrated L484W and L484H variants enhanced the flexibility of the side chain of residue 484 to some extent. Superposition of the residue 484 snapshots clearly showed fluctuations of Trp484 and His484 during simulations and it is hardly seen on Leu484 and Ala484 (Figure 4.11.C). Considering alanine and tryptophan both are nonpolar residue but the former has a much smaller side chain, while histidine has a similar size of side chain as tryptophan but a much lower hydrophobicity, the side chain structure, not hydrophobicity, plays an important role in the side-chain fluctuation.

In Section 3.12 and 3.13, I had mentioned L484W mainly caused a side-chain shift of Trp484 (Figure 3.12C) and then extended hydrophobic core and finally decreased SBD stability and the viability of cells under heat shock. Taking all together, L483W/H variant firstly increases the disturbance the side chain of residue 483, but does not influence the β-sheets structure of the backbone. Then disruption of the side chain radiates to the hydrophobic core and even whole SBD. Finally, the structure and function of full-length Ssa1 are altered through undefined short-range or long-range interactions.

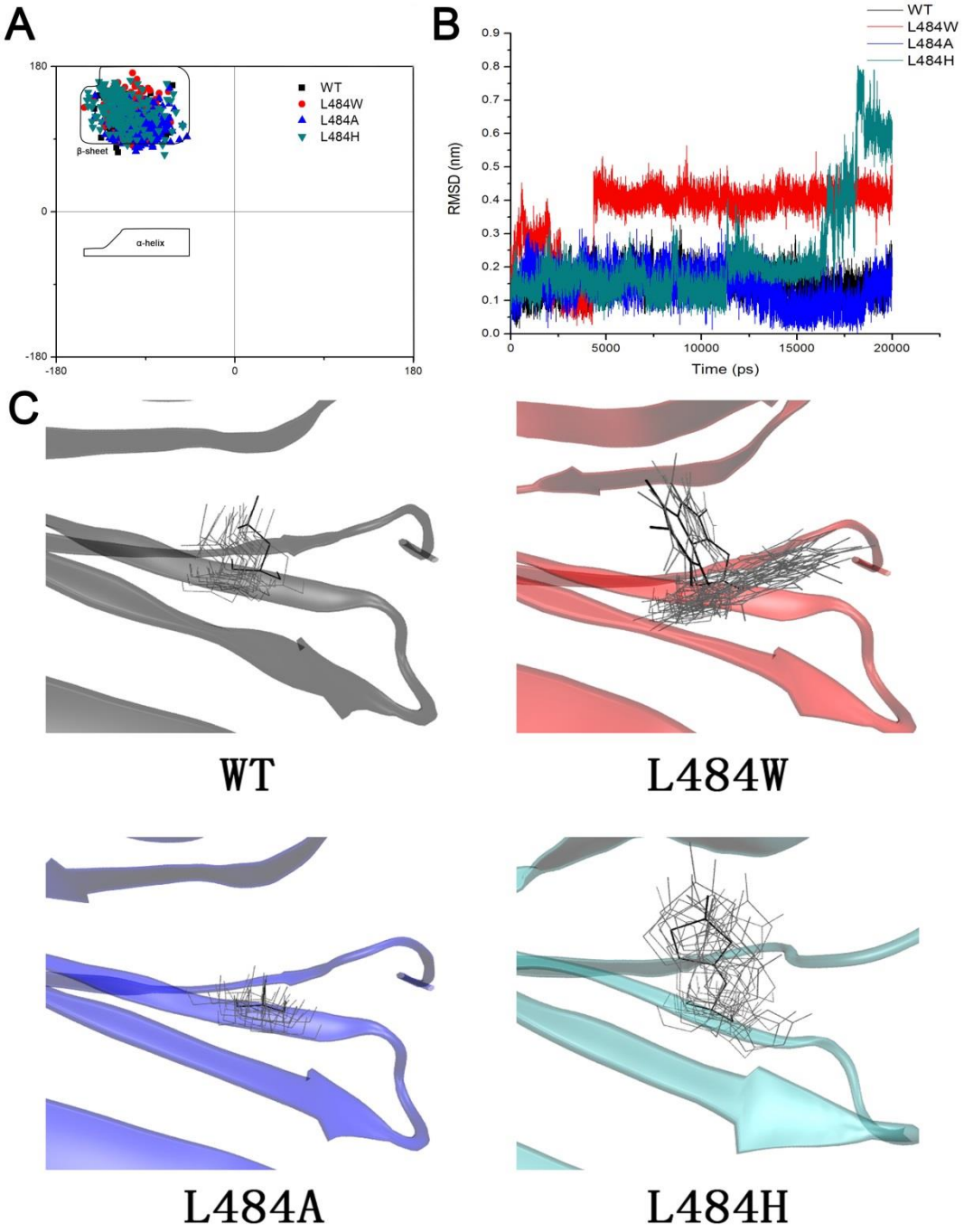

Figure 4.11. The flexibility of Ssa1 residue 484 induced by mutations. (A) Ramachandran plots generated from Leu484 mutations. The favoured regions of α-helix and β-sheets had been represented. (B) RMSDs of the side chain of residue 484 as a function of simulation time. (C) Superposition of the residue 484 snapshots for WT, L484W, L484A and L484H variants respectively. DnaK models were used for MD at 30 ℃.

4.12 Electrostatic potential surface rearrangement caused by Leu483 mutations

The electrostatic potential surface of proteins is a powerful way that has provided insights into conformational rearrangement. After simulations, average structures of the last 10 ns were loaded into PyMOL programme and potentials were mapped to an existing surface in Figure 4.12. Obviously, the electrostatic potential surfaces were rearranged on L484W, L484A and L484H variants. Remarkably, the negative charged interface comprised by loop 2,3, linker and other neighbouring residues rearranged to non-charged surface on L484W and L484H variants, which may alter the inter-domain communication between SBD and NBD enormously. L484A also induced the arrangement of the interface but still kept a part of negative changes. Taking all together, conformational rearrangements are ubiquitous following Leu484 mutation, but significant arrangements of the interface of L484W and L484H variants imply that the inter-domain communication is related to [PSI^{+}] propagation and heat shock response.

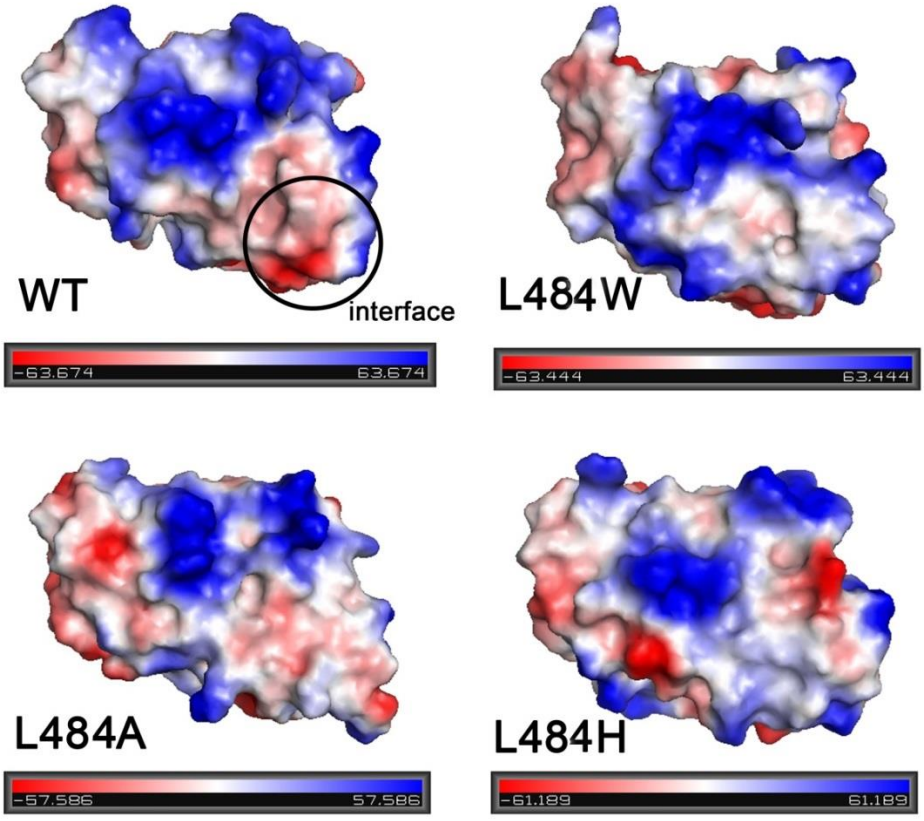

Figure 4.12. Electrostatic potential surfaces of Leu483 mutations. WT, L484W, L484A and L484H were displayed respectively. Negative changes represented in red and positive changes represented in blue.

4.13 Structural analysis of the full-length Ssa1 proteins

Although the disturbance of the Leu483 variants was observed from the SBD truncation model, it is not clear what kind of effects happened in the full-length Ssa1 protein. To clear this question, I expressed and purified the full-length Ssa1 mutations using *E. Coli* expression system. CD spectra revealed that there were several differences in the secondary structure of L483W and L483H variants in comparison to that of WT and L483A variants (Figure 4.13A). Briefly, those absorbance differences are focused on 208 nm, 222 nm (α-helix) and 215-217 nm (β-sheets). L483W and L483H variants obviously showed a decreasing absorbance at 215-217 nm which suggested that the content of β-sheets of SBD also decreased in full-length proteins (Figure 4.13A). Moreover, L483W and L483H mutations displayed decreased absorbance at 208 nm and 222 nm compared to that of WT and L483A, which implied the conformational changes happened to α-helix regions as well. Considering there are two mainly α-helix areas in full-length Ssa1, NBD and SBDα, I further assessed the intrinsic fluorescence of the tryptophan to monitor the conformational changes of the SBDα. Except a dramatic increasing of the intrinsic fluorescence on L483W which was caused by the extra tryptophan on residue 483, we did not see any changes of the intrinsic fluorescence intensity (Figure 4.13B), suggesting that Leu483 mutations did not cause conformational changes in the SBDα. Thus, it was speculated that the absorbance differences of CD spectra at 208 nm and 222 nm are mainly caused by conformation changes of the NBD. In another words, L483W and L483H variants alter the inter-domain communication and ATP hydrolysis of NBD perhaps. Moreover, CD spectra of all Leu483 variants displayed the slight changes at elevated temperatures (Figure 4.13 D and F), suggesting not all of those changes are directly and definitively related to enhancing the sensitivity of the L483W and L483H cells to heat shock at 39 ℃. Taking all together, the conformational changes of SBD and NBD are ubiquitous in L483W/A/H. Those changes happened for L483W and L483H variants at optimal and elevated temperatures, but only happened at elevated temperatures for L483A variants. Those conformational changes may be separated to independently regulate the temperature sensitivity of L483W and L483H cells, [PSI^{+}] propagation or other stresse responses.

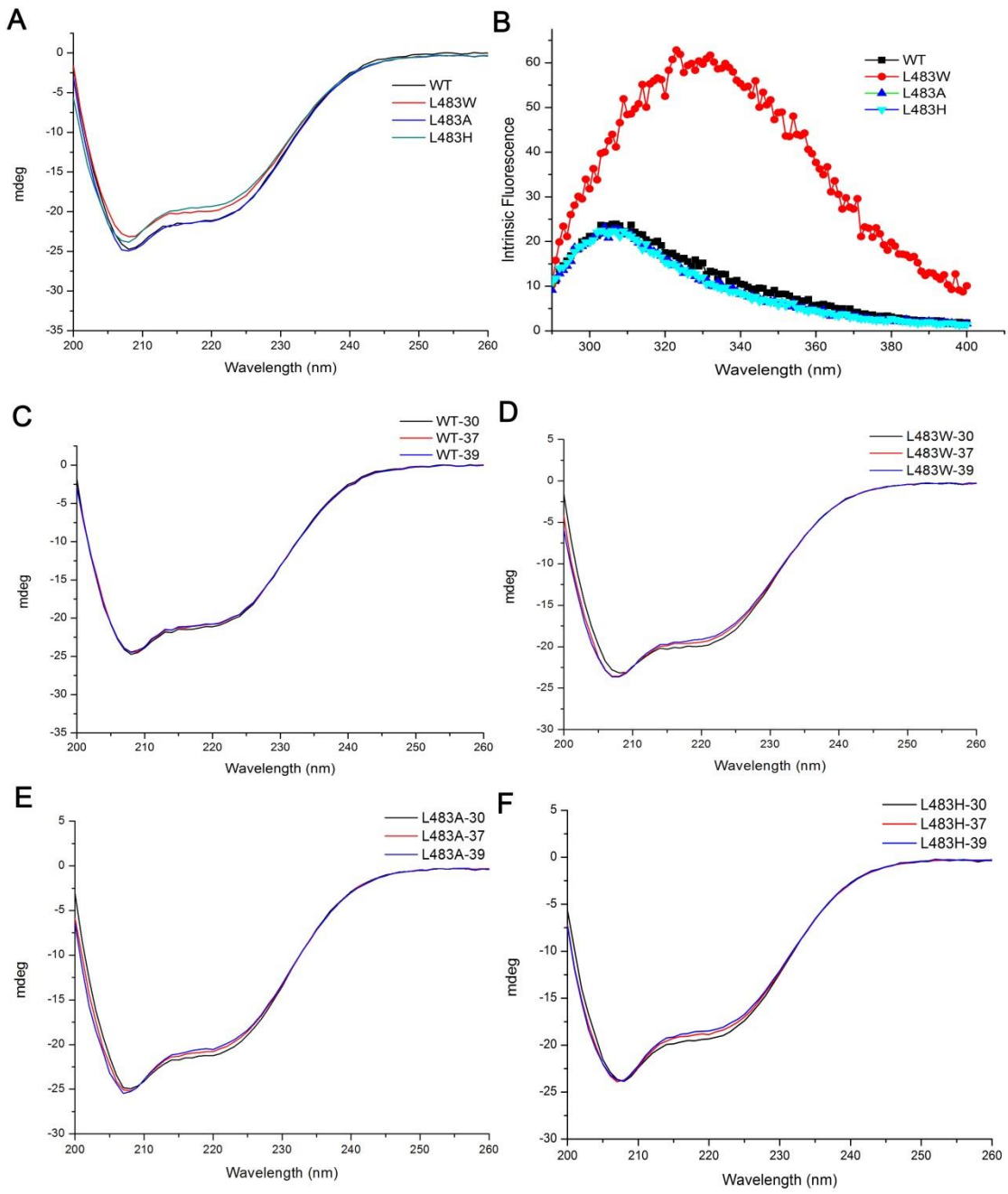

Figure 4.13. Structural analysis of the full-length Ssa1 proteins. (A) Secondary structure monitored by far-UV CD spectra for full-length Ssa1 at 30 ℃; (B) Intrinsic Fluorescence for full-length Ssa1 at RT. The dramatic increasing of the intrinsic fluorescence on L483W was caused by the extra tryptophan on residue 483.

4.14 ATPase activity of Leu483 mutations

To reveal the inter-domain communication and conformation changes of the α-helical NBD, I assessed the basal ATP hydrolysis of those mutants at optimal and elevated

temperatures (Figure 4.14). L483W and L483A slightly increased ATPase activities at 30 ℃ (roughly 1 fold) and ATPase activity of L483W and L483A mutations could be slightly stimulated by Ydj1 and substrate peptide. However, the basal ATP hydrolysis rate of L483H can be enhanced around 3 fold and cannot be stimulated by Ydj1 and peptide. ATPase activity was commonly increased by elevated temperatures. Taking all together, all three Leu483 mutations enhance the basal ATP turnover suggesting the conformational changes occurred in NBD. ATPase inhibition from SBD was almost abolished in the L483H variant by mimicking the co-chaperone-stimulated state or decreasing the affinity to Ydj1 and peptide. Like the F475S variant, the loss of ATPase inhibition from SBD may be related to temperature sensitivity and impairment of [*PSI*$^{+}$] propagation.

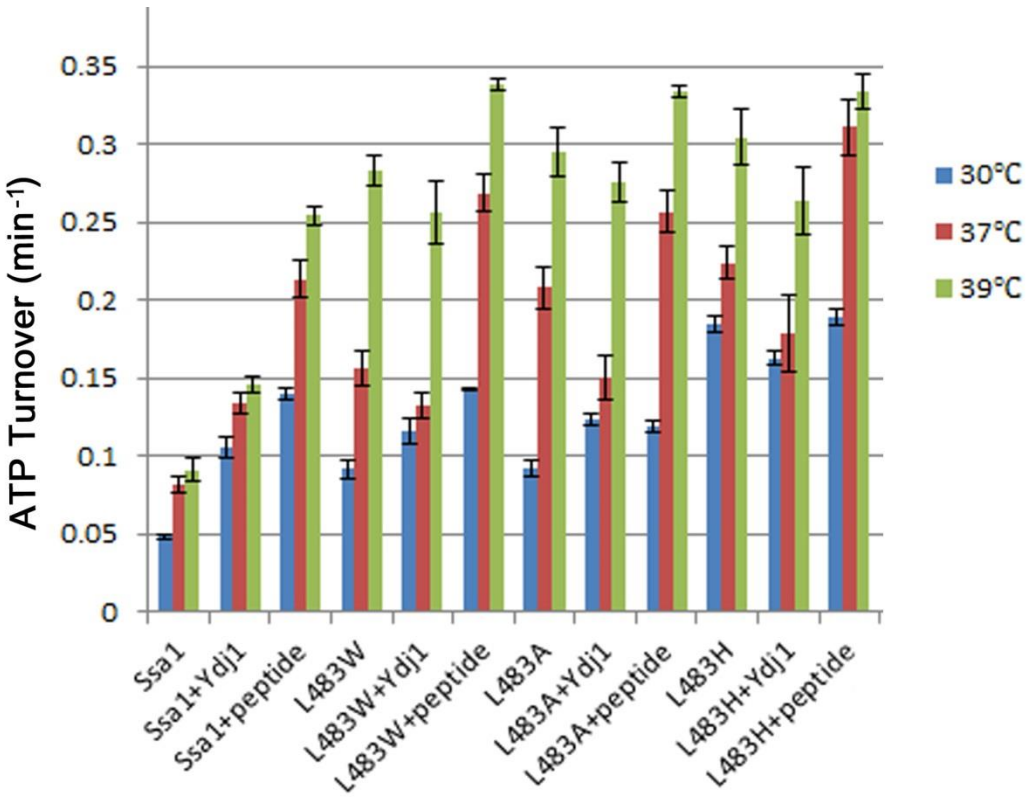

Figure 4.14. The ATPase activity of the mutants with or without Ydj1 or peptide at elevated temperatures. The unit of the ATP turnover rate is min^{-1}.

4.15 Luciferase refolding assay of Leu483 mutations

Hsp104/Hsp70/Hsp40 machinery is required to respond to heat shock and to refold misfolded proteins. Considering that the refolding activity of the Hsp104/Hsp70/Hsp40 machinery is required to produce prion "seeds", the luciferase assay was performed *in vivo*. As shown in Figure 4.15, L483W and L483H variants had lower refolding activity than that of WT and L483A. Interestingly, the order of refolding activity from highest to lowest is L483A, WT, L483H and L483W, which is totally in accordance with the intensity of [PSI^+] propagation *in vivo* (Figure 4.2). Therefore, the decreasing refolding activity is a reason of impairment of [PSI^+] propagation. It was considered that the loss of refolding activity influences the production of the functional "seeds". Moreover, as the accumulation of amorphous aggregation was increased in L483W and L483H cells, it may cause the sensitivity to response heat shock and other stresses.

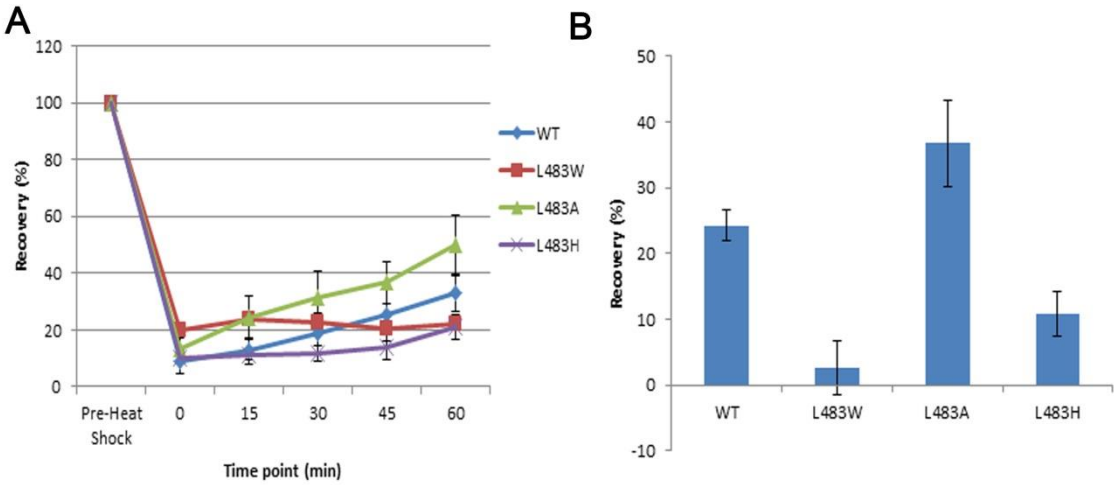

Figure 4.15. Luciferase refolding activity of mutations on Ssa1 residue 483. (A) Luciferase refolding profiles in a 60 min time course; (B) Luciferase recovery rate in 1 h. Fresh cultures were shifted to 37 ℃ for 30 min before 45 ℃ denaturation for 1 h. Denatured luciferase cultures were recovered at 25 ℃ for a 1 h period. Cycloheximide was used to prevent the protein synthesis during the recovery period.

4.16 Basal expression level of the Hsp70-Hsp40-Hsp104 machinery

Previous reports showed that expression levels of Hsp70, Hsp110, Hsp90, Hsp40 and small Hsps, mitochondrial chaperones such as Hsp10 and Hsp60 can be induced under

heat shock (Tan et al. 2015). To further characterize mutations on residue 483, I tested the intracellular expression level of main members of Hsp70 machinery (Ssa1, co-chaperones Ydj1 and Hsp104) using Western blotting. As seen in Figure 4.16, only a significant decrease of Ssa1 levels was observed in L483H cells. There was a slight decrease in Ssa1 level in L483W cells. L483A variant maintained the Ssa1 level well. Other co-chaperones, Hsp104 and Ydj1 were almost expressed without differences, suggesting expression levels of Hsp104 and Ydj1 do not contribute to thermotolerance or prion propagation. The expression level of Ssa1 in F475S cells was lower than that of WT (Figure 3.8), It was thus considered that expression level of Ssa1 was related to SBD disturbance and degradation. Indeed there may be multiple effects induced by mutations on residue 483, such as expression level, inter-domain communication, interactome and even more functions of the Ssa1.

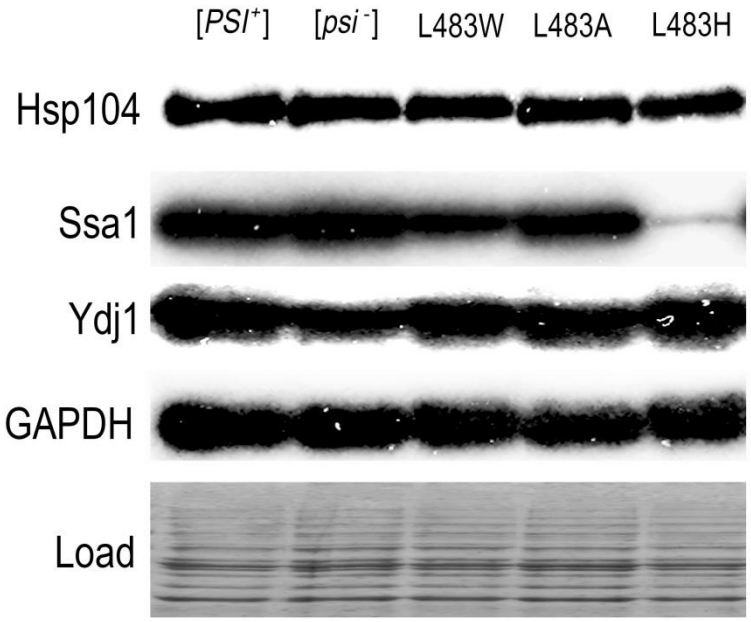

Figure 4.16. Abundance of chaperones in the Hsp70 machinery. Western blotting was performed to calculate the expression levels of Hsp104, Ssa1 and Ydj1. GAPDH and a stained SDS-PAGE running at the same conditions were used as double loading controls.

4.17 Specific SBD degradation

In order to confirm the stability of Leu483 mutations, I used N-terminal Flag-tagged Ssa1 to test the specific SBD degradation *in vivo*. Surprisingly, there were several

obvious bands around 40-50 KDa for L483W, L483H and F475S control sample, and they were hardly seen in WT and L483A samples (Figure 4.17). Following the conclusion mentioned in section 3.28, the degradation bands of L483W and L483H variants demonstrated the specific SBD degradation *in vivo*, which is consistent with the disturbance of SBD in earlier sections and temperature sensitivity of L483W and L483H cells at higher temperatures (Figure 4.3 and Figure 4.4). F475S is more sensitive at elevated temperatures than L483W and L483H variants, so it is reasonable that F475S had more degradation fragments (Figure 4.17).

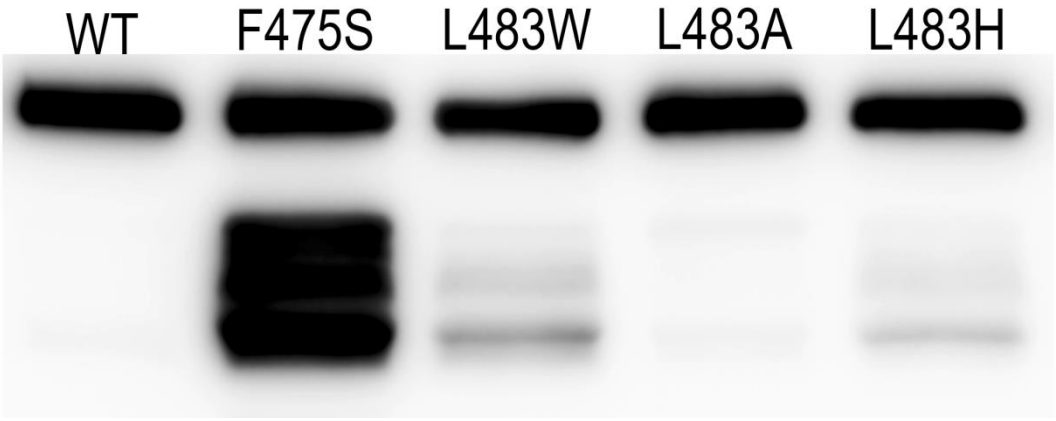

Figure 4.17. Specific SBD degradation of L483W and L483H variants. Anti-Flag was used to probe Flag-tagged Ssa1 proteins.

4.18 Co-IP analysis of interactions between Ssa1 and binding partners

In order to investigate the interaction changes between Leu483 variants and Ssa1 binding partners *in vivo*, I cultured cells with Flag tag and purified the Flag-Ssa1 interactomes using Anti-Flag M2 magnetic beads and then compared them by WB. Co-IP samples were probed by Hsp104, Ydj1, Hsp26 and Sup35 antibodies as before. Western blotting indicated that L483W and L483H variants enhanced the binding with Hsp26 (3 fold and 1.5 fold respectively) (Figure 4.18). Previous reports showed that Hsp26 impaired [PSI^+] prion propagation by inhibiting self-templating of molten oligomers in yeast (Duennwald et al. 2012). Therefore, it was hypothesized that the abundant Hsp26 interacted with Ssa1 and possibly inhibited self-templating of molten oligomers in yeast. Furthermore, the L483W variant interacted with more Hsp104 (Figure 4.18), which may cure [PSI^+] prion by accelerating prion degradation. Instead,

L483H was more likely to interact less with Hsp104 and Ydj1, which might prevent the formation of "seeds". Interestingly, L483W and L483H both hardly interact with Sup35 which also occurred in F475S variant (Figure 4.18), which is contradictive with our previous genetic and MD results (Jones & Masison 2003; Xu et al. 2013). One of the possible reasons is that WT and F475S/L483W/L483H variants have a variable affinity for oligomeric and monomeric Sup35. For instance, WT prefers to interact with oligomers and accelerate the formation of "seeds". However, F475S/L483W/L483H variant prefers to bind with monomers. Thus, there are not enough oligomers in [*psi*$^-$] cells, even if F475S/L483W/L483H variants have a better affinity with monomeric Sup35, and the quantity of interacted Sup35 is still more limited than that of low-affinity WT with oligomer binding.

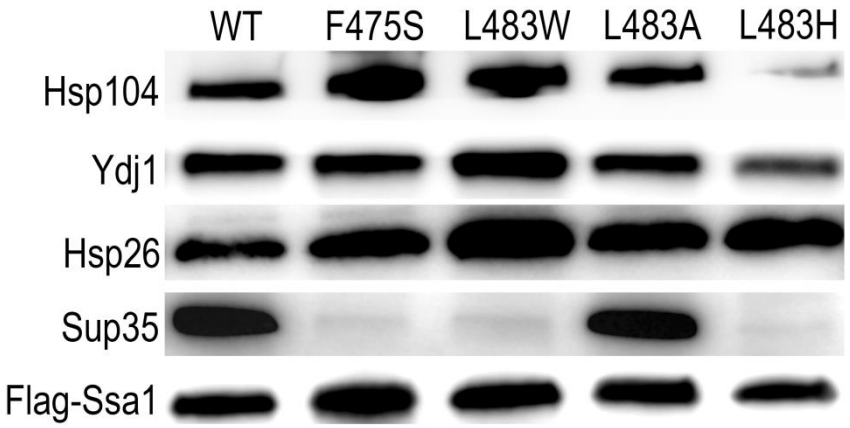

Figure 4.18. Leu483 mutations alter the Ssa1 interactions with clients. Flag-tagged Ssa1 was immunoprecipitatedfrom WT and mutationed cells and probed for Hsp104, Ydj1, Hsp26 and Sup35. Flag-Ssa1 was used as loading control.

4.19 SBD Stability of L483W variant as NMR sample

In Chapter 3, my work attempted to obtain more detailed and accurate information about conformation changes by NMR, which could be used to explain the temperature sensitivity and impairment of [*PSI*$^+$] propagation. However, as the serious signal attenuation of F475S variant, the exact CSPs cannot be calculated on more than 90% residues. Considering the L483W variant has both temperature sensitivity and impairment of [*PSI*$^+$] propagation phenotypes, I employed this classic SBD mutation to obtain more detailed and accurate information about conformation changes.

Unfortunately signal attenuation also occurred in L483W when we performed long-time collections of 3D NMR spectra at 30 ℃. Therefore, we attempted to enhance NMR signals by increasing collection temperature and decreasing ionic concentration in the sample buffer. In order to ensure that L483W variant is still stable enough at higher collection temperature for at least 24 h, I assessed the stability of L483W variant first. As shown in Figure 4.19, there are no any degraded fragments after 48 h incubation at 35 ℃, 37 ℃ and even 39 ℃. Finally, the 35 ℃ was used for all collections of 3D NMR spectra.

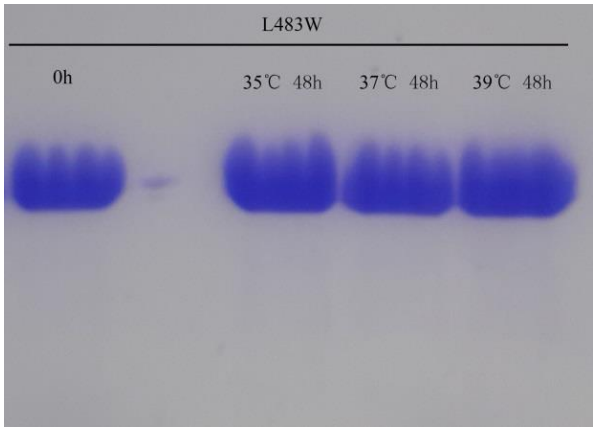

Figure 4.19. Assessment of the stability of L483W variant. 100 µl purified L483W was incubated at 35 ℃, 37 ℃ and 39 ℃ for 48 h respectively. After incubation, 10 µl was loaded for each lane on a 15% SDS-PAGE gel. The lane between 0 h and 35 ℃ 48 h actually was empty with a minute carryover from the 0 h sample (due to high protein concentration deployed).

4.20 Conformational changes of the L483W variant

As mentioned before, it is possible that SBD mutations or heat shock rearranges SBDβ and disrupts an interface between the NBD and SBD. However, the WT is not sensitive enough to assess the SBDβ rearrangement. Although F475S has the most sensitive characteristics in heat shock response and prion impairing, the assignment cannot be done as a surprising attenuation of the NMR signals was induced by the disordered structure. Therefore, we performed further NMR on L483W and more than 90% residues were assigned. Figure 4.20 showed a CSPs histogram of L483W compared to WT at 30 ℃. There are 5 regions identified with significant CSPs: (I) Val393 in linker; (II) Ile417 in loop 2,3; (III) Asp476, Vala477, Asp478, Ser479 Ile482, Leu483 and

Asn484 in β6, loop 6,7 and β7; (IV) Asn502, Asp503 and Lys504 in β8; (V) Ile512, Ile533, Lys547 and Ile548 in SBDα. Intriguingly, many residues in those regions have been reported playing critical roles in the SBDβ allosteric transition and inter-domain communication. The linker is very important to inter-domain communication and was buried into NBD cleft after docking (Mayer & Kityk 2015). Briefly, Val389, Leu391 and Asp393 in DnaK are known to be involved in the interface between NBD and SBD and to charge inter-domain communication directly (Mayer & Kityk 2015), suggesting Val393 may has the same effect. Pro418 in Ssa1 has been reported altering ATP cycling and interdomain communication (Needham et al. 2015a). Residues 414, 417-420 in DnaK have been identified as an important hinge region directly contacted with the linker (Zhuravleva & Gierasch 2015; Kityk et al. 2015; Kityk et al. 2012). Ile417 found in this study may have the same effect as a residue in the same loop 2,3. For region (III) F475S, V477I and L483W in this study have shown the critical roles and Leu484 and Asp481 in DnaK (homologous Leu483 and Asn480 in Ssa1) regulated signal transduction from the SBD to the NBD (Kityk et al. 2015). *In vivo*, neither DnaK-D481A or DnaK-D481K was able to complement the temperature-sensitive growth defect of the DdnaK52::Cm strain BB1553 (Kityk et al. 2015). Ile501 is the lynchpin residue of the hydrophobic core and Ile501 and Ser505 are both involved in the SBDβ allosteric network in DnaK (Zhuravleva & Gierasch 2015). M515I and S545F (closed to Lys547 and Ile548) has been identified impairing [PSI^{+}] propagation in this study. Ile512 found in this study near the D511E (residue number in DanK) which is located in the interface between SBDβ and lid and related with SBDβ allosteric regulation (Zhuravleva & Gierasch 2015).

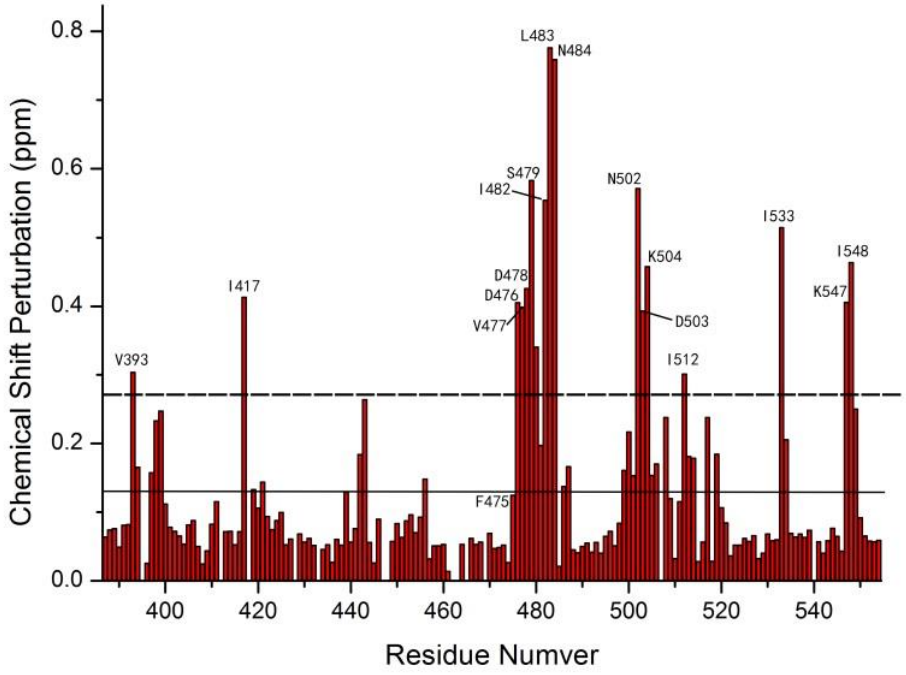

Figure 4.20. CSPs Histogram of L483W compared to WT at 30 ℃. The solid line showed the average of CSPs; the dotted line showed the average plus SD of CSPs.

4.21 Interface between SBD and NBD

To observe the structural position of identified residues with significant CSPs, I mapped them all on full-length and truncated DnaK models (Figure 4.21). Interestingly, a potential and clear surface was formed by those residues in regions of (I), (II), (III) and (IV) (Figure 4.21B). Considering the location of the surface, it must be the interface between SBD and NBD (Figure 4.21A). In another words, the temperature sensitivity and impairment of [PSI^+] propagation of L483W is related to inter-domain communication. Moreover, the region (V) may directly control the close and open of the α-helical lid (Figure 4.21A).

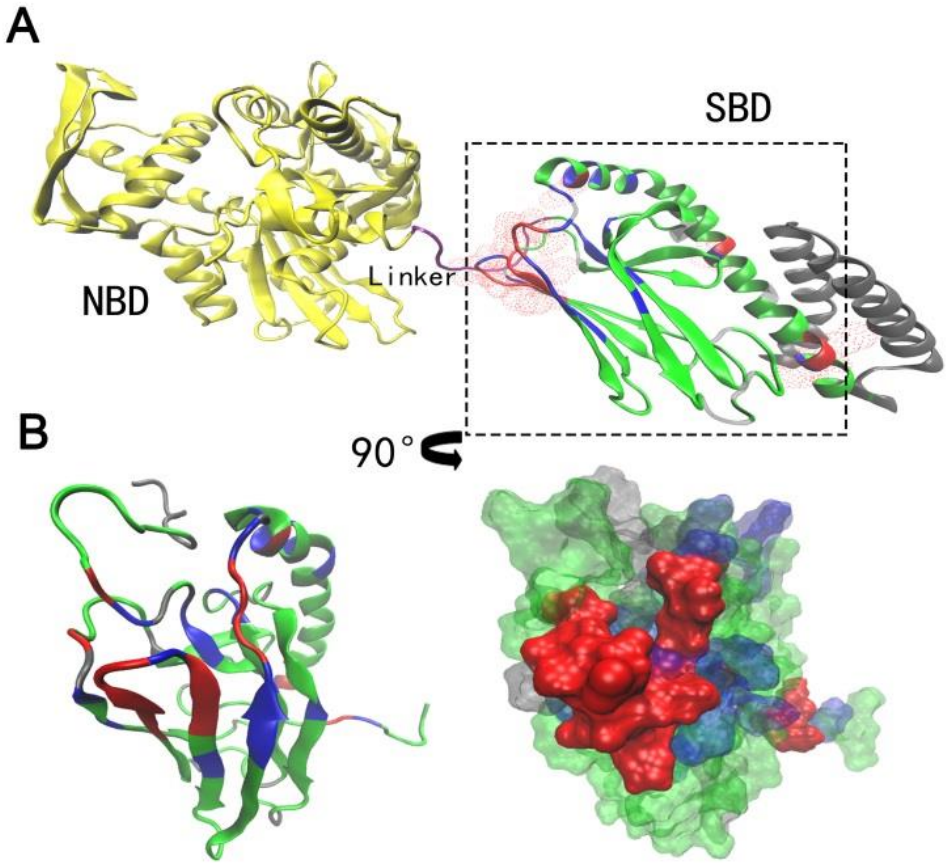

Figure 4.21. Interface between SBD and NBD. (A) Residues with significant CSPs were mapped onto the full-length DnaK structure (PDB: 2KHO); (B) Overlay of SBDβ with significant CSPs residues in the SBD model of DnaK (PDB: 1BPR). The SBDβ in (A) was rotated by 90◦ as arrow indicates in (B). The residues with significant CSPs over the average plus SD are in red; the residues with CSPs between the average plus SD and the average are in blue; the residues with CSPs below the average are in green; non-assigned residues are in grey.

4.22 Assessment of the interface mutations on [*PSI*$^+$] propagation

As the interface identified in Section 4.21 is from a special substitution model, L483W, we don't know whether the interface really plays significant role in conformational regulation and the general cellular functions of Hsp70. To determine the effects of the interface, I replaced the most of those residues with alanine to remove the contribution of side-chain hydrogen bonds, hydrophobic interactions and salt bridges. Then I constructed strains expressing those mutations as the only Ssa source. Firstly, I assessed the [*PSI*$^+$] propagation, and [*PSI*$^+$] and [*psi*$^-$] both phenotypes were expected to be seen. As shown in Figure 4.22, D478A, N480A and I482A are [*psi*$^-$] (red colonies on YPD

and lethal on -ADE); V393A cells are weak [*PSI*$^{+}$] (pink colonies on YPD and grow slowly on -ADE); the rest of mutations are [*PSI*$^{+}$] cells (white colonies on YPD and survived on -ADE). Therefore, I wondered if the interface identified is related to regulation of [*PSI*$^{+}$] propagation.

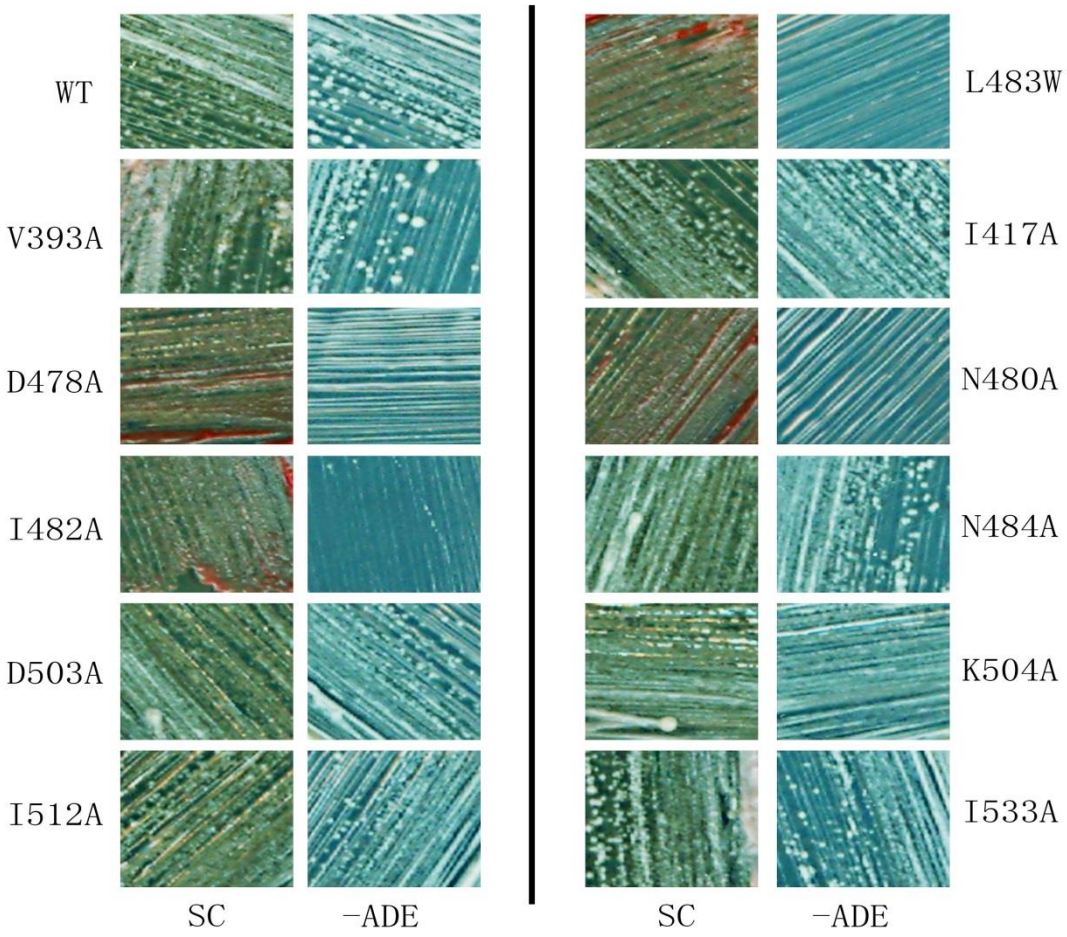

Figure 4.22. Assessment of the predicted mutations on [*PSI*$^{+}$] propagation. A single colony was striped on YPD and -ADE plates. Plates were incubated at RT for 5-7 days. As described in the Introduction, [*psi*$^{-}$] cells were red colonies on YPD and lethal on -ADE plates; [*PSI*$^{+}$] cells were white colonies on YPD and survived on -ADE plates.

4.23 Growth assay of the interface mutations at elevated temperatures

To see if the interface is related to heat shock response, I assessed the temperature sensitivity for those interface mutations. As shown in Figure 4.23, D478A, N480A, I482A and I512A variants are sensitive at elevated temperatures. The D478A and I482A

variants are as sensitive as F475S variant; N480A and I512A are both only sensitive at 39℃ like L483W and L483H variants. 1 M sorbitol did not significantly increase thermotolerance of those mutants compared to that of WT, which implied that temperature sensitivity of those mutations didn't cause a deficiency of the cell wall. Moreover, I also found a lethal variant D476A. Taking all together, the interface identified is involved in the heat shock response of Hsp70.

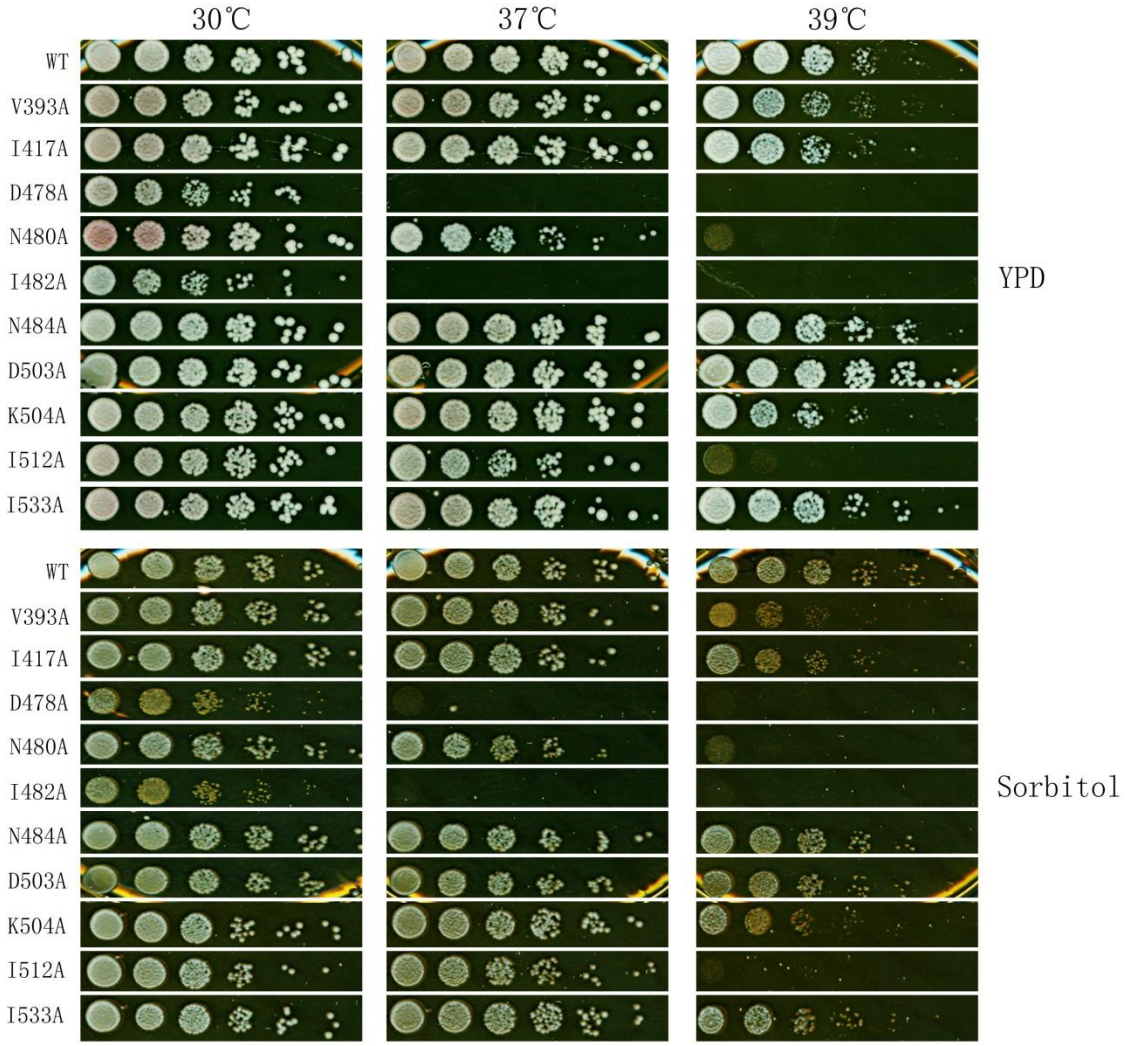

Figure 4.23. Growth assay of predicted mutations at elevated temperatures. Fresh cultures were spotted on YPD and YPD containing 1 M sorbitol as the description in the growth assay section.

4.24 Assessment of predicted mutations to respond other stresses

In addition to differences in other stresses in cells expressing those mutations on the interface, I also observed differences in response to SDS and H_2O_2 (Figure 4.24). Cells expressing V393A, D478A and I482A mutations as the only Ssa source are sensitive to H_2O_2. V393A, D478A, N480A, I482A and K504A mutations are sensitive under SDS stress. Therefore, the mutations on the interface may alter the basal structure and function of the Ssa1 so that cells have common deficiencies to response to different stresses. Moreover, cells expressing the different mutant as only Ssa source have the same or different ability to response to different stresses, implying that cells partly share same pathways to regulate different stresses.

Figure 4.24. Growth assay of predicted mutations under other stresses. YPD and SC medium were supplemented with cell-wall damage reagent SDS and oxidant reagent H_2O_2 respectively to achieve required concentrations. Fresh cultures were spotted on those plates as the description in growth assay section and incubated for 2 days at 30 ℃.

4.25 Conformation changes of Leu483 mutations

The extension of the hydrophobic core had been observed in F475S and L483W variants at optimal and elevated temperatures in earlier sections. Here, I was trying to demonstrate the regions with significant conformational changes only involved in regulation of heat shock response and [*PSI*$^{+}$] propagation. Therefore, I calculated the CSPs of L483A, L483W and L483H variants, respectively, compared with that of WT and mapped residues with significant CSPs on DnaK structure. Firstly, all Leu483 mutations induced a disruption of the hydrophobic core of the SBD at 30 ℃ as previously predicted. As L483W and L483H are similar with both temperature sensitivity and [*psi*$^{-}$] phenotype, unlike L483A, I eliminated those residues with significant CSPs in the L483A variant to specific regions which may be related to heat shock response and/or prion propagaation. As shown in Figure 4.25, one specific region highlighted with a circle was stable in L483A but was disturbed in L483W and L483H variants, which implied that it may be specifically related to regulation of the heat shock response and [*PSI*$^{+}$] propagation. Although D503A and K504A are located in the region, I did not detect any temperature sensitivity and [*psi*$^{-}$] phenotype for those two variants. One of the reasons is that alanine did not disrupt the stable α-helical structure and it is the case that additional mutations need to be designed in this region for further investigations.

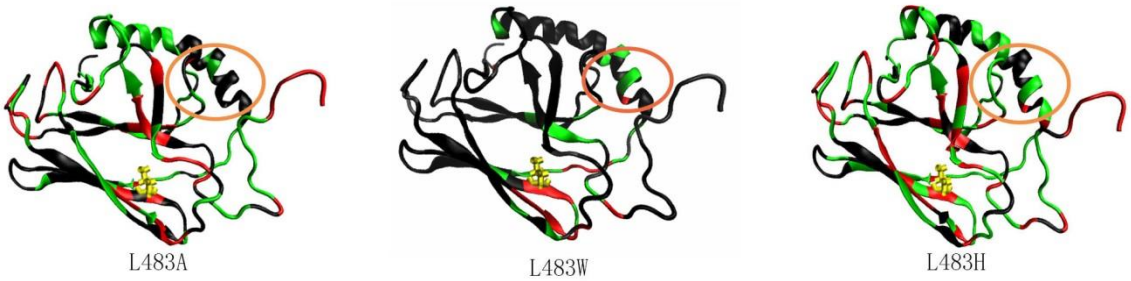

Figure 4.25. Conformational Changes of Leu483 mutations at 30 ℃ displayed on DnaK model. The residues with significant CSPs over the average plus SD are in red; the residues with CSPs between the average plus SD and the average are in green; the residues with CSPs below the average are in black; non-assigned residues are in grey.

4.26 Chapter conclusions

In the chapter, it was illuminated that the highly conserved residue 483 plays a crucial role in the conformational and functional changes of the Hsp70. Structurally, Leu483 and Phe475 are both located in a conserved β6-β7 region and are highly conserved in the Ssa family, *E.coli* DnaK and Human Hsp/c70. The L483W variant displayed deficiencies in [PSI^+] propagation and temperature sensitivity only at 39 ℃. It was found that a larger side chain of residue 483, though not necessarily hydrophobic, caused the disturbance of the side chain of residue 483 and then disruption of the side chain radiates to the hydrophobic core and even whole protein.

Interactions of Ssa1 with binding partners are more complicated for Leu483 mutations. Briefly, L483W increases affinity with Hsp104 and Hsp26. However, L483H only increases the affinity with Hsp26 but decreases the interactions with both Hsp104 and Ydj1. The changes in the interactome result in decreased refolding activity of the Hsp70 machinery. The loss of refolding activity finally influences the production of the functional "seeds" and causes the sensitivity to respond heat shock and other stresses by accumulating amorphous aggregation in L483W and L483H cells.

I also identified 5 regions with significant CSPs: (I) Val393 in linker; (II) Ile417 in loop 2,3; (III) Asp476, Val477, Asp478, Ser479 Ile482, Leu483 and Asn484 in β6, L67 and β7; (IV) Asn502, Asp503 and Lys504 in β8; (V) Ile512, Ile533, Lys547 and Ile548 in SBDα. Also, several residues in regions of (I), (II), (III) and (IV) form the interface between SBD and NBD. It was observed almost all of the expected phenotypes in those individual mutations (Table 4.1). V393A is weak [PSI^+] and heat-resistant. I417A, N484A, D503A, K504A and I533A are [PSI^+] and heat-resistant. I512A is [PSI^+] but temperature sensitive. D478A, N480A and I482A are [psi^-] and temperature sensitive. Moreover, I also identified a non-functional mutant, D476A, and the interface is also common in response to other stress such as cell-wall damage and oxidative stress to some degree (Table 4.1).

Table 4.1. Phenotypes of the interface mutations

	ts.	Prion	H_2O_2	SDS
V393A	N	weak	Y	Y
I417A	N	+	N	N
D476A	N/A	N/A	N/A	N/A
D478A	Y	-	Y	Y
N480A	Y	-	N	Y
I482A	Y	-	Y	Y
N484A	N	+	N	N
D503A	N	+	N	N
K504A	N	+	N	Y
I512A	Y	+	N	N
I533A	N	+	N	N

In combination, the disruption and degradation of the SBD are the definitive reasons for induction of temperature sensitivity of cells as the specific SBD degradation had also been observed in temperature sensitive mutations L483W and L483H. Moreover, the increasing of ATPase activity and the decreasing of refolding activity and interactions with Sup35 are related to the impairment of [PSI^+] propagation by decreasing the functional "seeds". [PSI^+] propagation and heat shock response are both closely related to the inter-domain communication of Hsp70.

CHAPTER FIVE

ACETYLATION OF HSP70 MEDIATES THE HEAT SHOCK RESPONSE

5.1 Acetylation of Hsp70 and heat shock response

Cells are challenged by acute and chronic stress like heat shock, oxidant stress, and variations in pH and salt concentrations, other toxic chemicals and so on. In stressed environments, proteins can be aggregated, unfolded or misfolded. Therefore, cells have to evolve specific networks to detect, monitor and respond to those stresses from the environment (Morimoto & Santoro 1998; Feder & Hofmann 1999; Lindquist & Craig 1988).

Protein post-translational modifications (PTM) have been widely reported to mediate cellular processes and stress responses. For instance, acetylation of proteins is important in the regulation of chromatin organization, mitochondrial metabolism, protein synthesis and other cellular processes (Henriksen et al. 2012). Lysine acetylation is an evolutionary conserved PTM from bacteria to mammalian cells, suggesting that its regulatory roles may be conserved during evolution (Yang & Seto 2007). Knockdown of histone deacetylase (HDAC), which deacetylates lysine residues in the ATP-dependent molecular chaperone Hsp90, induces reversible hyperacetylation and attenuates ATP binding and chaperone function of Hsp90 (Yang et al. 2008). Targeting extracellular hyperacetylated Hsp90 may undermine tumor invasion and metastasis (Yang et al. 2008). Human HSF1(Heat Shock Factor) is inducibly acetylated at the residue 80 which negatively regulates DNA-binding activity (Westerheide et al. 2009). Furthermore, a report on the phosphoproteome of *Saccharomyces cerevisiae* revealed that serine and threonine phosphorylation widely occur (Albuquerque et al. 2008). Sumoylation regulates many proteins which are involved in cancer, Huntington's, Alzheimer's and Parkinson's diseases (Sarge & Park-Sarge 2009).

As a highly conserved and complicated Hsp70, Ssa1 has been reported with multiple PTM sites (Table 1.2). Among them, highly conserved Thr36 phosphorylation in Ssa1 creates displacement of Ydj1, allowing binding between Ssa1 and the G1 cyclin Cln3 thus promoting its degradation (Truman et al. 2012). Oxidative modification of Cys264 and Cys303 abolish the repression of Ssa1 to Hsf1 and activate the transcription of heat shock genes (Wang et al. 2012). Recent research has shown that multiple acetylation sites and phosphorylation of Hsp70 contributes to dimer stability of itself (Morgner et al. 2015). However, it is not clear whether acetylation or phosphorylation of Hsp70 is specifically involved in heat shock response.

5.2 Acetylation and deacetylation of Ssa1

In the work presented in this chapter, we firstly identified modified residues under heat shock using mass spectrometry. There are two kinds of PTMs, phosphorylation and acetylation, observed after heat shock. Only two residues, Thr338 and Thr492, were phosphorylated and 23 lysine residues are involved in reversible hyperacetylation. Briefly, 23 lysine residues of Ssa1 are hyperacetylated at 30℃, but four of them (Lys86, Lys185, Lys354 and Lys562) are deacetylated after heat shock (Table 5.1). Considering the hyperacetylation of Ssa1, we only discuss whether the reversible acetylation of those special lysine residues regulates the heat shock response. Figure 5.1 showed a three-dimensional molecular structural model of Ssa1, which reveals all of the identified lysine residues distributed on NBD and SBD. Notably, three of four reversibly hyperacetylated residues are located in NBD and only one in the lid of SBDα, suggesting regulation of acetylation is more effective in NBD and inter-domain communication may be induced by those reversible hyperacetylations.

Table 5.1. Reversible hyperacetylations of Ssa1

Site	US-Mascot	HS-Mascot
K_{Ac}-54	K_{Ac}-54	K_{Ac}-54
K_{Ac}-69	K_{Ac}-69	K_{Ac}-69
K_{Ac}-86	**K_{Ac}-86**	**Absent**
K_{Ac}-126	K_{Ac}-126	K_{Ac}-126
K_{Ac}-157	K_{Ac}-157	K_{Ac}-157
K_{Ac}-185	**K_{Ac}-185**	**Absent**
K_{Ac}-186	K_{Ac}-186	K_{Ac}-186
K_{Ac}-248	K_{Ac}-248	K_{Ac}-248
K_{Ac}-316	K_{Ac}-316	K_{Ac}-316
K_{Ac}-322	K_{Ac}-322	K_{Ac}-322
K_{Ac}-325	K_{Ac}-325	K_{Ac}-325
K_{Ac}-345	K_{Ac}-345	K_{Ac}-345
K_{Ac}-354	**K_{Ac}-354**	**Absent**
K_{Ac}-446	K_{Ac}-446	K_{Ac}-446
K_{Ac}-448	K_{Ac}-448	K_{Ac}-448
K_{Ac}-497	K_{Ac}-497	K_{Ac}-497
K_{Ac}-523	K_{Ac}-523	K_{Ac}-523
K_{Ac}-536	K_{Ac}-536	K_{Ac}-536
K_{Ac}-556	K_{Ac}-556	K_{Ac}-556
K_{Ac}-562	**K_{Ac}-562**	**Absent**
K_{Ac}-567	K_{Ac}-567	K_{Ac}-567
K_{Ac}-568	K_{Ac}-568	K_{Ac}-568
K_{Ac}-592	K_{Ac}-592	K_{Ac}-592

The reversible acetylation residues are shown in bold. Acetylation sites were identified by Dr. Andrew W. Truman.

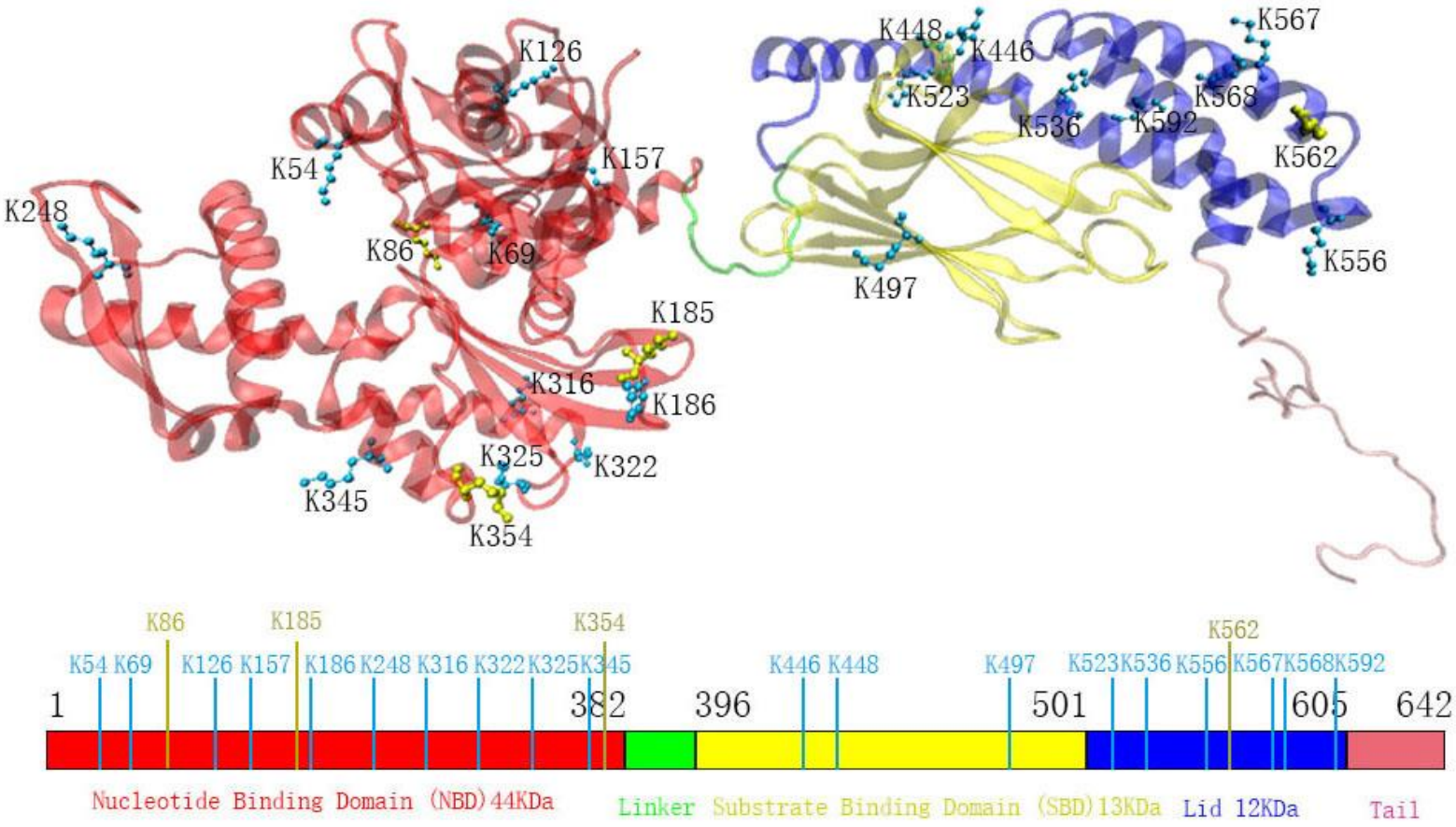

Figure 5.1. Locations of the reversible hyperacetylated residues in Ssa1 model. Ssa1 was modeling based on the full-length DnaK structure (PDB: 2KHO). All lysine residues acetylated in Table 5.1 were shown and four reversible hyperacetylated residues were highlighted in yellow. The lysine residues always maintaining acetylation were presented in blue.

5.3 Reversible hyperacetylated residues regulate cell thermotolerance

To assess the effects of reversibly hyperacetylated lysine residues on Hsp70 function, point mutations were introduced to create acetylation-deficient (lysine to arginine, K/R) and acetylation-mimetic (lysine to glutamine, K/Q) mutants based on the pC210 vector. First, I determined whether any of the residues affected the overall thermotolerance of the cells under heat shock conditions. As shown in Figure 5.2, none of the individual K/R or K/Q mutation showed a temperature sensitivity, implying individual acetylation or deacetylation did not induce significant changes of Hsp70 function. However, double mutant K86Q/K185Q was sensitive at 39℃ and the temperature sensitivity was observed for K86Q/K185Q/K354Q and K86Q/K185Q/K354Q/K562Q, but did not occur in corresponding K/R mutations (Figure 5.2). As mentioned in Table 5.1, those four residues were supposed to be deacetylated under heat shock, maintaining acetylation of those lysine residues thus negatively regulated the heat shock response of Hsp70. Notably, the regulation may rather happen in NBD because double mutation K86Q/K185Q (NBD mutation) has already shown sensitivity at high temperature.

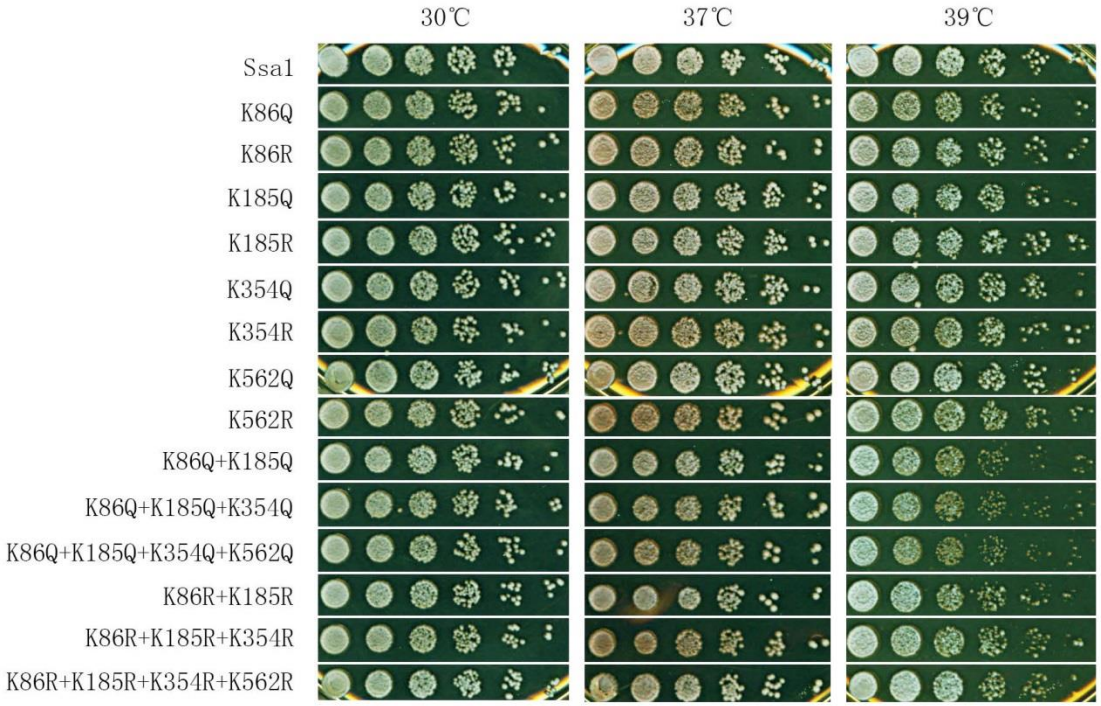

Figure 5.2. Growth assay of the reversible hyperacetylated mutations in Ssa1 at elevated temperatures. Fresh cultures were spotted on YPD as the description in the section of the growth assay.

5.4 Assessments of the thermotolerance at extreme temperature

To further compare the viability mediated by the four reversible hyperacetylated residues, I assessed the thermotolerance at extreme heat shock (47 ℃) by comparing the acetylation-mimetic variant 4Q (K86Q/K185Q/K354Q/K562Q) and acetylation-deficient variant 4R (K86R/K185R/K354R/K562R). As shown in Figure 5.3, 4Q obviously decreased the viability of cells at extreme temperature compared to that of WT and 4R as I observed from the Figure 5.2. Interestingly, the 4R variant slightly increased the survival of cells compared to that of WT. Two of the possible reasons can be used to explain this. Firstly, the deacetylation of those four residues may not completely occur in WT cells so that some of those four residues were maintaining acetylation even after heat shock. Secondly, the deacetylation process of those four residues was weakened/delayed by the extreme temperature (47 ℃) to some extent.

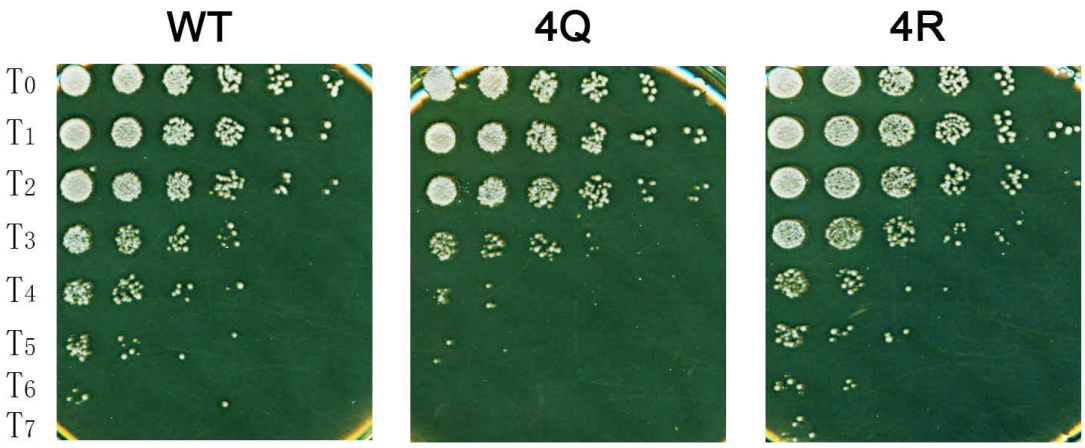

Figure 5.3. Thermotolerance assay of acetylation mutations in Ssa1 at extreme temperature. The fresh cultures were incubated at 47 ℃ incubator for a time course (T_0-T_7 mean 0, 5, 10, 15, 20, 25, 30 and 40 min respectively). Cells were spotted on YPD plates after a 1/5 dilution.

5.5 Assessments of the acquired thermotolerance

To assess the contribution of Hsp104 in association with Hsp70 mutations, cells containing the appropriate mutation as sole Ssa source were cultured and plated on YPD medium and YPD containing 3 mM Gdn-HCl which inhibits *in vivo* activity of Hsp104 (Jung & Masison 2001). As shown in Figure 5.4, 4Q variant decreased acquired

thermotolerance compared to WT Ssa1 and 4R on YPD, which is basically in line with their temperature sensitivity at 39 ℃ (Figure 5.2). However, 4R did not show a better survival than WT, implying there must be other regulations during the acetylated and deacetylated period. For instance, the acetylation of those four residues is necessary/required for the acetylation of the other lysine at 30 ℃ or the phosphorylation of Thr338 and Thr492 at 39 ℃. The thermotolerance of 4Q was almost the same with WT and 4R on YPD plates containing 3 mM Gdn-HCl (Figure 5.4), suggesting Hsp104 may be contributing to decreasing the acquired thermotolerance of the 4Q cells.

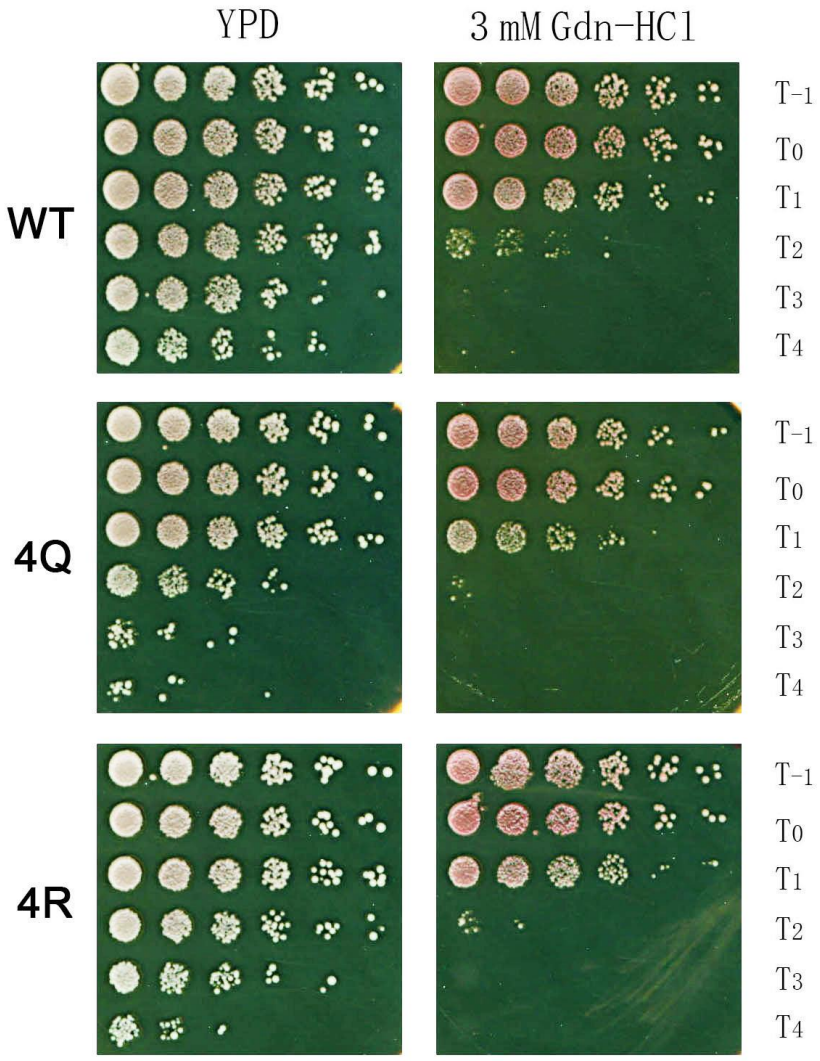

Figure 5.4. Acquired thermotolerance assay of Ssa1 acetylation mutations. The fresh cultures were incubated at 39 ℃ for 1 h to induce the expression of Hsp104 *in vivo*. Then cultures were moved to 47 ℃ incubator for a time course (T_0-T_4 mean 0, 10, 20, 30 and 40 min respectively). T_{-1} means cultures before 39 ℃ incubation. Cells were spotted on YPD plates and YPD containing 3 mM Gdn-HCl after a 1/5 dilution.

5.6 [*PSI*$^+$] prion independent from the temperature sensitivity

As shown in Figure 5.5, mutations on reversible hyperacetylated residues maintained the [*PSI*$^+$] prion (white colonies) in G402 cells and could be cured by 3 mM Gdn-HCl (cured cells are red and presented as [*psi*$^-$] cells). Previous reports have shown that [*PSI*$^+$] prion induced the read-through of the cells (Fitzpatrick et al. 2011) and altered the genome-wide translation (Baudin-Baillieu et al. 2014). In this section, I thus investigated the influence of [*PSI*$^+$] prion on the thermotolerance regulation of reversible hyperacetylated residues. [*psi*$^-$] cells were obtained by inoculating [*PSI*$^+$] colonies on YPD plates containing 3 mM Gdn-HCl. It is obviously that 4Q mutant, whether as [*PSI*$^+$] or [*psi*$^-$] cells, was sensitive at 39 ℃ (Figure 5.5). The 4R variants slightly increased the survival of cells compared to that of WT, which is in line with the finding in Figure 5.3. Therefore, the thermotolerance regulation of reversible hyperacetylated residues is independent from [*PSI*$^+$] prion and alteration of the genome-wide translation caused by the read-through.

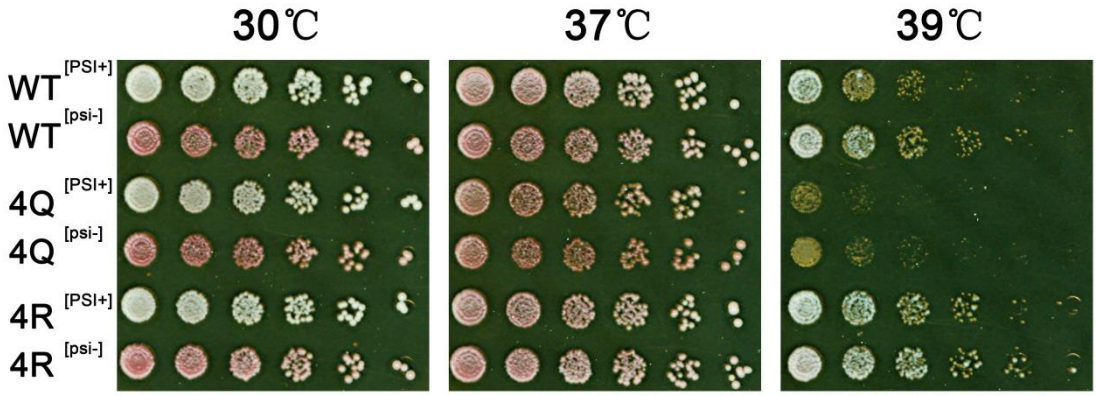

Figure 5.5. Effects of the [*PSI*$^+$] prion on the thermotolerance regulation of reversible hyperacetylated residues in Ssa1. [*psi*$^-$] cells were got by striping [*PSI*$^+$] colonies on YPD plates containing 3 mM Gnd-HCl for 2-3 days incubation. The cure of [*psi*$^-$] cells was repeated at least twice to get stable [*psi*$^-$] heritage. Fresh cultures were spotted on YPD as the description in the section of the growth assay.

5.7 Acquired thermotolerance assay of Ssa1 acetylation mutations in MH272 cells

To detect whether the temperature sensitivity of 4Q variant was strain-specific, we further transformed 4Q and 4R mutation into MH272 cells. As shown in Figure 5.6, the 4Q variant still decreased acquired thermotolerance compared to WT Ssa1 and 4R on YPD, and the thermotolerance of 4Q was almost same on YPD plates containing 3 mM Gdn-HCl compared to that of WT and 4R, which is totally in line with earlier observations in Figure 5.4. Therefore, the temperature sensitivity negatively regulated by acetylation was not cell type-specific, as it could be detected in G402 and MH272 cells.

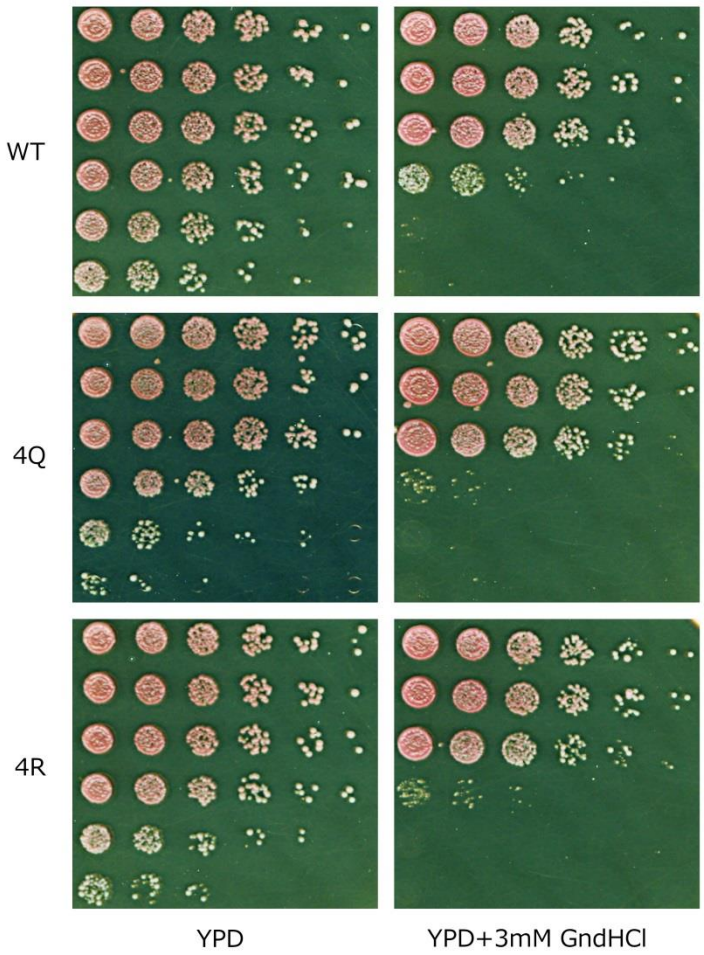

Figure 5.6. Acquired thermotolerance assay of mutations on the reversible hyperacetylated residues in MH272 cells. The fresh cultures were incubated at 39 ℃ for 1 h to induce the expression of Hsp104 *in vivo*. Then cultures were moved to 50 ℃ incubator for a time course (T_0-T_4 mean 0, 10, 20, 30 and 40 min respectively). T_{-1} means cultures before 39 ℃ incubation. Cells were spotted on YPD plates and YPD containing 3 mM Gdn-HCl after a 1/5 dilution.

5.8 Basal expression level of the Hsp70-Hsp40-Hsp104 machinery

To further investigate the expression levels of the main members of Hsp70 machinery, Western blotting was carried out to probe Ssa1, co-chaperones Ydj1 and Hsp104. As shown in Figure 5.7, none of them displayed a significant change of the basal expression level. Therefore, the reversible hyperacetylated residues did not influence the basal expression level of the Hsp70 machinery, but may rather regulate cellular functions of Ssa1, such as the inter-domain communication, interactome or dimerization.

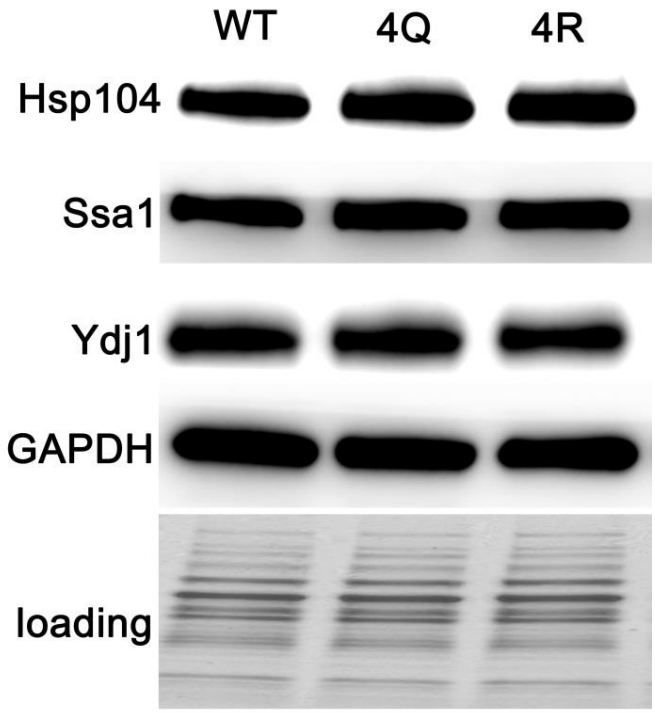

Figure 5.7. Abundance of chaperones in the Hsp70 machinery. Western blotting was performed to calculate the expression levels of Hsp104, Ssa1 and Ydj1. GAPDH and a stained SDS-PAGE running at the same conditions were used as double loading controls.

5.9 Influences of the different tags on acetylation mutations

In order to investigate the interaction changes between acetylation variants and Ssa1 binding partners *in vivo*, the 6×His tag or Flag tag was fused to N-terminal of Ssa1 and acetylation mutations based on the pC210 vector. The prion assessment showed that 6×His-tagged or Flag-tagged acetylation mutations still maintained the [PSI^+] phenotype (white colonies on YPD and survived on -ADE, Figure 5.8A). Furthermore,

Flag tag did not alter the temperature sensitivity of 4Q variant although all tagged mutations were generally more sensitive at elevated temperatures compared to untagged proteins (Figure 5.8B). Therefore, fusing N-terminal Flag-tagged acetylation mutations can be used for the further Co-IP assessment.

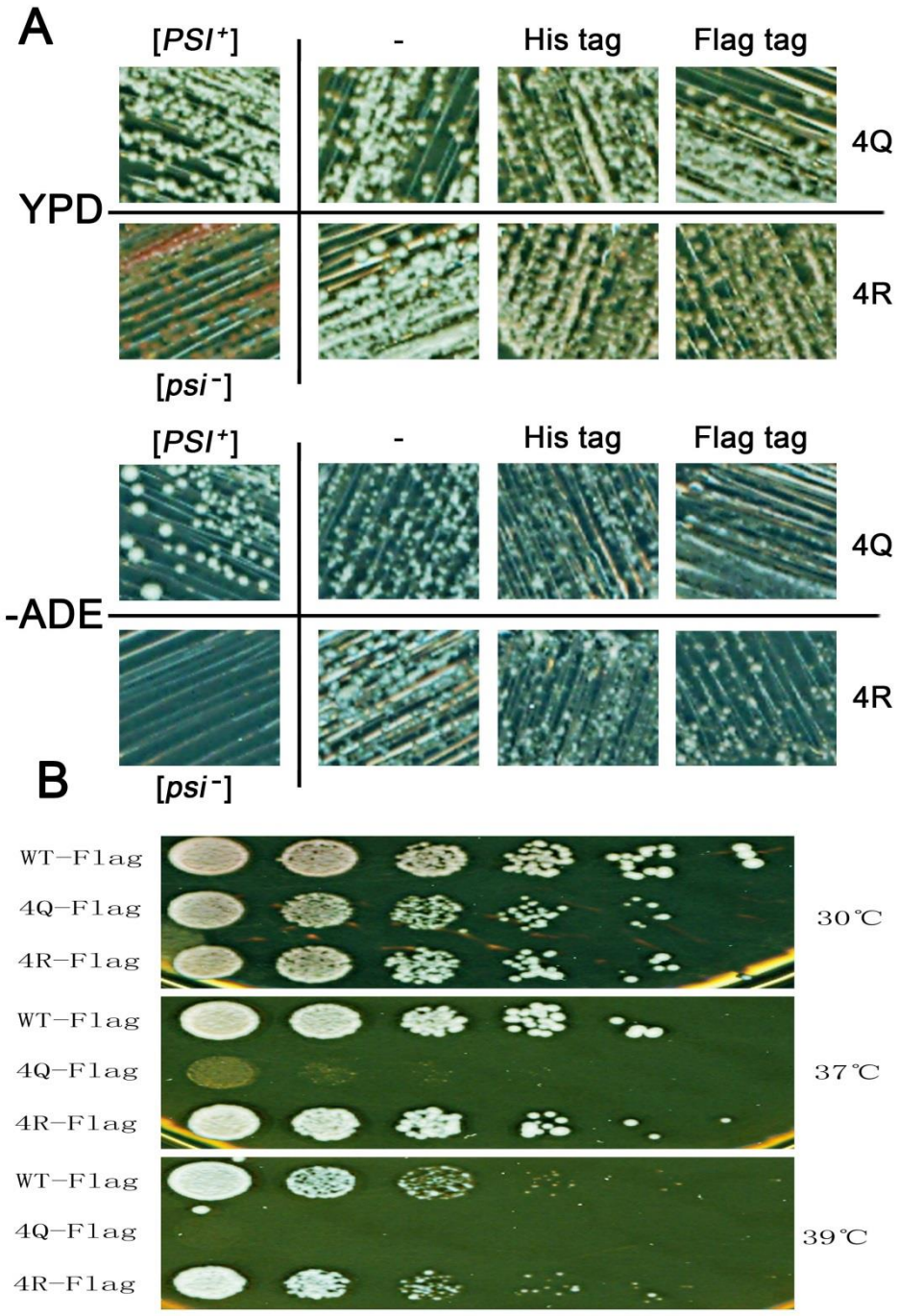

Figure 5.8. Phenotype assays of the tagged acetylation mutations. (A) Assessments of [*PSI*$^{+}$] propagation on tagged Ssa1 mutations; (B) Effects of elevated temperatures on tagged Ssa1 mutations.

5.10 Co-IP analysis of interactions between Ssa1 and binding partners

In the section, these mutants were analyzed for their ability to bind co-chaperones (Hsp104, Hsp40, Hsp26) and the substrate Sup35. Although none of the 4Q/4R mutants compromised the substrate binding (Figure 5.9A), but the acetylation-mimetic mutants (4Q) increased the affinity to all three co-chaperones (Figure 5.9A). The significance of this is unclear, although Hsp104, Hsp40 and Hsp26 had been considered to be involved in prion propagation in earlier chapters. Considering those four hyperacetylated residues are all distributed at the surface of the Ssa1 (Figure 5.9B), 4Q was considered to promote the formation of a tighter complex at 30 ℃ as glutamine brought extra negative changes to the surface of the Hsp70. Furthermore, in the last two chapters (3 & 4) I had found that the disturbance of SBD is related to elevated temperature, and F475S and L483W also increased interactions with co-chaperones (Hsp26,Ydj1 and Hsp104) to variant degree (Figure 4.18). It thus was speculated that 4Q might cause the disruption of SBD to some extent.

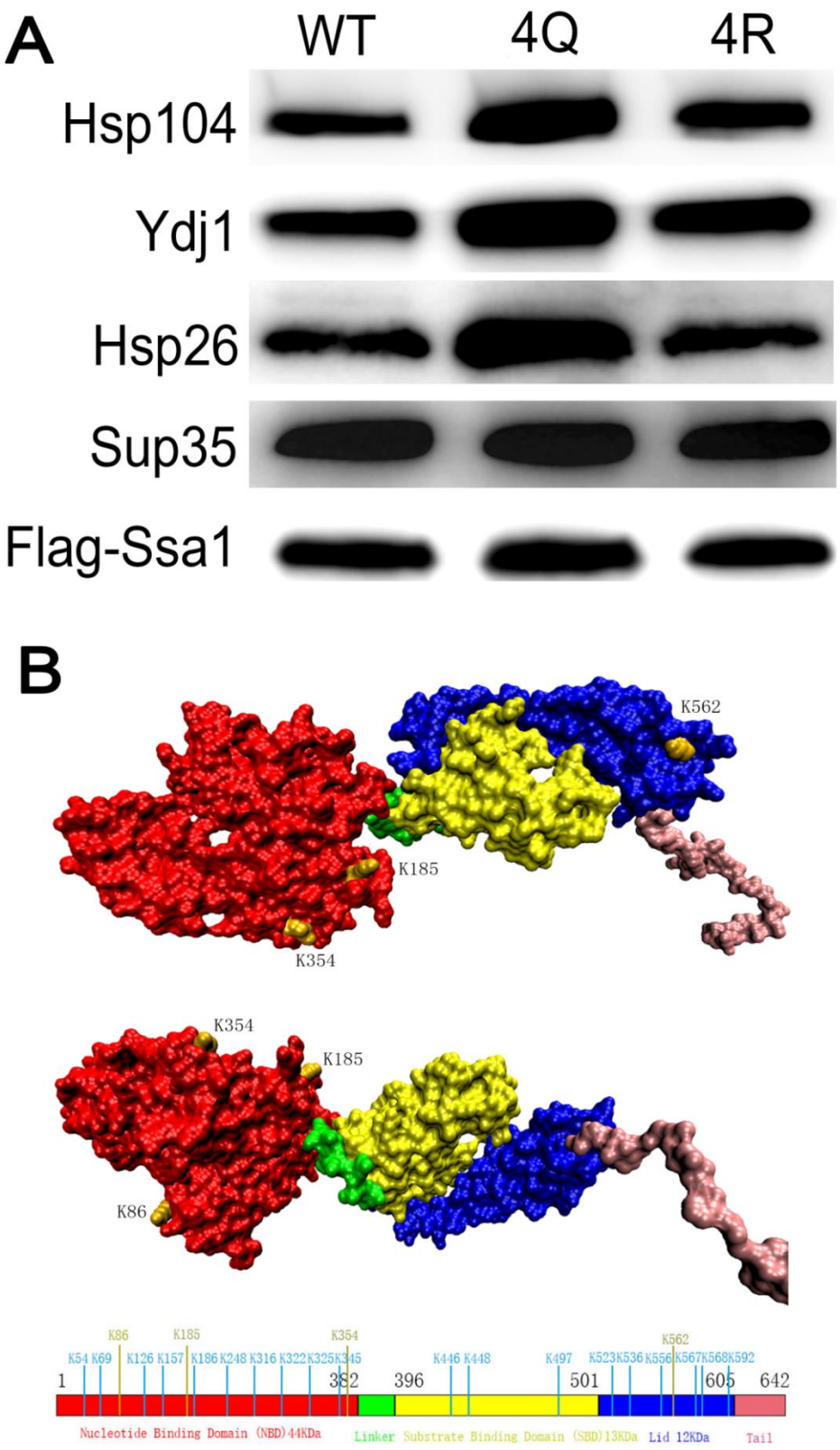

Figure 5.9. Acetylation mutations alter the Ssa1 interactions with clients. (A) Flag-tagged Ssa1 was pulled down from WT and mutations cells and probed for Hsp104, Ydj1, Hsp26 and Sup35. Flag-Ssa1 was used as loading control. (B) The space-filling Ssa1 model with the locations of hyperacetylated lysine residues (orange).

5.11 Specific SBD disruption caused by the acetylation

In order to investigate whether acetylation caused the SBD disruption of Ssa1, I used N-terminal fused Ssa1 to probe the specific SBD-degradation fragments *in vivo* like before. Interestingly, after extensive exposure, the image displayed a number of degradation fragments around 40-50 KDa in 4Q sample, and very slight degradation was observed in WT sample (Figure 5.10). Although the manner of disrupted SBD is not as clear as observed forF475S and L483W/H variants in Figure 4.17, it still implied that a very low percentage disruption of SBD exists in 4Q mutation and even WT at 30 ℃. It was thus predicted that the degraded fragments will be increased at elevated temperatures.

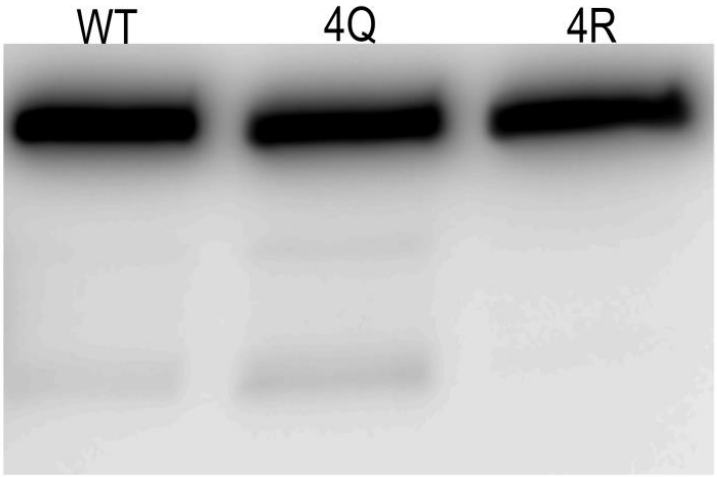

Figure 5.10. Specific SBD degradation of acetylation variants at 30 ℃. Anti-Flag was used to probe Flag-tagged Ssa1 proteins. The image was got after a long-time exposure.

5.12 Specific SBD disruption on heat shock

In order to confirm whether the SBD disturbance of 4Q mutation exists under heat shock, I incubated the cells with Flag-tagged Ssa1 at 39 ℃ for 2 h or 3 h. Degraded fragments were probed by anti-Flag as previously described. Surprisingly, there were several obvious bands around 40-50 KDa in WT and 4Q samples, and they were not seen in 4R samples (Figure 5.11A). This result supported that high temperature disturbed the SBD of Hsp70 and suggested that the acetylation of those four hyperacetylated residues negatively regulated the disruption of SBD at elevated temperature. However, WT Ssa1 should be deacetylated during 39 ℃ heat shock, so

that SBD degradation is not supposed to happen following the above hypothesis. The possible reasons are that low percentage of Ssa1 protein maintains the acetylated state even at heat shock condition or WT cells may take time to undergo complete deacetylation for all those four residues, which is in line with the growth assay under heat shock in Figure 5.3 and Figure 5.5. Following the prediction from the Figure 5.10, the SBD degradation of WT and 4Q variants had been found by stimulation at the high temperature in this section, rather than caused by cells apoptosis and autocatalysis during the heat shock process as all cells were survived after heat shock (Figure 5.11B). Therefore, the deacetylation of those four hyperacetylated residues maintains the abundance of the full-length Ssa1, in addition to the cellular functions of the Ssa1 under heat shock.

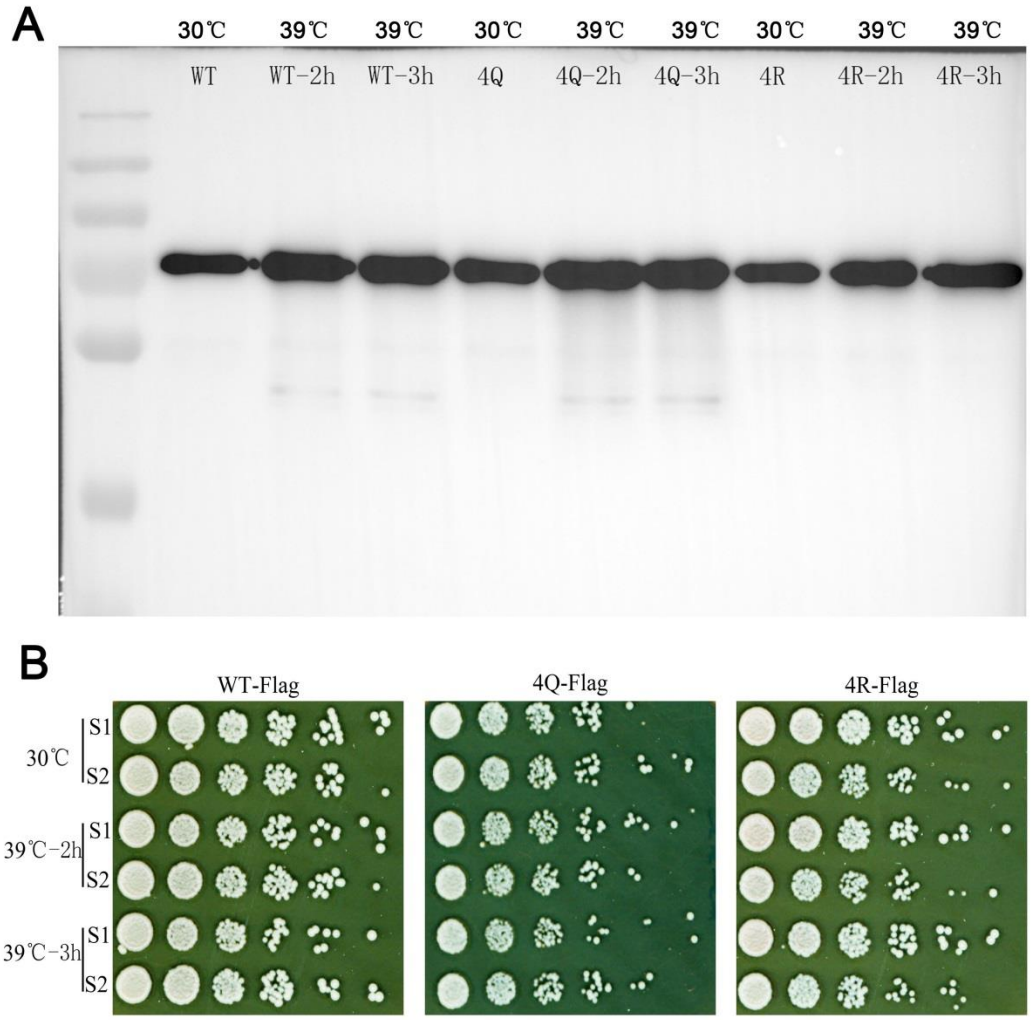

Figure 5.11. Specific SBD degradation of acetylation variants under heat shock. (A) Anti-Flag was used to probe Flag-tagged Ssa1 proteins. (B) Spot assay was employed to assess the viability of cells at 39 ℃ for 2 h or 3 h.

5.13 SBD disruption of Hsp70 independent from the pressure of misfolding proteins

Heat shock usually results in protein misfolding and brings the pressure of the denatured proteins to cells (Noor 2015; Morimoto 1998). L-Azatidine-2-carboxylic acid (AZC) is a ring analogue of L-proline and it is incorporated into proteins competitively with L-proline to cause the synthesis of misfolded proteins, thereby mimicking heat shock to some extent and preventing the cell growth (Shichiri et al. 2001). To investigate the effects of misfolded proteins induced by heat shock stress on the SBD disruption of Hsp70, I treated cells in SC medium containing 300 μg/ml AZC to induce the protein misfolding at 30 ℃ *in vivo*. Degraded fragments were probed by anti-Flag based on the Western blotting as the previous description. As shown in Figure 5.12, AZC did not effectively induce the SBD degradation compared to heat shock stress after 2 h treatment (Figure 5.12A) or longer (Figure 5.12B). Therefore, it was assumed that the specific SBD degradation of Hsp70 was independent from the stress of misfolded proteins in the cytoplasm. High temperature directly disturbs the stability of the SBD so that affects the structure and functions of full-length Hsp70.

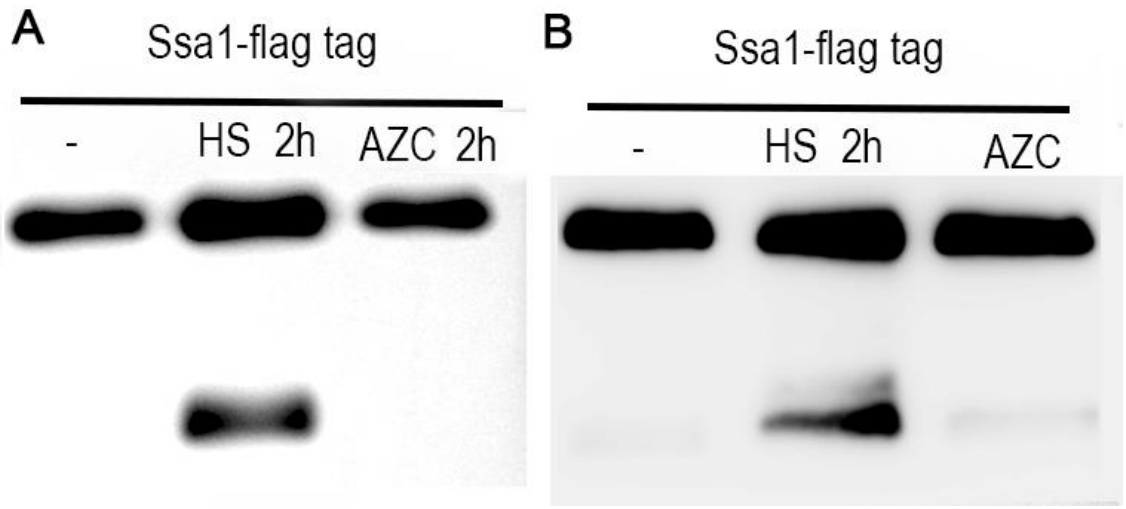

Figure 5.12. Specific SBD degradation induced by heat shock or AZC. (A) Cells were treated by 39 ℃ heat shock or 300 μg/ml AZC for 2 h. (B) Cells were treated by 39 ℃ heat shock for 2 h or cultured in SC containing 300 μg/ml AZC from 0.2 to 0.6 of OD_{600}. Anti-Flag was used to probe Flag-tagged Ssa1 proteins and degraded fragments.

5.14 Inhibitor of the vacuolar pathways rescues the Hsp70 abundance

I have demonstrated that specific SBD degradation existed in Ssa1-SBD mutants, F475S and L483W/H, and that it also occurred for WT and 4Q mutant at high temperature. In the section, I investigated which pathway regulated the degradation of the SBD. Proteins are degraded by two alternative breakdown pathways in *S. cerevisiae*. Normally, the degradation of short-lived proteins happens in proteasomes and is inhibited by carbobenzoxyl-leucinyl-leucinyl-leucinal (MG132); vacuolar proteases contributed to degrading long-lived proteins and are suppressed by phenylmethylsulfonyl fluoride (PMSF) (Lee & Goldberg 1996). To distinguish between the cytosolic or vacuolar proteolytic pathway contribution to SBD degradation, I added both classes of inhibitors into cultures to prevent protein degradation. As basal Ssa1 level of F475S mutant has a significant decrease even at 30 ℃ and F475S had been characterized to exhibit the best SBD-degradation, I employed F475S variant as the sensitive model in this section. Briefly, the fresh F475S cells were cultured at 30 ℃ in SC containing 0.1% (w/v) L-Proline to OD_{600} 0.5, then cells were harvested and resuspended into 20 ml fresh SC with 0.003% (w/v) SDS containing 75 μM MG132 or 1 mM PMSF for another 2 h incubation at 30 ℃. Western blotting showed that the basal Ssa1 level of F475S was increased slightly by MG132 inhibitor but enhanced approximately twice after the treatment of PMSF (Figure 5.13). Therefore, SBD degradation mainly happened in the vacuolar proteolytic pathway.

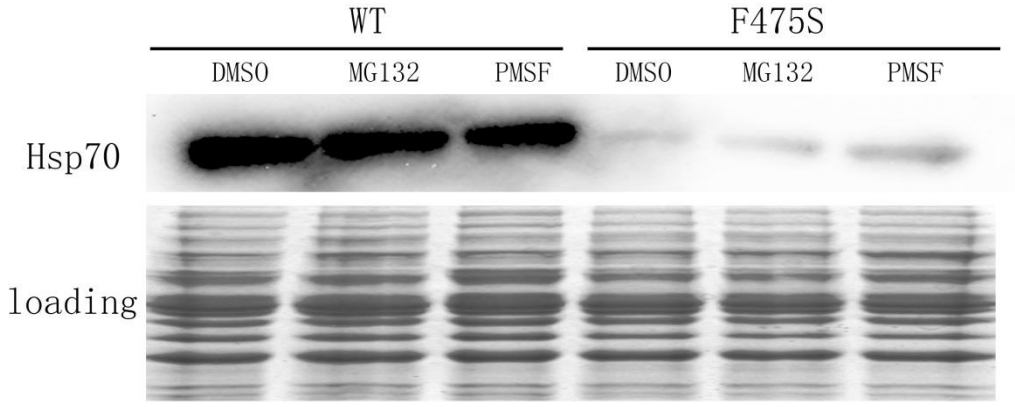

Figure 5.13. Effects of degradation inhibitors on the abundances of the Ssa1. Western blotting was performed to calculate the protein levels of Ssa1 at different conditions. DMSO was used to dissolve MG132 and PMSF, and the same volume of DMSO was added as a negative control in cells cultures. A stained SDS-PAGE running at the same conditions was used as the loading control.

5.15 Vacuolar carboxypeptidase (Pep4) contributes to the SBD degradation

To further confirm that SBD degradation mainly happened bythe vacuolar proteolytic pathway rather than the proteasomes, I assessed the SBD degradation of F475S variant in three knockout strains, ΔPEP4 (knockout vacuolar carboxypeptidase), ΔUFD2 (knockout ubiquitin fusion degradation factor) and ΔUBI4 (knockout ubiquitin precursor). Briefly, Flag-tagged F475S variant was transformed into those three backgrounds respectively. Cells were then cultured in SC-Leu and purified using magnetic anti-Flag beads. As shown in Figure 5.14, the level of full-length F475S variant was increased in ΔPEP4 cells by preventing the SBD degradation. The other two backgrounds, ΔUFD2 and ΔUBI4 did not rescue the breakdown of SBD. Moreover, there were a few degraded fragments of Ssa1 in ΔPEP4 cells, which implied that PEP4 may not fully be responsible for this degradation. Therefore, the specific SBD degradation of Hsp70 was mainly regulated by PEP4 of the vacuolar proteolytic pathway, but it is not the only protease which may contribute to SBD degradation.

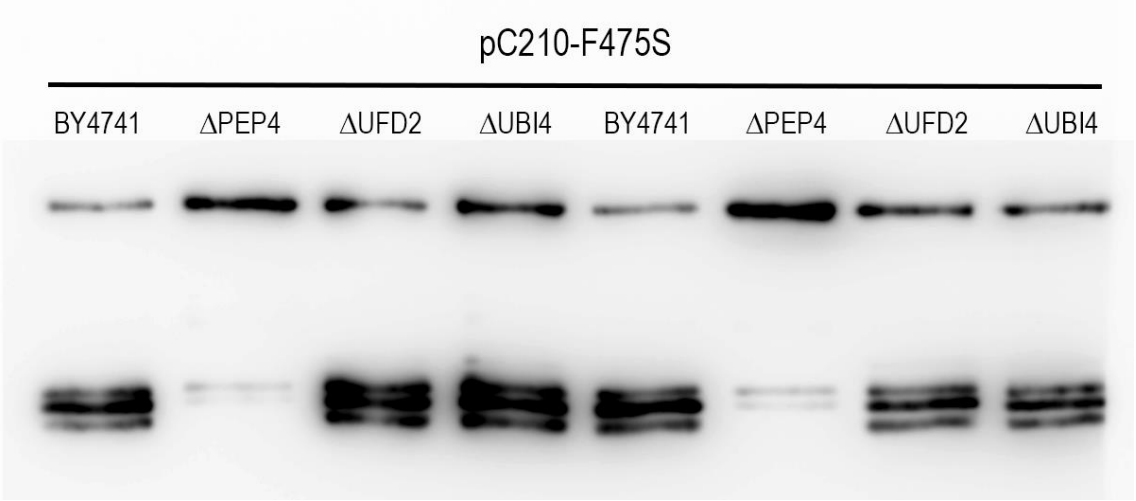

Figure 5.14. Vacuolar carboxypeptidase (Pep4) contributes to the SBD degradation. F475S variant was transformed into ΔPEP4, ΔUFD2 and ΔUBI4 cells respectively. After Co-IPs, anti-Flag was used to probe Flag-tagged Ssa1 proteins and degraded fragments. Duplicates were performed for each strain.

5.16 Effects of acetylation on HSF activation

Complexes of Hsp70 and HSF trimers have been detected during attenuation of the heat shock transcriptional response (Shi et al. 1998; Baler et al. 1992; Abravaya et al. 1992). Therefore, Hsp70 was considered as a negative regulator of Hsf1 to prevent the activation of heat shock genes (Morimoto 1998). To investigate how SBD degradation or acetylation influences Hsf1 activity, I employed lacZ reporter gene to assess the activation of HSF. Briefly, if Hsf1 is activated *in vivo*, it will increase the affinity with HSE and express the β-Galactosidase. As shown in Figure 5.15, acetylation-mimic mutation 4Q significantly activated Hsf1 after heat shock compared to the others. Interestingly, the SBD deficient variant, F475S, significantly decrease HSE-lacZ activity at 30 ℃ suggesting NBD only suppress the Hsf1 even more. Considering the three of four acetylated residues are located in NBD (Figure 5.1) and the Ssa1 nucleotide exchange factor Fes1, which interacts with NBD, is necessary for Hsf1 suppression (Wang et al. 2012), It was deduced that several specific conformational changes of NBD, which may be regulated by the acetylation/deacetylation process, are required for the activation/releasing of Hsf1. In other words, the acetylation of the four hyperacetylated residues accelerates the release of Hsf1 from Hsp70 complex, but SBD disturbance represses the release of Hsf1 at 30 ℃, but it is irrelevant to the release of Hsf1 at high temperature. Furthermore, the Hsf1 activation of 4Q variant at 39 ℃ did not rescue the deficiency at high temperature. It is unclear why this contradiction occurs, but there are three possible reasons: Firstly, 4Q over activated Hsf1 compared to WT and 4R so that a mass of genes were expressed at a short period. Those expressed proteins could not be fully folded to native structures so they aggregated and then brought misfolding-protein stress to cells. Secondly, over-activated Hsf1 promoted the expression of proteases and apoptosis genes, thus impairing the thermotolerance at high temperature. Finally, previous reports had shown that transcription of heat shock gene was prevented by overexpression of Hsp70 or Hsp40 (Sridhar K Rabindran et al. 1994; Mosser et al. 1993; Shi et al. 1998); therefore, the overexpression of Hsp70 or Hsp40 induced by the activation of Hsf1 suppressed the expression of the other requisite heat shock genes at high temperature.

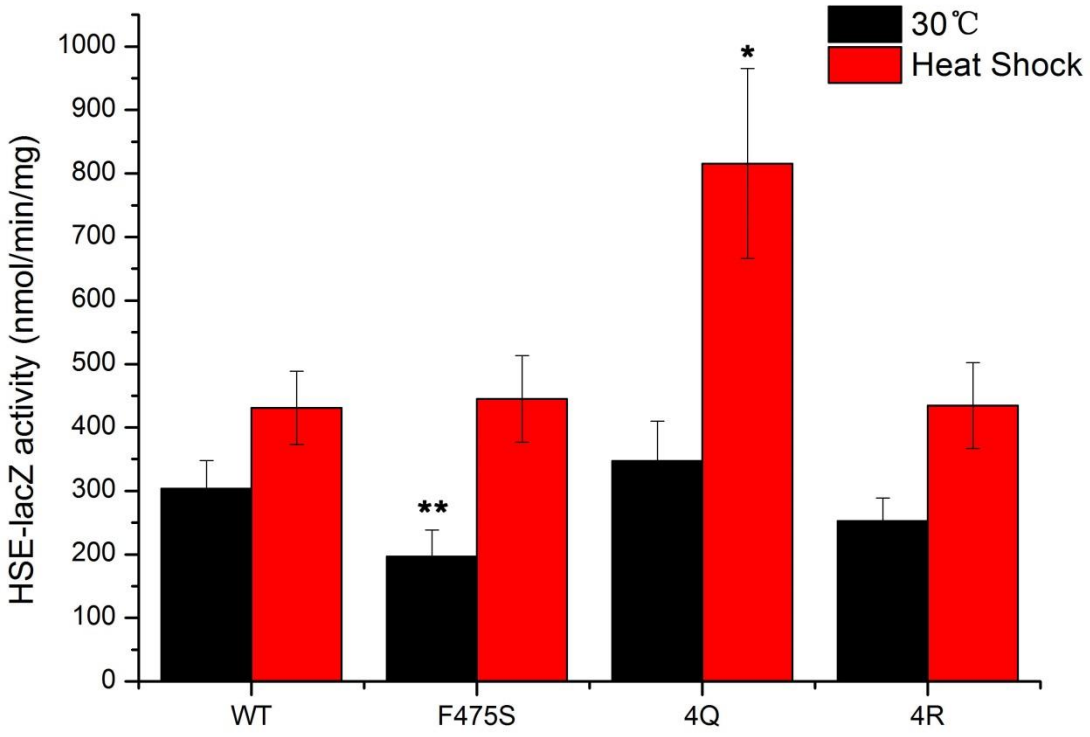

Figure 5.15. Effects of the acetylation of Ssa1 on the HSF activation. A plasmid with HSE-lacZ report gene was transformed into G402 cells. Cells were cultured at 30 ℃ or heat shock at 39 ℃ for 2 h. The activation of the Hsf1was calculated by measuring the expression of the β-Galactosidase under HSE. * represents $p<0.05$; ** represents $p<0.01$.

5.17 Luciferase refolding activity of lysine hyperacetylation

To assess the influence of acetylation of Ssa1 on the refolding activity of Hsp70 machinery, the luciferase refolding assay was performed *in vivo*. As shown in Figure 5.16, 4Q variant maintained the similar refolding activity as that of WT, but the 4R variant revealed slightly increased refolding activity. In earlier sections, 4R had been found to have the best growth at high temperature (Figure 5.3 and 5.5), thus it was considered that the increased refolding activity of 4R variant promoted the protein folding and refolding under heat shock. Therefore, the deacetylation of the four hyperacetylated residues enhances the refolding activity of Hsp70 machinery to adapt at elevated temperature.

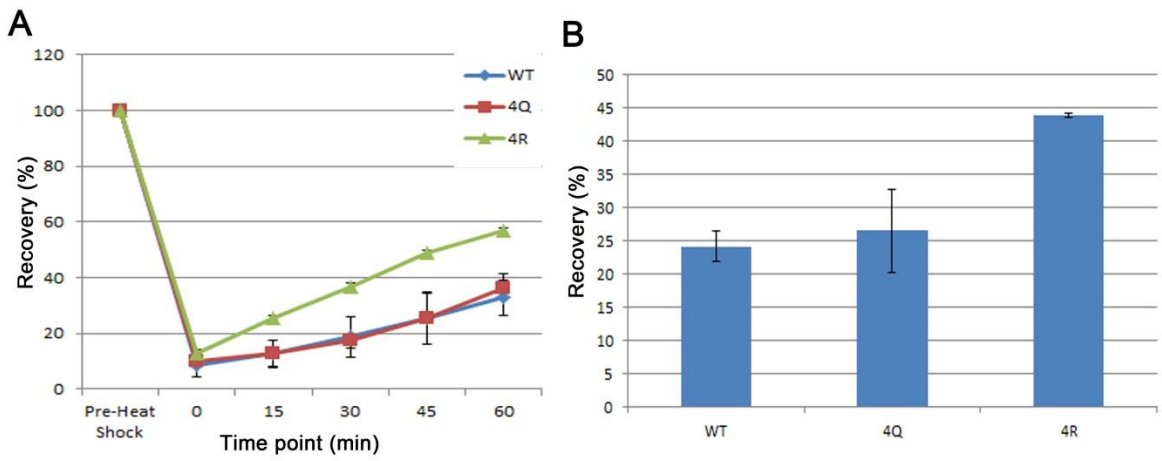

Figure 5.16. Luciferase refolding activity of acetylation mutations. (A) Luciferase refolding profiles in a 60 min time course; (B) Luciferase recovery rate in 1 h. Fresh cultures were shifted to 37 ℃ for 30 min before 45 ℃ denaturation for 1 h. Denatured luciferase cultures were recovered at 25 ℃ for a 1 h period. Cycloheximide was used to prevent the protein synthesis during the recovery period.

5.18 Investigation of acetylation mutations to respond other stresses

In order to further investigate the influence of acetylation mutations to respond stresses, I observed the viability of cells in the presence of SDS and H_2O_2, respectively. As shown in Figure 5.17, cells expressing the acetylation-mimetic 4Q variant as the only Ssa source were insensitive to SDS, but sensitive to H_2O_2, implying that 4Q variant did not excessively alter the basal structure and function of the Ssa1-like F475S mutation. Interestingly, 4R variant was more tolerant under H_2O_2 stress than WT. Thus, acetylation mutations have totally consistent responses to oxidant and heat shock stress, implying they may share the same stress-response pathway. A previous report had shown that Ssa1 is a sensor of oxidative stress and oxidative modification of C264 and C303 abolishes the repression of Ssa1 to binding Hsf1 and activates the transcription of heat shock genes (Wang et al. 2012). It has been found that acetylation of Ssa1 is involved in activation of Hsf1 (Figure 5.15). However, the activation of Hsf1 of the 4Q variant only happened at high temperature. It is still not known what kinds of effects on Hsf1 activation were caused by 4Q variant under oxidant stress.

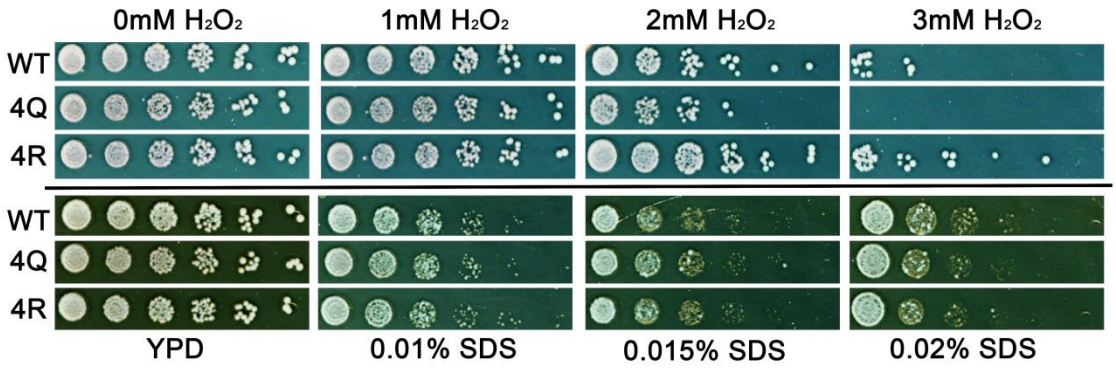

Figure 5.17. Growth assays of acetylation mutations under other stresses. YPD and SC medium were complemented with cell-wall damage reagent SDS and oxidant reagent H_2O_2 respectively to achieve required concentrations. Fresh cultures were spotted on those plates as the description in growth assay section and incubated for 2 days at 30 ℃.

5.19 Chapter conclusion

Ssa1 is hyperacetylated at 30 ℃ and four specific lysine residues, Lys86, Lys185, Lys354 and Lys562, distributed on NBD and SBD are deacetylated upon heat shock. Maintaining acetylation of those lysine residues would cause the sensitivity to high temperature. Thus, acetylation of those lysines negatively regulated the heat shock response. Furthermore, the thermotolerance regulation is independent from [*PSI*$^+$] prion and alteration of the genome-wide translation caused by the read-through. The reversible hyperacetylated residues did not influence the basal expression level of the Hsp70 machinery, but the acetylation-mimic variant 4Q was considered to promote the formation of a tighter Hsp70 complex at 30 ℃ as glutamine brought extra negative charges to the surface of the Hsp70. It was also found that high temperature disturbed the SBD of Hsp70 and that acetylation of those four hyperacetylated residues negatively regulated the disruption of SBD at elevated temperature. Moreover, SBD degradation mainly happened by the vacuolar proteolytic pathway rather than the proteasomes, and it represses Hsf1 activition at 30 ℃. The acetylation of those four hyperacetylated residues is one of the reasons accelerating the release of Hsf1 from Hsp70 complex at high temperature.

Figure 5.18 shows a three-dimensional space-filling molecular structural model of Hsp70 in the ATP state, which shows that all of the identified lysine residues on the

surface of the protein and thus accessible for modification. Notably, they are partially aligned along a line through NBD and SBD (Figure 5.18B) and three of four reversible hyperacetylated residues are located in NBD and one in the lid of SBDα, implying regulation of acetylation is involved in inter-domain communication and conformational changes of NBD.

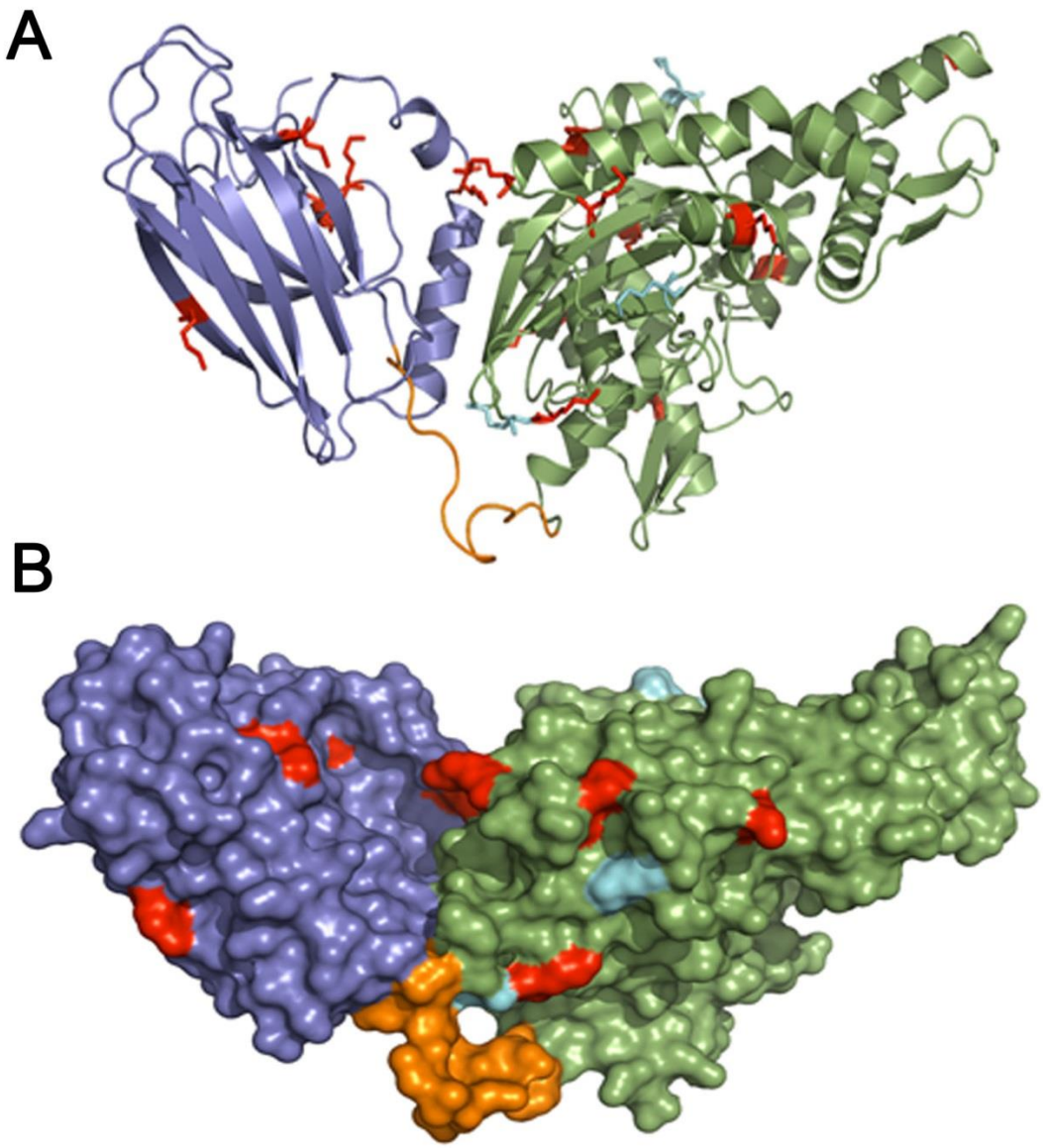

Figure 5.18. Three-dimensional molecular structural model of Hsp70 at ATP state. (A) the ribbon presentation; (B) the space-filling model. NBD is presented in dark green; and SBD is shown in dark blue; acetylated residues are in red; linker is presented in orange. Figure was produced by Dr. Andrew W. Truman.

Wild-type Ssa1 was rapidly clipped to a smaller form, which represents a species lacking the whole SBD or the C-terminal lid. Indeed, numerous studies also indicated that the 45 kDa NBD of Hsp70 is protease resistant whereas the SBD is proteolytically labile (Chappell et al. 1987; Buchberger et al. 1995; Needham et al. 2015b). It is not clear whether other stresses also cause the SBD disruption and whether SBD degradation is conserved in mammalian cells. Furthermore, phosphorylation and acetylation were both observed after heat shock. However, we only investigated the effects of acetylation in the work presented in this chapter. It is thus not clear, at present, whether phosphorylation and acetylation influence each other to respond heat shock stress.

CHAPTER SIX

GENERAL DISCUSSION AND FUTURE DIRECTIONS

6.1 Conclusions

In this thesis it was discovered that the highly conserved residues Phe475 and Leu483 located in the β6-β7 region of Hsp70 SBD play crucial roles in the structure and function of this protein. The particular structural significance of residue 475 requires a correctly sized side chain to maintain the hydrophobic core of the SBD. It was found that substitution of amino acids with much smaller amino acid side chains at residue 475, such as alanine and serine, resulted in temperature sensitivity and [PSI^+] impairment. When the side chain of residue 475 is larger than Cysteine, no matter if it is polar or nonpolar (tyrosine and phenylalanine), thermotolerance and [PSI^+] can be maintained. However, there is a limit to side-chain size at this residue as substitution with tryptophan caused structural instability and cell death. By contrast, residue 483 requires a smaller size amino acid to be at this site to maintain the hydrophobic core of SBD. Therefore, mutations at these two residues can significantly alter the integrity of SBD and promote degradation of SBD *in vitro* and *in vivo*.

Interestingly, we also identified 5 regions with significant CSPs: (I) Val393 in the linker; (II) Ile417 in loop 2,3; (III) Asp476, Val477, Asp478, Ser479 Ile482, Leu483 and Asn484 in β6, L67 and β7; (IV) Asn502, Asp503 and Lys504 in β8; (V) Ile512, Ile533, Lys547 and Ile548 in SBDα. Additionally, several residues in regions of (I), (II), (III) and (IV) also form the interface between the SBD and NBD. The residues with significant CSPs imply that the structural instability caused by substitutions of Phe475 or Leu483 may be transmitted through β6-β7 region to the interface region between the SBD and NBD. Therefore our data suggest that mutation of Phe475 or Leu483 can result in significant changes in the ability of the SBD and NBD to communicate and properly regulate the ATPase and substrate-binding cycles of Hsp70.

Functionally, the mutations F475S and L483W cause loss of SBD repression of ATP hydrolysis of the NBD, reduce protein refolding activity and enhance interactions with co-chaperones Hsp104 and Hsp26, but decrease the interaction with Sup35. The deficiency in binding Sup35 may be directly responsible for the prion propagation phenotypes observed with these mutants. Reduced interaction between Ssa1 and Sup35 may reduce the infectious “seeds” of [PSI^+] and result in prion loss. The enhanced degradation of the SBD in these mutants results in reduced abundance of Ssa1 in cells,

which is considered to be the primary cause of the temperature sensitivity phenotype. However, considering the results collectively, the increased ATPase activity, increased interaction with Hsp104 and Hsp26, and the decrease in refolding activity will all potentially contribute to [*PSI*$^{+}$] impairment and temperature sensitivity phenotypes observed.

The specific SBD degradation is observed in WT cells upon prolonged exposure to high temperature. SBD degradation appears regulated in part by the acetylation of Ssa1 at specific residues, and degradation occurs via the vacuolar proteolytic pathway rather than the proteasomal pathway. Ssa1 is hyperacetylated at 30℃ and four specific lysine residues, Lys86, Lys185, Lys354 and Lys562 are deacetylated upon heat shock. Maintaining acetylation at these lysine residues would be predicted to influence the ability of Ssa to function at optimum levels during heat shock. Seeing that Ssa1 harbouring acetylation-mimetic mutations at these sites had no [*PSI*$^{+}$]-related phenotypes, suggests prion propagation and thermotolerance are de-coupled in terms of Hsp70 acetylation [at these sites at least].

6.2 Discussion and future directions

6.2.1 Inter-domains communication of Hsp70

In Chapter 3, A394V was found significantly rescue the signal attenuation of F475S in the 2D ^{1}H-^{15}N HSQC spectrum (Figure 3.11). A394V/F475S also partially recovered thermotolerance of F475S cells at 37 ℃ (Figure 3.3, 3.4 and 6.1). Considering A394 is located in the linker of Hsp70, it may be a crucial site for inter-domain communication between NBD and SBD. A394V single mutant was characterised as having growth activity at elevated temperatures (Figure 6.1), and could possibly be utilised to investigate the inter-domain communication for mutants such as L484A in DnaK (Mayer & Kityk 2015).

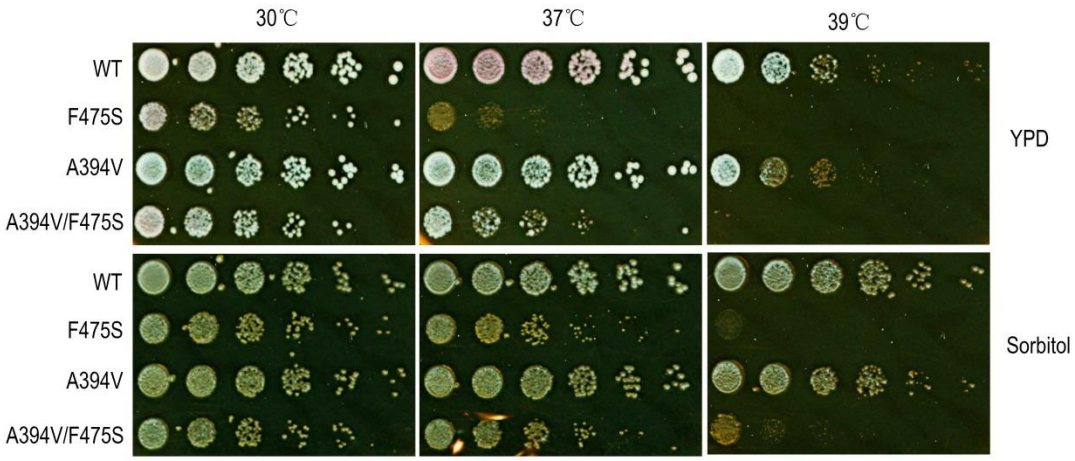

Figure 6.1. Growth assay at elevated temperatures. Fresh cultures were spotted onto YPD and YPD containing 1 M sorbitol as described in Section 2.16.1.

6.2.2 Assessment of highly conserved motif GGAP

The SBD of Hsp70 consists of β-sheet rich substrate-binding cavity, α-helical lid and a disordered tail of around 30 residues. Most of the mutations analysed in this thesis are located in the β-sheet rich substrate-binding cavity, and several mutations are located in the lid area. Previous reports showed that the highly conserved EEVD motif in the disordered tail interacts with co-chaperones such as Hop, Sti1 and Chip (Morshauser et al. 1985; Zhu et al. 1996; Mayer & Kityk 2015). Therefore the disordered tail of SBD was considered as possibly contributing to capture and/or recognising binding partners. In collaboration work with Prof. Perrett's group at the Chinese Academy of Sciences we have identified another highly conserved, the GGAP motif (608-GGAPGGAAGGAPGGFPGGAP-628), which is located in the SBD tail. Deletion (ΔGGAP) and introduction of mutants in this motif resulted in sensitivity at high temperature and other stresses (SDS and H_2O_2) (Figure 6.2B and C). Additionally, [PSI^+] propagation was slightly impaired in ΔGGAP cells (Figure 6.2A). Notably, the deficiency to response high temperature and other stresses is observed in three strain backgrounds (Figures 6.2 and 6.3). Mutagenesis of the GGAP motif also altered the secondary structure of Hsp70 (Figure 6.4A) and decreased the ATP hydrolysis (Figure 6.4B). However, we do not yet appreciate the relationship to mutations in this motif and alterations in Hsp70 function.

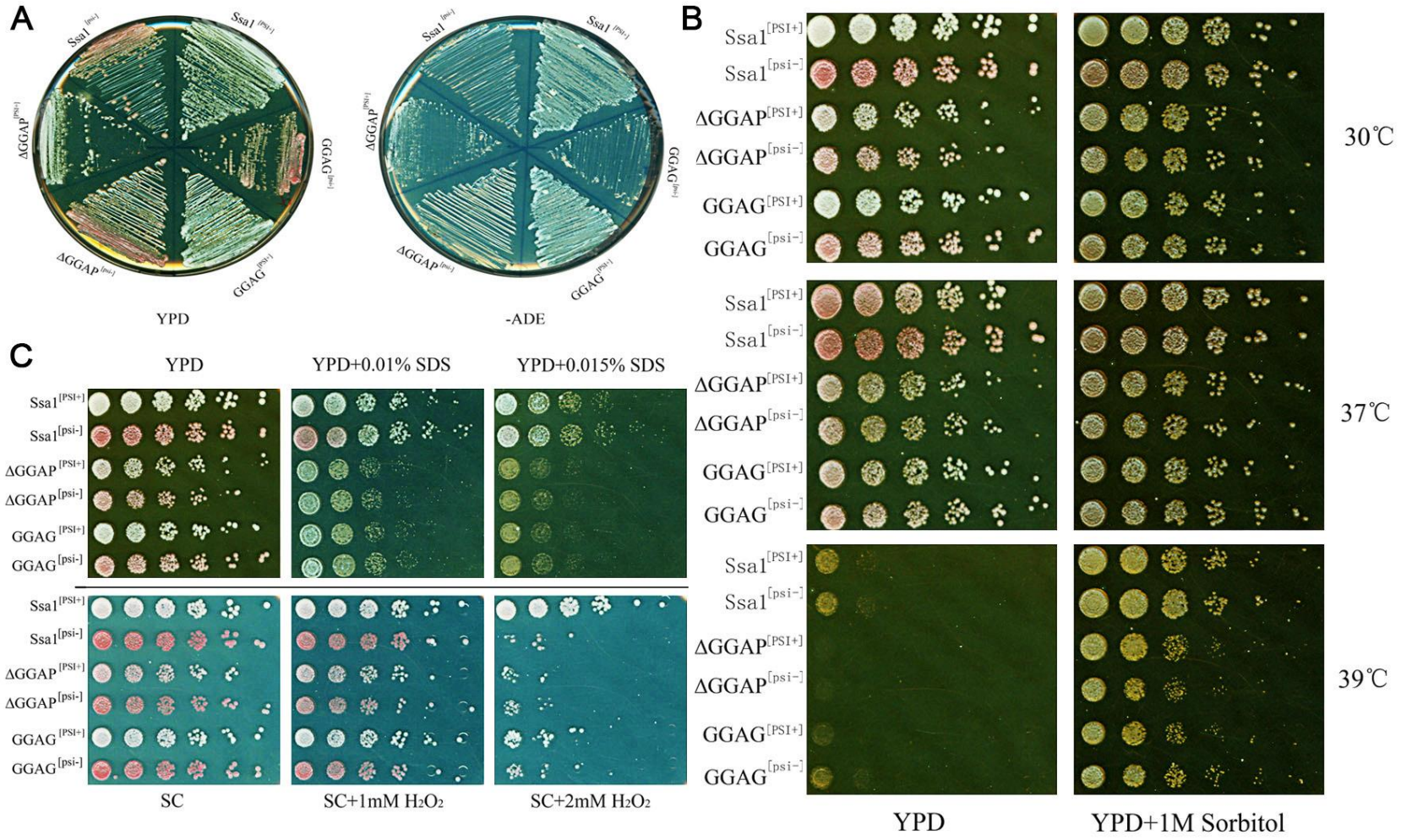

Figure 6.2. Phenotypic effects of the GGAP motif in G402 cells. (A) Assessment of [*PSI*$^{+}$] propagation; (B) Effects of the GGAP motif at elevated temperatures; (C) Effects of the GGAP motif to exposure of SDS and H_2O_2.

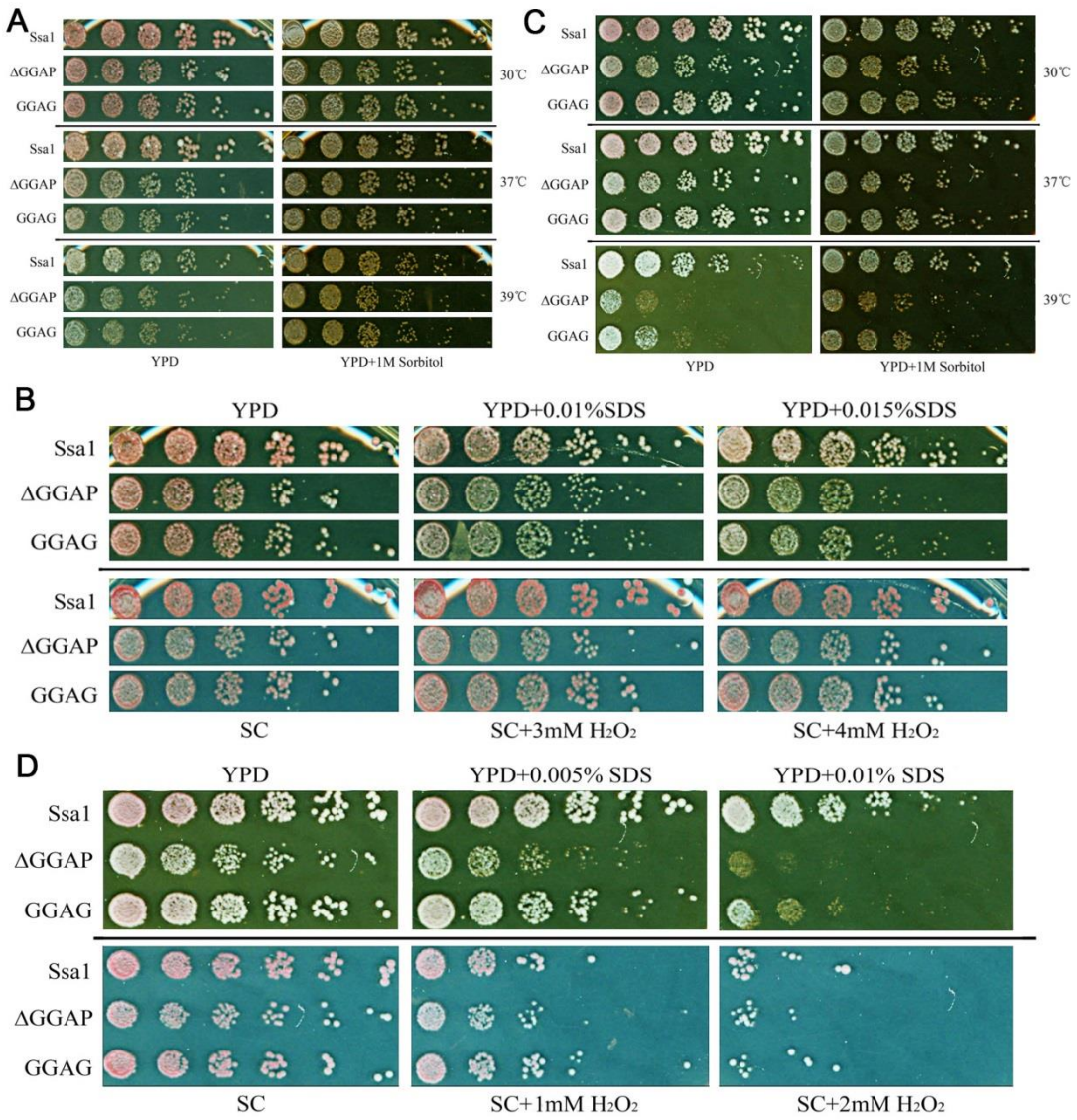

Figure 6.3. Phenotypic effects of the GGAP motif in MH272 or [*ure-0*] cells. (A) Effects of the GGAP motif at elevated temperatures in MH272 cells; (B) Effects of the GGAP motif to stresses of SDS and H_2O_2 in MH272 cells; (C) Effects of the GGAP motif at elevated temperatures in [*ure3-0*] cells; (D) Effects of the GGAP motif to stresses of SDS and H_2O_2 in [*ure3-0*] cells.

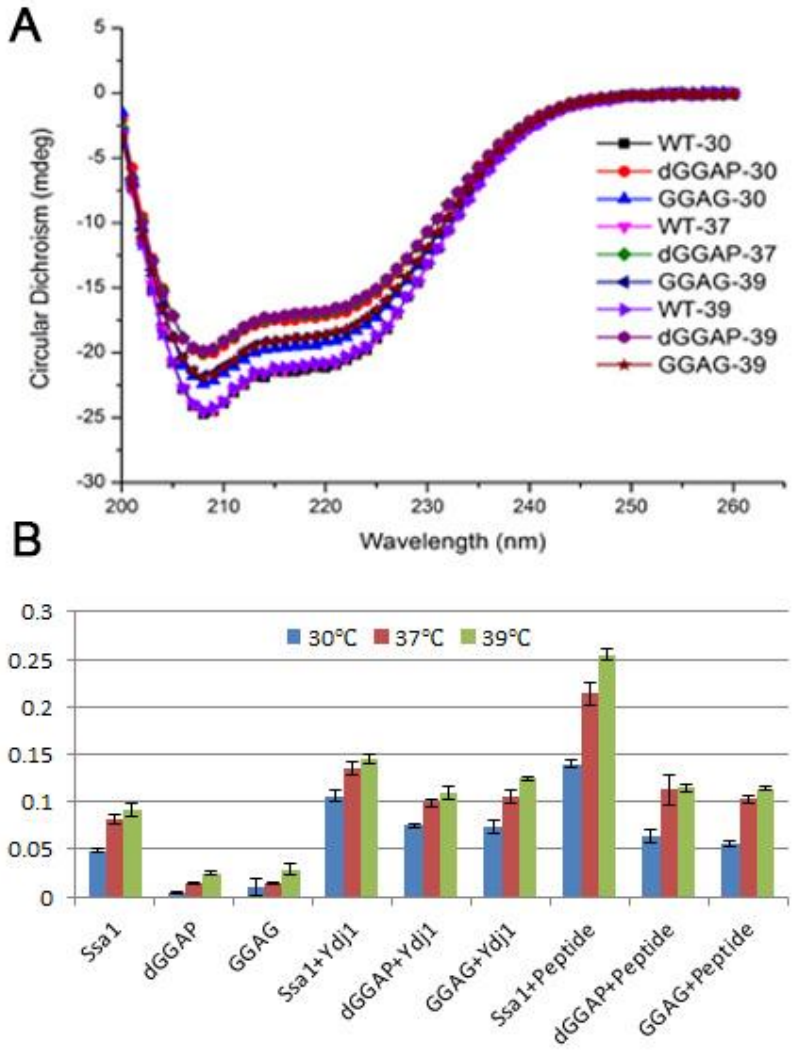

Figure 6.4. Structural and functional effects of the GGAP motif. (A) Secondary structure chnges monitored by far-UV CD spectra for full-length Ssa1. CD spectra were scanned at 30 ℃, 37 ℃ and 39 ℃ respectively. (B) ATPase activity of Ssa1 with or without Ydj1 or peptide stimulation at elevated temperatures.

6.2.3 Regulating Hsp70 inter-domain communication pathways

There is a bidirectional allosteric intramolecular regulation between NBD and SBD. Briefly, ATP binding and hydrolysis of the NBD regulate the substrate capture of the SBD and substrate binding of the SBD increases ATP hydrolysis (Mayer & Kityk 2015). The lid is able to detach from the substrate-binding pocket completely and dock onto one side of the NBD; also the linker region is buried into the cleft of the NBD and dictates the steering of the SBD docking with a new interface with the NBD (Kityk et al. 2012; Bertelsen et al. 2009). Several residues that are part of the NBD and SBD

interface have been reported as being important in this process and include, Arg151, Arg167, Asp326, Asp393, Lys414, Asp481 (residue numbers in DnaK) (Kityk et al. 2012; Kityk et al. 2015). Asp481 and Lys414 where found to contact the NBD subdomain IA and IIA respectively as a clamp to fix the NBD and SBD interaction in the ATP state, and thus strongly decrease intrinsic ATPase activity and lose stimulation through substrate binding and Hsp40 (Kityk et al. 2015). Figure 6.4 highlights two important residues (Phe475 and Leu483) characterised in this thesis and also several second-site suppressors of F475S variant or L483W reported previously (Jones & Masison 2003; Needham & Masison 2008). Interestingly, the vast majority of suppressors are located within nucleotide-binding cavity, linker, substrate-binding loops and the lid area (Figure 6.5). The distribution indicates that functional changes in Hsp70 caused by the SBD mutations, is most likely linked with the bidirectional allosteric intramolecular regulation between NBD and SBD. Furthermore, the P636S suppressor highlights a role for the disordered tail and promotes the significance of disorder tail (eg. GGAP motif) for further study.

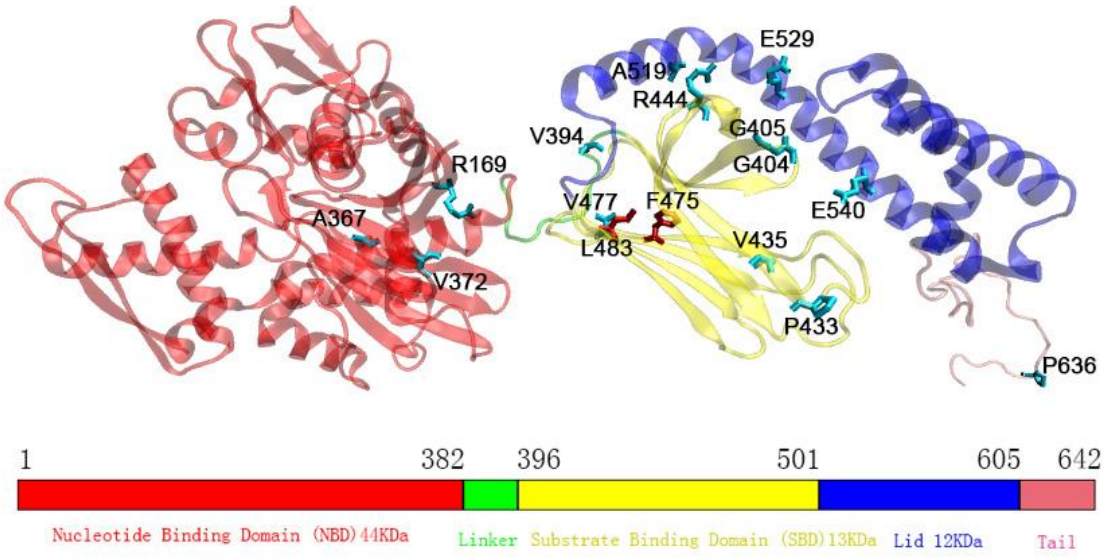

Figure 6.5. Locations of mutations in Ssa1 model. Red residues impair prion propagation and thermotolerance to some degree and those identified as second-site suppressing mutations are cyan.

6.2.4 Upstream regulation of SBD

The constitutive *SSA2* promoter was used in this thesis to assess protein function without the complicating factor of heat shock induction (Hasin et al. 2014). However, *SSA1* is regulated by Hsf1 at the *SSA1* promoter. It was noted that F475S under its native *SSA1* promoter in pJ120 vector is more tolerant to high temperature exposure compared to when under the *SSA2* promoter in pC210 (Figure 6.6). This finding raises the possibility of upstream regulation of SSA1 due to disruption and degradation of the SBD. However, due to lack of time this hypothesis could not further investigated.

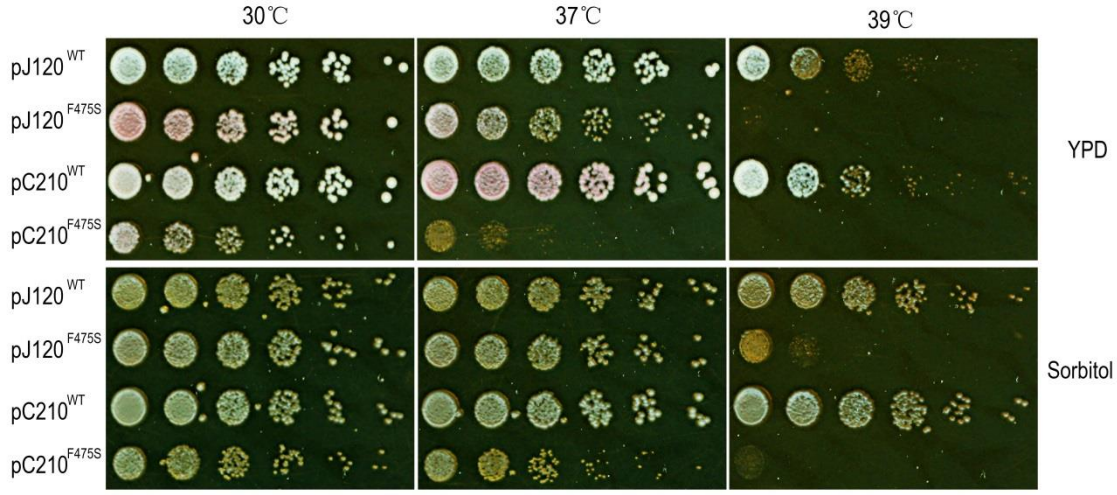

Figure 6.6. Growth assay of cells with Ssa1 F475S mutation under different promoters. Fresh cultures were spotted on YPD and YPD containing 1 M sorbitol as the description in Section 2.16.1. pJ120 is with *SSA1* promoter and pC210 is with *SSA2* promoter.

6.2.5 Finding the Acetylase(s) and deacetylase(s) for Hsp70

As shown in Chapter 5, acetylation of Ssa1 can negatively regulate the heat shock response. However, currently there is no direct evidence supporting the identification of the acetylase(s) or deacetylase(s) that target Ssa1. In global screening experiments, Hat1 (Histone AcetylTransferase) and Rpd3 (Histone deacetylase) were shown to interact with Ssa1 (Costanzo et al. 2010; Gong et al. 2009). We carried out preliminary experiments to investigate whether these proteins could be Ssa1-targeting acetylase and deacetylase. *HAT1* was successfully deleted in the genome and replaced with KanMX4 in the MH272 background (Figure 6.7A, lane 1: 2.4 Kb PCR product of flanking plus KanMX4; lane 2: 1 Kb PCR product of forward flanking plus a part of KanMX4; lane 3:

0.9 Kb PCR product of reverse flanking plus a part of KanMX4). Figure 6.7B showed that the Δ*HAT1* cells almost maintain the same thermotolerance as WT MH272 cells at elevated temperatures. However, it is still unknown whether *HAT1* knockout prevents the acetylation of Ssa1 directly. Although attempted on several occasions and with varying methodologies, we were unable to successfully delete the *RPD3* gene in the MH272 background when harbouring Ssa as the sole Hsp70-Ssa in the cell.

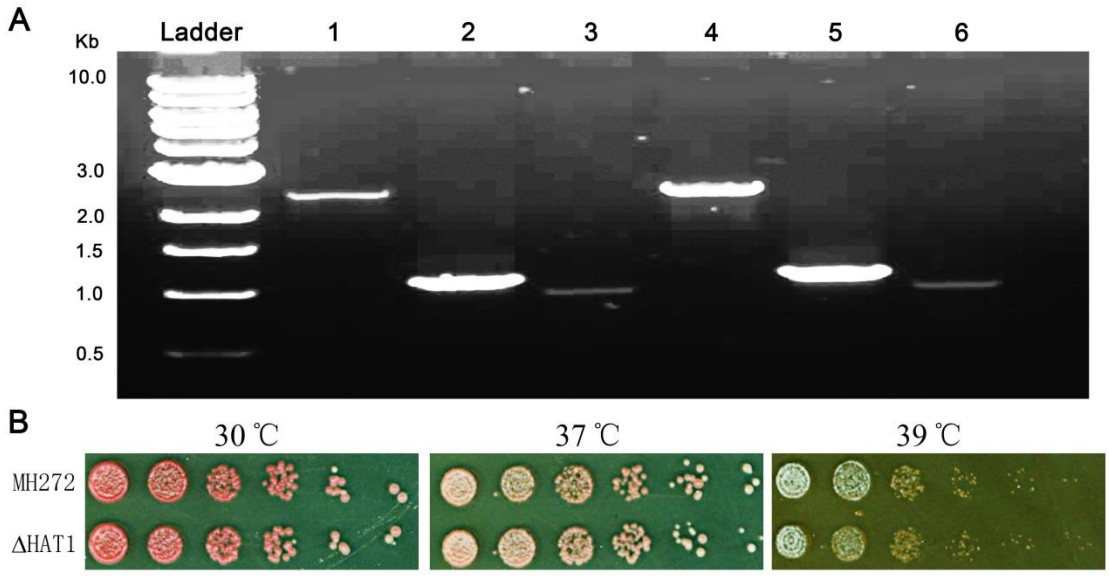

Figure 6.7. Effect of *HAT1* deletion on heat shock response. (A) colony PCR to assess the *HAT1* knockout by KanMX4 in MH272 cells. Duplicates are shown in lane 1and 4 are 2.4 Kb PCR products of flanking plus KanMX4; lane 2 and 5 are 1 Kb PCR products of forward flanking plus a part of KanMX4; lane 3 and 6 are 0.9 Kb PCR products of reverse flanking plus a part of KanMX4. (B) Growth assay of the *HAT1* knockout cells at elevated temperatures. Fresh cultures were spotted on YPD as the description in Section 2.16.1.

6.2.6 Reversible phosphorylated residues regulate thermotolerance in yeast

In Section 5.2, it was mentioned that in addition to lysine acetylation, two residues Thr338 and Thr492 were phosphorylated following heat shock. Thus, phosphorylation of Ssa1 is potentially also involved in the heat shock response. Figure 6.8 shows that the dephosphorylation-mimetic mutant T492A is sensitive at high temperatures and phosphorylation-mimetic mutant T492E has reduced growth even at 30℃. Therefore, phosphorylation of Ssa1 (specific residues) is perhaps also involved in response to heat shock?

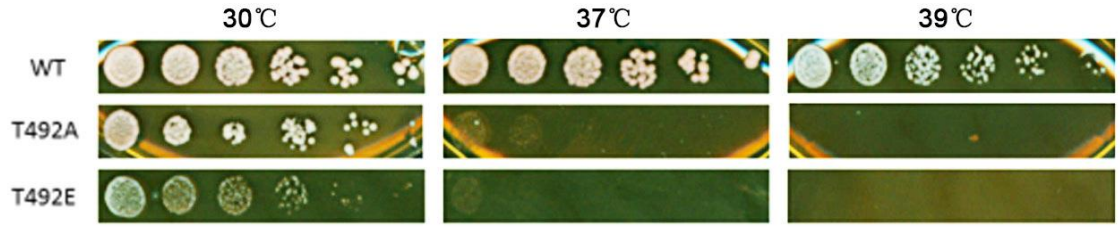

Figure 6.8. Growth assay of the reversible phosphorylated mutations in Ssa1 at elevated temperatures. Fresh cultures were spotted on YPD as the description Section 2.16.1.

6.2.7 SUMOylation of Hsp70

Small Ubiquitin-like Modifier (SUMO) is a well established PTM that can alter target protein function. As one of the PTMs, SUMOylation is involved in various cellular processes, such as nuclear-cytosolic transport, transcriptional regulation, apoptosis, protein stability, response to stress, and progression through the cell cycle (Hay 2005). Following on from showing ubiquitinylation of SBD is probably not involved in controlling degradation, we carried out preliminary analysis to investigate whether SUMOylation was involved. Two residues of Ssa1 (Lys106 and Lys523) have been identified as being SUMOylated. Thus, the K106R, K523R and K106R/K523R mutations were introduced into Ssa1 to prevent SUMOylation at these sites. As shown in Figure 6.9, none of these mutations alters the stress response (heat shock, SDS, H_2O_2) or prion propagation in G402 cells. One possibility is that SUMOylation is transferred to other residues after preventing SUMOylation on Lys106 and Lys523?

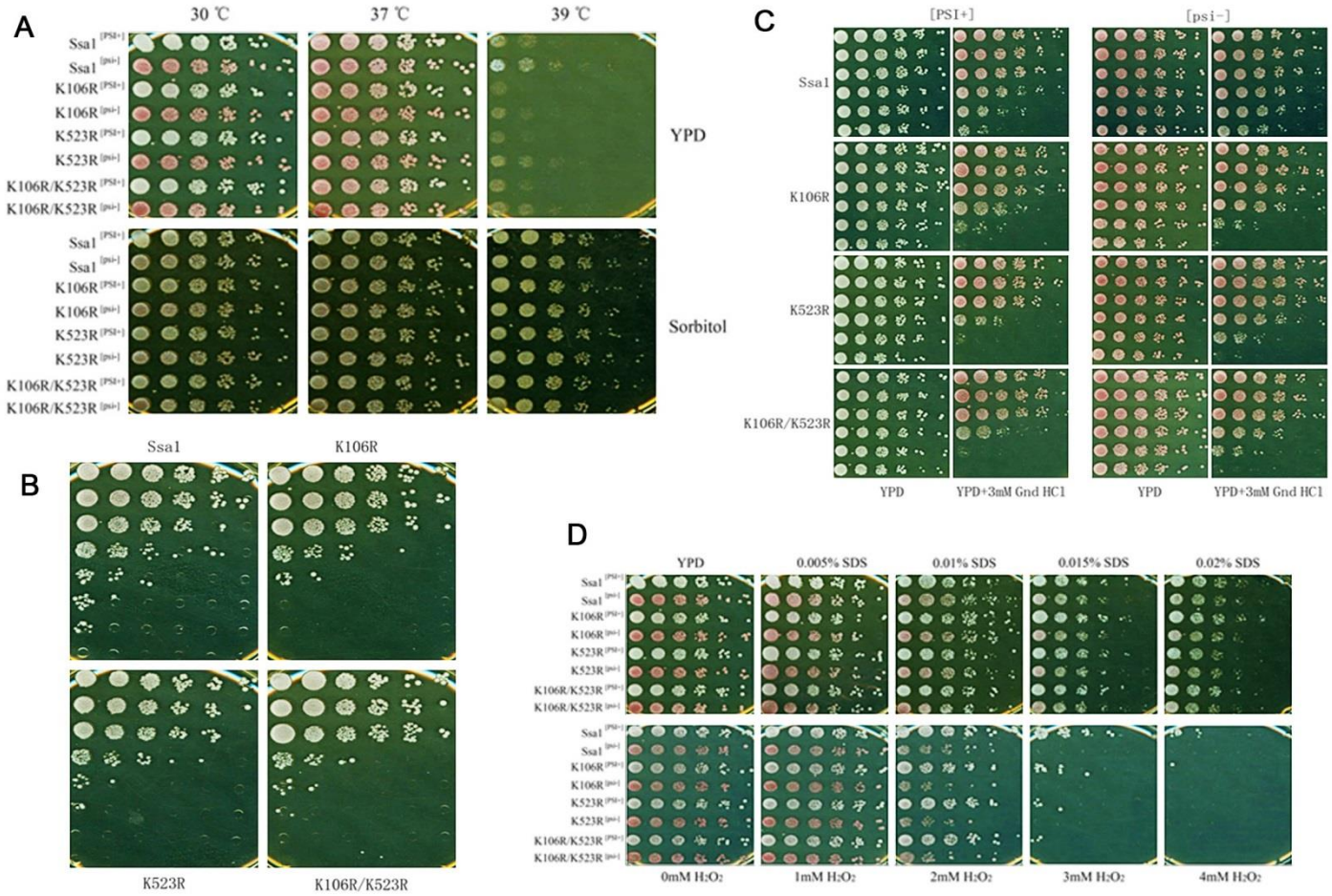

Figure 6.9. Phenotypic effects of the SUMOylation of Ssa1 in G402 cells. (A) Effects of the SUMOylation of Ssa1 at elevated temperatures; (B) Thermotolerance assay of SUMOylation mutations in Ssa1 at extreme temperature; (C) Acquired thermotolerance assay of Ssa1 SUMOylation mutations; (D) Effects of the Ssa1 SUMOylation to stresses of SDS and H_2O_2.

BIBLIOGRAPHY

Abbas-Terki, T., Donzé, O., Briand, P.-A., & Picard, D. (2001). Hsp104 interacts with Hsp90 cochaperones in respiring yeast. *Molecular and Cellular Biology*, *21*(22), 7569–7575. http://doi.org/10.1128/MCB.21.22.7569-7575.2001

Abravaya, K., Myers, M. P., Murphy, S. P., & Morimoto, R. I. (1992). The human heat shock protein hsp70 interacts with HSF, the transcription factor that regulates heat shock gene expression. *Genes and Development*, *6*(7), 1153–1164. http://doi.org/10.1101/gad.6.7.1153

Agarwal, M., Sahi, C., Katiyar-Agarwal, S., Agarwal, S., Young, T., Gallie, D. R., … Grover, A. (2003). Molecular characterization of rice hsp101: Complementation of yeast hsp104 mutation by disaggregation of protein granules and differential expression in indica and japonica rice types. *Plant Molecular Biology*, *51*(4), 543–553. http://doi.org/10.1023/A:1022324920316

Ahner, A., Gong, X., Schmidt, B. Z., Peters, K. W., Rabeh, W. M., Thibodeau, P. H., … Frizzell, R. a. (2012). Small heat shock proteins target mutant CFTR for degradation via a SUMO-dependent pathway. *Molecular Biology of the Cell*, mbc–E12. http://doi.org/10.1091/mbc.E12-09-0678

Albanèse, V., Yam, A. Y.-W., Baughman, J., Parnot, C., & Frydman, J. (2006). Systems analyses reveal two chaperone networks with distinct functions in eukaryotic cells. *Cell*, *124*(1), 75–88. http://doi.org/10.1016/j.cell.2005.11.039

Albuquerque, C. P., Smolka, M. B., Payne, S. H., Bafna, V., Eng, J., & Zhou, H. (2008). A multidimensional chromatography technology for in-depth phosphoproteome analysis. *Molecular & Cellular Proteomics : MCP*, *7*(7), 1389–1396. http://doi.org/10.1074/mcp.M700468-MCP200

Alexopoulos, J., Ahsan, B., Homchaudhuri, L., Husain, N., Cheng, Y. Q., & Ortega, J. (2013). Structural determinants stabilizing the axial channel of ClpP for substrate translocation. *Molecular Microbiology*, *90*(1), 167–180. http://doi.org/10.1111/mmi.12356

Allen, K. D. (2004). Hsp70 Chaperones as Modulators of Prion Life Cycle: Novel Effects of Ssa and Ssb on the Saccharomyces cerevisiae Prion [PSI+]. *Genetics*, *169*(3), 1227–1242. http://doi.org/10.1534/genetics.104.037168

Amberg, D. C., Burke, D. J., & Strathern, J. N. (2005). *Methods in Yeast Genetics*. Cold Spring Harbor Laboratory Press.

Antelmann, H., Engelmann, S., Schmid, R., Sorokin, A., Lapidus, A., & Hecker, M. (1997). Expression of a stress- and starvation-induced dps/pexB-homologous gene is controlled by the alternative sigma factor σB in Bacillus subtilis. *Journal of Bacteriology*, *179*(23), 7251–7256. Retrieved from http://jb.asm.org/cgi/content/abstract/179/23/7251

Arias-Palomo, E., O'Shea, V. L., Hood, I. V., & Berger, J. M. (2013). The bacterial DnaC helicase loader is a DnaB ring breaker. *Cell*, *153*(2), 438–448. http://doi.org/10.1016/j.cell.2013.03.006

Bai, F., Xi, J., Higashikubo, R., & Andley, U. P. (2004). Cell kinetic status of mouse lens epithelial cells lacking αA-and αB-crystallin. *Molecular and Cellular Biochemistry*, *265*(1-2), 115–122. http://doi.org/10.1023/B:MCBI.0000044365.48900.82

Bakthisaran, R., Tangirala, R., & Rao, C. M. (2015). Small heat shock proteins: Role in cellular functions and pathology. *Biochimica et Biophysica Acta*, *1854*(4), 291–319. http://doi.org/10.1016/j.bbapap.2014.12.019

Baler, R., Welch, W. J., & Voellmy, R. (1992). Heat shock gene regulation by nascent polypeptides and denatured proteins: hsp70 as a potential autoregulatory factor. *Journal of Cell Biology*, *117*(6), 1151–1159. http://doi.org/10.1083/jcb.117.6.1151

Baler, R., Zou, J., & Voellmy, R. (1996). Evidence for a role of Hsp70 in the regulation of the heat shock response in mammalian cells. *Cell Stress & Chaperones*.

Barbash, O., & Diehl, J. A. (2008). SCFFbx4/αB-crystallin E3 ligase: When one is not enough. *Cell Cycle*, *7*(19), 2983–2986.

Barnes, J. A., Collins, B. W., Dix, D. J., & Allen, J. W. (2002). Effects of heat shock protein 70 (Hsp70) on arsenite-induced genotoxicity. *Environmental and Molecular Mutagenesis*, *40*(4), 236–42. http://doi.org/10.1002/em.10116

Baudin-Baillieu, A., Legendre, R., Kuchly, C., Hatin, I., Demais, S., Mestdagh, C., … Namy, O. (2014). Genome-wide Translational Changes Induced by the Prion [PSI+]. *Cell Reports*, *8*(2), 439–448. http://doi.org/10.1016/j.celrep.2014.06.036

Bender, G. R., & Marquis, R. E. (1987). Membrane ATPases and acid tolerance of Actinomyces viscosus and Lactobacillus casei. *Applied and Environmental Microbiology*, *53*(9), 2124–2128.

Berson, J. F., Theos, A. C., Harper, D. C., Tenza, D., Raposo, G., & Marks, M. S. (2003). Proprotein convertase cleavage liberates a fibrillogenic fragment of a resident glycoprotein to initiate melanosome biogenesis. *Journal of Cell Biology*, *161*(3), 521–533. http://doi.org/10.1083/jcb.200302072

Bertelsen, E. B., Chang, L., Gestwicki, J. E., & Zuiderweg, E. R. P. (2009). Solution conformation of wild-type E. coli Hsp70 (DnaK) chaperone complexed with ADP and substrate. *Proceedings of the National Academy of Sciences of the United States of America*, *106*(21), 8471–8476. http://doi.org/10.1073/pnas.0903503106

Bierkens, J., Maes, J., & Plaetse, F. V. (1998). Dose-dependent induction of heat shock protein 70 synthesis in Raphidocelis subcapitata following exposure to different classes of environmental pollutants. *Environmental Pollution (Barking, Essex : 1987)*, *101*, 91–97. http://doi.org/10.1016/S0269-7491(98)00010-4

Blechinger, S. R., Warren, J. T., Kuwada, J. Y., & Krone, P. H. (2002). Developmental toxicology of cadmium in living embryos of a stable transgenic zebrafish line. *Environmental Health Perspectives*, *110*(10), 1041–1046.

http://doi.org/10.1289/ehp.021101041

Boorstein, W. R., Ziegelhoffer, T., & Craig, E. A. (1994). Molecular evolution of the HSP70 multigene family. *Journal of Molecular Evolution*, *38*(1), 1–17. http://doi.org/10.1007/BF00175490

Borrell-Pagès, M., Canals, J. M., Cordelières, F. P., Parker, J. A., Pineda, J. R., Grange, G., … Humbert, S. (2006). Cystamine and cysteamine increase brain levels of BDNF in Huntington disease via HSJ1b and transglutaminase. *Journal of Clinical Investigation*, *116*(5), 1410–1424. http://doi.org/10.1172/JCI27607

Boswell-Casteel, R. C., Johnson, J. M., Duggan, K. D., Tsutsui, Y., & Hays, F. A. (2014). Overproduction and biophysical characterization of human HSP70 proteins. *Protein Expression and Purification*, *106*, 57–65. http://doi.org/10.1016/j.pep.2014.09.013

Braun, N., Zacharias, M., Peschek, J., Kastenmüller, A., Zou, J., Hanzlik, M., … Weinkauf, S. (2011). Multiple molecular architectures of the eye lens chaperone αB-crystallin elucidated by a triple hybrid approach. *Proceedings of the National Academy of Sciences of the United States of America*, *108*(51), 20491–6. http://doi.org/10.1073/pnas.1111014108

Buchberger, A., Theyssen, H., Schroder, H., McCarty, J. S., Virgallita, G., Milkereit, P., … Bukau, B. (1995). Nucleotide-induced conformational changes in the ATPase and substrate binding domains of the DnaK chaperone provide evidence for interdomain communication. *Journal of Biological Chemistry*. http://doi.org/10.1074/jbc.270.28.16903

Bukau, B., & Horwich, A. L. (1998). The Hsp70 and Hsp60 chaperone machines. *Cell*, *92*(3), 351–366. http://doi.org/10.1016/S0092-8674(00)80928-9

Carlson, N., Rogers, S., & Rechsteiner, M. (1987). Microinjection of ubiquitin: Changes in protein degradation in HeLa cells subjected to heat-shock. *Journal of Cell Biology*, *104*(3), 547–555. http://doi.org/10.1083/jcb.104.3.547

Chang, L., Bertelsen, E. B., Wisén, S., Larsen, E. M., Zuiderweg, E. R. P., & Gestwicki, J. E. (2008). High-throughput screen for small molecules that modulate the ATPase activity of the molecular chaperone DnaK. *Analytical Biochemistry*, *372*(2), 167–176. http://doi.org/10.1016/j.ab.2007.08.020

Chapman, M. R., Robinson, L. S., Pinkner, J. S., Roth, R., Heuser, J., Hammar, M., … Hultgren, S. J. (2002). Role of Fiber Escherichia in coli Curli Operons Directing Formation Amyloid. *Science*, *295*(5556), 851–855. http://doi.org/10.1126/science.1067484

Chappells, T. G., Konforti, B. B., Schmids, S. L., & Rothmann, J. E. (1987). The ATPase core of a clathrin uncoating protein. *Journal of Biological Chemistry*, *262*(2), 746–751.

Cheetham, M. E., Brion, J. P., & Anderton, B. H. (1992). Human homologues of the bacterial heat-shock protein DnaJ are preferentially expressed in neurons. *The Biochemical Journal*, *284 (Pt 2*, 469–76. Retrieved from

http://www.pubmedcentral.nih.gov/articlerender.fcgi?artid=1132662&tool=pmcentrez&rendertype=abstract

Cheetham, M. E., & Caplan, A. J. (1998). Structure, function and evolution of DnaJ: conservation and adaptation of chaperone function. *Cell Stress & Chaperones*. http://doi.org/10.1379/1466-1268(1998)003<0028:SFAEOD>2.3.CO;2

Chen, B., Sysoeva, T. A., Chowdhury, S., Guo, L., De Carlo, S., Hanson, J. A., … Nixon, B. T. (2010). Engagement of Arginine Finger to ATP Triggers Large Conformational Changes in NtrC1 AAA+ ATPase for Remodeling Bacterial RNA Polymerase. *Structure*, *18*(11), 1420–1430. http://doi.org/10.1016/j.str.2010.08.018

Chernoff, Y. O., Lindquist, S. L., Ono, B. I., Inge-Vechtomov, S. G., & Liebman, S. W. (1995). Role of the chaperone protein Hsp104 in propagation of the yeast prion-like factor [psi+]. *Science*, *268*(5212), 880–884.

Chien, P., Weissman, J. S., & DePace, A. H. (2004). Emerging principles of conformation-based prion inheritance. *Annual Review of Biochemistry*, *73*(1), 617–656. http://doi.org/10.1146/annurev.biochem.72.121801.161837

Chiti, F., & Dobson, C. M. (2006). Protein Misfolding, Functional Amyloid, and Human Disease. *Annual Review of Biochemistry*, *75*(1), 333–366. http://doi.org/10.1146/annurev.biochem.75.101304.123901

Chowdary, T. K., Raman, B., Ramakrishna, T., & Rao, C. M. (2004). Mammalian Hsp22 is a heat-inducible small heat-shock protein with chaperone-like activity. *The Biochemical Journal*, *381*(Pt 2), 379–387. http://doi.org/10.1042/BJ20031958

Chung, C. T., & Miller, R. H. (1988). A rapid and convenient method for the preparation and storage of competent bacterial cells. *Nucleic Acids Research*, *16*(8), 20892–20892.

Cohen, A. S., Shirahama, T., & Skinner, M. (1982). Electron microscopy of amyloid. *Electron Microscopy of Proteins*, *3*, 165–205.

Costanzo, M., Baryshnikova, A., Bellay, J., Kim, Y., Spear, E. D., Sevier, C. S., … Prinz, J. (2010). The genetic landscape of a cell. *Science*, *327*(5964), 425–431.

COX, B. S. (1965). Ψ, A cytoplasmic suppressor of super-suppressor in yeast. *Heredity*, *20*(4), 505–521. http://doi.org/10.1038/hdy.1965.65

Dai, C., Whitesell, L., Rogers, A. B., & Lindquist, S. (2007). Heat Shock Factor 1 Is a Powerful Multifaceted Modifier of Carcinogenesis. *Cell*, *130*(6), 1005–1018. http://doi.org/10.1016/j.cell.2007.07.020

Darden, T., York, D., & Pedersen, L. (1993). Particle mesh Ewald: An N·log(N) method for Ewald sums in large systems. *The Journal of Chemical Physics*, *98*(12), 10089. http://doi.org/10.1063/1.464397

Davenport, K., Sohaskey, M., Kamada, Y., Levin, D. E., & Gustin, M. C. (1995). A second osmosensing signal transduction pathway in yeast. *The Journal of Biological Chemistry*,

270(50), 30157–30161. http://doi.org/10.1126/science.7681220

Davies, J. M., Tsuruta, H., May, A. P., & Weis, W. I. (2005). Conformational changes of p97 during nucleotide hydrolysis determined by small-angle X-ray scattering. *Structure*, *13*(2), 183–195. http://doi.org/10.1016/j.str.2004.11.014

De Angelis, M., & Gobbetti, M. (2004). Environmental stress responses in Lactobacillus: A review. *Proteomics*, *4*(1), 106–122. http://doi.org/10.1002/pmic.200300497

Desantis, M. E., & Shorter, J. (2012). The elusive middle domain of Hsp104 and ClpB: location and function. *Biochimica et Biophysica Acta*, *1823*(1), 29–39. http://doi.org/10.1016/j.bbamcr.2011.07.014

Duennwald, M. L., Echeverria, A., & Shorter, J. (2012). Small heat shock proteins potentiate amyloid dissolution by protein disaggregases from yeast and humans. *PLoS Biology*, *10*(6). http://doi.org/10.1371/journal.pbio.1001346

Dulle, J. E., Stein, K. C., & True, H. L. (2014). Regulation of the Hsp104 middle domain activity is critical for yeast prion propagation. *PLoS ONE*, *9*(1). http://doi.org/10.1371/journal.pone.0087521

Dutta, R., & Inouye, M. (2000). GHKL, an emergent ATPase/kinase superfamily. *Trends in Biochemical Sciences*, *25*(1), 24–28. http://doi.org/10.1016/S0968-0004(99)01503-0

Ebong, I. O., Morgner, N., Zhou, M., Saraiva, M. A., Daturpalli, S., Jackson, S. E., & Robinson, C. V. (2011). Heterogeneity and dynamics in the assembly of the Heat Shock Protein 90 chaperone complexes. *Proceedings of the National Academy of Sciences*, *108*(44), 17939–17944. http://doi.org/10.1073/pnas.1106261108

Echeverría, P. C., Bernthaler, A., Dupuis, P., Mayer, B., & Picard, D. (2011). An interaction network predicted from public data as a discovery tool: application to the Hsp90 molecular chaperone machine. *PloS One*, *6*(10), e26044. http://doi.org/10.1371/journal.pone.0026044

Ecroyd, H., & Carver, J. A. (2009). Crystallin proteins and amyloid fibrils. *Cellular and Molecular Life Sciences*, *66*(1), 62–81. http://doi.org/10.1007/s00018-008-8327-4

Erzberger, J. P., & Berger, J. M. (2006). Evolutionary Relationships and Structural Mechanisms of AAA+ Proteins. *Annual Review of Biophysics and Biomolecular Structure*, *35*(1), 93–114. http://doi.org/10.1146/annurev.biophys.35.040405.101933

Essmann, U., Perera, L., Berkowitz, M. L., Darden, T., Lee, H., & Pedersen, L. G. (1995). A smooth particle mesh Ewald method. *J Chem Phys*, *103*(1995), 8577–8593. http://doi.org/10.1063/1.470117

Fang, N. N., Chan, G. T., Zhu, M., Comyn, S. A., Persaud, A., Deshaies, R. J., … Mayor, T. (2014). Rsp5/Nedd4 is the main ubiquitin ligase that targets cytosolic misfolded proteins following heat stress. *Nat Cell Biol*, *16*(12), 1227–1237. http://doi.org/10.1038/ncb3054

Feder, M. E., & Hofmann, G. E. (1999). Heat-shock proteins, molecular chaperones, and the

stress response: Evolutionary and ecological physiology. *Annual Reviews of Physiology*, *61*, 243–282.

Fiaux, J., Horst, J., Scior, A., Preissler, S., Koplin, A., Bukau, B., & Deuerling, E. (2010). Structural analysis of the Ribosome-associated Complex (RAC) reveals an unusual Hsp70/Hsp40 interaction. *Journal of Biological Chemistry*, *285*(5), 3227–3234. http://doi.org/10.1074/jbc.M109.075804

Fiser, A., & Šali, A. (2003). MODELLER: Generation and Refinement of Homology-Based Protein Structure Models. *Methods in Enzymology*, *374*, 461–491. http://doi.org/10.1016/S0076-6879(03)74020-8

Fitzpatrick, D. a, O'Brien, J., Moran, C., Hasin, N., Kenny, E., Cormican, P., … Jones, G. W. (2011). Assessment of inactivating stop codon mutations in forty Saccharomyces cerevisiae strains: implications for [PSI+] prion- mediated phenotypes. *PloS One*, *6*(12), e28684. http://doi.org/10.1371/journal.pone.0028684

Flaherty, K. M., DeLuca-Flaherty, C., & McKay, D. B. (1990). Three-dimensional structure of the ATPase fragment of a 70K heat-shock cognate protein. *Nature*, *346*(6285), 623–628. http://doi.org/10.1038/346623a0

Freeman, B. C., Myers, M. P., Schumacher, R., & Morimoto, R. I. (1995). Identification of a regulatory motif in Hsp70 that affects ATPase activity, substrate binding and interaction with HDJ-1. *The EMBO Journal*, *14*(10), 2281–92. Retrieved from http://www.pubmedcentral.nih.gov/articlerender.fcgi?artid=398335&tool=pmcentrez&rendertype=abstract

Gao, X., Carroni, M., Helen, R., Mayer, M. P., & Bukau, B. (2015). Human Hsp70 Disaggregase Reverses Parkinson's-Linked α-Synuclein Amyloid Fibrils. *Molecular Cell*, *59*(5), 781–793. http://doi.org/10.1016/j.molcel.2015.07.012

Gautschi, M., Lilie, H., Fünfschilling, U., Mun, A., Ross, S., Lithgow, T., … Rospert, S. (2001). RAC, a stable ribosome-associated complex in yeast formed by the DnaK-DnaJ homologs Ssz1p and zuotin. *Proceedings of the National Academy of Sciences of the United States of America*, *98*(7), 3762–7. http://doi.org/10.1073/pnas.071057198

Gazit, E. (2002). Global analysis of tandem aromatic octapeptide repeats: the significance of the aromatic-glycine motif. *Bioinformatics (Oxford, England)*, *18*(6), 880–3. Retrieved from http://www.ncbi.nlm.nih.gov/pubmed/12075024

Gething, M. . (1997). *Guidebook to molecular chaperones and protein-folding catalysts*. Oxford University Press.

Gietz, R. D., & Schiestl, R. H. (2008). High-efficiency yeast transformation using the LiAc / SS carrier DNA / PEG method. *Nature Protocols*, *2*(1), 31–35. http://doi.org/10.1038/nprot.2007.13

Glaasker, E., Konings, W. N., & Poolman, B. (1996). Glycine betaine fluxes in Lactobacillus

plantarum during osmostasis and hyper- and hypo-osmotic shock. *Journal of Biological Chemistry*, *271*(17), 10060–10065. http://doi.org/10.1074/jbc.271.17.10060

Glover, J. R., Kowal, a S., Schirmer, E. C., Patino, M. M., Liu, J. J., & Lindquist, S. (1997). Self-seeded fibers formed by Sup35, the protein determinant of [PSI+], a heritable prion-like factor of S. cerevisiae. *Cell*, *89*(5), 811–819. http://doi.org/10.1016/S0092-8674(00)80264-0

Glover, J. R., & Lindquist, S. (1998). Hsp104, Hsp70, and Hsp40: A novel chaperone system that rescues previously aggregated proteins. *Cell*, *94*(1), 73–82. http://doi.org/10.1016/S0092-8674(00)81223-4

Gong, Y., Kakihara, Y., Krogan, N., Greenblatt, J., Emili, A., Zhang, Z., & Houry, W. a. (2009). An atlas of chaperone-protein interactions in Saccharomyces cerevisiae: implications to protein folding pathways in the cell. *Molecular Systems Biology*, *5*(275), 275. http://doi.org/10.1038/msb.2009.26

Gottesman, S. (1996). Proteases and their targets in Escherichia coli 1. *Annual Review of Genetics*, *30*, 465–506. http://doi.org/10.1146/annurev.genet.30.1.465

Graf, C., Stankiewicz, M., Kramer, G., & Mayer, M. P. (2009). Spatially and kinetically resolved changes in the conformational dynamics of the Hsp90 chaperone machine. *The EMBO Journal*, *28*(5), 602–13. http://doi.org/10.1038/emboj.2008.306

Grimminger-Marquardt, V., & Lashuel, H. A. (2010). Structure and function of the molecular chaperone Hsp104 from yeast. *Biopolymers*, *93*(3), 252–276. http://doi.org/10.1002/bip.21301

Gruschus, J. M., Greene, L. E., Eisenberg, E., & Ferretti, J. a. (2004). Experimentally biased model structure of the Hsc70/auxilin complex: substrate transfer and interdomain structural change. *Protein Science*, *13*(8), 2029–2044. http://doi.org/10.1110/ps.03390504

Guex, N., & Peitsch, M. C. (1997). SWISS-MODEL and the Swiss-PdbViewer: An environment for comparative protein modeling. *Electrophoresis*, *18*(15), 2714–2723. http://doi.org/10.1002/elps.1150181505

Gunasekera, T. S., Csonka, L. N., & Paliy, O. (2008). Genome-wide transcriptional responses of Escherichia coli K-12 to continuous osmotic and heat stresses. *Journal of Bacteriology*, *190*(10), 3712–3720. http://doi.org/10.1128/JB.01990-07

Guven, K., Duce, J. A., & de Pomerai, D. I. (1994). Evaluation of a stress-inducible transgenic nematode strain for rapid aquatic toxicity testing. *Aquatic Toxicology*. http://doi.org/10.1016/0166-445X(94)90052-3

Guven, K., Duce, J. A., & De Pomerai, D. I. (1995). Calcium moderation of cadmium stress explored using a stress-inducible transgenic strain of Caenorhabditis elegans. *Comparative Biochemistry and Physiology. Part C: Comparative*, *110*(1), 61–70. http://doi.org/10.1016/0742-8413(94)00071-H

Hainzl, O., Lapina, M. C., Buchner, J., & Richter, K. (2009). The charged linker region is an important regulator of Hsp90 function. *Journal of Biological Chemistry*, *284*(34), 22559–22567. http://doi.org/10.1074/jbc.M109.031658

Halloran, M. C., Sato-Maeda, M., Warren, J. T., Su, F., Lele, Z., Krone, P. H., … Shoji, W. (2000). Laser-induced gene expression in specific cells of transgenic zebrafish. *Development (Cambridge, England)*, *127*(9), 1953–1960.

Hasin, N., Cusack, S. a, Ali, S. S., Fitzpatrick, D. a, & Jones, G. W. (2014). Global transcript and phenotypic analysis of yeast cells expressing Ssa1, Ssa2, Ssa3 or Ssa4 as sole source of cytosolic Hsp70-Ssa chaperone activity. *BMC Genomics*, *15*(1), 194. http://doi.org/10.1186/1471-2164-15-194

Haslbeck, M., Franzmann, T., Weinfurtner, D., & Buchner, J. (2005). Some like it hot: the structure and function of small heat-shock proteins. *Nature Structural & Molecular Biology*, *12*(10), 842–6. http://doi.org/10.1038/nsmb993

Hattendorf, D. A., & Lindquist, S. L. (2002). Cooperative kinetics of both Hsp104 ATPase domains and interdomain communication revealed by AAA sensor-1 mutants. *EMBO Journal*, *21*(1-2), 12–21. http://doi.org/10.1093/emboj/21.1.12

Hatters, D. M., Lindner, R. A., Carver, J. A., & Howlett, G. J. (2001). The Molecular Chaperone, ??-Crystallin, Inhibits Amyloid Formation by Apolipoprotein C-II. *Journal of Biological Chemistry*, *276*(36), 33755–33761. http://doi.org/10.1074/jbc.M105285200

Hay, R. T. (2005). SUMO: A history of modification. *Molecular Cell*, *18*(1), 1–12. http://doi.org/10.1016/j.molcel.2005.03.012

Hayden, J. D., & Ades, S. E. (2008). The extracytoplasmic stress factor, σ E, is required to maintain cell envelope integrity in Escherichia coli. *PLoS ONE*, *3*(2). http://doi.org/10.1371/journal.pone.0001573

Hedhli, N., Wang, L., Wang, Q., Rashed, E., Tian, Y., Sui, X., … Depre, C. (2008). Proteasome activation during cardiac hypertrophy by the chaperone H11 Kinase/Hsp22. *Cardiovascular Research*, *77*(3), 497–505. http://doi.org/10.1093/cvr/cvm054

Hendershot, L., Wei, J., Gaut, J., Melnick, J., Aviel, S., & Argon, Y. (1996). Inhibition of immunoglobulin folding and secretion by dominant negative BiP ATPase mutants. *Proceedings of the National Academy of Sciences of the United States of America*, *93*(11), 5269–74. http://doi.org/10.1073/pnas.93.11.5269

Henriksen, P., Wagner, S. a., Weinert, B. T., Sharma, S., Bacinskaja, G., Rehman, M., … Choudhary, C. (2012). Proteome-wide analysis of lysine acetylation suggests its broad regulatory scope in Saccharomyces cerevisiae. *Molecular & Cellular Proteomics*, 1510–1522. http://doi.org/10.1074/mcp.M112.017251

Hess, B., Bekker, H., Berendsen, H. J. C., & Fraaije, J. G. E. M. (1997). Lincs: a Linear Constraint Solver for Molecular Simulations. *J. Comput. Chem.*, *18*(12), 1463–1472.

Hochberg, G. K. a, Ecroyd, H., Liu, C., Cox, D., Cascio, D., Sawaya, M. R., … Laganowsky, A. (2014). The structured core domain of αB-crystallin can prevent amyloid fibrillation and associated toxicity. *Proceedings of the National Academy of Sciences of the United States of America*, *111*(16), E1562–70. http://doi.org/10.1073/pnas.1322673111

Hong, S. W., & Vierling, E. (2001). Hsp101 is necessary for heat tolerance but dispensable for development and germination in the absence of stress. *Plant Journal*, *27*(1), 25–35. http://doi.org/10.1046/j.1365-313X.2001.01066.x

Hu, W., Wu, H., Zhang, H., Gong, W., & Perrett, S. (2015). Resonance assignments for the substrate binding domain of Hsp70 chaperone Ssa1 from Saccharomyces cerevisiae. *Biomolecular NMR Assignments*. http://doi.org/10.1007/s12104-015-9603-5

Huang, L., Yu, Z., Zhang, T., Zhao, X., & Huang, G. (2014). HSP40 interacts with pyruvate kinase M2 and regulates glycolysis and cell proliferation in tumor cells. *PLoS ONE*, *9*(3), 1–9. http://doi.org/10.1371/journal.pone.0092949

Huang, P., Gautschi, M., Walter, W., Rospert, S., & Craig, E. a. (2005). The Hsp70 Ssz1 modulates the function of the ribosome-associated J-protein Zuo1. *Nature Structural & Molecular Biology*, *12*(6), 497–504. http://doi.org/10.1038/nsmb942

Humphrey, W., Dalke, A., & Schulten, K. (1996). VMD: visual molecular dynamics. *J. Mol. Graph. Model.*, *14*(1), 33–38. http://doi.org/10.1016/0263-7855(96)00018-5

Ito, H., Kamei, K., Iwamoto, I., Inaguma, Y., & Kato, K. (2001). Regulation of the levels of small heat-shock proteins during differentiation of C2C12 cells. *Experimental Cell Research*, *266*(2), 213–21. http://doi.org/10.1006/excr.2001.5220

Iyer, L. M., Leipe, D. D., Koonin, E. V., & Aravind, L. (2004). Evolutionary history and higher order classification of AAA+ ATPases. *Journal of Structural Biology*, *146*(1-2), 11–31. http://doi.org/10.1016/j.jsb.2003.10.010

J, C., J, S., S, P., M, C., Chapple, J. P., van der Spuy, J., … Cheetham, M. E. (2004). Neuronal DnaJ proteins HSJ1a and HSJ1b: a role in linking the Hsp70 chaperone machine to the ubiquitin–proteasome system. *Biochemical Society Transactions*, *32*(Pt 4), 640–2. http://doi.org/10.1042/BST0320640

Jaiswal, H., Conz, C., Otto, H., Wolfle, T., Fitzke, E., Mayer, M. P., & Rospert, S. (2011). The Chaperone Network Connected to Human Ribosome-Associated Complex. *Molecular and Cellular Biology*, *31*(6), 1160–1173. http://doi.org/10.1128/MCB.00986-10

Jehle, S., Vollmar, B. S., Bardiaux, B., Dove, K. K., Rajagopal, P., Gonen, T., … Klevit, R. E. (2011). N-terminal domain of alphaB-crystallin provides a conformational switch for multimerization and structural heterogeneity. *Proceedings of the National Academy of Sciences of the United States of America*, *108*(16), 6409–6414. http://doi.org/10.1073/pnas.1014656108

Johnson, J. L. (2012). Evolution and function of diverse Hsp90 homologs and cochaperone

proteins. *Biochimica et Biophysica Acta - Molecular Cell Research*, *1823*(3), 607–613. http://doi.org/10.1016/j.bbamcr.2011.09.020

Jones, G., Song, Y., Chung, S., & Masison, D. C. (2004). Propagation of Saccharomyces cerevisiae [PSI+] prion is impaired by factors that regulate Hsp70 substrate binding. *Molecular and Cellular Biology*, *24*(9), 3928–37. http://doi.org/10.1128/MCB.24.9.3928

Jones, G. W., & Masison, D. C. (2003). Saccharomyces cerevisiae Hsp70 mutations affect [PSI+] prion propagation and cell growth differently and implicate Hsp40 and tetratricopeptide repeat cochaperones in impairment of [PSI+]. *Genetics*, *70*(February), 495–506.

Jones, G. W., & Tuite, M. F. (2005). Chaperoning prions: The cellular machinery for propagating an infectious protein? *BioEssays*, *27*(8), 823–832. http://doi.org/10.1002/bies.20267

Jung, G., Jones, G., Wegrzyn, R. D., & Masison, D. C. (2000). A role for cytosolic hsp70 in yeast [PSI(+)] prion propagation and [PSI(+)] as a cellular stress. *Genetics*, *156*(2), 559–70. Retrieved from http://www.pubmedcentral.nih.gov/articlerender.fcgi?artid=1461277&tool=pmcentrez&rendertype=abstract

Jung, G., & Masison, D. C. (2001). Guanidine hydrochloride inhibits Hsp104 activity in vivo: A possible explanation for its effect in curing yeast prions. *Current Microbiology*, *43*(1), 7–10. http://doi.org/10.1007/s002840010251

Kamada, Y., Jung, U. S., Piotrowski, R., & Levin, D. E. (1995). The Protein-Kinase C-Activated Map Kinase Pathway of Saccharomyces-Cerevisiae Mediates a Novel Aspect of the Heat-Shock Response. *Genes & Development*, *9*(13), 1559–1571. Retrieved from <Go to ISI>://A1995RK42200001

Kampinga, H. H., & Craig, E. A. (2010). The HSP70 chaperone machinery: J proteins as drivers of functional specificity. *Nature Reviews. Molecular Cell Biology*, *11*(8), 579–92. http://doi.org/10.1038/nrm2941

Kappé, G., Franck, E., Verschuure, P., Boelens, W. C., Leunissen, J. A. M., & de Jong, W. W. (2003). The human genome encodes 10 alpha-crystallin-related small heat shock proteins: HspB1-10. *Cell Stress & Chaperones*, *8*(1), 53–61. http://doi.org/10.1379/1466-1268(2003)8<53:THGECS>2.0.CO;2

Karlin, S., & Brocchieri, L. (1998). Heat shock protein 70 family: multiple sequence comparisons, function, and evolution. *Journal of Molecular Evolution*, *47*(5), 565–577. http://doi.org/10.1007/PL00006413

Kasjet, E. R. (1987). Bioenergetics of lactic acid bacteria: citoplasmic pH and osmotolerance. *FEMS Microbiology Reviews*, *46*, 233–244. http://doi.org/10.1016/0378-1097(87)90110-8

Kim, W. S., Perl, L., Park, J. H., Tandianus, J. E., & Dunn, N. W. (2001). Assessment of stress

response of the probiotic Lactobacillus acidophilus. *Current Microbiology*, *43*(5), 346–350. http://doi.org/10.1007/s002840010314

King, C. Y., & Diaz-Avalos, R. (2004). Protein-only transmission of three yeast prion strains. *Nature*, *428*(6980), 319–323. http://doi.org/10.1038/nature02400.Published

Kityk, R., Kopp, J., Sinning, I., & Mayer, M. P. (2012). Structure and Dynamics of the ATP-Bound Open Conformation of Hsp70 Chaperones. *Molecular Cell*, *48*(6), 863–874. http://doi.org/10.1016/j.molcel.2012.09.023

Kityk, R., Vogel, M., Schlecht, R., Bukau, B., & Mayer, M. P. (2015). Pathways of allosteric regulation in Hsp70 chaperones. *Nature Communications*, *6*, 1–11. http://doi.org/10.1038/ncomms9308

Kleizen, B., & Braakman, I. (2004). Protein folding and quality control in the endoplasmic reticulum. *Current Opinion in Cell Biology*, *16*(4), 343–349. http://doi.org/10.1016/j.ceb.2004.06.012

Knowles, T. P. J., Vendruscolo, M., & Dobson, C. M. (2014). The amyloid state and its association with protein misfolding diseases. *Nature Reviews Molecular Cell Biology*, *15*(6), 384–396. http://doi.org/10.1038/nrm3810

Kolawa, N., Sweredoski, M. J., Graham, R. L. J., Oania, R., Hess, S., & Deshaies, R. J. (2013). Perturbations to the ubiquitin conjugate proteome in yeast δubx mutants identify Ubx2 as a regulator of membrane lipid composition. *Molecular & Cellular Proteomics*, *12*, 2791–803. http://doi.org/10.1074/mcp.M113.030163

Kominek J, Marszalek J, Neuvéglise C, Craig EA, W. B. (2013). The complex evolutionary dynamics of Hsp70s: A genomic and functional perspective. *Genome Biology and Evolution*, *5*(12), 2460–2477. http://doi.org/10.1093/gbe/evt192

Kryndushkin, D. S., Smirnov, V. N., Ter-Avanesyan, M. D., & Kushnirov, V. V. (2002). Increased expression of Hsp40 chaperones, transcriptional factors, and ribosomal protein Rpp0 can cure yeast prions. *Journal of Biological Chemistry*, *277*(26), 23702–23708. http://doi.org/10.1074/jbc.M111547200

Kudva, Y. C., Hiddinga, H. J., Butler, P. C., Mueske, C. S., & Eberhardt, N. L. (1997). Small heat shock proteins inhibit in vitro A??1-42 amyloidogenesis. *FEBS Letters*, *416*(1), 117–121. http://doi.org/10.1016/S0014-5793(97)01180-0

Kumar, S., Stecher, G., & Tamura, K. (2016). MEGA7: Molecular Evolutionary Genetics Analysis version 7.0 for bigger datasets. *Molecular Biology and Evolution*, msw054.

Kushnirov, V. V., Kryndushkin, D. S., Boguta, M., Smirnov, V. N., & Ter-Avanesyan, M. D. (2000). Chaperones that cure yeast artificial [PSI+] and their prion-specific effects. *Current Biology*, *10*(22), 1443–1446. http://doi.org/10.1016/S0960-9822(00)00802-2

Landry, S. J. (2003). Structure and energetics of an allele-specific genetic interaction between dnaJ and dnaK: Correlation of nuclear magnetic resonance chemical shift perturbations in

the J-domain of Hsp40/DnaJ with binding affinity for the ATPase domain of Hsp70/DnaK. *Biochemistry*, *42*(17), 4926–4936. http://doi.org/10.1021/bi027070y

Lavery, L. A., Partridge, J. R., Ramelot, T. A., Elnatan, D., Kennedy, M. A., & Agard, D. A. (2014). Structural Asymmetry in the Closed State of Mitochondrial Hsp90 (TRAP1) Supports a Two-Step ATP Hydrolysis Mechanism. *Molecular Cell*, *53*(2), 330–343. http://doi.org/10.1016/j.molcel.2013.12.023

Lee, D. H., & Goldberg, A. L. (1996). Selective Inhibitors of the Proteasome-dependent and Vacuolar Saccharomyces cerevisiae Selective Inhibitors of the Proteasome-dependent and Vacuolar Pathways of Protein Degradation in Saccharomyces cerevisiae. *The Journal of Biological Chemistry*, *271*(44), 27280–27284. http://doi.org/10.1074/jbc.271.44.27280

Lee, D. H., Sherman, M. Y., & Goldberg, a L. (1996). Involvement of the molecular chaperone Ydj1 in the ubiquitin-dependent degradation of short-lived and abnormal proteins in Saccharomyces cerevisiae. *Molecular and Cellular Biology*, *16*(9), 4773–4781.

Levin, D. E., & Bartlett-Heubusch, E. (1992). Mutants in the S. cerevisiae PKC1 gene display a cell cycle-specific osmotic stability defect. *Journal of Cell Biology*, *116*(5), 1221–1229. http://doi.org/10.1083/jcb.116.5.1221

Li, J., & Sha, B. (2003). Crystal structure of the E. coli Hsp100 ClpB N-terminal domain. *Structure*, *11*(3), 323–328. http://doi.org/10.1016/S0969-2126(03)00030-3

Lin, D. I., Barbash, O., Kumar, K. G. S., Weber, J. D., Harper, J. W., Klein-Szanto, A. P., … Diehl, J. A. (2006). Phosphorylation-dependent ubiquitination of cyclin D1 by the SCF FBX4-αB crystallin complex. *Molecular Cell*, *24*(3), 355–366. http://doi.org/10.1016/j.molcel.2006.09.007

Lindquist, S., & Craig, E. A. (1988). the Heat-Shock Proteins. *Annual Review of Genetics*, *22*(1), 631–678. http://doi.org/10.1146/annurev.ge.22.120188.003215

Liu, J. J., Sondheimer, N., & Lindquist, S. L. (2002). Changes in the middle region of Sup35 profoundly alter the nature of epigenetic inheritance for the yeast prion [PSI+]. *Proceedings of the National Academy of Sciences of the United States of America*, *99 Suppl 4*, 16446–53. http://doi.org/10.1073/pnas.252652099

Liu, Q., Krzewska, J., Liberek, K., & Craig, E. A. (2001). Mitochondrial Hsp70 Ssc1: Role in Protein Folding. *Journal of Biological Chemistry*, *276*(9), 6112–6118. http://doi.org/10.1074/jbc.M009519200

Loovers, H. M., Guinan, E., & Jones, G. W. (2007). Importance of the Hsp70 ATPase domain in yeast prion propagation. *Genetics*, *175*(2), 621–630. http://doi.org/10.1534/genetics.106.066019

Mahalingam, D., Swords, R., Carew, J. S., Nawrocki, S. T., Bhalla, K., & Giles, F. J. (2009). Targeting HSP90 for cancer therapy. *British Journal of Cancer*, *100*(10), 1523–9. http://doi.org/10.1038/sj.bjc.6605066

Mayer, M. P., & Kityk, R. (2015). Insights into the molecular mechanism of allostery in Hsp70s. *Frontiers in Molecular Biosciences*, *2*(October). http://doi.org/10.3389/fmolb.2015.00058

Mayer, M. P., & Le Breton, L. (2015). Hsp90: breaking the symmetry. *Molecular Cell*, *58*(1), 8–20. http://doi.org/10.1016/j.molcel.2015.02.022

Mccormick, M. L., Buettner, G. R., Britigan, B. E., & Cormick, M. L. M. C. (1998). Endogenous superoxide dismutase levels regulate iron-dependent hydroxyl radical formation in Escherichia coli exposed to hydrogen peroxide. *Journal of Bacteriology*, *180*(3), 622–625.

Merchant, a M., Zhu, Z., Yuan, J. Q., Goddard, A., Adams, C. W., Presta, L. G., & Carter, P. (1998). Stress-inducible responses and heat shock proteins: new pharmacologic targets for cytoprotection. *Nature Biotechnology*, *16*(10), 291–294. http://doi.org/10.1038/nbt0898-773

Mizuno, S., Nakazaki, Y., Yoshida, M., & Watanabe, Y. H. (2012). Orientation of the amino-terminal domain of ClpB affects the disaggregation of the protein. *FEBS Journal*, *279*(8), 1474–1484. http://doi.org/10.1111/j.1742-4658.2012.08540.x

Morgner, N., Schmidt, C., Beilsten-Edmands, V., Ebong, I., Patel, N. A., Clerico, E. M., … Robinson, C. V. (2015). Hsp70 Forms Antiparallel Dimers Stabilized by Post-translational Modifications to Position Clients for Transfer to Hsp90. *Cell Reports*, 1–11. http://doi.org/10.1016/j.celrep.2015.03.063

Morimoto, R. I. (1998). Regulation of the heat-shock transcriptional response: cross talk between a family of heat-shock factors, molecular chaperones, and negative regulators. *Genes Dev*, *12*, 3788–3796. http://doi.org/10.1101/gad.12.24.3788

Morimoto, R. I. (2008). Proteotoxic stress and inducible chaperone networks in neurodegenerative disease and aging. *Genes and Development*, *22*(11), 1427–1438. http://doi.org/10.1101/gad.1657108

Morimoto, R. I., & Santoro, M. G. (1998). Stress-inducible responses and heat shock proteins: new pharmacologic targets for cytoprotection. *Nature Biotechnology*, *16*(February), 833–838. http://doi.org/10.1038/nbt0998-833

Morshauser, R. C., Wang, H., Flynn, G. C., & Zuiderweg, E. R. (1985). The Peptide-Binding Domain of the Chaperone Protein Hsc7O Has an Unusual Secondary Structure Topology. *Biochemistry*, *34*(19), 6261–6266.

Mosser, D. D., Duchaine, J., & Massie, B. (1993). shock transcription factor is regulated in vivo The DNA-Binding Activity of the Human Heat Shock Transcription Factor Is Regulated In Vivo by hsp7O. *Molecular and Cellular Biology*, *13*(9), 5427–5438. http://doi.org/10.1128/MCB.13.9.5427.Updated

Nadeau, D., Corneau, S., Plante, I., Morrow, G., & Tanguay, R. M. (2001). Evaluation for Hsp70 as a biomarker of effect of pollutants on the earthworm Lumbricus terrestris. *Cell*

Stress & Chaperones, *6*(2), 153–163. http://doi.org/10.1379/1466-1268(2001)006<0153:EFHAAB>2.0.CO;2

Needham, P. G., & Masison, D. C. (2008). Prion-impairing mutations in Hsp70 chaperone Ssa1: effects on ATPase and chaperone activities. *Archives of Biochemistry and Biophysics*, *478*(2), 167–74. http://doi.org/10.1016/j.abb.2008.07.023

Needham, P. G., Patel, H. J., Chiosis, G., Thibodeau, P. H., & Brodsky, J. L. (2015a). Mutations in the yeast Hsp70, Ssa1, at P417 alter ATP cycling, interdomain coupling, and specific chaperone functions. *Journal of Molecular Biology*. http://doi.org/10.1016/j.jmb.2015.04.010

Needham, P. G., Patel, H. J., Chiosis, G., Thibodeau, P. H., & Brodsky, J. L. (2015b). Mutations in the yeast Hsp70, Ssa1, at P417 alter ATP cycling, interdomain coupling, and specific chaperone functions. *Journal of Molecular Biology*, 1–18. http://doi.org/10.1016/j.jmb.2015.04.010

Neupert, W., & Herrmann, J. M. (2007). Translocation of proteins into mitochondria. *Annual Review of Biochemistry*, *76*, 723–749. http://doi.org/10.1146/annurev.biochem.76.052705.163409

Nilsson, M. R. (2004). Techniques to study amyloid fibril formation in vitro. *Methods*, *34*(1), 151–160. http://doi.org/10.1016/j.ymeth.2004.03.012

Nollen, E. A., & Morimoto, R. I. (2002). Chaperoning signaling pathways: molecular chaperones as stress-sensingheat shock'proteins. *Journal of Cell Science*, *115*(14), 2809–2816.

Noor, R. (2015). Mechanism to control the cell lysis and the cell survival strategy in stationary phase under heat stress. *SpringerPlus*, *4*(1), 599. http://doi.org/10.1186/s40064-015-1415-7

Nover, L., Mumsche, D., Neumann, D., Ohme, K., & Scharf, K. (1986). Control of ribosome biosynthesis in plant cell cultures under heat-shock conditions. *European Journal of Biochemistry*, *160*(2), 297–304. Retrieved from http://www.ncbi.nlm.nih.gov/pubmed/3769929

Nunes, S. L., & Calderwood, S. K. (1995). Heat shock factor-1 and the heat shock cognate 70 protein associate in high molecular weight complexes in the cytoplasm of NIH-3T3 cells. *Biochemical and Biophysical Research Communications*, *213*(1), 1–6.

O'Brien, M. C., & McKay, D. B. (1993). Threonine 204 of the chaperone protein Hsc70 influences the structure of the active site, but is not essential for ATP hydrolysis. *Journal of Biological Chemistry*, *268*(32), 24323–24329.

Oguchi, Y., Kummer, E., Seyffer, F., Berynskyy, M., Anstett, B., Zahn, R., … Bukau, B. (2012). A tightly regulated molecular toggle controls AAA+ disaggregase. *Nature Structural & Molecular Biology*, *19*(12), 1338–46. http://doi.org/10.1038/nsmb.2441

Parag, H. A., Raboy, B., & Kulka, R. G. (1987). Effect of heat shock on protein degradation in mammalian cells: involvement of the ubiquitin system. *The EMBO Journal*, *6*(1), 55–61. Retrieved from http://www.pubmedcentral.nih.gov/articlerender.fcgi?artid=553356&tool=pmcentrez&rendertype=abstract

Paravicini, G., Cooper, M., Friedli, L., Smith, D. J., Carpentier, J. L., Klig, L. S., & Payton, M. A. (1992). The osmotic integrity of the yeast cell requires a functional PKC1 gene product. *Molecular and Cellular Biology*, *12*(11), 4896–4905. http://doi.org/10.1128/MCB.12.11.4896.Updated

Parcellier, A., Schmitt, E., Gurbuxani, S., Seigneurin-Berny, D., Pance, A., Chantôme, A., … Garrido, C. (2003). HSP27 is a ubiquitin-binding protein involved in I-kappaBalpha proteasomal degradation. *Molecular and Cellular Biology*, *23*(16), 5790–5802. http://doi.org/10.1128/MCB.23.16.5790

Parsell, D. A., Kowal, A. S., Singer, M. A., & Lindquist, S. (1994). Protein disaggregation mediated by heat-shock protein Hsp104. *Nature*. http://doi.org/10.1038/372475a0

Parsell, D. A., Kowal, A. S., Singer, M. A., & Lindquist, S. (1994). Protein disaggregation mediated by heat-shock protein Hspl04. *Nature*, *372*(6505), 475–478.

Peisker, K., Chiabudini, M., & Rospert, S. (2010). The ribosome-bound Hsp70 homolog Ssb of Saccharomyces cerevisiae. *Biochimica et Biophysica Acta - Molecular Cell Research*, *1803*(6), 662–672. http://doi.org/10.1016/j.bbamcr.2010.03.005

Pellecchia, M., Montgomery, D. L., Stevens, S. Y., Vander Kooi, C. W., Feng, H. P., Gierasch, L. M., & Zuiderweg, E. R. (2000). Structural insights into substrate binding by the molecular chaperone DnaK. *Nature Structural Biology*, *7*(4), 298–303. http://doi.org/10.1038/74062

Peng, J., Schwartz, D., Elias, J. E., Thoreen, C. C., Cheng, D., Marsischky, G., … Gygi, S. P. (2003). A proteomics approach to understanding protein ubiquitination. *Nature Biotechnology*, *21 VN - r*(8), 921–926. http://doi.org/10.1038/nbt849

Perrett, S., & Jones, G. W. (2008). Insights into the mechanism of prion propagation. *Current Opinion in Structural Biology*, *18*(1), 52–59. http://doi.org/10.1016/j.sbi.2007.12.005

Petesch, S. J., & Lis, J. T. (2012). Overcoming the nucleosome barrier during transcript elongation. *Trends in Genetics*, *28*(6), 285–294. http://doi.org/10.1016/j.tig.2012.02.005

Piard, J. C., & Desmazeaud, M. (1991). Inhibiting factors produced by lactic acid bacteria. 1. Oxygen metabolites and catabolism end-products. *Le Lait*, *71*(5), 525–541. http://doi.org/10.1051/lait:1991541

Pietrosiuk, A., Lenherr, E. D., Falk, S., Bönemann, G., Kopp, J., Zentgraf, H., … Mogk, A. (2011). Molecular basis for the unique role of the AAA + chaperone ClpV in type VI protein secretion. *Journal of Biological Chemistry*, *286*(34), 30010–30021.

http://doi.org/10.1074/jbc.M111.253377

Piper, P. W., Ortiz-Calderon, C., Holyoak, C., Coote, P., & Cole, M. (1997). Hsp30, the integral plasma membrane heat shock protein of Saccharomyces cerevisiae, is a stress-inducible regulator of plasma membrane H(+)-ATPase. *Cell Stress Chaperones*. http://doi.org/10.1379/1466-1268(1997)002<0012:HTIPMH>2.3.CO;2

Porankiewlcz, J., Wang, J., & Clarke, A. K. (1999). New insights into the ATP-dependent Clp protease: Escherichia coli and beyond. *Molecular Microbiology*, *32*(3), 449–458. http://doi.org/10.1046/j.1365-2958.1999.01357.x

Prodromou, C., Siligardi, G., O'Brien, R., Woolfson, D. N., Regan, L., Panaretou, B., … Pearl, L. H. (1999). Regulation of Hsp90 ATPase activity by tetratricopeptide repeat (TPR)-domain co-chaperones. *EMBO Journal*, *18*(3), 754–762. http://doi.org/10.1093/emboj/18.3.754

Qian, Y. Q., Patel, D., Hartl, F. U., & McColl, D. J. (1996). Nuclear magnetic resonance solution structure of the human Hsp40 (HDJ- 1) J-domain. *Journal of Molecular Biology*, *260*(2), 224–235. http://doi.org/10.1006/jmbi.1996.0394

Qiu, X. B., Shao, Y. M., Miao, S., & Wang, L. (2006). The diversity of the DnaJ/Hsp40 family, the crucial partners for Hsp70 chaperones. *Cellular and Molecular Life Sciences*, *63*(22), 2560–2570. http://doi.org/10.1007/s00018-006-6192-6

Queitsch, C. (2000). Heat Shock Protein 101 Plays a Crucial Role in Thermotolerance in Arabidopsis. *The Plant Cell Online*, *12*(4), 479–492. http://doi.org/10.1105/tpc.12.4.479

Rabindran, S. K., Wisniewski, J., Li, L., Li, G. C., & Wu, C. (1994). Interaction between heat shock factor and hsp70 is insufficient to suppress induction of DNA-binding activity in vivo. *Molecular and Cellular Biology*, *14*(10), 6552–60. Retrieved from http://www.pubmedcentral.nih.gov/articlerender.fcgi?artid=359185&tool=pmcentrez&rendertype=abstract

Rabindran, S. K., Wisniewski, J., Li, L., Li, G. C., & Wu, C. (1994). Interaction between heat shock factor and hsp70 is insufficient to suppress induction of DNA-binding activity in vivo. *Molecular and Cellular Biology*, *14*(10), 6552–60. Retrieved from http://www.pubmedcentral.nih.gov/articlerender.fcgi?artid=359185&tool=pmcentrez&rendertype=abstract

Ritossa, F. (1962). A new puffing pattern induced by temperature shock and DNP in drosophila. *Experientia*, *18*(12), 571–573.

Rose, B. M., & Botsten, D. (1983). *Construction and use of gene fusions to lacZ (β-galactosidase) that are expressed in yeast*. *Methods in enzymology* (Vol. 101). http://doi.org/10.1016/0076-6879(83)01012-5

Rüdiger, S., Germeroth, L., Schneider-Mergener, J., & Bukau, B. (1997). Substrate specificity of the DnaK chaperone determined by screening cellulose-bound peptide libraries. *EMBO*

Journal, *16*(7), 1501–1507. http://doi.org/10.1093/emboj/16.7.1501

Rutherford, S. L., & Lindquist, S. (1998). Hsp90 as a capacitor for morphological evolution. *Nature*, *396*(6709), 336–342.

Sacchettini, J. C., & Kelly, J. W. (2002). Therapeutic Strategies for Human Amyloid Diseases. *Biochemistry*, *1*(April). http://doi.org/10.1038/nrd769

Sanchez, Y., & Lindquist, S. L. (1990). HSP104 required for induced thermotolerance. *Science*, *248*(12), 1112–1115. http://doi.org/10.1126/science.2188365

Sarge, K. D., & Park-Sarge, O.-K. (2009). Sumoylation and human disease pathogenesis. *Trends in Biochemical Sciences*, *34*(4), 200–205. http://doi.org/10.1016/j.tibs.2009.01.004

Schirmer, E. C., Lindquist, S., & Vierling, E. (1994). An Arabidopsis heat shock protein complements a thermotolerance defect in yeast. *The Plant Cell*, *6*(December), 1899–1909. http://doi.org/10.1105/tpc.6.12.1899

Schirmer, E. C., Queitsch, C., Kowal, S., Parsell, D. a, Kowal, A. S., & Lindquist, S. (1998). The ATPase Activity of Hsp104 , Effects of Environmental Conditions and Mutations The ATPase Activity of Hsp104 , Effects of Environmental Conditions and Mutations. *Journal of Biological Chemistry*, *273*(25), 15546–15552. http://doi.org/10.1074/jbc.273.25.15546

Schirmer, E. C., Ware, D. M., Queitsch, C., Kowal, a S., & Lindquist, S. L. (2001). Subunit interactions influence the biochemical and biological properties of Hsp104. *Proceedings of the National Academy of Sciences of the United States of America*, *98*(3), 914–919. http://doi.org/10.1073/pnas.031568098

Schlenstedt, G., Harris, S., Risse, B., Lill, R., & Silver, P. A. (1995). A yeast dnaj homolog, scj1p, can function in the endoplasmic-reticulum with bip/kar2p via a conserved domain that specifies interactions with hsp70s . *Journal of Cell Biology* , *129*(N4), 979–988.

Schlesinger, M. J. (1990). Heat Shock Proteins. *The Journal of Biological Chemistry*, *265*(21 (July 25)), 12111–12114. http://doi.org/10.1586/erv.11.124

Schröder, H. C., Batel, R., Hassanein, H. M. A., Lauenroth, S., Jenke, H. S., Simat, T., … Müller, W. E. G. (2000). Correlation between the level of the potential biomarker, heat-shock protein, and the occurrence of DNA damage in the dab, Limanda limanda: A field study in the North Sea and the English Channel. *Marine Environmental Research*, *49*(3), 201–215. http://doi.org/10.1016/S0141-1136(99)00065-3

Serpell, L. C., Sunde, M., Benson, M. D., Tennent, G. A., Pepys, M. B., & Fraser, P. E. (2000). The protofilament substructure of amyloid fibrils. *Journal of Molecular Biology*, *300*(5), 1033–1039. http://doi.org/10.1006/jmbi.2000.3908

Seyffer, F., Kummer, E., Oguchi, Y., Winkler, J., Kumar, M., Zahn, R., … Mogk, A. (2012). Hsp70 proteins bind Hsp100 regulatory M domains to activate AAA+ disaggregase at aggregate surfaces. *Nature Structural & Molecular Biology*, *19*(12), 1347–55. http://doi.org/10.1038/nsmb.2442

Shi, Y., Mosser, D. D., & Morimoto, R. I. (1998). Molecular chaperones as HSF1-specific transcriptional repressors. *Genes and Development*, *12*(5), 654–666. http://doi.org/10.1101/gad.12.5.654

Shi, Y. Y., Hong, X. G., & Wang, C. C. (2005). The C-terminal (331-376) sequence of Escherichia coli DnaJ is essential for dimerization and chaperone activity: A small angle X-ray scattering study in solution. *Journal of Biological Chemistry*, *280*(24), 22761–22768. http://doi.org/10.1074/jbc.M503643200

Shichiri, M., Hoshikawa, C., Nakamori, S., & Takagi, H. (2001). A Novel Acetyltransferase Found in Saccharomyces cerevisiae Σ1278b that Detoxifies a Proline Analogue, Azetidine-2-carboxylic Acid. *Journal of Biological Chemistry*, *276*(45), 41998–42002. http://doi.org/10.1074/jbc.C100487200

Shorter, J., & Lindquist, S. (2005). Prions as adaptive conduits of memory and inheritance. *Nature Reviews. Genetics*, *6*(6), 435–450. http://doi.org/10.1038/nrg1616

Shorter, J., & Lindquist, S. (2006). Destruction or Potentiation of Different Prions Catalyzed by Similar Hsp104 Remodeling Activities. *Molecular Cell*, *23*(3), 425–438. http://doi.org/10.1016/j.molcel.2006.05.042

Shorter, J., & Lindquist, S. (2008). Hsp104, Hsp70 and Hsp40 interplay regulates formation, growth and elimination of Sup35 prions. *Embo J*, *27*(20), 2712–2724. http://doi.org/10.1038/emboj.2008.194\remboj2008194 [pii]

Shyy, T. T., Subjeck, J. R., Heinaman, R., & Anderson, G. (1986). Effect of growth state and heat shock on nucleolar localization of the 110,000-Da heat shock protein in mouse embryo fibroblasts. *Cancer Research*, *46*(9), 4738–4745.

Sikorski, R. S., & Hieter, P. (1989). A system of shuttle vectors and yeast host strains designed for efficient manipulation of DNA in Saccharomyces cerevisiae. *Genetics*, *122*(1), 19–27. http://doi.org/0378111995000377 [pii]

Sipe, J. D., & Cohen, a S. (2000). Review: history of the amyloid fibril. *Journal of Structural Biology*, *130*(2-3), 88–98. http://doi.org/10.1006/jsbi.2000.4221

Song, Y., Wu, Y. X., Jung, G., Tutar, Y., Eisenberg, E., Greene, L. E., & Masison, D. C. (2005). Role for Hsp70 chaperone in Saccharomyces cerevisiae prion seed replication. *Eukaryotic Cell*, *4*(2), 289–297. http://doi.org/10.1128/EC.4.2.289-297.2005

Song, Y., Xu, L., Shen, M., & He, J. (2013). Roles of hydrophobic and hydrophilic forces on maintaining amyloid-prone cystatin structural stability. *Journal of Biomolecular Structure & Dynamics*, (January 2013), 37–41. http://doi.org/10.1080/07391102.2012.748535

Sorger, P. K. (1991). Heat shock factor and the heat shock response. *Cell*, *65*(3), 363–366. http://doi.org/10.1016/0092-8674(91)90452-5

Sreedhar, A. S., & Csermely, P. (2004). Heat shock proteins in the regulation of apoptosis: new strategies in tumor therapy: a comprehensive review. *Pharmacology & Therapeutics*,

101(3), 227–257.

Sreedhar, A. S., Vanathi, P., & Rao, K. (2010). Stress proteins in biology and medicine : evolution , adaptation and clinical evaluation. *International Journal of Pharma and Bio Sciences*, *1*(3), 1–36.

Stankiewicz, M., & Mayer, M. P. (2012). The universe of Hsp90. *Biomolecular Concepts*, *3*(1), 79–97. http://doi.org/10.1515/bmc.2011.054

Stansfield, I., Jones, K. M., Kushnirov, V. V, Dagkesamanskaya, a R., Poznyakovski, a I., Paushkin, S. V, … Tuite, M. F. (1995). The products of the SUP45 (eRF1) and SUP35 genes interact to mediate translation termination in Saccharomyces cerevisiae. *The EMBO Journal*, *14*(17), 4365–4373.

Stebbins, C. E., Russo, a a, Schneider, C., Rosen, N., Hartl, F. U., & Pavletich, N. P. (1997). Crystal structure of an Hsp90-geldanamycin complex: targeting of a protein chaperone by an antitumor agent. *Cell*, *89*(2), 239–250. http://doi.org/10.1016/S0092-8674(00)80203-2

Stevens, S. Y., Cai, S., Pellecchia, M., & Zuiderweg, E. R. P. (2003). The solution structure of the bacterial HSP70 chaperone protein domain DnaK (393 – 507) in complex with the peptide NRLLLTG. *Protein Science*, *12*(11), 2588–2596. http://doi.org/10.1110/ps.03269103.BiP

Subjeck, J. R., Shyy, T., Shen, J., & Johnson, R. J. (1983). Association between the mammalian 110,000-dalton heat-shock protein and nucleoli. *Journal of Cell Biology*, *97*(5 I), 1389–1395.

Summers, D. W., Wolfe, K. J., Ren, H. Y., & Cyr, D. M. (2013). The Type II Hsp40 Sis1 Cooperates with Hsp70 and the E3 Ligase Ubr1 to Promote Degradation of Terminally Misfolded Cytosolic Protein. *PLoS ONE*, *8*(1), 1–10. http://doi.org/10.1371/journal.pone.0052099

Swaney, D. L., Beltrao, P., Starita, L., Guo, A., Rush, J., Fields, S., … Villén, J. (2013). Global analysis of phosphorylation and ubiquitylation cross-talk in protein degradation. *Nature Methods*, *10*(7), 676–82. http://doi.org/10.1038/nmeth.2519

Sweeny, E. A., Jackrel, M. E., Go, M. S., Sochor, M. A., Razzo, B. M., DeSantis, M. E., … Shorter, J. (2015). The Hsp104 N-Terminal Domain Enables Disaggregase Plasticity and Potentiation. *Molecular Cell*, *57*(5), 836–849. http://doi.org/10.1016/j.molcel.2014.12.021

Sweeny, E. A., & Shorter, J. (2015). Mechanistic and structural insights into the prion-disaggregase activity of Hsp104. *Journal of Molecular Biology*, *104*, 38–41. http://doi.org/10.1016/j.jmb.2015.11.016

Sysoeva, T. A., Chowdhury, S., Guo, L., & Tracy Nixon, B. (2013). Nucleotide-induced asymmetry within ATPase activator ring drives ??54-RNAP interaction and ATP hydrolysis. *Genes and Development*, *27*(22), 2500–2511. http://doi.org/10.1101/gad.229385.113

Taipale, M., Jarosz, D. F., & Lindquist, S. (2010). HSP90 at the hub of protein homeostasis: emerging mechanistic insights. *Nature Reviews. Molecular Cell Biology*, *11*(7), 515–28. http://doi.org/10.1038/nrm2918

Tan, K., Fujimoto, M., Takii, R., Takaki, E., Hayashida, N., & Nakai, A. (2015). Mitochondrial SSBP1 protects cells from proteotoxic stresses by potentiating stress-induced HSF1 transcriptional activity. *Nature Communications*, *6*, 6580. http://doi.org/10.1038/ncomms7580

Teixeira, P., Castro, H., Mohácsi-Farkas, C., & Kirby, R. (1997). Identification of sites of injury in Lactobacillus bulgaricus during heat stress. *Journal of Applied Microbiology*, *83*(2), 219–226. http://doi.org/10.1046/j.1365-2672.1997.00221.x

Ter-Avanesyan, M. D., Dagkesamanskaya, A. R., Kushnirov, V. V., & Smirnov, V. N. (1994). The SUP35 omnipotent suppressor gene is involved in the maintenance of the non-Mendelian determinant [psi+] in the yeast Saccharomyces cerevisiae. *Genetics*, *137*(3), 671–676.

Tonsor, S. J., Scott, C., Boumaza, I., Liss, T. R., Brodsky, J. L., & Vierling, E. (2008). Heat shock protein 101 effects in A. thaliana: Genetic variation, fitness and pleiotropy in controlled temperature conditions. *Molecular Ecology*, *17*(6), 1614–1626. http://doi.org/10.1111/j.1365-294X.2008.03690.x

Truman, A. W., Kristjansdottir, K., Wolfgeher, D., Hasin, N., Polier, S., Zhang, H., … Kron, S. J. (2012). CDK-Dependent Hsp70 phosphorylation controls G1 cyclin abundance and cell-cycle progression. *Cell*, *151*(6), 1308–1318. http://doi.org/10.1016/j.cell.2012.10.051

Tsai, J., & Douglas, M. G. (1996). A conserved HPD sequence of the J-domain is necessary for YDJ1 stimulation of Hsp70 ATPase activity at a site distinct from substrate binding. *Journal of Biological Chemistry*, *271*(16), 9347–9354. http://doi.org/10.1074/jbc.271.16.9347

Tuite, M. F., & Cox, B. S. (2003). Propagation of yeast prions. *Nature Reviews. Molecular Cell Biology*, *4*(11), 878–890. http://doi.org/10.1038/nrm1247

Tyedmers, J., Mogk, A., & Bukau, B. (2010). Cellular strategies for controlling protein aggregation. *Nature Reviews Molecular Cell Biology*, *11*(11), 777–788. http://doi.org/10.1038/nrm2993

Vabulas, R. M., Raychaudhuri, S., Hayer-hartl, M., & Hartl, F. U. (2010). Protein folding in the cytoplasm and the heat shock response. *Cold Spring Harb Perspect Biol*, *2:a004390*, 1–18. http://doi.org/10.1101/cshperspect.a004390

Van Der Spoel, D., Lindahl, E., Hess, B., Groenhof, G., Mark, A. E., & Berendsen, H. J. C. (2005). GROMACS: Fast, flexible, and free. *Journal of Computational Chemistry*, *26*(16), 1701–1718. http://doi.org/10.1002/jcc.20291

Van Huizen, R., Martindale, J. L., Gorospe, M., & Holbrook, N. J. (2003). P58IPK, a novel

endoplasmic reticulum stress-inducible protein and potential negative regulator of eIF2α signaling. *Journal of Biological Chemistry*, *278*(18), 15558–15564. http://doi.org/10.1074/jbc.M212074200

Vaughan, C. K., Piper, P. W., Pearl, L. H., & Prodromou, C. (2009). A common conformationally coupled ATPase mechanism for yeast and human cytoplasmic HSP90s. *FEBS Journal*, *276*(1), 199–209. http://doi.org/10.1111/j.1742-4658.2008.06773.x

Wahid, A., Gelani, S., Ashraf, M., & Foolad, M. R. (2007). Heat tolerance in plants: An overview. *Environmental and Experimental Botany*, *61*(3), 199–223. http://doi.org/10.1016/j.envexpbot.2007.05.011

Wallace, E. W. J., Kear-Scott, J. L., Pilipenko, E. V., Schwartz, M. H., Laskowski, P. R., Rojek, A. E., … Drummond, D. A. (2015). Reversible, Specific, Active Aggregates of Endogenous Proteins Assemble upon Heat Stress. *Cell*, *162*(6), 1286–1298. http://doi.org/10.1016/j.cell.2015.08.041

Walter, G. M., Smith, M. C., Wisén, S., Basrur, V., Elenitoba-Johnson, K. S. J., Duennwald, M. L., … Gestwicki, J. E. (2011). Ordered assembly of heat shock proteins, Hsp26, Hsp70, Hsp90, and Hsp104, on expanded polyglutamine fragments revealed by chemical probes. *Journal of Biological Chemistry*, *286*(47), 40486–40493. http://doi.org/10.1074/jbc.M111.284448

Wang, F., Zhang, Y., Zhao, H., Chen, L., Shi, Y.-X., & Zhang, L. (2010). Validation of a clinical prognostic model in Chinese patients with metastatic and advanced pretreated non-small cell lung cancer treated with gefitinib. *Medical Oncology*, 331–335. http://doi.org/10.1007/s12032-010-9451-1

Wang, H., Kurochkin, A. V., Pang, Y., Hu, W., Flynn, G. C., & Zuiderweg, E. R. P. (1998). NMR solution structure of the 21 kDa chaperone protein DnaK substrate binding domain: A preview of chaperone-protein interaction. *Biochemistry*, *37*(22), 7929–7940. http://doi.org/10.1021/bi9800855

Wang, N., Li, Q., Feng, N.-H., Cheng, G., Guan, Z.-L., Wang, Y., … Sistonen, L. (2013). Heat shock factors: integrators of cell stress, development and lifespan. *Nature Reviews. Molecular Cell Biology*, *11*(6), 735–41. http://doi.org/10.1038/aja.2013.80

Wang, Y., Gibney, P. a., West, J. D., & Morano, K. a. (2012). The yeast Hsp70 Ssa1 is a sensor for activation of the heat shock response by thiol-reactive compounds. *Molecular Biology of the Cell*, *23*(17), 3290–3298. http://doi.org/10.1091/mbc.E12-06-0447

Weinert, B. T., Schölz, C., Wagner, S. A., Iesmantavicius, V., Su, D., Daniel, J. A., & Choudhary, C. (2013). Lysine succinylation is a frequently occurring modification in prokaryotes and eukaryotes and extensively overlaps with acetylation. *Cell Reports*, *4*(4), 842–851. http://doi.org/10.1016/j.celrep.2013.07.024

Weitzel, G., Pilatus, U., & Rensing, L. (1987). The cytoplasmic pH, ATP content and total

protein synthesis rate during heat-shock protein inducing treatments in yeast. *Experimental Cell Research*, *170*(1), 64–79. http://doi.org/10.1016/0014-4827(87)90117-0

Welch, W. J., & Suhan, J. P. (2012). Cellular and Biochemical Events in Mammalian Cells from Physiological Stress during and after Recovery. *Cell*, *103*(5), 2035–2052.

Werner-Washburne, M., Stone, D. E., & Craig, E. A. (1987). Complex interactions among members of an essential subfamily of hsp70 genes in Saccharomyces cerevisiae. *Molecular and Cellular Biology*, *7*(7), 2568–77. http://doi.org/10.1128/MCB.7.7.2568.Updated

Westerheide, S. D., Anckar, J., Jr, S. M. S., Sistonen, L., & Morimoto, R. I. (2009). Stress-Inducible Regulation of Heat Shock Factor 1 by thr Deacetylase SIRT1. *Science*, *323*(5917), 1063–1066. http://doi.org/10.1126/science.1165946.Stress-Inducible

Whitesell, L., Sutphin, P. D., Pulcini, E. J., Martinez, J. D., & Cook, P. H. (1998). The physical association of multiple molecular chaperone proteins with mutant p53 is altered by geldanamycin, an hsp90-binding agent. *Molecular and Cellular Biology*, *18*(3), 1517–1524.

Wickner, R. B. (1994). [URE3] as an altered URE2 protein: evidence for a prion analog in Saccharomyces cerevisiae. *Science*, *264*(April), 566–569. http://doi.org/10.1126/science.7909170

Wickner, R. B., Edskes, H. K., Roberts, B. T., Baxa, U., Pierce, M. M., Ross, E. D., & Brachmann, A. (2004). Prions: Proteins as genes and infectious entities. *Genes and Development*, *18*(5), 470–485. http://doi.org/10.1101/gad.1177104

Wickner, R. B., Edskes, H. K., Shewmaker, F., Kryndushkin, D., & Nemecek, J. (2009). Prion variants, species barriers, generation and propagation. *Journal of Biology*, *8*(5), 47. http://doi.org/10.1186/jbiol148

Wilhelmus, M. M. M., Otte-Höller, I., Wesseling, P., De Waal, R. M. W., Boelens, W. C., & Verbeek, M. M. (2006). Specific association of small heat shock proteins with the pathological hallmarks of Alzheimer's disease brains. *Neuropathology and Applied Neurobiology*, *32*(2), 119–130. http://doi.org/10.1111/j.1365-2990.2006.00689.x

Williams, J. H., Farag, A. M., Stansbury, M. A., Young, P. A., Bergman, H. L., & Petersen, N. S. (1996). Accumulation of Hsp70 in Juvenile and Adult Rainbow Trout Gill Exposed To Metal-Contaminated Water and/or Diet. *Environmental Toxicology and Chemistry*, *15*(8), 1324–1328.

Wu, C. (1995). HEAT SHOCK TRANSCRIPTION FACTORS : Structure and Regulation translocation , higher order assembly , and protein degradation. *Annual Review of Cell and Developmental Biology*, *11*(1), 441–469.

Xia, D., Esser, L., Singh, S. K., Guo, F., & Maurizi, M. R. (2004). Crystallographic investigation of peptide binding sites in the N-domain of the ClpA chaperone. *Journal of*

Structural Biology, *146*(1-2), 166–79. http://doi.org/10.1016/j.jsb.2003.11.025

Xu, L., Hasin, N., Shen, M., He, J., Xue, Y., Zhou, X., … Jones, G. W. (2013). Using Steered Molecular Dynamics to Predict and Assess Hsp70 Substrate-Binding Domain Mutants that Alter Prion Propagation. *PLoS Computational Biology*, *9*(1). http://doi.org/10.1371/journal.pcbi.1002896

Xu, W., & Neckers, L. (2007). Targeting the molecular chaperone heat shock protein 90 provides a multifaceted effect on diverse cell signaling pathways of cancer cells. *Clinical Cancer Research*, *13*(6), 1625–1629. http://doi.org/10.1158/1078-0432.CCR-06-2966

Yang, C., Miao, S., Zong, S., Koide, S. S., & Wang, L. (2005). Identification and characterization of rDJL, a novel member of the DnaJ protein family, in rat testis. *FEBS Letters*, *579*(25), 5734–5740. http://doi.org/10.1016/j.febslet.2005.09.046

Yang, X., & Seto, E. (2007). HATs and HDACs: from structure, function and regulation to novel strategies for therapy and prevention. *Oncogene*, *26*(37), 5310–5318. http://doi.org/10.1038/sj.onc.1210599

Yang, Y., Rao, R., Shen, J., Tang, Y., Fiskus, W., Nechtman, J., … Bhalla, K. (2008). Role of Acetylation and Extracellular Location of Heat Shock Protein 90A in Tumor Cell Invasion. *Cancer Research*, *68*(12), 4833–4842. http://doi.org/10.1158/0008-5472.CAN-08-0644

Zahn, M., Berthold, N., Kieslich, B., Knappe, D., Hoffmann, R., & Sträter, N. (2013). Structural studies on the forward and reverse binding modes of peptides to the chaperone DnaK. *Journal of Molecular Biology*, *425*(14), 2463–2479. http://doi.org/10.1016/j.jmb.2013.03.041

Zhang, H., Yang, J., Wu, S., Gong, W., Chen, C., & Perrett, S. (2016). Glutathionylation of the Bacterial Hsp70 Chaperone DnaK Provides a Link Between Oxidative Stress and the Heat Shock Response. *Journal of Biological Chemistry*, jbc.M115.673608. http://doi.org/10.1074/jbc.M115.673608

Zhang, T., Ploetz, E. A., Nagy, M., Doyle, S. M., Wickner, S., Smith, P. E., & Zolkiewski, M. (2012). Flexible connection of the N-terminal domain in ClpB modulates substrate binding and the aggregate reactivation efficiency. *Proteins: Structure, Function and Bioinformatics*, *80*(12), 2758–2768. http://doi.org/10.1002/prot.24159

Zheng, S., Wang, J., Feng, Y., Wang, J., & Ye, K. (2012). Solution Structure of MSL2 CXC Domain Reveals an Unusual Zn3Cys9 Cluster and Similarity to Pre-SET Domains of Histone Lysine Methyltransferases. *PLoS ONE*, *7*(9).

Zhou, X., Shimanovich, U., Herling, T. W., Wu, S., Dobson, C. M., Knowles, T. P. J., & Perrett, S. (2015). Enzymatically Active Microgels from Self-Assembling Protein Nano fi brils for Micro fl ow Chemistry. *ACS Nano*, *9*(6), 5772–5781.

Zhu, X., Zhao, X., Burkholder, W. F., Gragerov, A., Craig, M., Gottesman, M. E., … Ogata, C. M. (1996). Structural Analysis by the Binding Chaperone of Substrate Molecular DnaK.

Science, *272*(5268), 1606–1614.

Zhuravleva, A., & Gierasch, L. M. (2015). Substrate-binding domain conformational dynamics mediate Hsp70 allostery. *Proceedings of the National Academy of Sciences*, *112*(22), E2865–E2873. http://doi.org/10.1073/pnas.1506692112

Zou, J., Guo, Y., Guettouche, T., Smith, D. F., & Voellmy, R. (1998). Repression of heat shock transcription factor HSF1 activation by HSP90 (HSP90 complex) that forms a stress-sensitive complex with HSF1. *Cell*, *94*(4), 471–480. http://doi.org/10.1016/S0092-8674(00)81588-3